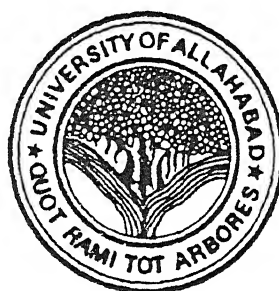


Study of Ultrasonic Attenuation in Condensed Materials



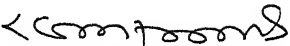
Devraj Singh
Department of Physics
University of Allahabad,
Allahabad-211 002
INDIA

Thesis
Submitted to the
University of Allahabad
For the Degree of
Doctor of Philosophy
in
Science
2002

Dedicated
to
my parents

CERTIFICATE

This is to certify that the candidate Mr. Devraj Singh has fulfilled all the requirements for the submission of a D.Phil. thesis to the University of Allahabad, Allahabad-211 002 (INDIA).


(Dr. Raja Ram Yadav)

Supervisor

ACKNOWLEDGEMENT

I am indebted to my supervisor Dr. Raja Ram Yadav, Reader in Physics, University of Allahabad for his keen interest, noble guidance, constructive criticism, thoughtful suggestions and constant encouragement during the course of research work.

I wish to express my sincere thank to Prof. Gopal Krishna Pandey, Head of Physics Department, University of Allahabad for providing necessary facilities in the Department.

I am highly grateful to Prof. Sushil Kumar Kor (D.Sc.) and Prof. Bal Krishna Agrawal (F.N.A.) for the valuable discussions during the research work.

I offer thank to my research colleagues Mr. Arvind Kumar Tiwari, Mr. Devendra Kumar Singh, Mr. Devendra Kumar Mishra, Mr. Ambesh Dixit, Mr. Rakesh Kumar and Mr. Santosh Kumar for their help in numerous ways.

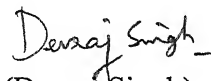
The help rendered to me by computer operators Mr. Ved Prakash Mishra and Mr. Ajay Singh is highly acknowledged.

The work carried out in this thesis would not have been possible without the emotional support from my family members, who always inspired me to take up new challenges.

Last but not the least, I express my gratitude to the official staff, library staff and Mr. Ramji Dwivedi of Physics Department, University of Allahabad.

Dated: 29.07.2002

Place Allahabad


(Devraj Singh)

List of Publications

- [1.] "Ultrasonic characterization of intermetallics"
Raja Ram Yadav and **Devraj Singh**
15th World conference on non-destructive testing,
Roma(Italy)-15-21October, (2000), Idn.386.
- [2.] "Temperature dependence of Ultrasonic absorption
in Lanthanum Monochalcogenides"
Raja Ram Yadav and **Devraj Singh**
Journal of the Acoustical Society of India
Vol. 28, No. 1-4, (2000), pp.191-198.
- [3] "Behaviour of ultrasonic attenuation in intermetallics"
Raja Ram Yadav and **Devraj Singh**
Intermetallics (Elsevier-Cambridge)
Vol.9,(2001), pp.189-194.
- [4] "Ultrasonic attenuation in Lanthanum Monochalcogenides"
Raja Ram Yadav and **Devraj Singh**
Journal of the Physical Society of Japan
Vol.70, No.6, (2001), pp.1825-1832.
- [5] "Ultrasonic attenuation in semi-metallic GdX single crystals
(X=P,As,Sb and Bi) in the temperature range 10 to 300K"
S.K.Kor, Govind Pandey and **Devraj Singh**
Indian Journal of Pure and Applied Physics
Vol.39, (2001), pp. 510-513.
- [6] "Ultrasonic attenuation in Gadolinium Monopnictides"
Devraj Singh and Raja Ram Yadav
Journal of the Acoustical Society of India
Vol. 29, No. 1, (2001), pp.176-184.

- [7] "Absorption at low temperatures"
Raja Ram Yadav and **Devraj Singh**
Journal of the Acoustical Society of India
Vol. 29, No. 1, (2001), pp.220-224.
- [8] "Ultrasonic attenuation in Lanthanum Monochalcogenides
from 5K to 500K"
S.K.Kor, Govind Pandey and **Devraj Singh**
Acustica
Communicated.
- [9] "Ultrasonic attenuation in semiconductors"
Devraj Singh, R.R.Yadav and Arvind Kumar Tiwari
Indian Journal of Pure and Applied Physics
Submitted.
- [10] "Ultrasonic studies of CTAB in Glycol"
S.K.Kor, R.R.Yadav and **Devraj Singh**
Molecular Crystals and Liquid Crystals
Communicated.
- [11] "Effect of thermal conductivity on ultrasonic attenuation
in Praseodymium Monochalcogenides"
Raja Ram Yadav and **Devraj Singh**
Acoustical Physics (USSR)
Submitted.
- [12] "Acoustical investigations on plutonium monochalcogenides"
Raja Ram Yadav and **Devraj Singh**
Journal of the Acoustical Society of India
Communicated.
- [13] "The thermal conductivity and ultrasonic absorption in
dielectric crystals"
Devraj Singh and Raja Ram Yadav
Journal of the Acoustical Society of India
Communicated.

[15] “Ultrasonic evaluations in rare-earth metals”

Raja Ram Yadav, **Devraj Singh** and Arvind Kumar Tiwari

Journal of the Acoustical Society of India

Communicated.

[16] “Effect of compositions on ultrasonic attenuation in metallic alloys at room temperature”

Raja Ram Yadav, **Devraj Singh** and Priyanka Awasthi

Journal of the Acoustical Society of India

Communicated.

[17] “Acoustical investigations on intermetallic compounds”

Raja Ram Yadav, **Devraj Singh** and Arvind Kumar Tiwari

Acta Physica Polonica A

Communicated.

Contents

Chapters	Particulars	Page No.
1	Introduction	1-3
2	Theory of Second and Third Order Elastic Constants of Face Centered Cubic Crystal and Ultrasonic Attenuation due to Electron-Phonon interaction, Phonon-Phonon interaction and Thermoelastic Loss	4-30
3	Temperature Dependence of Ultrasonic Attenuation in Metallic Crystals	31-48
4	Effect of Thermal Conductivity on Ultrasonic Attenuation in Dielectric Crystals	49-64
5	Ultrasonic Attenuation in Semiconductors	65-85

6	Effect of Concentration on Ultrasonic Attenuation in Metallic Alloys at Room Temperature	86-99
7	Ultrasonic Attenuation in Intermetallics	100-138
8	Ultrasonic Attenuation in Semi-Metallic Single Crystals	139-164
9	Application of Morse Potential to Evaluate the Ultrasonic Attenuation in Semi-Metallic GdX Single Crystals (X=P, As, Sb and Bi) in the Temperature Range 10 to 300K	165-184
10	Behaviour of Acoustical Phonons in BCC Metals in Low Temperature Region using Morse Potential	185-194
11A	Experimental Techniques and Methodology	195-207
11B	Ultrasonic Measurements in Lyotropic Liquid Crystal	208-216
	Appendix-A	217-222

CHAPTER-1

Introduction

Increased competition and needs of higher productivity and better products from material producing industries are creating more stringent requirements for process and quality control and call for advances in non-destructive techniques which can be used to characterize materials not only after production but during processing as well, progress in characterizing techniques is also needed by more wide spread use of advanced materials and demands for the non-destructive measurements of their mechanical properties.

Ultrasonics offer the possibility to detect and characterize microstructural properties as well as deformation processes in materials controlling material's behaviour based on the physical mechanism to predict future performance of the materials. Structural inhomogeneities or flaw size atomistic (interstitials), elastic parameters, precipitates, dislocations, grain, phase transformation, porosity and cracks, electrical resistivity, thermal conductivity are well connected with the frequency, concentration of the contents in alloys, pressure, magnetization, crystallographic direction or temperature dependence of the ultrasonic attenuation and velocity evaluations. Ultrasonic measurements provide a direct method for obtaining information about the mean free path of phonons of particular type (i.e. phonons constituting the sound wave). This is contrast to thermal conductivity or heat pulse measurement which only provide the mean free path averaged over that part of the phonon spectrum thermally excited.

In the present investigation quantitative ultrasonic evaluations in condensed materials now aims to establish a theoretical approach for the evaluations and to detect and characterize microstructural properties as well as deformation processes in the materials based on the physical mechanism controlling material behaviour (especially mechanical properties) to predict future performance, safety and reliability of the materials components and structures.

Elastic properties of a solid are important because they relate to various fundamental solid-state phenomena such as interatomic potentials, equations of state and phonon spectra. Elastic properties are also linked thermodynamically with specific heat, thermal expansion, Debye temperature and the Grüneisen parameter. Most importantly,

knowledge of elastic constants is essential for many practical applications related to the mechanical properties of a solid: load deflection, thermoelastic stress, internal strain (residual stress), sound velocity and fracture toughness.

In the present investigation second and higher order elastic constants play an important role for the evaluations of ultrasonic attenuation through non-linearity parameter. Higher order elastic constants are important for studying anharmonicity i.e. thermal expansion and other properties dependent on phonon interaction, which is the mechanism used for ultrasonic absorption.

Therefore upto 10th chapter we have also evaluated second and third order elastic constants of the materials taken for the ultrasonic evaluations starting from only two basic parameters (lattice parameter and hardness parameter).

Continuing the work finally we have evaluated ultrasonic absorption, velocity as a function of frequency and other related parameters like thermal relaxation time, non-linearity parameter (acoustic coupling constants) Grüneisen numbers etc. at different physical conditions like different temperatures concentration of content in alloys, crystallographic directions.

In the current status major part of the work on ultrasonic investigations has been done in the materials like metals, dielectric crystals, few semiconducting materials, few metallic alloys at room temperature and at low temperature in metals along few crystallographic directions. On the other side the extensive experimental work on ultrasonic absorption and velocity has been done by previous workers mostly in liquids only. No work has been done in liquid crystals.

For the present investigations the technologically important metals Ce, Yb and Th are chosen. For these metals no work has been done by previous workers.

Although a lot of work in dielectric crystals has been done by previous workers but temperature and orientation dependence of ultrasonic absorption in AgCl, LiF and MnO is not found in the available literature. Therefore the evaluations of ultrasonic absorption and velocity in AgCl, LiF and MnO from 100-573K, temperatures based on phonon-phonon interaction mechanism have been made.

In the literature very few quantity of work on semiconductors has been found at room temperature along one or two orientation of the crystals. Therefore ultrasonic parameters

from 100 to 300K in the first time attempted SnTe, EuSe, CdO, SmS, NpS, NpSe, PuS, PuSe and PuTe semiconducting materials have been evaluated and discussed. Some results are seen very characterizing features of the materials.

In the recent years so many properties like crystalline structure, magnetoresistance etc. are directly dependent on the content of the metallic alloys [1]. The effect of concentration of the partner of the alloys Cu-Pt, Ag-Pt and Au-Pt on ultrasonic parameters at room temperature is discussed in the present investigation

Intermetallic compounds or 'intermetallics' for short have received extensive attention in recent years [2]. Therefore ultrasonic studies are made first time in intermetallics viz. LaS, LaSe, LaTe, PrS, PrSe, PrTe, CeS, CeSe, CeTe, NdS, NdSe and NdTe at 5K to 500K temperature range. Interesting characteristic features have been discussed.

In the continuation first time taken semi-metallics as GdX (X=P, As, Sb and Bi), NpTe are also taken for the ultrasonic evaluation in the 8th and 9th chapters. For the study in semi-metallics both type of interaction potentials, Born-Mayer and Morse potentials have been utilized.

In the 10th.chapter three bcc metals V, Nb and Ta are also taken for the ultrasonic evaluation at lower temperature based on electron-phonon interaction

In the last chapter the experiment has been set for the measurements of ultrasonic absorption and velocity in lyotropic liquid crystal in non-aqueous solution taking ethylene glycol as solvent which has a relaxation frequency. This type of work has been started because of wide application of liquid crystals in a number of technological important areas including medical.

References:

1. S.Ram and P.S.Frankwicz, Phys. Stat. Sol. (a)188,1129(2001).
2. R.W.Cahn; Contemporary Physics 42, 365(2001).

CHAPTER- 2

Theory of Second and Third Order Elastic Constants of Face-Centered Cubic Crystal and Ultrasonic Attenuation in Solids due to Electron-Phonon Interaction, Phonon-Phonon Interaction and Thermoelastic Loss

2.1 Introduction

In the second chapter the theory has been discussed to be established for the evaluations of the ultrasonic attenuation and other related parameters in different temperature region along various direction of propagation for all type of solids reviewing the earlier work done by various investigators [1-12]. Evaluation of ultrasonic parameters will be aimed to establish the ultrasonic theoretical approach and behavior of ultrasonic attenuation and other associated parameters under different physical conditions as the characteristic features of the materials.

The second and third order elastic constants (SOEC & TOEC) play a versatile role for the evaluations of the ultrasonic velocities longitudinal as well as shear, Grüneisen parameters etc. and finally ultrasonic attenuation. Hence our theory of present investigation categorized into two parts

- (a) Calculation of SOEC and TOEC using Coulomb and Born Mayer Potential
- (b) Ultrasonic attenuation in solids

2.2 Calculations of SOEC and TOEC using Coulomb and Born-Mayer Potential

K. Brugger [13] defined the elastic constant of the n^{th} order ← check into this

$$C_{ijklmn} = (\partial^n F / \partial \eta_{ij} \partial \eta_{kl} \partial \eta_{mn}) \quad (2.1)$$

Here F is the free energy density of undeformed material and $\partial \eta_{ij} = [(\partial x_i / \partial a_k) (\partial x_j / \partial a_k) - \delta_{ij}]$ is the component of the Lagrangian strain tensor (i,j,k=1,2,3) where a and x are initial and final positions of the material point, and δ_{ij} is the Kronecker's delta. Summation on repeated indices is always implied for components of vector and tensor quantities. The Voigt notation (which has been adopted in the present investigation) C_{IJK} ...have been used instead of tensor

ne a

notation C_{ijklmn} for notation of elastic constants. for using (ij)→I according to the scheme (11)→1 etc. and (23) →4 etc. for cubic crystals. due to symmetry only three independent SOEC and six TOEC exist. The total free energy F is expanded in terms of strain η , can be written (using Taylor's series expansion) as

$$F = \sum_{n=0}^{\infty} F_n = \sum_{n=0}^{\infty} \frac{1}{n!} (\partial^n F / \partial \eta_{ij} \partial \eta_{kl} \partial \eta_{mn}) \eta_{ij} \eta_{kl} \eta_{mn} \quad (2.2)$$

Expanding free energy in terms of strain η_{ij} , square and cubic terms are obtained as

$$F_2 = \frac{1}{2!} C_{ijkl} \eta_{ij} \eta_{kl}$$

$$F_2 = [(1/2)C_{11}(\eta_{11}^2 + \eta_{22}^2 + \eta_{33}^2) + C_{12}(\eta_{11}\eta_{22} + \eta_{11}\eta_{33} + \eta_{22}\eta_{33}) + 2C_{44}(\eta_{12}^2 + \eta_{23}^2 + \eta_{31}^2)] \quad (2.3)$$

and

$$F_3 = \frac{1}{3!} C_{ijklmn} \eta_{ij} \eta_{kl} \eta_{mn}$$

$$F_3 = [(1/6)C_{111}(\eta_{11}^3 + \eta_{22}^3 + \eta_{33}^3) + (1/2)C_{112}\{\eta_{11}^2(\eta_{22} + \eta_{33}) + \eta_{22}^2(\eta_{33} + \eta_{11}) + \eta_{33}^2(\eta_{11} + \eta_{22})\} + C_{123}\eta_{11}\eta_{22}\eta_{33} + 2C_{166}\{\eta_{12}^2(\eta_{11} + \eta_{22}) + \eta_{23}^2(\eta_{22} + \eta_{33}) + \eta_{31}^2(\eta_{33} + \eta_{11})\} + 8C_{456}\eta_{12}\eta_{23}\eta_{31}] \quad (2.4)$$

Where η_{ij} are Lagrangian strain components C_{IJ} are second order elastic constants, and C_{IJK} are third order elastic constants (TOEC) in Brugger's notation [13].

The free energy density of a crystal at a finite temperature T is [14]

$$F = U + F^{\text{vib}} \quad (2.5)$$

$$F = \frac{kT}{NV_c} \sum_{i=0}^{3sN} \ln 2 \sinh(h\omega_i / 2kT) \quad (2.6)$$

Where U is the internal energy of unit volume of the crystal when all ions are at rest on their point. F^{vib} is the vibrational free energy, V_c is the volume of elementary cell, N is the number of the cells in the crystal, and s ($=2$) is the number of ions per unit cell for f.c.c. crystals, ω_i is vibrational frequency corresponding to i^{th} mode of atomic vibration.

Elastic constants of second and third order at T K , can be written as

$$C_{IJ} = C_{IJ}^0 + C_{IJ}^{\text{vib}}$$

$$C_{IJK} = C_{IJK}^0 + C_{IJK}^{\text{vib}} \quad (2.7)$$

Where C_{IJ}^0 and C_{IK}^0 are static and C_{IJ}^{Vib} and C_{IK}^{Vib} are vibrational contribution to SOEC and TOEC respectively.

The energy U can be expressed as

$$U = \frac{1}{2} V_C \sum_{v=1}^2 \sum_{\substack{(m) \\ (n) \neq (o)}} \phi_{\mu v}(R_{\mu v}^{mo}) \cong \frac{1}{2} V_C \sum \phi_{\mu v}(R) \quad , \quad (2.8)$$

where $R_{\mu v}^{mo}$ is the distance between v^{th} ion in the o^{th} cell and μ^{th} ion in the m^{th} cell and $\phi_{\mu v}$ is the interaction potential between ions. The indices (v,o) and (μ,m) are dropped where no confusion occurs. $\phi_{\mu v}$ is assumed to be sum of long range electrostatic (i.e Coulomb) and short range Born-Mayer [15] potentials given as

$$\phi_{\mu v}(R) = \pm(e^2 / R) + A \exp(-R / b) = \phi(R) \quad (2.9)$$

Where e is electronic charge, \pm sign is used for like and unlike ions and A and b are strength parameter and hardness parameter respectively. Taking interactions into account upto second neighbor distance, the following form for the short range potential is obtained:

- (a) Unlike charges $A_{ij} \cdot \exp (-r_1/b)$,
- (b) Like +ive charges $A_{ii} \cdot \exp (-r_2/b)$ and
- (c) Like -ive charges $A_{jj} \cdot \exp (-r_2/b)$,

where i, j =1, 2 for positive and negative ions and r_1 and r_2 are nearest neighbor and next neighbor distance respectively. In this form of potential there would be six parameters for interactions between like (ii) and (jj) and unlike (ij) ions. For the simplicity it has been assumed that A is same for like and unlike charges, here b is hardness parameter [16] and can be obtained from equilibrium condition:

$$(\partial \phi / \partial r)_{r=r_0} = 0 \quad (2.10)$$

and using experimental value of compressibility or cohesive energy or one of the SOEC at absolute zero and A is given by

$$A = b Z_0 (e^2 / r_0^2) [6 \exp(-r_0/b) + 12 \sqrt{2} \exp(-r_0 \sqrt{2} / b)]^{-1} \quad (2.11)$$

Where Z_0 =Madelung's constants for face centered cubic crystal=1.74756, and e is the electronic charge=4.803X10⁻¹⁰esu. The value of b can be used to evaluate $\phi_{\mu v}(R)$. One has used the set of “b” by Tosi [16] making use of the Hinderbrand equation of state.

When the crystal is deformed homogeneously the distant between ions R is given by

$$R=[(R_{\mu\nu}^{m\circ})^2-(r_{\mu\nu}^{m\circ})^2]^{1/2} \quad (2.12)$$

where $r_{\mu\nu}^{m\circ}$ and $R_{\mu\nu}^{m\circ}$ are the position of the ion in equilibrium and deformed state respectively. The distance can be expressed in terms of Lagrangian strain tensor as

$$(R_{\mu\nu}^{m\circ})^2-(r_{\mu\nu}^{m\circ})^2=2\xi_{\mu\nu_i}^{m\circ}\xi_{\mu\nu_j}^{m\circ}\eta_{ij}\cong 2\rho_{\mu\nu}^{m\circ} \quad (2.13)$$

where $\xi_{\mu\nu_i}^{m\circ}$ is the i^{th} Cartesians components of vector $r_{\mu\nu}^{m\circ}$.

The internal energy U_1 can be expanded in terms of ρ and cubic and the quadratic terms are:

$$\begin{aligned} U_2 &= (2V_C)^{-1} \sum [\rho^2 D^2 \phi(R) / 2!]_{R=r} \\ &= (4V_C)^{-1} [\eta_{ij}\eta_{kl} \sum \xi_i \xi_j \xi_k \xi_l D^2 \phi(R)]_{R=r} \end{aligned} \quad (2.14)$$

$$\begin{aligned} U_3 &= (2V_C)^{-1} \sum [\rho^3 D^3 \phi(R) / 3!]_{R=r} \\ &= (12V_C)^{-1} [\eta_{ij}\eta_{kl}\eta_{mn} \sum \xi_i \xi_j \xi_k \xi_l \xi_m \xi_n D^3 \phi(R)]_{R=r} \end{aligned} \quad (2.15)$$

with the abbreviation $D=R^{-1}(d/dR)$ and V_C is the volume of the elementary cell ($=2r_0^3$ for NaCl-type crystals).

The SOEC and TOEC at zero degree K have been obtained in Table 2.1 by comparing eqns. (2.3) and (2.4) with eqns. (2.14) and (2.15).

Table 2.1 Expression for the SOEC and TOEC at 0 K

$$\begin{aligned} C_{11}^0 &= (2V_C)^{-1} [\sum \xi_1^4 D^2 \phi(R)]_{R=r}, \quad C_{12}^0 = (2V_C)^{-1} [\sum \xi_1^2 \xi_2^2 D^2 \phi(R)]_{R=r}, \\ C_{44}^0 &= (2V_C)^{-1} [\sum \xi_1^2 \xi_2^2 D^2 \phi(R)]_{R=r}, \quad C_{111}^0 = (2V_C)^{-1} [\sum \xi_1^6 D^3 \phi(R)]_{R=r}, \\ C_{112}^0 &= (2V_C)^{-1} [\sum \xi_1^4 \xi_2^2 D^3 \phi(R)]_{R=r}, \quad C_{123}^0 = (2V_C)^{-1} [\sum \xi_1^2 \xi_2^2 \xi_3^2 D^3 \phi(R)]_{R=r}, \\ C_{144}^0 &= (2V_C)^{-1} [\sum \xi_1^2 \xi_2^2 \xi_3^2 D^3 \phi(R)]_{R=r}, \quad C_{166}^0 = (2V_C)^{-1} [\sum \xi_1^4 \xi_2^2 D^3 \phi(R)]_{R=r}, \\ \text{and } C_{456}^0 &= (2V_C)^{-1} [\sum \xi_1^2 \xi_2^2 \xi_3^2 D^3 \phi(R)]_{R=r}, \end{aligned}$$

Cauchy's relations for second and third order elastic constants (SOEC & TOEC) are satisfied as given in Table 2.1 i.e.

$$C_{12}^0 = C_{44}^0; \quad C_{112}^0 = C_{166}^0; \quad C_{123}^0 = C_{144}^0 = C_{456}^0 \quad (2.16)$$

Now taking the case of f.c.c crystals for obtaining the elastic constants. The cartesian coordinates of ions are represented as $\xi_1=l_1r_0$, $\xi_2=l_2r_0$, $\xi_3=l_3r_0$. ($l_1, l_2, l_3=0, \pm 1, \pm 2, \dots$), where r_0 is the nearest neighbor distance, the volume of elementary cell $V_C=2 r_0^3$.

The Coulomb interactions are considered between the ions in the crystal and the lattice sum defined by

$$S_N^{(n_1, n_2, n_3)} = \sum_{l_1, l_2, l_3} (-1)^{l_1, l_2, l_3} \frac{l_1^{2n_1} l_2^{2n_2} l_3^{2n_3}}{(l_1^2 + l_2^2 + l_3^2)^{N/2}} \quad (2.17)$$

Thus the lattice sums have been obtained as shown in Table 2.3. For the short range repulsive potential interaction between the nearest neighbor ($l_1, l_2, l_3=\pm 1, 0, 0$ etc.) and second nearest neighbor ($l_1, l_2, l_3=\pm 1, \pm 1, 0$) are taken into account.

For face centered cubic crystals (present investigation) SOEC and TOEC at 0 K can be obtained using expressions as in Tables 2.2 and 2.3.

Table 2.2 Static SOE and TOE constants C_{IJ}^0 and C_{IJK}^0

$$C_{11}^0 = \frac{3e^2}{2r_0^4} S_5^{(2)} + \frac{1}{br_0} \left(\frac{1}{r_0} + \frac{1}{b} \right) \phi(r_0) + \frac{2}{br_0} \left(\frac{\sqrt{2}}{2r_0} + \frac{1}{b} \right) \phi(\sqrt{2}r_0),$$

$$C_{12}^0 = C_{44}^0 = \frac{3e^2}{2r_0^4} S_5^{(1,1)} + \frac{1}{br_0} \left(\frac{\sqrt{2}}{2r_0} + \frac{1}{b} \right) \phi(\sqrt{2}r_0),$$

$$C_{111}^0 = -\frac{15e^2}{2r_0^4} S_7^{(3)} - \frac{1}{b} \left(\frac{3}{r_0^2} + \frac{3}{br_0} + \frac{1}{b^2} \right) \phi(r_0) - \frac{1}{2b} \left(\frac{3\sqrt{2}}{r_0^2} + \frac{6}{br_0} + \frac{2\sqrt{2}}{b^2} \right) \phi(\sqrt{2}r_0)$$

$$C_{112}^0 = C_{166}^0 = -\frac{15e^2}{2r_0^4} S_7^{(2,1)} - \frac{1}{4b} \left(\frac{3\sqrt{2}}{r_0^2} + \frac{6}{br_0} + \frac{2\sqrt{2}}{b^2} \right) \phi(\sqrt{2}r_0)$$

$$C_{123}^0 = C_{144}^0 = C_{456}^0 = -\frac{15e^2}{2r_0^4} S_7^{(1,1,1)}$$

Here r_0 is the short range parameter, b is the hardness parameter

$$\phi(r_0) = A \exp(-r_0/b) \quad \text{and} \quad \phi(\sqrt{2} r_0) = A \exp(-\sqrt{2} r_0/b)$$

A is the parameter given by

$$A = -3b(e^2/r_0^2) [6 \exp(-r_0/b) + 12\sqrt{2} \exp(-r_0\sqrt{2}/b)]^{-1}$$

Table 2.3 Values of lattice sum.

$S_3^{(1)} = -0.58252, S_5^{(2)} = -1.04622, S_5^{(1,1)} = 0.23185$
$S_7^{(3)} = -1.36852, S_7^{(2,1)} = 0.16115, S_7^{(1,1,1)} = -0.09045$

2.3 Vibrational Elastic Constants or Temperature Variation of SOEC and TOEC using approximation $\hbar \omega_0 \ll kT$

The vibrational energy density at temperature T is given as in equ.(2.6), which for $\hbar \omega_0 \ll kT$ [19] becomes as:

$$F^{\text{vib}} = kT \sum_{i=1}^{3sN} \ln 2 (\hbar \omega_i / kT) \quad (2.18)$$

An approximation [14,17,18] used in eqn. (2.18) is valid only in higher temperature limit, hence subsequent expressions for thermal coefficients. Here using the theorem that the spur of a matrix is invariant under coordinate transformation and $\sum \omega_i^2 = 3sN \langle \omega^2 \rangle_{\text{av}}$. Following Born's suggestion, ω_i in eqn.(2.18) is replaced by $(\langle \omega^2 \rangle)^{1/2}$ as the average of ω_i^2 is generally shown to be

$$\langle \omega^2 \rangle_{\text{av}} = (3s)^{-1} \sum (M_v)^{-1} \Delta \phi_{\mu\nu}(R) \cong \omega_0^2 \quad (2.19)$$

where M_v is the mass of the v^{th} ion. In the present case, only the short range repulsive potential $\phi(R) = A \exp(-R/b)$ is taken into consideration for the interaction energies, because Coulombic contribution vanishes due to $\Delta(e^2/r) = 0$. When the repulsive interactions up to the second neighbor are considered, it follows that

$$\omega_0^2 = \left(\frac{1}{M_+} + \frac{1}{M_-} \right) \frac{1}{br_0} \left\{ \left(\frac{r_0}{b} - 1 \right) \phi(r_0) + 2 \left(\frac{r_0}{b} - \sqrt{2} \right) \phi(\sqrt{2}r_0) \right\} \quad (2.20)$$

At a temperature T^0K , lattice parameter changes from equilibrium r_0 to $r_0 + \delta r_0$. For cubic crystals the thermal expansion is isotropic and assuming that it is independent of temperature then:

$$\delta r = l_1 kT. \quad (2.21)$$

where k is Boltzmann constant and l_1 will be defined latter.

One now imposes the condition of equilibrium reduced to

$$V_c \sum C_{ik,jl} \eta_{ij}^{\text{th}} - 3skT \gamma_{ik} = 0 \quad (2.22)$$

Where $\gamma_{ik} = -(1/2)(\partial \ln \langle \omega^2 \rangle_{av} / \partial \eta_{ik})$ is the generalized Grüneisen constants and $C_{ik,jl}$ are the SOEC. For cubic crystal $\gamma_{ik} = \delta_{ik} \gamma$, Then

$$\frac{\delta r}{r_0} = \eta_{11}^{th} = (skT / V_c)(\text{bulk modulus})^{-1} \gamma \quad (2.23)$$

The thermal strain is defined as

$$\eta_{ij}^{th} \delta_{ij} = \frac{\delta r}{r_0} \quad (2.24)$$

The expressions for l_1 can be easily written down. For face centered cubic crystal

$$l_1 = -\frac{b}{2} \frac{[(2 + 2\rho_0 - \rho_0^2)\phi(r_0) + 2\sqrt{2}(1 + \sqrt{2}\rho_0 - \rho_0^2)\phi(r_0\sqrt{2})]}{[(\rho_0 - 2)\phi(r_0) + 2(\rho_0 - \sqrt{2})\phi(r_0\sqrt{2})][(\rho_0 - 2)\phi(r_0) + 4(\rho_0 - \sqrt{2})\phi(r_0\sqrt{2})]}, \quad (2.25)$$

where $\rho_0 = r_0 / b$, $\phi(r) = A \exp(-r/b)$.

Now expanding the vibrational part of the free energy of the deformed crystal in square and cubic terms one gets;

$$\begin{aligned} f_2^{vib} &= (kT / 8\omega_0^2) \left(\sum_{ij} \sum_{i'j'} \eta_{ij} \eta_{i'j'} \sum_{\nu=1}^2 M_{\nu}^{-1} \xi_i \xi_j \xi_{i'} \xi_{j'} [D^2 \Delta \phi_{\mu\nu}(R)]_{R=r_{\mu\nu}^{m_0}} \right) - (2\omega_0^2)^{-1} \\ &\quad \left\{ \sum_{\nu\nu'} \sum_{\left(\begin{smallmatrix} m \\ \mu \end{smallmatrix}\right) \neq \left(\begin{smallmatrix} o \\ \nu \end{smallmatrix}\right)} \sum_{\left(\begin{smallmatrix} m' \\ \mu' \end{smallmatrix}\right) \neq \left(\begin{smallmatrix} o' \\ \nu' \end{smallmatrix}\right)} M_{\nu}^{-1} M_{\nu'}^{-1} \xi_i \xi_j \xi_{i'} \xi_{j'} [D \Delta \phi_{\mu\nu}(R)]_{R=r_{\mu\nu}^{m_0}} [D \Delta \phi_{\mu'\nu'}(R)]_{R=r_{\mu'\nu'}^{m'_0 o'_0}} \right\} \quad (2.26) \\ f_3^{vib} &= (kT / 24\omega_0^2) \left(\sum_{ij} \sum_{i'j'} \sum_{i''j''} \eta_{ij} \eta_{i'j'} \eta_{i''j''} \sum_{\nu=1}^2 M_{\nu}^{-1} \xi_i \xi_j \xi_{i'} \xi_{j'} \xi_{i''} \xi_{j''} [D^3 \Delta \phi_{\mu\nu}(R)]_{R=r_{\mu\nu}^{m_0}} \right) \\ &\quad - (2\omega_0^2)^{-1} \left\{ \sum_{\nu\nu'} \sum_{\left(\begin{smallmatrix} m \\ \mu \end{smallmatrix}\right) \neq \left(\begin{smallmatrix} o \\ \nu \end{smallmatrix}\right)} \sum_{\left(\begin{smallmatrix} m' \\ \mu' \end{smallmatrix}\right) \neq \left(\begin{smallmatrix} o' \\ \nu' \end{smallmatrix}\right)} M_{\nu}^{-1} M_{\nu'}^{-1} \xi_i \xi_j \xi_{i'} \xi_{j'} \xi_{i''} \xi_{j''} [D^2 \Delta \phi_{\mu'\nu'}(R)]_{R=r_{\mu'\nu'}^{m'_0 o'_0}} \right. \\ &\quad \left. [D \Delta \phi_{\mu\nu}(R)]_{R=r_{\mu\nu}^{m_0}} + (18\omega_0^4)^{-1} \left\{ \sum_{\nu\nu'\nu''} \sum_{\left(\begin{smallmatrix} m \\ \mu \end{smallmatrix}\right) \neq \left(\begin{smallmatrix} o \\ \nu \end{smallmatrix}\right)} \sum_{\left(\begin{smallmatrix} m' \\ \mu' \end{smallmatrix}\right) \neq \left(\begin{smallmatrix} o' \\ \nu' \end{smallmatrix}\right)} \sum_{\left(\begin{smallmatrix} m'' \\ \mu'' \end{smallmatrix}\right) \neq \left(\begin{smallmatrix} o'' \\ \nu'' \end{smallmatrix}\right)} M_{\nu}^{-1} M_{\nu'}^{-1} M_{\nu''}^{-1} \xi_i \xi_j \right.} \\ &\quad \left. \xi_{i'} \xi_{j'} \xi_{i''} \xi_{j''} [D \Delta \phi_{\mu\nu}(R)]_{R=r_{\mu\nu}^{m_0}} [D \Delta \phi_{\mu'\nu'}(R)]_{R=r_{\mu'\nu'}^{m'_0 o'_0}} [D \Delta \phi_{\mu''\nu''}(R)]_{R=r_{\mu''\nu''}^{m''_0 o''_0}} \right\} \right\} \quad (2.27) \end{aligned}$$

where ω_0^2 is the mean square frequency of undeformed crystal ($\omega_0^2 = \langle \omega_0^2 \rangle$ [given in eqn.(2.20)] and $\xi_z = \xi_{\mu\nu}$, $\xi_z = \xi_{\mu\nu}$ and $\xi_z = \xi_{\mu\nu}$ $z=i, j, i', j', i''$ and j'' .

Rearranging the terms one gets f_{ij}^{vib} and f_{ijk}^{vib} (f_1^{vib} being vibrational energy per unit cell)

$$f_2^{vib} = \frac{1}{2} f_{11}^{vib} (\eta_{11}^2 + \eta_{22}^2 + \eta_{33}^2) + f_{12}^{vib} (\eta_{11} \eta_{22} + \eta_{22} \eta_{33} + \eta_{33} \eta_{11})$$

$$+ f_{11}^{\text{vib}} (\eta_{11}^2 + \eta_{22}^2 + \eta_{33}^2) \quad (2.28)$$

$$\begin{aligned} f_3^{\text{vib}} = & \frac{1}{6} f_{111}^{\text{vib}} (\eta_{11}^3 + \eta_{22}^3 + \eta_{33}^3) + \frac{1}{2} f_{112}^{\text{vib}} \{ \eta_{11}^2 (\eta_{22} + \eta_{33}) + \eta_{22}^2 (\eta_{33} + \eta_{11}) \\ & + \eta_{22}^2 (\eta_{11} + \eta_{22}) \} + f_{123}^{\text{vib}} \eta_{11} \eta_{22} \eta_{33} + 2 f_{144}^{\text{vib}} (\eta_{11} \eta_{23}^2 + \eta_{22} \eta_{31}^2 + \eta_{33} \\ & \eta_{12}^2) + 2 f_{166}^{\text{vib}} \{ \eta_{12}^2 (\eta_{11} + \eta_{22}) + \eta_{23}^2 (\eta_{22} + \eta_{33}) + \eta_{31}^2 (\eta_{33} + \eta_{11}) \} \\ & + 8 f_{456}^{\text{vib}} \eta_{12} \eta_{23} \eta_{31} \end{aligned} \quad (2.29)$$

where

$$\begin{aligned} f_{11}^{\text{vib}} &= \frac{kT}{4} (G_2 - \frac{G_1^2}{6}); \quad f_{12}^{\text{vib}} = kT (G_{1,1} - \frac{G_1^2}{6}); \quad f_{44}^{\text{vib}} = kT \frac{G_{1,1}}{4}; \\ f_{111}^{\text{vib}} &= \frac{kT}{4} (G_3 - \frac{1}{2} G_2 G_1 + \frac{G_1^3}{18}); \quad f_{112}^{\text{vib}} = \frac{kT}{4} (G_{2,1} - \frac{1}{3} G_{1,1} G_1 - \frac{1}{6} G_2 G_1 + \frac{G_1^3}{18}); \\ f_{123}^{\text{vib}} &= \frac{kT}{4} (G_{1,1,1} - \frac{1}{2} G_{2,1} G_1 + \frac{G_1^3}{18}); \quad f_{144}^{\text{vib}} = \frac{kT}{4} (G_{1,1,1} - \frac{1}{2} G_{1,1} G_1); \\ f_{166}^{\text{vib}} &= \frac{kT}{4} (G_{1,1,1} - \frac{1}{2} G_{1,1} G_1) \quad \text{and} \quad f_{456}^{\text{vib}} = kT \frac{G_{1,1,1}}{4}. \end{aligned}$$

and

$$\begin{aligned} G_1 &= \omega_0^{-2} \sum M_{\nu}^{-1} \xi_1^2 [D \Delta \phi_{\mu\nu}]_{R=r_{\mu\nu}^{\text{mo}}}; \quad G_2 = \omega_0^{-2} \sum M_{\nu}^{-1} \xi_1^4 [D^2 \Delta \phi_{\mu\nu}]_{R=r_{\mu\nu}^{\text{mo}}}; \\ G_3 &= \omega_0^{-2} \sum M_{\nu}^{-1} \xi_1^6 [D^3 \Delta \phi_{\mu\nu}]_{R=r_{\mu\nu}^{\text{mo}}}; \quad G_{1,1} = \omega_0^{-2} \sum M_{\nu}^{-1} \xi_1^2 \xi_2^2 [D^2 \Delta \phi_{\mu\nu}]_{R=r_{\mu\nu}^{\text{mo}}}; \\ G_{2,1} &= \omega_0^{-2} \sum M_{\nu}^{-1} \xi_1^4 \xi_2^2 [D^3 \Delta \phi_{\mu\nu}]_{R=r_{\mu\nu}^{\text{mo}}}; \quad \text{and} \quad G_{1,1,1} = \omega_0^{-2} \sum M_{\nu}^{-1} \xi_1^2 \xi_2^2 \xi_3^2 [D^3 \Delta \phi_{\mu\nu}]_{R=r_{\mu\nu}^{\text{mo}}}; \end{aligned}$$

On further evaluation of G_1 , G_2 , G_3 , $G_{1,1}$, $G_{2,1}$ and $G_{1,1,1}$ in the approximation of second nearest neighbor interactions.

$$\begin{aligned} G_1 &= [2(2\rho_0 + 2\rho_0^2 - \rho_0^3)\phi(r_0) + 2(2\rho_2 + 2\rho_2^2 - \rho_2^3)\phi(r_0\sqrt{2})]\Lambda; \\ G_2 &= [2(-6\rho_0 - 6\rho_0^2 - \rho_0^3 + \rho_0^4)\phi(r_0) + (-6\rho_0 - 6\rho_0^2 - \rho_0^3 + \rho_0^4)\phi(r_0\sqrt{2})]\Lambda; \\ G_3 &= [2(30\rho_0 + 30\rho_0^2 + 9\rho_0^3 - \rho_0^4 - \rho_0^5)\phi(r_0) + (1/2)(30\rho_0 + 30\rho_0^2 + 9\rho_0^3 - \rho_0^4 - \rho_0^5)\phi(r_0\sqrt{2})]\Lambda; \\ G_{1,1} &= [(1/2)(-6\rho_0 - 6\rho_0^2 - \rho_0^3 + \rho_0^4)\phi(r_0\sqrt{2})]\Lambda; \\ G_{2,1} &= [(1/4)(30\rho_0 + 30\rho_0^2 + 9\rho_0^3 - \rho_0^4 - \rho_0^5)\phi(r_0\sqrt{2})]\Lambda; \quad \text{and} \quad G_{1,1,1}=0 \\ \Lambda &= \{ \rho_0^2 - 2\rho_0 \} \phi(r_0) + 2 \{ \rho_2^2 - 2\rho_2 \} \phi(\sqrt{2} r_0) \}^{-1}, \end{aligned}$$

$\rho_0=r_0/b$ and $\rho_2= \sqrt{2} r_0/b$ and $\phi(r)=A \exp(-r/b)$.

SOEC and TOEC at T^0K with lattice parameter $r=r_0+\delta r_0$ can be written as

$$\begin{aligned} C_{ij} &= C_{ij}(r_0) + \delta r (\partial C_{ij}^0 / \partial r)_{r=r_0} + V_c^{-1} f_{ij}^{Vib} \\ &= C_{ij}^o + C_{ij}^{Vib} \end{aligned} \quad (2.30)$$

and

$$\begin{aligned} C_{ijk} &= C_{ijk}(r_0) + \delta r (\partial C_{ijk}^0 / \partial r)_{r=r_0} + V_c^{-1} f_{ijk}^{Vib} \\ &= C_{ijk}^o + C_{ijk}^{Vib} \end{aligned} \quad (2.31)$$

$$C_{ij}^0 = l_1 k (\partial C_{ij}^0 / \partial r)_{r=r_0} + (TV_c)^{-1} f_{ij}^{Vib} \quad (2.32)$$

$$C_{ijk}^0 = l_1 k (\partial C_{ijk}^0 / \partial r)_{r=r_0} + (TV_c)^{-1} f_{ijk}^{Vib} \quad (2.33)$$

2.4 Temperature variation of SOEC and TOEC without any approximation:

In the case of short range interaction repulsive potential $\phi(r)$ is taken into account for interaction energies because the contribution due to Coulombic part vanishes being relation $(\Delta e^2/r)=0$. Considering interaction upto second nearest neighbor expressions for ω^2_0 becomes as eqn. (2.20).

Similar to internal energy U_l the vibrational F^{Vib} is expanded in terms of η_{ij} and the square and cubic terms are given as

$$F_2^{Vib} = [(1/2!V_c) \sum \sum \rho \rho' (DD') F^{Vib}]_{\rho=0}, \quad \cong (1/2!V_c) \eta_{ij} \eta_{kl} f_{ijkl} \quad (2.34)$$

$$F_3^{Vib} = [(1/3!V_c) \sum \sum \sum \rho \rho' \rho'' (D''D'D) F^{Vib}]_{\rho=0, \dots} \cong (1/3!V_c) \eta_{ij} \eta_{kl} \eta_{mn} f_{ijklmn} \quad (2.35)$$

where

$$f_{ijkl} = \sum \sum [\xi_i \xi_j \xi'_k \xi'_l (D'D) F^{Vib}]_{R=r,} \quad (2.36)$$

$$f_{ijklmn} = \sum \sum \sum [\xi_i \xi_j \xi'_k \xi'_l \xi''_m \xi''_n (D''D'D) F^{Vib}]_{R=r,} \quad (2.37)$$

Here the abbreviation $\rho_{\mu'\nu'}^{m'o'} \rightarrow \rho'$, $(1/R_{\mu'\nu'}^{m'o'}) (d/dR_{\mu'\nu'}^{m'o'}) \rightarrow D'$ etc are used.

By comparing eqns. (2.3) and (2.4) with eqns.(2.34) and (2.35), the vibrational elastic consants, C_{IJ}^{Vib} and C_{IJK}^{Vib} . The explicit formulae are obtained by calculating f_{ijk} . After taking into consideration that $D\langle\omega^2\rangle=1/6 M_v^{-1} D\Delta\phi_{\mu\nu}(R)$. The results for C_{IJ}^{Vib} and C_{IJK}^{Vib} .obtained

thus are presented in Table 2.4. Where C_{IJ}^{Vib} and C_{IJK}^{Vib} are represented as G_n 's. These f^n 's and G_n 's can be conveniently calculated by taking crystal symmetry into account and their expressions are shown in Tables 2.5 and 2.6. By adding C_{IJ} to static constants C_{IJ}^0 and C_{IJK}^0 , the SOEC and TOEC at required temperature can be obtained.

Two parameters A and b in the Born-Mayer potential have been determined using the equilibrium condition that total energy (F) should be minimum i.e. $(\partial F/\partial \eta_{ij})_{r=r_0}=0$, where r_0 is the lattice parameter. In cubic crystals, it can be shown that $\partial F/\partial \eta_{11}=\partial F/\partial \eta_{22}=\partial F/\partial \eta_{33}$ and $\partial F/\partial \eta_{23}=\partial F/\partial \eta_{31}=\partial F/\partial \eta_{12}=0$. Therefore, the equilibrium condition is

$$(\partial F/\partial \eta_{ij})_{r=r_0}=0 \quad (2.38)$$

and the explicit form

$$-\frac{e^2}{r_0} S_3^{(1)} - \frac{2r_0}{b} \phi(r_0) - \frac{4\sqrt{2}r_0}{b} \phi(\sqrt{2}r_0) + \frac{\hbar\omega_0}{4} G_1 \coth x = 0 \quad (2.39)$$

Table 2.4 Vibrational SOE and TOE constants C_{IJ}^{Vib} and C_{IJK}^{Vib}

$$\begin{aligned} C_{11}^{Vib} &= f^{(1,1)} G_1^2 + f^{(2)} G_2, \\ C_{12}^{Vib} &= f^{(1,1)} G_1^2 + f^{(2)} G_{1,1}, \\ C_{44}^{Vib} &= f^{(2)} G_{1,1}, \\ C_{111}^{Vib} &= f^{(1,1,1)} G_1^3 + 3f^{(2,1)} G_2 G_1 + f^{(3)} G_3, \\ C_{112}^{Vib} &= f^{(1,1,1)} G_1^3 + f^{(2,1)} G_1 (2G_{1,1} + G_2) + f^{(3)} G_{2,1}, \\ C_{123}^{Vib} &= f^{(1,1,1)} G_1^3 + 3f^{(2,1)} G_1 G_{1,1} + f^{(3)} G_{1,1,1}, \\ C_{144}^{Vib} &= f^{(2,1)} G_1 G_{1,1} + f^{(3)} G_{1,1,1}, \\ C_{166}^{Vib} &= f^{(2,1)} G_1 G_{1,1} + f^{(3)} G_{2,1}, \\ C_{456}^{Vib} &= f^{(3)} G_{1,1,1} \end{aligned}$$

Table 2.5 Expressions of $f^{(n)}$

$$f^{(2)} = f^{(3)} = \frac{1}{2r_0^3} \frac{\hbar\omega_0}{4} \coth x;$$

$$f^{(1,1)} = f^{(2,1)} = -\frac{1}{2r_0^3} \frac{\hbar\omega_0}{48} \left\{ \frac{\hbar\omega_0}{2kT \sinh^2 x} + \coth x \right\};$$

$$f^{(1,1,1)} = \frac{1}{2r_0^3} \frac{\hbar\omega_0}{192} \left\{ \frac{(\hbar\omega_0)^2 \coth x}{6(kT)^2 \sinh^2 x} + \frac{\hbar\omega_0}{2kT \sinh^2 x} + \coth x \right\}.$$

Table2.6 Expressions of G_n

$$G_1 = 2 \{ (2 + 2\rho_0 - \rho_0^2) \phi(r_0) + 2(\sqrt{2} + 2\rho_0 - \sqrt{2}\rho_0^2) \phi(\sqrt{2}r_0) \} H$$

$$G_2 = 2 \{ (-6 - 6\rho_0 - \rho_0^2 + \rho_0^3) \phi(r_0) + (-3\sqrt{2} - 6\rho_0 - \sqrt{2}\rho_0^2 + 2\rho_0^3) \phi(\sqrt{2}r_0) \} H$$

$$G_3 = 2 \{ \{ (30 + 30\rho_0 + 9\rho_0^2 - \rho_0^3 - \rho_0^4) \phi(r_0) + \{ (15/2)\sqrt{2} + 15\rho_0 + (9/2)\sqrt{2}\rho_0^2 - \rho_0^3 - \sqrt{2}\rho_0^4 \} \phi(\sqrt{2}r_0) \} \} H$$

$$G_{1,1} = \{ -3\sqrt{2} - 6\rho_0 - \sqrt{2}\rho_0^2 + 2\rho_0^3 \} \phi(\sqrt{2}r_0) H$$

$$G_{2,1} = \{ (15/2)\sqrt{2} + 15\rho_0 + (9/2)\sqrt{2}\rho_0^2 - \rho_0^3 - \sqrt{2}\rho_0^4 \} \phi(\sqrt{2}r_0) H$$

$$G_{1,1,1} = 0$$

$$H = \{ \rho_0 - 2 \} \phi(r_0) + 2(\rho_0 - \sqrt{2}) \phi(\sqrt{2}r_0) \}^{-1}$$

$$\phi(r_0) = A \exp.(-\rho_0) \text{ and } \phi(\sqrt{2}r_0) = A \exp.(-\sqrt{2}\rho_0)$$

$$\rho_0 = r_0/b \quad \text{where } r_0 \text{ is nearest neighbor distance and } b \text{ being hardness parameter}$$

2.5. Ultrasonic attenuation in Solids

The solids have greater binding forces between their constitute atoms than the fluids, hence in general they support shear stress and may also have anisotropy. Since solid can support shear stress, both longitudinal and shear waves can be propagated. For any direction of propagation in a solid the different modes with mutually orthogonal displacements are possible. However these modes will neither be pure longitudinal nor pure shear waves. Solids have a number of contributions to ultrasonic attenuation. These contributions could be estimated under different conditions of concerned medium. One can study the particular cause of attenuation and eliminate the other contribution by having control over the physical properties of materials.

Most of the energy absorbed from acoustic beam is converted into heat and dissipated in the material. As pointed out earlier [3-7, 9-10] the absorption of ultrasonic waves in solids may be attributed mostly to the dissipate type of absorption but there are non-dissipated type absorption also. Various dissipated type of ultrasonic absorption may be classified [20] as being due to

- (a) Electron-phonon interaction
- (b) Phonon-phonon interaction
- (c) Thermoelastic loss
- (d) Ferromagnetic and ferroelectric loss
- (e) Lattice imperfections
- (f) NMR and thermal relaxation
- (g) Dislocations etc.

If it is assumed that the hypothetical crystal under study is perfect and non ferromagnetic and non-ferroelectric, then there will be only three causes viz-electron-phonon interaction (at low temperature), Phonon-phonon interaction, and thermoelastic loss at room temperature (at higher temperature). In the present work these types of losses have been studied.

2.5.1 Electron-phonon interaction

When an ultrasonic wave propagates through a solid, the coupling between the wave and the conduction electrons dissipates some of the acoustic energy. Debye theory of specific heat suggests that the energy exchange occur in metals' free electrons and interacting lattice at low temperature. ~~As the matter of fact~~ the electron-phonon interaction in a conducting solid can be understood in three different ways

- (1) Attenuation of acoustic wave [21]
- (2) Velocity dispersion[22]
- (3) The presence of acoustoelectric field[23]

The Physical mechanism by which acoustic phonons interact with conduction electrons can be classified into four categories

- (1) **Purely electromagnetic coupling** [5, 24]

This kind of coupling arises in solids in which two atoms are ionized or have a high density of ionized impurities.

- (2.) **Deformation potential coupling** [25,26]

is due to detailed band structure of solids and mechanism is dominant one in most conducting solids at high enough frequency.

(3.) Piezo-electric coupling [27]

It arises in piezoelectric semiconductors.

(4.) Magneto-elastic coupling [28]

It is effective in those conducting solids in which magnetostrictive effect is large. It is dominant in ferromagnetic conductors.

The electron-phonon interaction becomes very important tool and can be used in studying the electronic band structure of matter. The information that can be obtained in this manner includes carrier effective masses, the dimensions of the Fermi-surface. This kind of interaction also provides a method for amplifying and generating phonon of very high frequency [29], effect of trapping[30,31,32] attenuation of ultrasound [33]; to generate[34] and study hot electrons[35,36] in semiconductors.

The attenuation of ultrasonic wave due to this effect becomes an important matter of extensive study below 100K. At still lower temperature ^{in addition to} besides other factors, dislocation losses also vanish and the loss only due to electron-phonon interaction remains effective. However in superconducting state lattice is not able to transfer momentum to electron gas and the damping disappears.

Mason's formulation for the attenuation of Ultrasonic waves due to Electron-phonon interaction

At low temperature in pure metals [5,6,37,38], when the mean free path of conduction electrons becomes large is comparable to the wavelength of the acoustic wave.

According to Mason [37,39] analysis the energy of electrons in normal state is carried to and from the lattice vibration by means of transfer of momentum. The momentum given to it by the vibrating lattice is not returned to the lattice immediately and viscous loss occurs.

The electron viscosity [40] η_e for the ideal gas may be given by

$$\eta_e = \frac{N \bar{l} m \bar{V}}{3} \quad (2.40)$$

where N is the number of electron per cc, m their mass \bar{l} the mean free path (in this case between electrons and lattice atom (phonon) and \bar{V} the mean velocity. The last two quantities can be evaluated from the theory of free electron gas [41] and are

$$\bar{V}^2 = \frac{3\hbar^2}{5m^2}(3\pi^2N)^{1/2} \quad ; \quad \bar{l} = \frac{\sigma m \bar{V}}{Ne^2}; \quad (2.41)$$

where e is the charge on the electron, \hbar is the Planck's constants divided by 2π and σ is the electrical resistivity in cgs system. Introducing eqn.(2.41) in eqn.(2.40) and substituting

$\sigma = \frac{9 \times 10^{11}}{R}$ where R is the electrical resistivity in ohm cm, the value of η_e becomes

$$\eta_e = \frac{9 \times 10^{11} \hbar^2}{5e^2 R} (3\pi^2 N)^{2/3} \quad (2.42)$$

The attenuation of ultrasonic waves caused by the energy loss due to shear and compressional viscosities of the electron gas for longitudinal and shear waves in the lattice is given as

$$(\alpha)_{\text{long}} (\text{Np/cm}) = \frac{2\pi^2 f^2}{\rho V_l^3} \left(\frac{4}{3} \eta_e + \chi \right) \quad (2.43)$$

$$(\alpha)_{\text{shear}} (\text{Np/cm}) = \frac{2\pi^2 f^2}{\rho V_s^3} \eta_e \quad (2.44)$$

where ρ is the density of the crystal, f is the frequency, η_e the shear viscosity, χ the compressional viscosity, V_l and V_s are directly related with second order elastic constants C_{ij} , as

$$V_l = \sqrt{\frac{C_{11}}{\rho}} \quad \text{and} \quad V_s = \sqrt{\frac{C_{44}}{\rho}} \quad (2.45)$$

χ is taken to be zero on the basis of measurement made in metals[34].

Mason also discussed Bömmel's result in terms of the equivalent shear viscosity of the electron gas. The discussion of Mason [37] and Morse [6] leads the similar results. However the two approaches are differ at high frequencies. Not this but leading term of Pippards [5] gives the similar results as obtained by Morse and Mason. Hence the basic assumption lying in explaining the phenomenon is the same.

Schrey [42] measured the e-p interaction attenuation in Copper and they have also predicted the results, which are good agreement with this theory.

Thus in the present work we have used Mason's approach for evaluating the ultrasonic attenuation due to e-p interaction at lower temperatures.

2.5.2 Phonon-phonon interaction

At higher temperature i.e. at 100K and above the ultrasonic attenuation arises mainly due to interaction of acoustical phonons and thermal phonons in solids.

Two distinct theoretical approaches have been found useful in estimating velocity and attenuation due to p-p interaction:

- (1) Landau-Rumer's theory
- (2) Akhiezer theory

2.5.2 A Landau-Rumer's theory:

In Landau-Rumer's theory [43], the acoustic and thermal waves are treated microscopically, which are valid at low temperature i.e. when $\omega\tau \gg 1$, where ω is the frequency of the ultrasonic waves and τ is the thermal relaxation time. The acoustic wave is considered as a beam of low energy phonons and the attenuation is calculated by obtaining the rate at which these acoustic phonons are scattered by elastic collisions with thermal phonons. Anisotropy and velocity dispersions are ignored in the original theory. Various investigators have extended the theory and have considered how the attenuation is affected by anisotropy and dispersion. The correction to the sound velocity due to interaction with thermal phonons, may also be calculated as the presence of thermal phonons changes the energy of each acoustic phonon by a small amount, which causes the changes in the velocity and can be evaluated by second order quantum mechanical perturbation theory. Recently Bonnet et al.[44] have measured attenuation due to p-p interaction for NaCl and KCl in a wide temperature region using hypersonic waves in Brillouin scattering and they found good agreement with Landau-Rumer theory.

2.5.2B Akhiezer's theory:

In the Landau's theory, interaction between thermal phonons and acoustic phonons has been taken into account by considering these interactions. Boltzmann distribution equation can be used for the evaluation of ultrasonic attenuation. According to Akhiezer [45] the sound wave modulates the thermal phonon distribution of the medium through which it propagates. The modulated phonons are no longer in equilibrium but tends to relax back to equilibrium via phonon-phonon interaction caused by anharmonic interaction. In the process

of relaxing back, entropy is produced and energy is absorbed from the propagating sound waves. The sound waves are treated macroscopically and the strain of sound waves as the driving force on the system of thermal phonons. Earlier this theory restricted to high temperatures i.e. under the conditions $\omega\tau \ll 1$. However the theory was further developed by Woodruff and Ehrenreich [4] and extended to the condition $\omega\tau \gg 1$.

When $\omega\tau \ll 1$, Boltzmann equation is applied to consider the interaction between the individual thermal phonons. Boltzmann equation is given by

$$\frac{\partial N(\vec{k}J)}{\partial T} = \omega_{ij}(\vec{k}J) \left(\frac{\partial \eta_{ij}}{\partial x_k} \frac{\partial N(\vec{k}J)}{\partial k_k} - V_i(\vec{k}J) \frac{\partial N(\vec{k}J)}{\partial t} \right) + \left[\frac{\partial N(\vec{k}J)}{\partial t} \right]_{\text{Coll}} \quad (2.46)$$

Where $N(kJ)$ is total number of phonons (k is the wave vector of ultrasonic wave and J is polarization direction), $V(kJ)$ is phase velocity, $\tau(kJ)$ is life time for acoustical phonons.

$$\omega_{ij}(\vec{k}J) = \frac{\partial \omega(\vec{k}J)}{\partial \eta_{ij}} \quad (2.47)$$

and η_{ij} is lagrangian strain tensor defined as

$$\eta_{ij} = \frac{1}{2} \left[\frac{\partial U_i}{\partial X_j} + \frac{\partial U_j}{\partial X_i} + \frac{\partial U_k}{\partial X_i} \frac{\partial U_k}{\partial X_j} \right] \quad (2.48)$$

Where U is the displacement and X the position in the equation motion. The three different types of collision between thermal phonon may take place, which are briefly discussed below:

(i) Normal Process:

These collisions arises due to anharmonicity with the involvement of three phonons process in general. In this process the total energy E_{ph} of thermal phonons and the total quasi momentum (p) remains conserved. One therefore obtains

$$E_{ph} = \sum_{kJ} N(k'J) \hbar \omega(k'J) = \text{Constant} \quad (2.49)$$

$$p = \sum_{kJ} N(k'J) \hbar k = \text{Constant} \quad (2.50)$$

Here
$$\sum_{kJ} \left[\frac{\partial N(\vec{k}J)}{\partial t} \right]_{\text{Coll}} \hbar k = 0 \quad (2.51)$$

and

$$\left[\frac{\partial N(\vec{k}J)}{\partial t} \right]_{\text{Coll}} \hbar k = 0 \quad (2.52)$$

It can further shown that Normal process results in a distribution function which after simplification reduces to

$$N_N(k'J) = \left[\exp \frac{\hbar \omega(\vec{k}J) - \hbar \vec{V}_d k}{k_B T \rho} \right] \quad (2.53)$$

Where V_d is the drift velocity and T_l corresponds to local temperature. Because of the conservation law on the quasi momentum, N-process alone are not able to bring arbitrary initial distribution of thermal phonons into thermal equilibrium.

(ii) Umklapp Process:

Umklapp process is different from the normal process as in this process the momentum is not conserved and therefore the following expression gives the energy

$$\sum_{\vec{k}J} \left[\frac{\partial N(\vec{k}J)}{\partial t} \right]_{\text{Coll}} \hbar k = 0 \quad (2.54)$$

The equilibrium is completed by non-equilibrium distribution of phonons and distribution is given as follows

$$N_u(\vec{k}J) = \left[\exp \frac{\hbar \omega(\vec{k}J)}{k_B T_l \rho} - 1 \right]^{-1} \quad (2.55)$$

Where T_l is the local temperature, unlike N-processes it can bring non-equilibrium of phonon to complete the equilibrium.

(iii) Elastic Scattering:

In this process acoustic phonon collide with impurities etc. and mostly the scattering process is elastic. The frequency remains unchanged but the wave vector changes and the conserved energy can be mathematically expressed as given below

$$\sum_{\vec{k}J} \left[\frac{\partial N(\vec{k}J)}{\partial t} \right]_{\text{Coll}} \delta[\omega - \omega(\vec{k}J)] = 0 \quad (2.56)$$

In this case the distribution takes the form

$$N_E(\vec{k}J) = \left[\exp \frac{\hbar \omega(\vec{k}J)}{k_B T \omega(\vec{k}J)} - 1 \right]^{-1} \quad (2.57)$$

Elastic processes also do not produce complete equilibrium when acting by themselves. However E and N processes acting together to produce equilibrium. When many Umklapp processes are considered and one restricted to the case $\omega\tau_{th} \ll 1$, where τ_{th} is the average time between Umklapp processes, a finite value for the attenuation is obtained as follows:

$$\alpha = \frac{\omega^2 e_i(\vec{k}J)\vec{k}_j e_k(\vec{k}J)\vec{k}_l V_{ijkl}}{2\rho V^3(\vec{k}J)} + \frac{\omega^2 T \vec{k}_{\lambda\mu} \vec{k}_\lambda \vec{k}_\mu}{2\rho V^5(\vec{k}J)C^2} [e_i(\vec{k}J)\vec{k}_j C_{ijkl} \alpha'_{lm}]^2 \quad (2.58)$$

Where C_{ijkl} is second order elastic constant, C is the specific heat per unit volume, V is the phase velocity. The first term arises from phonon-viscosity and the second term from heat conduction. However, the relation (2.58) is not very useful as there is no practical way of evaluating V_{ijkl} (viscosity tensor). The relation seems to be useful as it provides the relations between attenuation of waves of different polarization and propagation direction. In case of cubic crystals the viscosity tensor has three independent components V_{11} , V_{12} and V_{44} . The attenuation due to viscosity may be given as

$$\alpha_v = \frac{\omega^2 V_{eff}}{2\rho V^3(\vec{k}J)} \quad (2.59)$$

Where V_{eff} can be given in terms of V_{11} , V_{12} and V_{44} . Similarly the loss due to thermal conduction for cubic symmetry also takes a simpler form because the conductivity and thermal conduction tensor are isotropic. Thus

$$K_{\lambda\mu} = K \delta_{\lambda\mu} \alpha_{lm} = \alpha \delta_{\gamma\delta} \quad (2.60)$$

and hence attenuation due to heat conduction is given as:

$$\alpha_{th} = \frac{\omega^2 T \alpha'^2 k}{2V^5(\vec{k}J)C^2} (C_{11} + 2C_{12})^2 [\vec{e}_j(\vec{k}J) - \vec{k}_j] \quad (2.61)$$

For pure shear wave $e(kJ)$ is perpendicular to k and thus $e_j(kJ) \cdot k_j = 0$, Hence there is no heat conduction. For the pure longitudinal wave $e(kj) \cdot k_j = 1$. Many workers viz Bömmel and Dransfeld [3], Lamb and Ritcher [46], Lewis and Patterson [47] have studied the attenuation and found that the attenuation due to thermal conduction is not very appreciable and can be ignored. The quadratic dependence on attenuation is shown in eq.(2.58) and (2.61) and was verified by Lamb and Ritcher [46], by measuring attenuation in quartz, fused silica, silicon and Germanium between 100 to 1000MHz at room temperature. However a simplified approach was taken up by Woodruff and Ehrenreich [4] and they took the time independent

Boltzmann transport equation to describe the process. The collision integral is written explicitly and exclusively in terms of three phonon transition probabilities. They have avoided to separate the absorption into heat flow and discuss damping part because $\omega\tau_{th}=1$, the separation is difficult to justify. The expression for the case $\omega\tau_{th}<<1$ is

$$\alpha = \frac{CT\gamma^2\omega^2\tau}{3\bar{V}^3} \quad (2.62)$$

where $K=C\bar{V}^2/3$ and for $\omega\tau>>1$

$$\alpha = \frac{\pi CT\gamma^2\omega}{4\rho\bar{V}^3} \quad (2.63)$$

It is interesting to note that this expression is independent of τ and has the same dependence on ω and T as that arrived by Landau and Rumer [43] quantum mechanical treatment for $\omega\tau>1$. Here γ is the some form of Grüneisen constants respectively the non-linearity of the elastic moduli and is given as

$$\gamma = \frac{3\alpha'k}{C} \quad (2.64)$$

α' and k are thermal expansion coefficient and bulk modulus. The thermal relaxation time τ (represented as τ_{th} here after) is determined by the time required to transfer the acoustic energy into thermal phonon and the time to equalize the temperature difference of the phonons. Experimentally Herring [48] has obtained that the thermal phonon relaxation time for longitudinal τ_l and shear wave τ_s as

$$\tau_{th}=\tau_{sh}=\frac{1}{2}\tau_{long}=\frac{3K}{C_v\bar{V}^2} \quad (2.65)$$

where K is the thermal conductivity, C_v is the specific heat per unit volume, \bar{V} is the Debye average velocity of ultrasonic wave as:

$$\frac{3}{\bar{V}^3} = \frac{1}{V_l^3} + \frac{2}{V_s^3} \quad (2.66)$$

where V_l and V_s are the ultrasonic longitudinal and shear wave velocities respectively. However the method of Woodruff and Ehrenreich [4] is also not found very useful for quantitative value of attenuation due to insufficient information available for γ used in

expression. In 1983 Bonnet et al.[44] have studied experimentally few alkali halides and concluded that attenuation is successfully explained in Akhiezer region [45].

(iv) Mason's approach:

Akhiezer [45] was first to propose the phonon-viscosity mechanism, but he did not include the finite value of relaxation time for thermal equilibrium process. Bömmel and Dransfeld [3] later modified this work considering the relaxation time to be finite. They have obtained results comparable to the experimental results. Further Woodruff and Ehrenreich used the Boltzmann equation method to evaluate the steady state distribution of thermal phonons and acoustical attenuation. But due to insufficient information regarding γ ; Mason [9] has used Grüneisen constants $\langle\gamma_i^j\rangle$ which is related to second and third order elastic constants and this approach is found to be very useful for the estimation of the ultrasonic attenuation in various crystals.

At room temperature and in a wide temperature region also, thermal relaxation time, τ_{th} varies from 10^{-10} sec to 10^{-13} sec from metallic to dielectric crystals. As the temperature increases, τ_{th} decreases. Hence condition $\omega\tau_{th}\ll 1$ holds good and at the same time the individual phonon losses its significance and idea of the phonon gas having macroscopic parameters is described. The sudden application of acoustical pressure on a body at temperature T causes different temperature increments for different phonon modes, which relax back to new equilibrium at temperature $T+\Delta T$ through the phonon-phonon collision. This temperature difference lags behind the periodic stress and causes a relaxational absorption.

The relation between the attenuation and ΔC_e (change in the elastic constant due to non-equilibrium temperature separation of the phonon modes by the applied strain) is given as

$$\alpha = \frac{\Delta C_e \omega^2 \tau_{th}}{2\rho V^3 (1 + \omega^2 \tau_{th}^2)} \quad (2.67)$$

Where α is the attenuation in Np/cm, ρ is density, ω is the angular frequency of the ultrasonic waves and V is the velocity of the wave.

When the strain S_j is applied to the crystal, there is change in mode frequency given by

$$\omega_i = \omega_{i0} (1 - \sum_{j=1} \gamma_i^j S_j) \quad (2.68)$$

ω_{10} is the frequency of the mode in the standard state. By measurement of SOEC and TOEC, it could be predicted that $\langle \gamma_i^j \rangle$ do not much and when the above expression is differentiated, one obtains

$$\gamma_i^j = -\frac{\partial \omega_i / \partial S_j}{\omega_{10}} \quad (2.69)$$

γ_i^j is known as Gruneisen number, Brugger has given a general formula for γ_i^j by in terms of the tensor notation-

$$\gamma_i^j = -\gamma_i^{jk} = U_j U_k + (N_p N_q / 2C)(C_{jkpq} + U_r U_s C_{jkpqrs}) \quad (2.70)$$

where j, k are the two index symbols for strain S_j , N_p and N_q are the direction cosines for the propagation direction and C_e is the required elastic constants determined by the type of wave and the direction of propagation U_j and U_k are the direction cosines for the particle displacement, C_{jkpq} and C_{jkpqrs} are the SOEC and TOEC in tensor notations. Now suddenly applied strain neither changes the number of modes nor their entropy. Mason considered thermal energy of the modes under Debye approximation

$$U_{th} = 3\hbar \sum_i \frac{N_i}{\omega_{gi}^3} \int_0^{\omega_{gi}} \frac{\omega^3 d\omega}{e^{h\omega/k_B T} - 1} \quad (2.71)$$

Differentiating the sum of the elastic energy plus total thermal energy of all modes one obtains

$$\begin{aligned} T_j &= \partial U_{th} / \partial S_j \\ &= C_{ij}^s S_j + 3\hbar \frac{\partial}{\partial S_j} \left[\sum_i \frac{N_i}{\omega_{gi}^3} \int_0^{\omega_{gi}} \frac{\omega^3 d\omega}{e^{h\omega/k_B T} - 1} \right] \end{aligned} \quad (2.72)$$

and finally one obtains

$$T_j = [C_{ij}^s + 3 \sum_i E_i (\gamma_i^j)] S_j + 3 \sum_i E_i \gamma_i^j \quad (2.73)$$

T_j is the stress associated with the strain S_j , C_{ij}^s is the corresponding elastic constants resulting from no entropy exchanges between any of the modes and γ_i^j is Gruneisen number,

Ei is the thermal energy associated with each direction and each mode. The above expression clearly shows the increase in elastic moduli

$$\Delta C = 3 \sum E_i (\gamma_i^j)^2 \quad (2.74)$$

This is valid for shear modes for which the average rise in temperature is zero. For longitudinal modes, the increase in modulus resulting from the difference between the adiabatic and isothermal conditions is to be subtracted and it is given by

$$\Delta C = [3 \sum E_i (\gamma_i^j)^2 - \gamma^2 C T] \quad (2.75)$$

replacing the value of ΔC in eqn.(2.67)

$$\alpha = \frac{\omega^2 \tau_{th} E_0 (D/3)}{2\rho V^3 (1 + \omega^2 \tau_{th}^2)} \quad (2.76)$$

for $\omega \tau_{th} \ll 1$

$$\alpha = \frac{\omega^2 \tau_{th} E_0 (D/3)}{2\rho V^3} \quad (2.77)$$

Eqn. (2.77) reduced to

$$(\alpha / f^2)_{long} = \frac{4\pi^2 \tau_{th} E_0 (D/3)}{2\rho V_l^3} \quad (2.78)$$

$$(\alpha / f^2)_{shear} = \frac{4\pi^2 \tau_{th} E_0 (D/3)}{2\rho V_s^3} \quad (2.79)$$

For longitudinal and shear wave respectively; here D is the non linearity constants or acoustic coupling constant.

$$D = 9 \langle (\gamma_i^j)^2 \rangle - \frac{3 \langle \gamma_i^j \rangle^2 C_V T}{E_0} \quad (2.80)$$

Mason and coworkers [7,9,49] have obtained a number of tables of SOEC and TOEC to evaluate $\langle \gamma_i^j \rangle$ and $\langle (\gamma_i^j)^2 \rangle$ for different directions of propagation and polarization. In Appendix-A various equations have been given for calculating Grüneisen numbers along directions of propagation viz $\langle 100 \rangle$, $\langle 110 \rangle$ and $\langle 111 \rangle$. The average have been taken over various modes. Though Barret and Holland [50] have criticized this method by arguing that strain wave modulate the frequency and energy and density of thermal phonons. This modulation creates a variation in the instantaneous population of mode from its equilibrium

value. Their next objection is that the present approach involves the product of specific heat and absolute temperature i.e. $C_v T$, instead of thermal energy E_0 . Both C_v and E_0 are Debye function of (θ_D/T) and differ by a numerical factor only. But these two effects do not cause any appreciable effect on the value the ultrasonic attenuation when $\omega\tau_{th} \ll 1$. Maris [51] has also reviewed this approach and concluded that the approach is not good for Silicon and Germanium but for the other crystals it would give reliable results. Nava et al.[52,53] have included anisotropies and acoustic dispersion in their formulation to obtain ultrasonic attenuation defining ultrasonic Gruneisen parameters. The expression for attenuation is under the condition $\omega^2(1-\beta_n/V_j)\tau_{th} \ll 1$

$$\alpha_j = \frac{3K_k T \omega^2 \Gamma_j^2}{\rho V_j^3 \bar{V}^2} \quad (2.81)$$

where

$$\Gamma_j^2 = \frac{1}{K_k} \sum_{q_n} [\bar{q}_n \Gamma_{nj}^2(q)] \quad (2.82)$$

Where V_j is the ultrasonic velocity, j is the polarization direction, ω is the angular frequency K_k is thermal conductivity along k , \bar{V} is the Debye average velocity and n is the projection of the phonon velocity along the second waves propagation directions and Γ_j is Ultrasonic gruneisen parameter (UGP) defined as

$$\Gamma_j^2 = \bar{V}^2 \frac{[\gamma_{nj}^2 - \gamma \gamma_{nj}(1 - \beta_n^2)/V_j \delta_j]}{n^2} \quad (2.83)$$

Where γ_{nj} is the generalized Grüneisen parameter which describes the change in the mode frequency caused by strain of the sound wave, γ is the calculated value of the Grüneisen number and δ_{jl} is the Kronecker delta that arises from local equilibrium effects associated with longitudinal sound wave.

The main difficulty in applying the above approach is that one lacks sufficiently detailed knowledge about the dispersion and polarization dependence of relevant microscopic quantities like Grüneisen parameters and relaxation times of thermal phonon modes coupled to external wave. Hence it is preferred to calculate UGP by taking experimental values of attenuation. Therefore due to these complexities and unknown factors involved in other

approaches the Mason [9] approach still seems most suitable and will be widely used to obtain ultrasonic attenuation under different physical condition in present investigation.

2.5.3 Thermoelastic loss

In an isotropic polycrystalline solid when a stress is applied, there will be a variation of strain from one grain to another [54]. Here the substance is isotropic due to random orientation of grains. The individual grain may be an isotropic. The propagation of longitudinal ultrasonic waves creates compression and rarefaction throughout the lattice. The rarefied regions are colder than that of compressed regions and hence there is a flow of heat between the two regions and direction of flow of the energy will reversed after every half cycle. Since this is a relaxational phenomenon, hence there is a loss of energy. The attenuation due to this effect is given by [9]

$$\alpha_{Np/cm} = \frac{2\pi f^2}{\rho V^3} \left[\frac{K}{C_V} \frac{C_{nn}^\sigma - C_{nn}^\theta}{C_{nn}} \right] \quad (2.84)$$

Where C_{nn}^σ and C_{nn}^θ are adiabatic and isothermal elastic moduli, K is the thermal conductivity and C_V is the specific heat per gm. The difference between these two values may be obtained with the help of SOEC and TOEC. The loss is not so important in case of insulating and semiconducting crystals due to less free electrons. The contribution due to mechanism is negligible in comparison to phonon viscosity mechanism. In the case of metals, thermal conduction arises due to electronic and lattice contribution to total ultrasonic attenuation. In case of shear waves propagation there towards be no loss due to this mechanism as there is no compression and rarefaction resulting to heat effect. However the expression for attenuation given by Mason for longitudinal wave is

$$\alpha = \frac{\omega^2 \langle \gamma_i^j \rangle^2 KT}{2\rho V_{long}^5} \quad (2.85)$$

or in simple form

$$(\alpha/f^2)_{th} = \frac{4\pi^2 \langle \gamma_i^j \rangle^2 KT}{2\rho V_{long}^5} \quad (2.86)$$

Where K is thermal conductivity, for shear wave $\alpha_{thrm}=0$ as $\langle \gamma_i^j \rangle=0$.

If it is assumed that the hypothetical crystal under investigation is perfect, non-ferromagnetic, non-ferroelectric; there would be only three principal thermal causes of

attenuation viz: electron-phonon interaction, phonon-phonon interaction and thermoelastic relaxation. At room temperature and above the loss due electron-phonon interaction can be ignored.

In the present work, ultrasonic attenuation due to above causes has been discussed in wide temperature range in metals, dielectrics, semiconductors, semimetallics, intermetallics and metallic alloys.

References

1. T.Gupta and D.M.Gaitonde, Mod.Phys.Lett. 2,269(2001).
2. S.Rajgopalan and D.N.Joharapurkar, J.Appl.Phys. 55,275(1984).
3. H.E.Bömmel and K. Dransfeld, Phys. Rev. Lett. 2,298(1959) and Phys. Rev.117,1245(1960).
4. T.O.Woodruff and H. Ehrenreich, Phys. Rev.123,1553(1961).
5. A.B.Pippard, Proc. Roy. Soc. (London) A257, 165(1960).
6. R.W.Morse, A.Myers and C.T.Walker, Phys. Rev.Lett. 4,605(1960).
7. W.P.Mason and A. Rosenberg, J.Acoust. Soc.Am.45,470(1969).
8. S.Seiro, H.R.Salva, M.Saint-Paul, A.A.Ghilarducci, P.Lejay, P.Monceaux, M.Nunez-Reguiro and A.Sulpia, J.Phys.: Condes.Matter 14,3973(2002).
9. W.P.Mason ed., Physical Acoustics (Academic Press, New York, 1965). Vol. IIIB, pp.237-286.
10. H.H.Barret and M.G.Holland, Phys. Rev. B1,2538(1970).
11. S.A.Ahmed and R.B.Thomson, Rev.of Progress in quantative non destructive evaluation,San Diego, CA (27 July-1Aug.1997); (New York, NY, USA, Plenum 1998) Vol.2 pp.1649-1655..
12. R.Nava, M.P.Vecchi, J.Romero and B.Fernandez, Phys. Rev. B14,800(1976).
13. K.Brugger, Phys. Rev 133, A1611(1964).
14. G.Leibfried and W.Ludwig, in Solid State Physics, edited by F.Seitz and D. Turnbull (Academic Press Inc., New York (1961) Vol.12, pp.275-444.
15. M.Born and J.E.Mayer, Z.Phys,75,1(1932)
16. M.P.Tosi, in Solid State Physics, edited by F.Seitz and D. Turnbull (Academic Press Inc., New York (1965) Vol.16, pp.1-120.

17. P.B.Ghate, Phys. Rev 139, A1666(1965).
18. H.B.Huntigton, in Solid State Physics, edited by F.Seitz and D. Turnbull (Academic Press Inc., New York (1958), Vol.7, pp.213-351.
19. S.Mori and Y.Hiki, J.Phys. Soc.Jpn., 45,1449(1978).
20. J.Blitz, Fundamentals of Ultrasonics, Butterwoth and Company Publishers Ltd. London (1967) p.153.
21. B.I.Blount, Phys. Rev 114, 418(1959).
22. D.Bohm and P.T.Slater, Phys. Rev 84, 836(1952).
23. R.H.Parmenter, Phys. Rev 89, 990(1953).
24. M.H.Cohen, Phys. Rev 117, 927(1960).
25. M.J.Harrison, Phys. Rev 119, 1260(1960).
26. H.N.Spector, Phys. Rev 127, 1084(1964).
27. H.R.Hutson and D.L.White, J.Appl.Phys.33,40(1962).
28. G.Simon, Phys. Rev 128, 161(1962).
29. H.N.Spector, Phys. Rev 127, 1084(1962).
30. I.Uchides et al., J.Phys.Soc.Jpn., 19,674(1964).
31. P.D.Southgate and H.N.Spector, J.Appl.Phys.(USA) 36,3728(1965).
32. C.A.A.Greebe, Phys.Lett., 4,45(1966).
33. H.E.Bömmel, Phys.Rev.96,220(1954).
34. B.V.Parajape, Physica 30,1641(1964).
35. P.J.Prise, IBB J.Res.Dev.9,69(1965).
36. E.M.Conwell, Proc.IEEE,52,964(1964).
37. W.P.Mason, Phys Rev., 97,557(1955).
38. Robert T.Beyer and Stephen Letcher, Physical Ultrasonics, (Academic Press, New York, 1969), p.325
39. W.P.Mason, "Piezoelectric Crystal and their applications to ultrasonics", (D. Van Nostrand and Co., New York,1950) p.478.
40. G.Joos, Theoretical Physics, (Hofner Publishing Co.,New York (1950) ,p.562.
41. C.Kittle, Introduction to Solid State Physics(John Wiley and Company, New York,1953)Chapter12.
42. P.Scry et al., J.Phys.Colloq.42,671(1981).

43. L.Landau and G.Rumer,Z.Phys.,11,18(1937).
44. J.P.Bonnet, M.Boisser, C.Vedel and R.Vacher. J.Phys.Chem.Solids,44,515(1983).
45. A.Akhiezer, Z.Phys.1,277(1939).
46. J.Lamb and R.Richter, Proc.Roy.Soc.(London), A293.47(1966).
47. M.F.Lewis and E.Palterson,J.Appl.Phys.39,1932(1968)
48. C.Herring, Phys Rev.96,1163(1954).
49. W.P.Mason and T.B.Batemann, J.Acoust.Soc.Am.40,852(1966).
50. H.H.Barret and M.G.Holland, Phys.Rev.B1,2538(1970).
51. H.J.Maris, in Physical Acoustics, edited by W.P.Mason and R.N.Thurston, (Academic Press Inc., New York, 1971), Vol.VIII,.
52. R.Nava, M.D.Vecchi and J.Romero,Phys. Rev. B11,800(1970).
53. R.Nava and J.Romero, J.Acoust.Soc.Am.64,529(1978).
54. K.Lücke, J.Appl.Phys.,27,1433(1956).

CHAPTER-3

Temperature Dependence of Ultrasonic Attenuation in Metallic Crystals

3.1 Introduction

Studies of ultrasonic attenuation have been carried out in solids, at different physical conditions in different ways of the materials [1-4] recently.

In this chapter, ultrasonic attenuation due to electron-phonon interaction, phonon-phonon interaction and thermoelastic loss has been studied in the temperature range 5 to 373.2K in f-block elements (rare-earths) of the Periodic Table in which two lanthanides cerium(Ce) and ytterbium(Yb), and one actinide thorium (Th) possessing face centered cubic crystalline structure. The ultrasonic attenuation due to electron-phonon interaction has been studied from 5 to 80K, while the attenuation due to phonon- phonon interaction and thermoelastic loss at 273.2K, 298.2K and 373.2K temperatures is studied along $\langle 100 \rangle$, $\langle 110 \rangle$ and $\langle 111 \rangle$ crystallographic direction for longitudinal and shear waves polarized along $\langle 100 \rangle$, $\langle 001 \rangle$ & $\langle 1\bar{1}0 \rangle$ and $\langle \bar{1}10 \rangle$ directions respectively. For the evaluation of ultrasonic absorption coefficient, the second and third order elastic constants (SOEC & TOEC) have been evaluated. In the present work, Ce, Yb and Th have been chosen because they have some different properties from the other metals.

Cerium is the most abundant of metals of the so called rare earth. It is found in a number of minerals including allanite. Cerium is a component misch metal, which is extensively used in manufacture of pyrophoric alloys for agarth lighters etc. It with other rare-earths, is used in carbon-arc lighting, especially in the motion picture industry.

Ytterbium occurs along with other rare earths in the number of rare minerals. It is commercially recovered principally from monazite sand. Ytterbium has bright silvery luster, is soft, malleable and quite ductile. While the element is fairly stable. Ytterbium normally has two allotropic forms with a transformation point at 798⁰C. The α -form is room temperature, face centred cubic modification, while the higher temperature β -form is a body centered cubic form. Another body centered cubic phase has recently been

found to stable at high pressures at room temperature. α -form ordinarily has metallic type conductivity, becomes a semiconductor when the pressure is increased about 16000 atm. Natural Ytterbium is a mixture of seven stable isotopes. Ytterbium metal has possible use in improving the grain refinement, strength and other mechanical properties of stainless steel. One isotope is reported to have been used as a radiation source as a substitute for a portable X-ray machine where electricity is unavailable.

Thorium metal is a source of nuclear power. Thorium was originally assigned a position in Group IV of the Periodic Table. It is now considered to be the second member of the actinide series of the elements. This is a silvery-white metal. Thorium stores more energy than all the @92 plus the fossil fuels of the coal and oil combined.

Much of the three metals have a technological and industrial importance therefore we have chosen these metals for the study of ultrasonic investigations at different physical conditions to make them more useful for the world welfare.

3.2 Theory

As one has indicated in the introduction that SOEC & TOEC are playing very important role to evaluate the ultrasonic attenuation. Hence theory is divided into two phases.

3.2.1 Theory of second and third order elastic constants

In the primary phase we have computed SOEC and TOEC following Brugger's definition of elastic constants at absolute 0 K (C_{IJ}^0 and C_{IJK}^0) [5-6]. The SOEC and TOEC at different temperature are obtained by method developed by Leibfried and Haln [7], Ludwig [8], Ghate [9] and Mori and Hiki [10] for face centered cubic crystal. Here it is assumed that $\phi_{\mu\nu}(r)$ -the interaction potential is the sum of the Coulomb and Born-Mayer short range potential i.e.

$$\phi_{\mu\nu}(r) = \pm \left(\frac{e^2}{r} \right) + A \exp\left(-r/b\right) \quad (3.1)$$

The electronic charge is e, the nearest neighbor distance r and \pm signs apply to like and unlike charges and A and b are the parameters. Further assumption was that A and b are the same for interactions between like and unlike[10] ions.

All the formulations used in the calculations of SOEC and TOEC are given as follows:

An elastic constant can be separated in two

$$C_{IJK} = C_{IJ}^0 + C_{IJK}^0 \quad (3.2)$$

Explicit expressions for the elastic constants have been given in Tables 2.2, 2.3, 2.7, 2.8 etc. in the chapter II

3.2.2 (a) Ultrasonic attenuation due to e-p interaction:

In the pure metals, at the low temperatures the electron mean free path increases and is of the same magnitude as the mean free path of the acoustical phonons at high frequency. Hence the probability of interaction between conducting electrons and phonons increases as explained by Pippard [11], Morse [12] and Mason [13]. When the ultrasonic wave is passed through a solid, a coupling between electrons and acoustical phonons occurs below 80K.

The attenuation of ultrasonic wave due shear and compressional viscosities of the lattice at low temperature for longitudinal and shear wave approached by Mason [13,14] used in this evaluation are as:

$$(\alpha / f^2)_{\text{long}} = \frac{2\pi^2}{\rho V_l^3} \left(\frac{4}{3} \eta_e + \chi \right) \quad (3.3)$$

$$(\alpha / f^2)_{\text{shear}} = \frac{2\pi^2}{\rho V_s^3} \eta_e \quad (3.4)$$

$$\eta_e = \frac{9 \times 10^{11} \eta^2}{5e^2 R} (3\pi^2 N)^{2/3} \quad (3.4a)$$

Where η_e -stands for electron viscosity, V_l and V_s -velocities of longitudinal and shear waves, f -the frequency of the wave, χ -compressional viscosity, ρ -density of the material, R -electrical resistivity, N -electronic density and η -the Planck's constants divided by 2π .

3.2.2.b Ultrasonic attenuation due to p-p interaction:

The phonon-phonon interaction processes occur mainly at higher temperatures as described in the proceeding chapter II. At higher temperatures two main causes of ultrasonic attenuation in solid are known as (i) Akhiezer loss and (ii) thermoelastic loss. Akhiezer [15] first proposed the ultrasonic attenuation due to phonon viscosity mechanism. Bömmel and Dransfeld [16] and Woodruff and Ehrenreich [17] made improvement and finally expression for ultrasonic attenuation has been given by Mason [18]. Ultrasonic attenuation due to phonon-phonon interaction is caused by interaction of

thermal phonons and acoustical phonons in the frequency range $\omega\tau_{th} \ll 1$ [15] (ω is angular frequency of ultrasonic wave and τ_{th} is the thermal relaxation time) is obtained as [18]:

$$\left(\alpha/f^2\right) = \frac{2\pi^2 E_0 (D/3) \tau}{\rho V^3} \quad (3.5)$$

where E_0 is the energy density, ρ is the density, D is non-linearity parameters for longitudinal/shear waves as $D = 9 \langle (\gamma_l^j)^2 \rangle - \frac{(3 \langle \gamma_l^j \rangle^2 C_V T)}{E_0}$; $\langle \gamma_l^j \rangle$ is the average of Grünesisen parameters, V is ultrasonic velocity for longitudinal/shear waves, τ is thermal relaxation time as $\tau_{th} = \tau_s = \frac{1}{2} \tau_l = \frac{3K}{C_V \bar{V}^2}$, τ_l and τ_s are thermal relaxation time for longitudinal and shear wave respectively, K is thermal conductivity, C_V is specific heat per unit volume, \bar{V} is the Debye average velocity of ultrasonic wave as $\frac{3}{\bar{V}^3} = \frac{1}{V_l^3} + \frac{2}{V_s^3}$. V_l and V_s are longitudinal and shear waves as $V_l = \sqrt{C_{11}/\rho}$ and $V_s = \sqrt{C_{44}/\rho}$; C_{11} and C_{44} are the second order elastic constants.

The expression to evaluate ultrasonic attenuation due to thermoelastic loss is as

$$\left(\alpha/f^2\right)_{th} = \frac{4\pi^2 \langle \gamma \rangle^2 K T}{2\rho V_l^5} \quad (3.6)$$

where symbols have their meaning as described in chapter II.

3.3 Evaluations, results and discussions

The attenuation caused by electron-phonon interaction, phonon-phonon interaction and thermoelastic relaxation is evaluated using Born-Mayer (hardness) parameter and nearest neighbor distance for Ce, Yb and Th respectively at different temperatures. Proceeding with first part C_{IJ} and C_{IJK} at different temperatures are evaluated from nearest neighbor distance [19] $r_0=3.65, 3.88$ and 3.60 (all in \AA) for Ce, Yb and Th and hardness parameter $b=0.303, 0.298$ and 0.313 (all in \AA) for Ce, Yb and Th respectively. The SOEC and TOEC have been evaluated at different temperatures using the theory given in section 2.1 of chapter II (Tables 2.2-2.6). SOEC at the temperature range 5K to 80K, density (ρ) and ultrasonic velocities (V_l and V_s) are presented in Tables 3.1, 3.2 and 3.3 at

the temperature range 5-80K. Electron viscosity (η_e) has been evaluated using thermal component of electrical resistivity (R) [20,21,22]. The values of density from the literature [23] Ultrasonic attenuation coefficient over frequency square (α/f^2) due to electron-phonon interaction have been evaluated from temperature 5K to 80K using the eqs.(3.3) and (3.4). The values of electrical resistivity (R), calculated values of electron-viscosity (η_e) and ultrasonic attenuation due to electron-phonon interaction [$(\alpha/f^2)_{\text{long}}$ for longitudinal wave and $(\alpha/f^2)_{\text{shear}}$ for shear wave] are presented in Tables 3.4-3.6 for these metals. The temperature variation of ultrasonic attenuation due to electron-phonon interaction and temperature vs $\ln(R)$ have been plotted in Figs. 3.1 to 3.9 for Ce, Yb and Th for longitudinal and shear waves.

SOEC and TOEC at the temperatures 273.2K, 298.2K and 373.2K are presented in Tables 3.7,3.8 and 3.9. Which have been used to obtain Grüneisen parameters [18] $\langle\gamma_i^j\rangle$ and $\langle(\gamma_i^j)^2\rangle$ along $\langle 100 \rangle$ direction for longitudinal wave over 39 modes and for shear wave over 18 modes; along $\langle 110 \rangle$ direction for longitudinal wave over 39 modes and for shear wave polarized along $\langle 001 \rangle$ direction over 14 modes & polarized along $\langle 1\bar{1}0 \rangle$ direction over 20 modes and along $\langle 111 \rangle$ direction for longitudinal wave over 39 modes and for shear wave polarized along $\langle \bar{1}10 \rangle$ direction over 14 modes. Grüneisen parameters are evaluated by using Mason's table (Appendix A). Thermal relaxation time has been evaluated taking lattice thermal conductivity [20-22], using eqn.(2.65) as in chapter II. Specific heat per unit volume and Energy density of crystals have been evaluated as a function of θ_D/T [23]; where θ_D is Debye temperature. Non-linearity constants D has been obtained at different temperature using equ.(2.80) as in chapter II. The values of Grüneisen parameters $\langle\gamma_i^j\rangle$ and $\langle(\gamma_i^j)^2\rangle$ and non-linearity constants D are presented in Tables 3.9-3.11. Ultrasonic attenuation due to p-p interaction have been evaluated at these temperature along $\langle 100 \rangle$, $\langle 110 \rangle$ and $\langle 111 \rangle$ directions for longitudinal and shear waves using eqn.(3.5) and are presented in Tables 3.12 to 3.14. Ultrasonic attenuation due to thermoelastic mechanism $(\alpha/f^2)_{\text{th}}$ at different higher temperatures has been evaluated using total thermal conductivity taken from the literature [20-22] using eqn. (3.6) and are presented in Tables 3.12-3.14. All calculations have been done by self developed computer program in C++ language.

Obviously from eqn. (2.42) as in chapter II, electron viscosity (η_e) is inversely proportional to electrical resistivity (R). The ultrasonic attenuation for both longitudinal and shear wave is directly proportional to electron viscosity (η_e) from the eqns. 3.3 and 3.4. It can be observed from Tables 3.4 to 3.6 and Figs 3.1 to 3.9 that the attenuation of ultrasonic waves normally decreases rapidly with electron viscosity (η_e) and with the temperature, except one anomalous kink at 20K in case of Yb.

It is clear from the Figs. 3.1 to 3.6 and 3.7 to 3.9 that the behavior of temperature dependence of ultrasonic attenuation gives the clear indication that the possibility of electron-phonon interaction becomes small beyond 80K and loss due to this effect also ceases. The variation of attenuation of ultrasonic waves with temperature is not linear and similar to the variation of $\ln(1/R)$ with temperature. This shows that α is directly related with electrical conductivity of the metals. One anomalous kink at 20K in the behavior of temperature dependence of ultrasonic attenuation in Ytterbium at lower temperature is due to effect of electrical resistivity at that temperature [22]. Order of the ultrasonic attenuation in Ce, Yb and Th for longitudinal wave is the same as compared with other metals [25-27]. Thus the trend of the behavior of temperature dependence of ultrasonic attenuation at lower temperature is normally same as compared to other metals [25-27] except one peak in Ytterbium at 20K and describe the characteristic features of the metals.

It is seen from the Table 3.8 that thermal relaxation time (τ_{th}) in all the three temperatures has the same order as in previously studied metals [18]. Thermal relaxation time (τ_{th}) has positive temperature dependence in Yb and Th. It is obvious from the Table 3.8 that the values of thermal conductivity in these metals are approximately same for 273.2K, 298.2K and 373.2K temperatures. It can be seen from Tables 3.12 to 3.14 that the thermoelastic loss $(\alpha f^2)_{th}$ is negligible in comparison to Akhieser type attenuation $(\alpha f^2)_{Akh}$ (loss due to p-p interaction). This is due to low values of thermal conductivity of these metals and higher values of Debye average velocities of the waves along all the three propagating directions. Positive temperature dependence of the thermoelastic loss $(\alpha f^2)_{th}$ in Cerium, Ytterbium and Thorium is approximately the same as in other metals [25-27].

Attenuation of longitudinal wave is more than that of the shear wave along $\langle 100 \rangle$ and $\langle 110 \rangle$ direction polarized along $\langle 001 \rangle$. A Greater the value of ultrasonic attenuation for longitudinal wave along $\langle 100 \rangle$ in comparison to shear wave attenuation is due to greater value of non-linearity parameters (D_l). In the case of wave propagating along $\langle 110 \rangle$ direction and shear wave polarizing along $\langle 001 \rangle$, although D_{S1} is greater than the (D_l), the value of $(\alpha T^2)_{\text{Akh long}}$ are greater than $(\alpha T^2)_{\text{Akh shear}}$. This behavior is due to smaller value of C_{44} (SOEC) in comparison to C_{11} affecting the wave velocity. In the case of the wave propagating along $\langle 111 \rangle$ and shear wave polarizing along $\langle 110 \rangle$; shear wave attenuation $(\alpha T^2)_{\text{Akh shear2}}$ is greater than the longitudinal wave attenuation $(\alpha T^2)_{\text{Akh long}}$. This is due to greater value of shear wave a non-linearity constant D_s in comparison to longitudinal wave a non-linearity constant D_l .

It can be understood from the Tables 3.12-3.14 that ultrasonic absorption (Akhiezer type or thermoelastic loss) for all the three metals has positive temperature dependence and maximum at 373.2K. This positive temperature dependence of ultrasonic absorption is due to the fact that p-p interaction occurs at higher temperatures mainly at room temperatures. Since the whole computation is made starting from only nearest neighbour distance and hardness parameters, one may conclude that the behaviour of temperature dependence of ultrasonic absorption and other allied parameters in Ce, Yb and Th is characteristic one for the materials taken and supports our theoretical approach.

Table 3.1

SOEC(C_{11} , C_{12} and C_{44})[in 10^{11} Dyne/cm²], density ρ (g/cm³) and ultrasonic velocities (V_l for longitudinal wave and V_s for shear wave)[in 10^5 cm/sec] of Cerium at temperature range 5-80K.

Temp.[K]	C_{11}	C_{12}	C_{44}	ρ	V_l	V_s
5	2.946	0.471	0.485	7.255	2.015	0.818
10	2.946	0.471	0.485	7.251	2.015	0.818
20	2.947	0.469	0.485	7.247	2.016	0.818
30	2.951	0.464	0.485	7.243	2.018	0.818
40	2.958	0.458	0.485	7.240	2.021	0.819
50	2.968	0.451	0.485	7.236	2.025	0.819
60	2.979	0.448	0.485	7.232	2.030	0.819
70	2.991	0.438	0.486	7.228	2.034	0.819
80	3.004	0.432	0.486	7.224	2.039	0.820

Table 3.2 SOEC(C_{11} , C_{12} and C_{44})[in 10^{11} Dyne/cm²], density ρ (g/cm³) and ultrasonic velocities (V_l for longitudinal wave and V_s for shear wave)[in 10^5 cm/sec] of Thorium at temperature range 5-80K.

Temp.[K]	C_{11}	C_{12}	C_{44}	ρ	V_l	V_s
5	2.865	0.509	0.519	12.600	1.508	0.642
10	2.865	0.508	0.519	12.555	1.511	0.643
20	2.866	0.505	0.519	12.551	1.511	0.643
30	2.873	0.500	0.519	12.446	1.519	0.646
40	2.882	0.494	0.519	12.441	1.522	0.646
50	2.893	0.487	0.519	12.437	1.525	0.646
60	2.905	0.481	0.520	12.432	1.529	0.646
70	2.918	0.475	0.520	12.428	1.532	0.647
80	2.931	0.469	0.520	12.422	1.534	0.647

Table 3.3 SOEC(C_{11} , C_{12} and C_{44})[in 10^{11} Dyne/cm²], density ρ (g/cm³) and ultrasonic velocities (V_L for longitudinal wave and V_S for shear wave)[in 10^5 cm/sec] of Ytterbium at temperature range 5-80K.

Temp.[K]	C_{11}	C_{12}	C_{44}	ρ	V_L	V_S
5	2.606	0.361	0.373	8.255	1.777	0.672
10	2.606	0.361	0.373	8.250	1.777	0.672
20	2.607	0.358	0.373	8.242	1.779	0.672
30	2.613	0.352	0.373	8.240	1.781	0.673
40	2.623	0.346	0.373	8.236	1.784	0.673
50	2.631	0.340	0.373	8.231	1.788	0.673
60	2.644	0.334	0.373	8.224	1.793	0.673
70	2.656	0.327	0.373	8.221	1.798	0.674
80	2.669	0.321	0.373	8.215	1.803	0.674

Table 3. 4.

Electrical resistivity (R) [in $10^{-6}\Omega$ cm], Viscosity (η_e)[in 10^{-3} g/cm s] and ultrasonic attenuation $\{(\alpha/f^2)_L$ for longitudinal waves and $(\alpha/f^2)_S$ for shear wave}[in 10^{-18} Np s²/cm] of Cerium at temperature range from 5-80K.

Temperature in K	R	η_e	$(\alpha/f^2)_L$	$(\alpha/f^2)_S$
5	20.798	0.729	0.319	3.309
10	22.897	0.662	0.290	3.004
20	26.344	0.575	0.252	2.609
30	28.263	0.536	0.234	2.430
40	30.341	0.499	0.217	2.262
50	32.322	0.468	0.203	2.121
60	34.028	0.445	0.191	2.013
70	35.879	0.421	0.180	1.907
80	37.620	0.402	0.171	1.817

Table 3.5. Electrical resistivity (R) [in $10^{-6}\Omega$ cm], Viscosity (η_e)[in 10^{-3} g/cm s] and ultrasonic attenuation $\{(\alpha/f^2)_L$ for longitudinal waves and $(\alpha/f^2)_S$ for shear wave} [in 10^{-18} Np s²/cm] of Thorium at temperature range from 5-80K.

Temperature in K	R	η_e	$(\alpha/f^2)_L$	$(\alpha/f^2)_S$
5	0.622	25.167	15.149	136.032
10	0.753	20.731	12.457	111.854
20	0.911	17.138	10.286	92.439
30	1.264	12.282	7.317	65.952
40	1.825	8.503	5.039	45.629
50	2.325	6.674	3.932	35.794
60	2.974	5.214	3.053	27.947
70	3.403	4.557	2.650	24.407
80	4.044	3.833	2.214	20.517

Table 3.6. Electrical resistivity (R) [in $10^{-6}\Omega$ cm], Viscosity (η_e)[in 10^{-3} g/cm s] and ultrasonic attenuation $\{(\alpha/f^2)_L$ for longitudinal waves and $(\alpha/f^2)_S$ for shear wave} [in 10^{-18} Np s²/cm] of Ytterbium at temperature range from 5-80K.

Temperature in K	R	η_e	$(\alpha/f^2)_L$	$(\alpha/f^2)_S$
5	3.012	4.763	2.675	34.248
10	3.502	4.096	2.299	29.440
20	3.657	3.920	2.198	28.159
30	6.125	1.667	0.932	11.972
40	8.597	1.667	0.927	11.962
50	11.136	1.286	0.710	9.224
60	13.738	1.042	0.571	7.467
70	16.179	0.884	0.482	6.336
80	18.667	0.766	0.414	5.485

Table 3.7 SOEC and TOEC of Ce, Yb and Th at temperatures 273.2K, 298.2K and 373.2K [$\times 10^{11}$ Dyne/cm²]

Metal	Temp .[K]	C ₁₁	C ₁₂	C ₄₄	C ₁₁₁	C ₁₁₂	C ₁₂₃	C ₁₄₄	C ₁₆₆	C ₄₅₆
Ce	273.2	3.472	0.289	0.485	-63.0	-0.89	-0.69	0.899	-1.87	0.884
	298.2	3.511	0.271	0.485	-63.2	-0.80	-0.83	0.901	-1.88	0.884
	373.2	3.629	0.218	0.487	-64.0	-0.53	-1.26	0.905	-1.88	0.884
Yb	273.2	2.891	0.200	0.376	-53.3	-0.53	-0.77	0.702	-1.44	0.690
	298.2	2.926	0.185	0.376	-53.5	-0.45	-0.90	0.703	-1.44	0.690
	373.2	3.031	0.152	0.365	-54.2	-0.21	-1.30	0.706	-1.45	0.690
Th	273.2	3.492	0.328	0.521	-62.2	-1.09	-0.54	0.957	-2.03	0.940
	298.2	3.530	0.310	0.521	-62.4	-1.00	-0.68	0.959	-2.03	0.940
	373.2	3.647	0.259	0.522	-63.2	-0.75	-1.08	0.964	-2.04	0.940

Table 3.8

Thermal conductivity (K), density (ρ), specific heat (C_V), energy density (E₀), Debye average velocity (\bar{V}), thermal relaxation time (τ_{th}) of the metals at temperatures 273.2K, 298.2K and 373.2K.

Metals	Temp (K)	K X10 ⁵ (J/cm s K)	ρ (g/cm ³)	C _V X10 ⁷ (erg/cm ³ K)	E ₀ X10 ⁸ (erg/cm ³)	\bar{V} X10 ⁴ (cm/sec)	τ_{th} X10 ⁻¹¹ (sec)
Ce	273.2	1.08	7.00	1.230	2.783	9.340	3.020
	298.2	1.13	6.90	1.214	3.042	9.412	3.152
	373.2	1.28	6.81	1.208	3.908	9.488	3.531
Yb	273.2	3.54	7.05	1.010	2.361	8.197	15.650
	298.2	3.49	7.02	1.009	2.596	8.217	15.367
	373.2	3.43	6.91	0.995	3.299	8.294	15.032
Th	273.2	5.40	11.90	1.258	2.757	7.416	23.413
	298.2	5.40	11.70	1.241	3.018	7.483	23.310
	373.2	5.43	11.30	1.203	3.811	7.626	23.282

Table 3.9 Average Grüneisen numbers $\langle \gamma_l^j \rangle_l$ for longitudinal wave, average square Grüneisen numbers $\langle (\gamma_l^j)^2 \rangle_l$ for longitudinal wave, average square Grüneisen numbers $\langle (\gamma_l^j)^2 \rangle_s$ for shear wave, non-linearity parameters D_l and D_s for longitudinal and shear wave [all along $\langle 100 \rangle$ direction].

Metals	Temp.(K)	$\langle \gamma_l^j \rangle$	$\langle (\gamma_l^j)^2 \rangle_l$	$\langle (\gamma_l^j)^2 \rangle_s$	D_l	D_s
Ce	273.2	0.485	2.760	0.130	23.988	1.172
	298.2	0.479	2.720	0.130	23.663	1.170
	373.2	0.462	2.612	0.129	22.765	1.165
Yb	273.2	0.483	2.890	0.131	25.193	1.178
	298.2	0.477	2.849	0.131	24.850	1.177
	373.2	0.459	2.734	0.130	23.897	1.173
Th	273.2	0.484	2.630	0.130	22.795	1.166
	298.2	0.478	2.592	0.130	22.485	1.164
	373.2	0.462	2.487	0.129	21.627	1.159

Table 3.10 Average Grüneisen numbers $\langle \gamma_l^j \rangle_l$ for longitudinal wave, average square Grüneisen numbers $\langle (\gamma_l^j)^2 \rangle_l$ for longitudinal wave, average square Grüneisen numbers $\langle (\gamma_l^j)^2 \rangle_{s1}$ for shear wave polarized along $\langle 001 \rangle$ direction, average square Grüneisen numbers $\langle (\gamma_l^j)^2 \rangle_{s2}$ for shear wave polarized along $\langle 110 \rangle$ direction, non-linearity parameters D_l for longitudinal wave, D_{s1} for shear wave polarized along $\langle 001 \rangle$ direction and D_{s2} for shear wave polarized along $\langle 1\bar{1}0 \rangle$ direction [all along $\langle 110 \rangle$ direction].

Metals	Temp. (K)	$\langle \gamma_l^j \rangle_l$	$\langle (\gamma_l^j)^2 \rangle_l$	$\langle (\gamma_l^j)^2 \rangle_{s1}$	$\langle (\gamma_l^j)^2 \rangle_{s2}$	D_l	D_{s1}	D_{s2}
Ce	273.2	-0.689	2.571	0.078	4.664	21.420	41.971	0.699
	298.2	-0.677	2.518	0.076	4.627	21.025	41.643	0.688
	373.2	-0.643	2.374	0.073	4.531	19.936	40.782	0.657
Yb	273.2	-0.681	2.690	0.072	4.975	22.583	44.770	0.646
	298.2	-0.668	2.635	0.071	4.954	22.163	44.476	0.636
	373.2	-0.632	2.485	0.068	4.854	21.016	43.688	0.609
Th	273.2	-0.692	2.448	0.084	4.385	20.244	39.465	0.756
	298.2	-0.680	2.396	0.083	4.347	19.867	39.126	0.743
	373.2	-0.647	2.256	0.078	4.247	18.825	38.220	0.706

Table 3.11 Average Grüneisen numbers $\langle \gamma_l^l \rangle_l$ for longitudinal wave, average square Grüneisen numbers $\langle (\gamma_l^l)^2 \rangle_l$ for longitudinal wave, average square Grüneisen numbers $\langle (\gamma_l^l)^2 \rangle_s$ for shear wave polarized along $\langle 110 \rangle$ direction, non-linearity parameters D_l for longitudinal wave and D_s for shear wave polarized along $\langle \bar{1}10 \rangle$ direction [all along $\langle 111 \rangle$ direction].

Metals	Temp.(K)	$\langle \gamma_l^l \rangle$	$\langle (\gamma_l^l)^2 \rangle_l$	$\langle (\gamma_l^l)^2 \rangle_s$	D_l	D_s
Ce	273.2	-0.638	2.004	3.155	16.564	28.397
	298.2	-0.629	1.955	3.131	16.180	28.174
	373.2	-0.605	1.819	3.065	15.108	27.587
Yb	273.2	-0.643	2.059	3.360	17.080	30.238
	298.2	-0.634	2.006	3.337	16.660	30.035
	373.2	-0.608	1.861	3.276	15.502	29.483
Th	273.2	-0.629	1.935	2.970	15.934	26.732
	298.2	-0.621	1.888	2.945	15.572	26.506
	373.2	-0.598	1.759	2.877	14.563	25.897

Table 3.12 Ultrasonic attenuation $(\alpha/f^2)_{th}$, $(\alpha/f^2)_{Akh \text{ long}}$ and $(\alpha/f^2)_{Akh \text{ shear}}$ along $\langle 100 \rangle$ crystallographic direction [$\times 10^{-17} \text{ Np s}^2 / \text{cm}$].

Metals	Temp.(K)	$(\alpha/f^2)_{th}$	$(\alpha/f^2)_{Akh \text{ long}}$	$(\alpha/f^2)_{Akh \text{ shear}}$
Ce	273.2	0.033	31.285	14.634
	298.2	0.035	34.382	16.539
	373.2	0.041	44.999	23.465
Yb	273.2	0.169	190.814	95.293
	298.2	0.171	199.135	102.545
	373.2	0.175	224.027	125.589
Th	273.2	0.354	295.164	131.145
	298.2	0.358	309.539	141.331
	373.2	0.369	351.529	173.746

Table 3.13 Ultrasonic attenuation $(\alpha/f^2)_{th}$, $(\alpha/f^2)_{Akh\ long}$, $(\alpha/f^2)_{*Akh\ shear}$ and $(\alpha/f^2)_{\#Akh\ shear}$ along $\langle 110 \rangle$ crystallographic direction [$X 10^{-17} Np\ s^2/cm$]

Metals	Temp.(K)	$(\alpha/f^2)_{th}$	$(\alpha/f^2)_{Akh\ long}$	$(\alpha/f^2)_{*Akh\ shear}$	$(\alpha/f^2)_{\#Akh\ shear}$
Ce	273.2	0.066	27.933	8.732	524.059
	298.2	0.069	30.549	9.722	588.443
	373.2	0.080	39.408	13.227	821.183
Yb	273.2	0.337	171.040	52.263	3621.937
	298.2	0.336	177.607	55.396	3873.17
	373.2	0.335	198.807	65.234	4677.538
Th	273.2	0.724	262.136	85.058	4438.784
	298.2	0.724	273.498	90.178	4750.278
	373.2	0.722	305.986	105.925	5731.977

*and # polarized along $\langle 001 \rangle$ and $\langle 1\bar{1}0 \rangle$ respectively.

Table 3.14 Ultrasonic attenuation $(\alpha/f^2)_{th}$, $(\alpha/f^2)_{Akh.long}$ and $(\alpha/f^2)_{Akh.shear}$ along $\langle 111 \rangle$ crystallographic direction [$X 10^{-17} Np\ s^2/cm$].

Metals	Temp.(K)	$(\alpha/f^2)_{th}$	$(\alpha/f^2)_{Akh\ long}$	$(\alpha/f^2)_{Akh\ shear}$
Ce	273.2	0.056	21.600	354.536
	298.2	0.059	23.507	398.125
	373.2	0.071	29.864	555.498
Yb	273.2	0.299	129.365	2446.272
	298.2	0.302	133.501	2615.624
	373.2	0.306	145.322	3156.652
Th	273.2	0.599	206.326	3006.717
	298.2	0.604	214.373	3218.068
	373.2	0.617	236.720	3883.871

\prime polarized along $\langle \bar{1}10 \rangle$

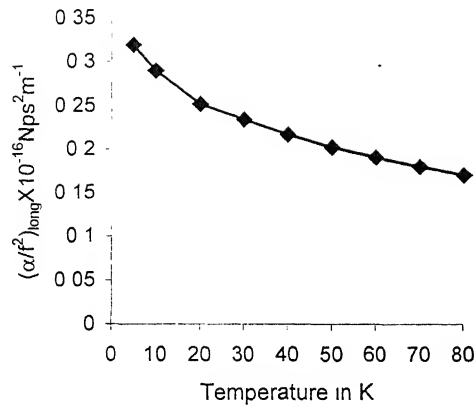


Fig 3 1 $(\alpha/f^2)_{\text{long}}$ vs temperature of Cerium

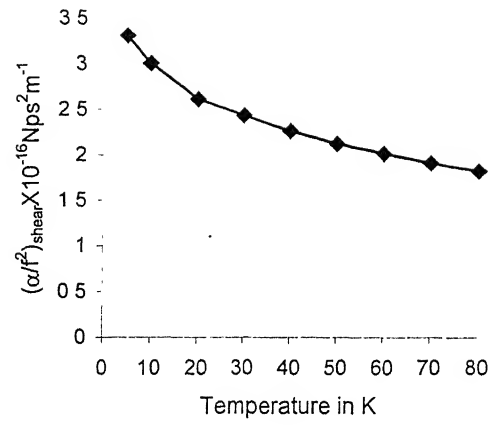


Fig 3 2 $(\alpha/f^2)_{\text{shear}}$ vs. Temperature of Cerium

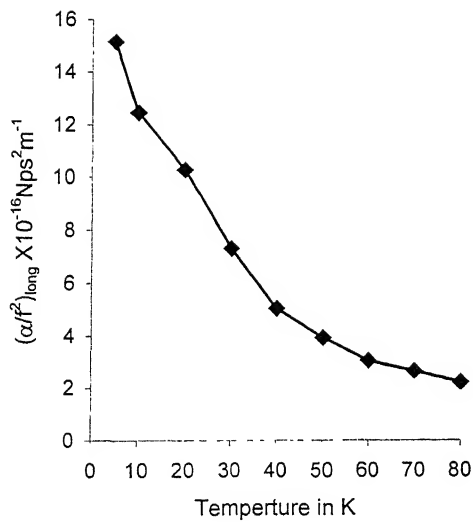


Fig.3.3 $(\alpha/f^2)_{\text{long}}$ vs. temperature of Thorium

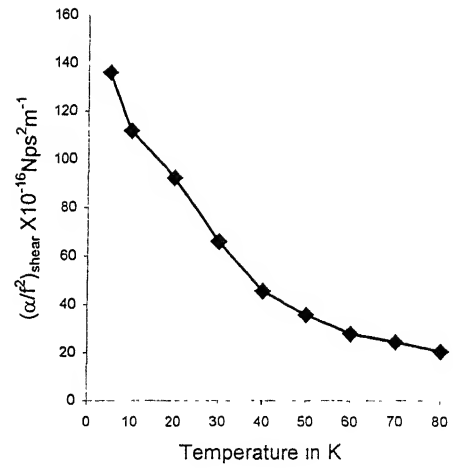


Fig 3.4 $(\alpha/f^2)_{\text{shear}}$ vs temperature of Thorium

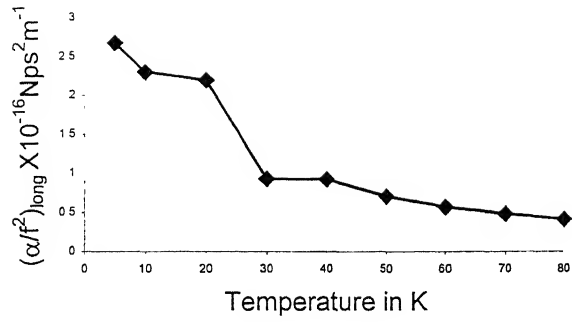


Fig 3.5 $(\alpha/f^2)_{\text{long}}$ vs temperature of Ytterbium

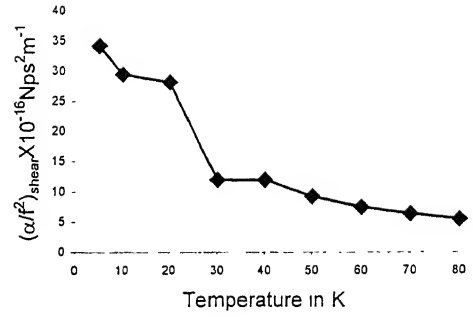


Fig.3 6 $(\alpha/f^2)_{\text{shear}}$ vs. temperature of Ytterbium

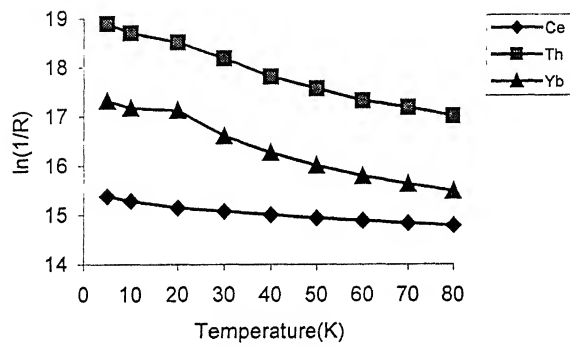


Fig.3 7 $\ln(1/R)$ vs temperature

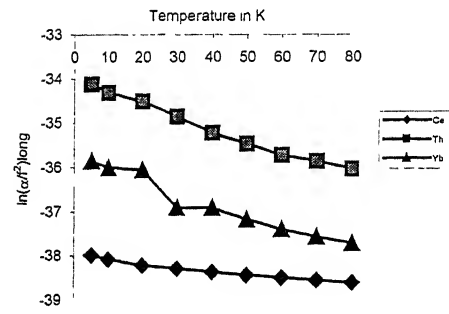


Fig 3 8 $\ln(\alpha/f^2)$ vs temperature

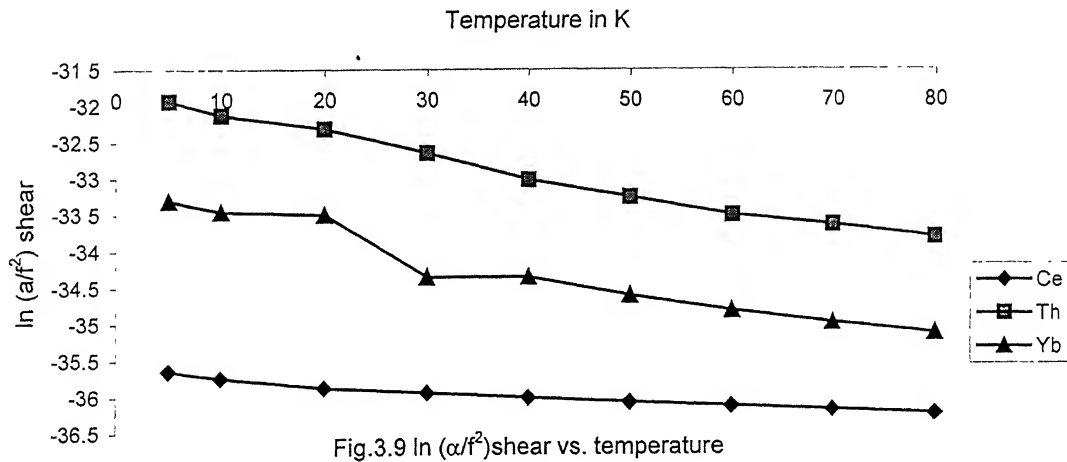


Fig.3.9 $\ln (\alpha/f^2)_{\text{shear}}$ vs. temperature

References

1. M.S.Ojha, G.C.Rout and S.N.Behera; Ind.J,Pure Appl.Phys.76A,79(2002).
2. T.Gupta and D.M.Gaitonde; Mod.Phys.Lett. B15(9&10),269(2001).
3. I.Vekhtar, E.J.Nicol and J.P.Carbotte, Phys.Rev. B59,7123(1999).
4. M.J.Graf, S.K.Yip and J.P.Saul; Phys.Rev. B62,14393(2000).
5. K.Brugger, Phys.Rev. A133,1611(1999).
6. M.Born and J.E.Mayer, Z.Phys. 75,1(1932)
7. G.Leibfried and H.Hahn; Z.Phys.150,497(1958).
8. G.Leibfried and W.Ludwig, in Solid State Physics edited by F.Seitz and D.Turnbull, (Academic Press, New York 1961), Vol.12.
9. P.B.Ghate, Phys.Rev 139, A1666(1965).
10. S.Mori and Y.Hiki, J.Phys. Soc.Jpn., 45,1449(1978).
11. A.B.Pippard; Philos.Mag. 45,1104(1955).
12. R.W.Morse ; Phys.Rev. 97,1716(1955).
13. W.P.Mason, Phys.Rev. 97, 557(1955).
14. W.P.Mason edited “Piezoelectric Crystals and their applications to ultrasonics” (D.Van Nostrand and Co., Princeton 1950), p.479.
15. A.Akhiezer,; J.Phys.(USSR)1,277(1939).
16. H.E.Bömmel and K. Dransfeld, Phys. Rev. Lett. 2,298(1959) and Phys. Rev.117,1245(1960).
17. T.O.Woodruff and H. Ehrenreich, Phys. Rev.123,1553(1961).
18. W.P.Mason, Physical Acoustics (Academic Press, New York 1965) Vol. IIIB, Chapter 6.
19. C.Kittel; Introduction to Solid State Physics, (John Wiley Press, New York 1996), 7th edition.
20. Y.S.Touloukian et al.;TPRC series (IFI/Plenum-New York 1970), Vol.I pp.50 and 446.
21. P.Haen and G.T.Meaden; Cryogenics,5,191(1965).
22. M.A.Curry, S.Legvold and F.H.Spedding; Phys.Rev. B117,953(1960).
23. D.E. Gray ed., AIP Handbook, (McGraw Hill Book Co. Inc. New York) IIIrd edition.

24. D.R.Lide ed., Hand book of Chemistry and Physics, (CRC Press, New York 1998-99), 79th edition.
25. S.K.Kor, Kailash, K. Shanker and P.Mehrotra, J.Phys.Soc.Jpn. 56,2428(1987).
26. S.K.Kor and R.R.Yadav; J.Pure Appl.Ultrason. 8,89(1986).
27. R.R.Yadav and D.Singh; Intermetallics 9,189(2001).

CHAPTER—4

Effect of Thermal Conductivity on Ultrasonic Attenuation in Dielectric Crystals

4.1 Introduction

In recent years ultrasonic attenuation studies [1-8] have been stretched out all type materials. In the present investigation NaCl-type crystals (AgCl, LiF and MnO) have been chosen for a number of reasons. These are one of the most structurally perfect crystals and have simple cubic face centered lattice structure. # AgCl (Silver chloride) is useful material for deep infrared (IR) applications where sensitivity to moisture is a problem. This soft crystal deforms under heat and pressure and can be forged against polished die to create IR windows and lenses. A major use in the manufacture of small disposable cell windows for spectroscopy is known as 'mini-cell'. These windows have a depression of controlled thickness pressed into the surface. The inherent cost of material is affect against ease of manufacture. # LiF (Lithium Fluoride) is the material with most extreme UV transmission of all and used for special UV optics. It transmits well into the VUV region at the hydrogen Lyman-alpha line (121nm) and beyond. It is also used for X-ray monochromator plates where its lattice spacing makes it the most useful analysis crystal. # MnO (Manganous Oxide) is an olive green powder containing black specks of free carbon;odorless, having bulk density-94 pounds/cu ft, melting point->2900⁰ F and insoluble in water. Above 108⁰C, half of the oxygen disassociates to produce MnO, a flux which immediately reacts with silica to produce violet colours in the absence of alumina, browns in its presence. Manganese browns have a different, often more pleasant character than iron browns. In glazes below 108⁰C, it can give coffee colour brown when used with tin and dull browns in lead and low alkaline glazes. Very pleasing tan-brown reduction fired glazes can be achieved with 5% manganese oxide reduction. Small manganous oxide particles embedded into the skin of worker can cause localized inflammatory reactions. Inhalations of manganous oxide fume can cause metal fume inflammatory reactions. Inhalation of manganous oxide fume-can cause metal fume fever, where 4 to 6

hours after exposure the worker experiences coughing, fever, chills and a tight feeling in the chest. These symptoms should subside in less than 24 hours.

Attenuation in acoustic wave in LiF [9,27] experimentally have been studied, but theoretically investigations [10,11] have been made mainly at room temperature. In dielectric crystals, attenuation at ultrasonic frequencies arises mainly from the interaction between acoustic and thermal phonons. In metals, semiconductors and intermetallics; particularly at low temperature free electrons also play important role in attenuation of acoustic energy interacting with thermal phonons.

In the preceding chapter ultrasonic attenuation has been studied in metals as a function of temperature, frequency and direction of propagation. In this chapter ultrasonic attenuation due to phonon-phonon interaction and thermoelastic loss have been studied in dielectric crystals Viz. AgCl, LiF and MnO in the temperature range 100-500K, 100-300K and 100-573K respectively, along $\langle 100 \rangle$, $\langle 110 \rangle$ and $\langle 111 \rangle$ direction of propagation. Ultrasonic Grüneisen parameters and non-linearity constants have also been evaluated in these dielectric crystals.

4.2 Theory

4.2.1 Theory of the second and third order elastic constants (SOEC & TOEC)

Using electrostatic ($\pm e^2/r$) and repulsive potential [12] and taking nearest neighbor distance and hardness parameter as input data, second and third order elastic constants (SOEC & TOEC) have been obtained at 0K, following Brugger's [13] definition of elastic constants as in Table 2.2-2.3 in chapter-II. Anharmonic theory of lattice dynamics developed by Leibfried and Ludwig [14], Leibfried and Hahn [15], Ghate [16] and finally Mori and Hiki [17] has been used to obtain SOEC and TOEC at different temperatures. Explicit expressions for elastic constants have been given in Table 2.2-2.6 in chapter-II.

4.2.2 Ultrasonic attenuation due to p-p interaction and thermoelastic loss

To establish the theory of ultrasonic absorption in these dielectric crystals. Akhieser [18] first proposed the attenuation of ultrasonic waves, which was modified by Bömmel and Dransfeld [19] and finally by Mason [20]. In the present investigation Mason's approach is used to evaluate ultrasonic absorption over frequency square $(\alpha f^2)_{\text{Akh long}}$ for longitudinal wave and $(\alpha f^2)_{\text{Akh shear}}$ for shear wave due to phonon-phonon interaction and $(\alpha f^2)_{\text{th}}$ due to thermoelastic loss using eqs. (2.78), (2.79) and (2.86) in chapter-II.

4.3 Evaluations, Results and Discussions

C_{IJ} and C_{IJK} at different temperatures are evaluated using Born-Mayer parameter [21] ($\text{AgCl}=0.313 \text{ \AA}^0$, $\text{LiF}=0.270 \text{ \AA}^0$ and $\text{MnO}=0.298 \text{ \AA}^0$) and nearest neighbor distance [22] ($\text{AgCl}=2.774 \text{ \AA}^0$, $\text{LiF}=2.014 \text{ \AA}^0$ and $\text{MnO}=2.22 \text{ \AA}^0$). With the values of second and third order elastic constants (SOEC & TOEC) C_{IJ} and C_{IJK} at different higher temperatures Grüneisen parameters $\langle \gamma_i^1 \rangle$ and $\langle (\gamma_i^1)^2 \rangle$ have been evaluated using Grüneisen Table[17] (Appendix A) along $\langle 100 \rangle$, $\langle 110 \rangle$ and $\langle 111 \rangle$ direction of propagation for longitudinal and shear waves. Non-linearity parameters 'D' are calculated using the eqn.(2.80) in chapter II with the help of $\langle \gamma_i^1 \rangle$ and $\langle (\gamma_i^1)^2 \rangle$, specific heat (C_V) data and energy density (E_0) values taken from the literature [24]. Non-linearity parameters 'D' are presented in Tables 4.5, 4.6 and 4.7. The thermal relaxation time τ_{th} are obtained using eqn.(2.65) with thermal conductivity data for AgCl [23], LiF [20,23] and MnO [23] and specific heat data [24] and presented in Tables 4.1-4.3. From the values of τ_{th} , one can check that for the ultrasonic frequency ranges, condition $\omega \tau_{th} \ll 1$ is well satisfied. Phonon viscosity loss $(\alpha/f^2)_{Akh}$ and thermoelastic loss $(\alpha/f^2)_{th}$ at different temperatures are obtained and the values are shown in Tables 4.8,4.9 and 4.10.

The best check for the validity of the present investigation will be to compare values of SOEC and TOEC, thermal relaxation time (τ_{th}), non-linearity coupling constants (D) and phonon-viscosity loss (α/f^2) with other similar solids.

(i) Second and third order elastic constants

The calculated values of SOEC and TOEC for these dielectric crystals are shown in Tables 4.1, 4.2 and 4.3. The evaluated values of SOEC of AgCl at 300K are $C_{11}=53.89 \text{ GPa}$, $C_{12}=13.85 \text{ GPa}$ and $C_{44}=16.34 \text{ GPa}$; While in the available literature [20,25,26], these are as $C_{11}=60.1 \text{ GPa}$, $C_{12}=36.2 \text{ GPa}$ and $C_{44}=6.25 \text{ GPa}$. The values of SOEC and TOEC of LiF are presented in Table 4.2, our calculated values of C_{11} , C_{12} and C_{44} for LiF have good agreement with the theoretical and experimental values of those available in the literature [17,20,25-27]. Trend of SOEC and TOEC of ~~MnO~~ ~~is the same as~~ other associated dielectric crystal.

(ii) Non-linearity coupling constants(D)

Non-linearity parameters for these three dielectric crystals are shown in Tables 4.5, 4.6 and 4.7 along $\langle 100 \rangle$, $\langle 110 \rangle$ and $\langle 111 \rangle$ crystallographic directions respectively.

Comparison of values of D_l and D_s have been made in the Table 4.11 for LiF. In which one has made comparison of LiF especially and found very good match with available experimental as well as theoretical data by Handson [27] and Kor et al [28] at room temperature. Besides LiF two other crystals AgCl and MnO are having the same trend of D_l and D_s as other NaCl-type crystals [8]

(iii) Thermal relaxation time

Clearly the values of thermal relaxation time is of the order of pico second (Table 4.4); which is as expected. Its value is greatest at 100K and decreases exponentially with temperature and one may propose the relation: $\tau_{th} = \tau_0 \exp(-T/\lambda)$, where τ_0 and λ being constants. Such type of nature is as expected. It can be seen from Table 4.4 that one may obtain saturation state after certain temperature which follows the proposed above expression and is in accordance with our expectation. It is also found to be the same order in other NaCl-type materials [27,28].

(iv) Phonon-viscosity loss

The temperature dependence of ultrasonic attenuation due to phonon-phonon interactions is shown in Tables 4.8 4.10 and Figs. 4.1-4.10 for AgCl, LiF and MnO dielectric crystals. The thermal conductivity played very important role for the ultrasonic absorption. As we are seeing the relation $(\alpha/f^2) \propto \tau$ and τ thermal relaxation time is directly proportional to thermal conductivity of the material. In the case of AgCl first (α/f^2) increases with temperature upto 400K and then decreases due to the values of thermal conductivity. The order of attenuation is the same as that of other rocksalt type crystals [27,28].

In case of LiF the results are very interesting being compared with the available theoretical and experimental results in the literature [27,10]. In this single crystal, the lattice thermal conductivity is playing very important role and affected the attenuation results. It can be seen with the Table 4.11 that at 300K our values of ultrasonic absorption coefficient (α) are good agreement with evaluated by Hanson [27] and experimental values of that given by Handson [28].

In case of MnO the values of attenuation for longitudinal wave along $\langle 111 \rangle$ direction is $1.62 \times 10^{-18} \text{ Np s}^2/\text{cm}$ and for shear wave along $\langle 111 \rangle$ direction polarized along $\langle 110 \rangle$ direction is $1.63 \times 10^{-18} \text{ Np s}^2/\text{cm}$ at 100K, while in same conditions in KCl [28] which is

well known dielectric crystal, these are $3.10 \times 10^{-18} \text{ Np s}^2/\text{cm}$ and $5.40 \times 10^{-18} \text{ Np s}^2/\text{cm}$ for longitudinal and shear wave respectively. Thus the order of attenuation of ultrasonic waves is the same as in rocksalt type KCl crystal [28]. The ultrasonic attenuation due to Akhieser loss for longitudinal and shear waves is maximum at 300K. It is obvious from the Table 4.4 and Tables 4.8-4.10 that the behaviour of temperature dependence of ultrasonic absorption coefficient in MnO is the same as the behaviour of temperature dependence of the lattice part of the thermal conductivity value of MnO. The attenuation of Ultrasonic waves is greatest at 300K (\approx room temperature). This is clearly support that ultrasonic attenuation mainly occurs at room temperature in dielectric crystals.

(iv) Thermoelastic loss

The ultrasonic attenuation due to thermoelastic loss is negligible in comparison to loss due to phonon-phonon interaction (Akhiezer loss) and also directly affected with the values of total thermal conductivity values. However there are no experimental result available in thermoelastic loss for comparasion; but the trend is the same as other NaCl-type materials [8].

Thus behaviour of temperature dependence of ultrasonic attenuation in these dielectric crystals clearly supports the Mason's approach, which is employed for the evaluation of ultrasonic parameters in this chapter.

Table4.1: Second and third order elastic constants (SOEC & TOEC) in 10^{11} Dyne/cm² and ultrasonic velocities (V_l for longitudinal wave, V_s for shear wave and \bar{V} for Debye average velocity in 10^5 cm/s and thermal relaxation time (τ_{th}) in 10^{-11} sec. of AgCl in temperature range 100-500K

Temp.K→ SOEC/TOEC↓	100	200	300	400	500
C_{11}	5.041	5.212	5.389	5.568	5.747
C_{12}	1.537	1.461	1.385	1.309	1.233
C_{44}	1.620	1.627	1.634	1.641	1.648
C_{111}	-79.333	-80.130	-80.991	-81.869	-82.753
C_{112}	-6.319	-6.042	-5.766	-5.491	-5.215
C_{123}	2.219	1.796	1.372	0.949	0.525
C_{144}	2.663	2.683	2.704	2.724	2.745
C_{166}	-6.625	-6.653	-6.682	-6.712	-6.742
C_{456}	2.643	2.643	2.643	2.643	2.643
V_l	2.995	3.076	3.162	3.269	3.341
V_s	1.698	1.718	1.741	1.775	1.789
V	1.865	1.890	1.917	1.956	1.973
τ_{th}	0.1285	0.1285	0.098	0.0964	0.07902

Table4.2: Second and third order elastic constants (SOEC & TOEC) in 10^{11} Dyne/cm² and ultrasonic velocities (V_l for longitudinal wave, V_s for shear wave and \bar{V} for Debye average velocity in 10^5 cm/s and thermal relaxation time (τ_{th}) in 10^{-11} sec. of LiF in temperature range 100-300K

Temp.K→ SOEC/TOEC↓	100	200	300
C_{11}	9.575	9.639	9.798
C_{12}	6.301	6.218	6.112
C_{44}	6.482	6.491	6.508
C_{111}	-128.178	-128.008	-128.260
C_{112}	-25.684	-25.535	-25.261
C_{123}	9.062	8.660	8.226
C_{144}	9.587	9.625	9.676
C_{166}	-26.346	-26.362	-26.407
C_{456}	9.512	9.512	9.512
V_l	5.901	5.974	6.091
V_s	4.855	4.902	4.964
V	5.054	5.106	5.178
τ_{th}	1.663	0.1922	0.0985

Table 4.3: Second and third order elastic constants (SOEC & TOEC) in 10^{11} Dyne/cm² and ultrasonic velocities (V_l for longitudinal wave, V_s for shear wave and \bar{V} for Debye average velocity in 10^5 cm/s and thermal relaxation time (τ_{th}) in 10^{-11} sec. of MnO in temperature range 100-300K

Temp.K→ SOEC/TOEC↓	100	200	300	400	500	573
C_{11}	7.848	7.989	8.186	8.402	8.626	8.792
C_{12}	4.120	4.027	3.931	3.835	3.739	3.669
C_{44}	4.241	4.253	4.268	4.283	4.300	4.312
C_{111}	-111.246	-111.246	-111.907	-112.719	-113.599	-114.265
C_{112}	-16.939	-16.680	-16.393	-16.107	-15.822	-15.615
C_{123}	5.994	5.570	5.146	4.723	4.299	3.991
C_{144}	6.459	6.498	6.539	6.580	6.621	6.651
C_{166}	-17.345	-17.380	-17.731	-17.487	-17.546	-17.590
C_{456}	6.415	6.415	6.415	6.415	6.415	6.415
V_l	3.813	3.853	3.912	3.966	4.046	4.091
V_s	2.803	2.811	2.823	2.832	2.857	2.865
\bar{V}	2.982	2.995	3.013	3.028	3.059	3.072
τ_{th}	0.7614	0.216	0.1778	0.1198	0.08936	0.06199

Table 4.4: Density(ρ) in g/cc, thermal conductivity (K) in 10^5 erg/cm s K, specific heat (C_v) in 10^6 erg/cc K and internal energy (E_0) in 10^8 erg/cc of the materials in their temperature range.

Material	Temp.in K	ρ	K	C_v	E_0
AgCl	100	5.62	1.615	8.795	5.483
	200	5.51	1.453	9.501	14.661
	300	5.39	1.150	9.581	24.206
	400	5.21	1.150	9.352	32.852
	500	5.16	0.950	9.262	41.626
LiF	100	2.750	65.00	4.590	16.000
	200	2.641	26.00	15.570	18.170
	300	2.605	16.00	18.170	24.740
MnO	100	5.399	21.540	9.540	3.310
	200	5.381	10.050	15.540	16.020
	300	5.353	9.230	17.150	32.321
	400	5.340	6.540	17.840	48.741
	500	5.268	5.000	17.940	67.703
	573	5.254	3.500	18.010	80.534

Table 4.5: Average Grüneisen parameters $\langle \gamma_l^j \rangle_l$ longitudinal wave, average of square of Grüneisen parameters $\langle (\gamma_l^j)^2 \rangle_l$ for longitudinal wave average of square of Grüneisen parameters $\langle (\gamma_l^j)^2 \rangle_s$ for shear wave and non linearity parameters (D_l for longitudinal wave and D_s for shear wave) along $\langle 100 \rangle$ direction of the materials in their temperature range.

Material	Temp.in K	$\langle\gamma_i^j\rangle_l$	$\langle(\gamma_i^j)^2\rangle_l$	$\langle(\gamma_i^j)^2\rangle_s$	D_l	D_s
AgCl	100	0.523	2.037	.0145	17.017	1.309
	200	0.504	1.912	0.143	16.219	1.294
	300	0.486	1.801	0.141	15.371	1.285
	400	0.470	1.705	0.138	14.586	1.245
	500	0.455	1.619	0.136	13.883	1.228
LiF	100	0.603	2.139	0.352	15.246	3.165
	200	0.589	2.029	0.337	15.508	3.027
	300	0.567	1.868	0.313	14.685	2.814
MnO	100	0.557	1.900	0.218	14.423	1.959
	200	0.539	1.787	0.210	14.388	1.890
	300	0.520	1.670	0.202	13.739	1.816
	400	0.502	1.566	0.194	12.983	1.750
	500	0.486	1.475	0.188	12.334	1.692
	573	0.475	1.415	0.184	11.872	1.654

Table 4.6: Average Grüneisen parameters $\langle\gamma_i^j\rangle_l$ for longitudinal wave average of square of Grüneisen parameters $\langle(\gamma_i^j)^2\rangle_l$, average of square of Grüneisen parameters $[\langle(\gamma_i^j)^2\rangle_{s1}]$ (for shear wave polarized along $\langle 001 \rangle$ direction) and $\langle(\gamma_i^j)^2\rangle_{s2}$ (for shear wave polarized along $\langle 1\bar{1}0 \rangle$ direction) and non linearity parameters (D_l for longitudinal wave, D_{s1} for shear wave polarized along $\langle 001 \rangle$ direction and D_{s2} for shear wave polarized along $\langle 1\bar{1}0 \rangle$ direction) along $\langle 110 \rangle$ direction of the materials in their temperature range.

Material	Temp.in K	$\langle\gamma_i^j\rangle_l$	$\langle(\gamma_i^j)^2\rangle_l$	$\langle(\gamma_i^j)^2\rangle_{s1}$	$\langle(\gamma_i^j)^2\rangle_{s2}$	D_l	D_{s1}	D_{s2}
AgCl	100	-0.827	2.411	0.646	2.894	18.407	5.811	26.043
	200	-0.785	2.163	0.530	2.760	17.076	4.767	24.842
	300	-0.746	1.954	0.444	2.638	15.605	3.997	23.741
	400	-0.711	1.778	0.380	2.527	14.274	3.421	22.745
	500	-0.679	1.628	0.331	2.427	13.114	2.980	21.844
LiF	100	-1.168	7.049	2.435	1.741	48.405	48.405	15.673
	200	-1.129	6.458	2.665	1.715	48.032	48.032	15.432
	300	-1.068	5.599	3.152	1.670	42.846	42.846	15.290
MnO	100	-0.983	3.932	43.089	2.118	27.026	3.878	19.060
	200	-0.939	3.511	136.30	2.051	26.463	12.267	18.460
	300	-0.892	3.093	140.00	1.9772	24.031	12.60	17.787
	400	-0.848	2.734	147.68	1.904	21.440	13.29	17.137
	500	-0.808	2.435	35.219	1.836	19.318	3.16	16.528
	573	-0.782	2.248	18.738	1.790	17.880	1.68	16.110

Table 4.7: Average Grüneisen parameters $\langle \gamma_i^j \rangle_l$ for longitudinal wave, average of square of Grüneisen parameters $\langle (\gamma_i^j)^2 \rangle_l$, for longitudinal wave, average of square of Grüneisen parameters $\langle (\gamma_i^j)^2 \rangle_s$ (shear wave polarized along $\langle \bar{1}10 \rangle$) and non linearity parameters (D_l for longitudinal wave and D_s for shear wave polarized along $\langle \bar{1}10 \rangle$) along $\langle 111 \rangle$ direction of the materials in their temperature range.

Material	Temp.in K	$\langle \gamma_i^j \rangle_l$	$\langle (\gamma_i^j)^2 \rangle_l$	$\langle (\gamma_i^j)^2 \rangle_s$	D_l	D_s
AgCl	100	-0.631	1.898	1.950	15.163	17.552
	200	-0.603	1.732	1.861	14.169	16.753
	300	-0.578	1.587	1.781	13.097	16.026
	400	-0.555	1.463	1.708	12.113	15.372
	500	-0.534	1.354	1.643	11.239	14.784
LiF	100	-0.686	2.691	1.189	19.032	10.703
	200	-0.601	2.540	1.168	19.322	10.514
	300	-0.641	2.319	1.134	18.157	10.203
MnO	100	-0.647	2.185	1.428	16.051	12.850
	200	-0.624	2.023	1.381	15.940	12.427
	300	-0.598	1.855	1.329	14.991	11.958
	400	-0.574	1.706	1.279	13.904	11.511
	500	-0.553	1.575	1.233	12.966	11.097
	573	-0.538	1.491	1.202	12.304	10.816

Table 4.8: Ultrasonic attenuation due to p-p interaction $((\alpha/f^2)_{Akh \text{ long}})$ for longitudinal wave and $(\alpha/f^2)_{Akh \text{ shear}}$ for shear wave) and thermoelastic loss $((\alpha/f^2)_{th})$ of the materials in their temperature range:(in $10^{-18} \text{Np s}^2/\text{cm}$) along $\langle 100 \rangle$ direction

Material	Temp.in K	$(\alpha/f^2)_{th}$	$(\alpha/f^2)_{Akh \text{ long}}$	$(\alpha/f^2)_{Akh \text{ shear}}$
AgCl	100	0.0059	1.1743	0.2478
	200	0.0087	2.2868	0.5197
	300	0.0086	2.5675	0.6326
	400	0.0093	3.0465	0.8128
	500	0.0079	2.8540	0.8220
LiF	100	0.02165	0.6733	0.1254
	200	0.01582	0.7328	0.1274
	300	0.01256	0.7198	0.1274
MnO	100	0.0276	1.4586	0.2494
	200	0.0230	1.9425	0.3286
	300	0.0275	2.9605	0.5199
	400	0.0227	2.7292	0.5053
	500	0.0186	2.5654	0.4999
	573	0.0135	1.971	0.3999

Table 4.9: Ultrasonic attenuation due to p-p interaction $((\alpha/f^2)_{\text{Akh long}}$ for longitudinal wave, $(\alpha/f^2)_{\text{Akh shear1}}$ for shear wave polarized along $\langle 001 \rangle$ direction and $(\alpha/f^2)_{\text{Akh shear2}}$ for shear wave polarized along $\langle 1\bar{1}0 \rangle$ and thermoelastic loss $((\alpha/f^2)_{\text{th}})$ of the materials in their temperature range: (in $10^{-18} \text{Np s}^2/\text{cm}$) along $\langle 110 \rangle$ direction

Material	Temp.in K	$(\alpha/f^2)_{\text{th}}$	$(\alpha/f^2)_{\text{Akh long}}$	$(\alpha/f^2)_{\text{Akh shear1}}$	$(\alpha/f^2)_{\text{Akh shear2}}$
AgCl	100	0.0147	1.2703	1.1006	4.9320
	200	0.0212	2.4077	1.9273	10.0420
	300	0.0282	2.6067	1.9999	11.8800
	400	0.0215	2.9813	2.2335	14.8500
	500	0.0184	2.6960	1.9957	14.6290
LiF	100	0.0811	2.1377	0.6214	0.8690
	200	0.0581	2.2697	0.6598	1.0255
	300	0.0445	2.1004	0.6805	1.2845
MnO	100	0.0862	2.7332	2.42656	49.3701
	200	0.0698	3.5729	3.2092	213.2462
	300	0.0810	5.1785	5.0920	360.6929
	400	0.0646	4.5079	4.9487	383.8100
	500	0.0514	4.0180	4.8842	93.6600
	573	0.0367	2.9691	3.8944	40.7680

Table 4.10: Ultrasonic attenuation due to p-p interaction $((\alpha/f^2)_{\text{Akh long}}$ for longitudinal wave and $(\alpha/f^2)_{\text{Akh shear}}$ for shear wave polarized along $\langle 1\bar{1}0 \rangle$ and thermoelastic loss $((\alpha/f^2)_{\text{th}})$ of the materials in their temperature range: (in $10^{-18} \text{Np s}^2/\text{cm}$) along $\langle 111 \rangle$ direction

Material	Temp.in K	$(\alpha/f^2)_{\text{th}}$	$(\alpha/f^2)_{\text{Akh long}}$	$(\alpha/f^2)_{\text{Akh shear}}$
AgCl	100	0.0085	1.0464	3.3242
	200	0.0126	1.9978	6.7726
	300	0.0122	2.1878	6.7726
	400	0.0131	2.5299	10.0364
	500	0.0137	2.3104	9.9011
LiF	100	0.0280	0.8405	0.4244
	200	0.0204	0.9130	0.4500
	300	0.0161	0.8901	0.4620
MnO	100	0.0373	1.6233	1.6359
	200	0.0308	2.1520	2.1603
	300	0.0364	3.2303	3.4232
	400	0.0296	2.9229	3.3240
	500	0.0241	2.7524	2.9936
	573	0.0173	2.0431	2.6147

Table 4.11: Comparison data for LiF at room temperature and 900MHz frequency.

Prop direction	Polrization	$\alpha(\text{exp.})[27]$ in dB/ μsec	$\alpha(\text{theo.})$ dB/ μsec	in	D(exp.) [27]	D(theo.) Present case	D(theo.) Hanson[27]
<100>	Long.	3.5	3.1		38.0	15.0	35.0
<100>	shear	0.8	0.5		4.50	3.0	3.0
<110>	Long.	1.3	8.8		17.0	42.0	28.0
<110>	Shear <001>	0.8	2.4		4.5	28.0	3.0
<110>	Shear < $\bar{1}\bar{1}0$ >	10.0	4.5		35.0	15.0	9.0
<111>	Long.	0.8	3.8		11.0	18.0	27.
<111>	Shear < $\bar{1}\bar{1}0$ >	5.0	1.8		10.0	10.0	7.0

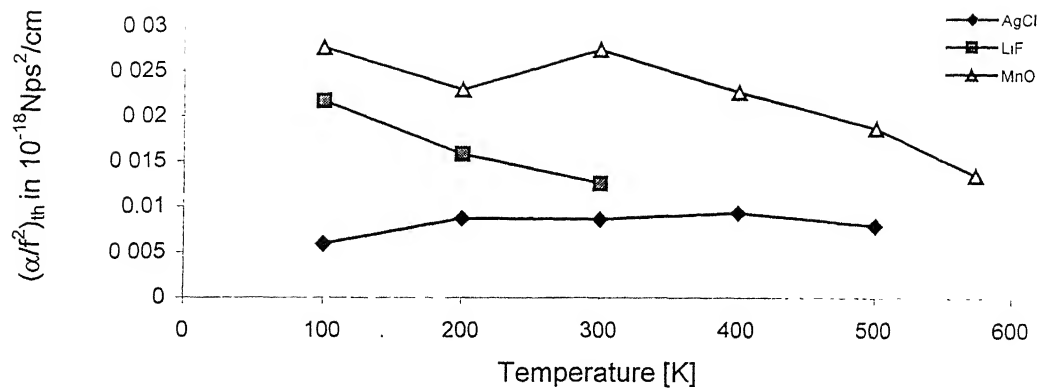


Fig.4.1 $(\alpha/f^2)_{th}$ vs. temperature along $\langle 100 \rangle$ direction

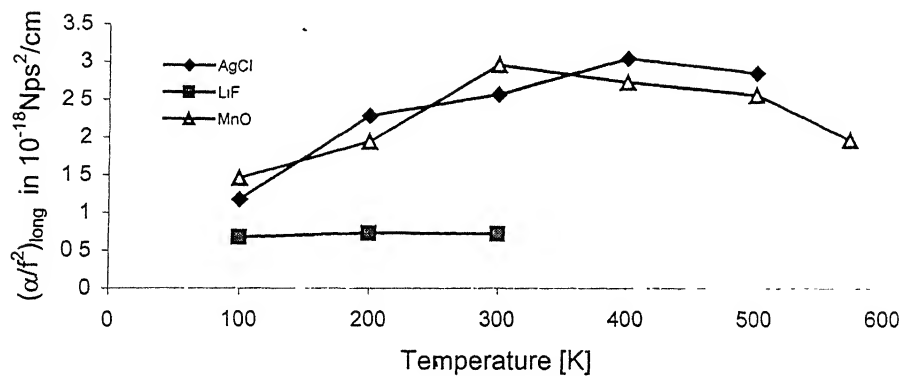


Fig.4.2 $(\alpha/f^2)_{Akh\ long}$ vs. temperature along $\langle 100 \rangle$ direction

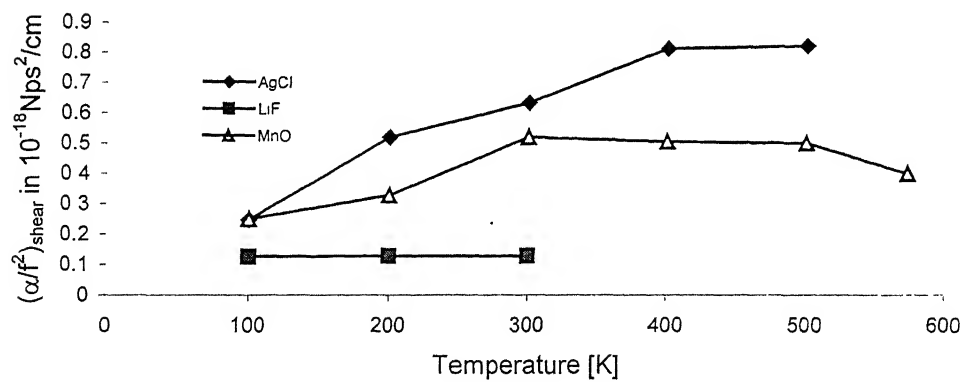


Fig.4.3 $(\alpha/f^2)_{Akh\ shear}$ vs. temperature along $\langle 100 \rangle$ direction

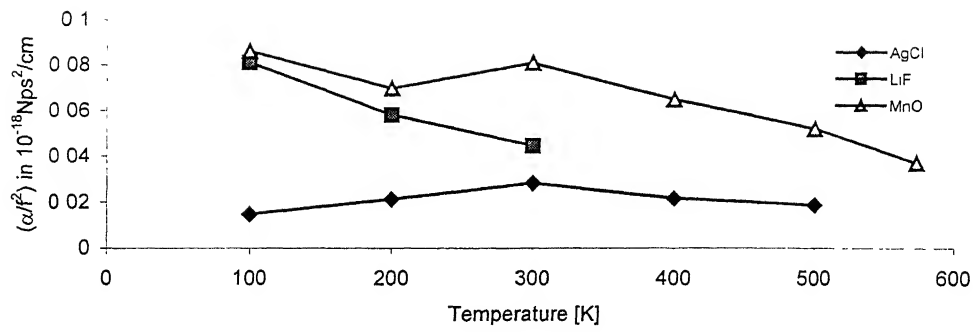


Fig.4.4 $(\alpha/f^2)_{th.}$ vs. temperature along $\langle 110 \rangle$ direction

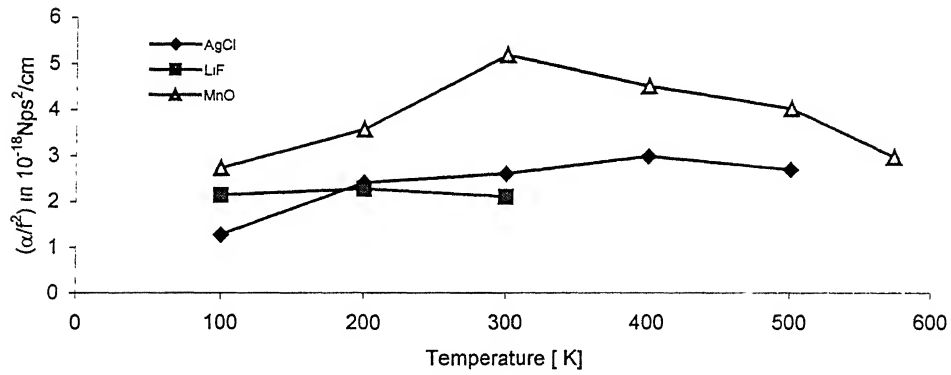


Fig.4.5 $(\alpha/f^2)_{Akh, long}$ vs. temperature along $\langle 110 \rangle$ direction

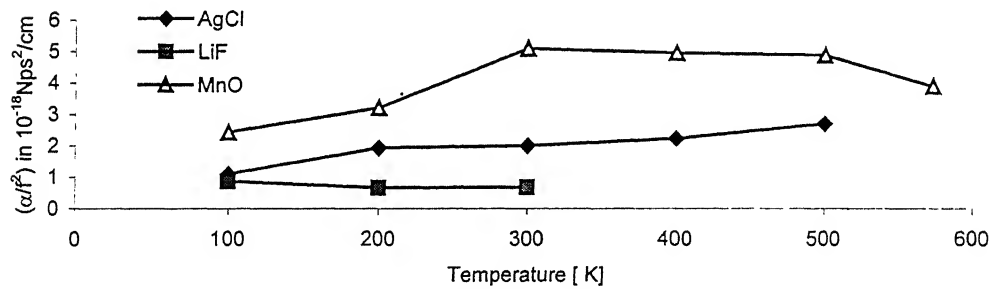


Fig.4.6 $(\alpha/f^2)_{Akh, shear}$ vs. temperature along $\langle 110 \rangle$ direction polarized along $\langle 001 \rangle$ direction

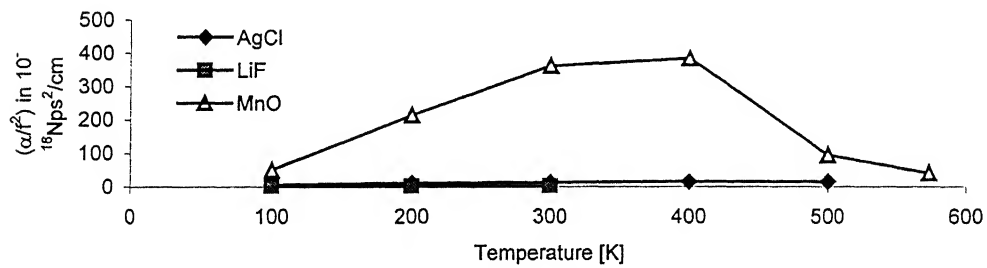


Fig.4.7 $(\alpha/f^2)_{Akh, shear}$ vs. temperature along $\langle 110 \rangle$ direction polarized along $\langle 110 \rangle$ direction

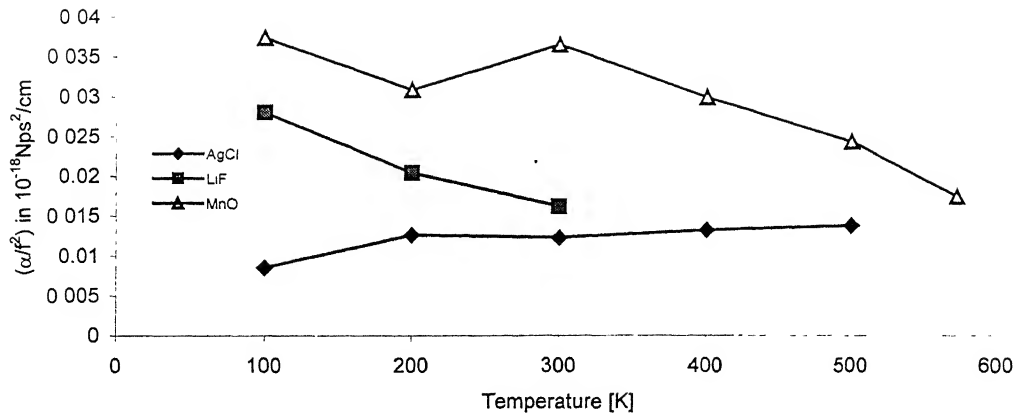


Fig.4.8 $(\alpha/f^2)_{th}$ vs. temperature along $\langle 111 \rangle$ direction

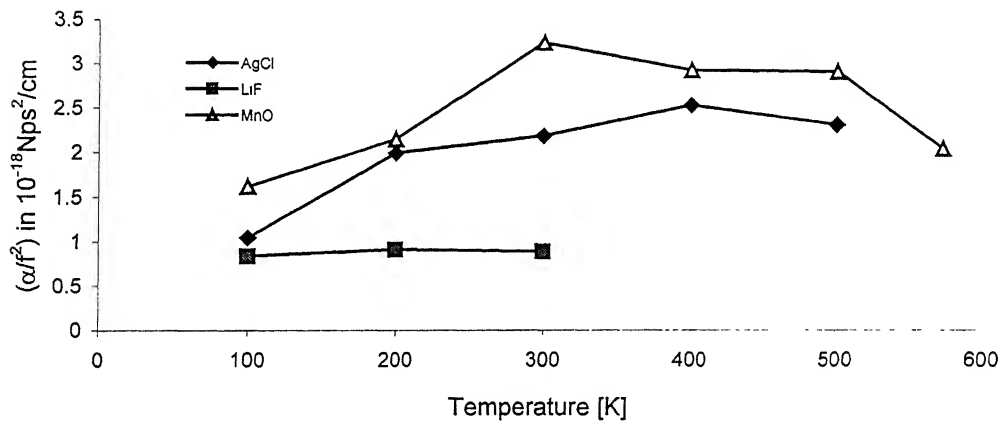


Fig.4.9 $(\alpha/f^2)_{long}$ vs. temperature along $\langle 111 \rangle$ direction

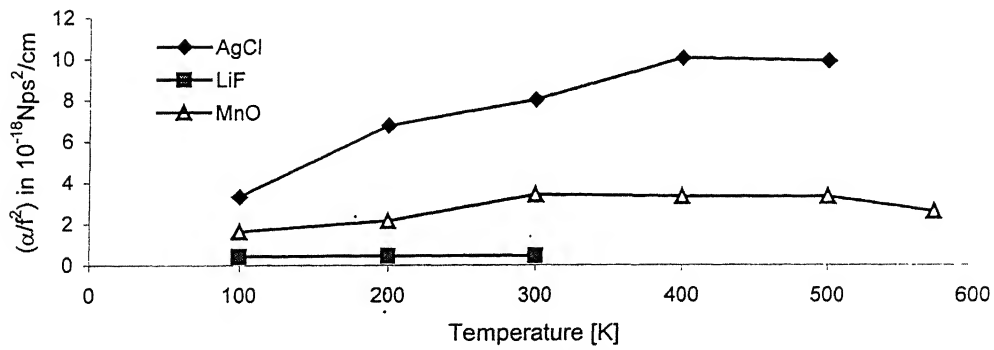


Fig.4.10 $(\alpha/f^2)_{shear}$ vs. temperature along $\langle 111 \rangle$ direction

References:

1. S.Seiro, H.R.Salva, M.Saint-paul, A.A Ghilarducci, P.Lejay, P.Monceau, M.Nunez-Regueiro and A.Sulpice, J.Phys.:Condens.Matter 14,3973(2002).
2. V.Müller, D.Maurer, K.deGroot, E.Bucherand H.E.Bömmel, Phy.Rev.Lett. 56, 248 (1986).
3. Y.Kawai, Jpn.J.Appl.Phys., 37,2970(1997).
4. S.Rajgopalan and D.N.Joharapurkar, J.Appl.Phys. 56,1333(1984).
5. F.Bert, G.Bellessa, A.Quivy and Y.Calvayrac, Phy.Rev.B 64 32(2000).
6. M.Hirao, H.Ogi, N.Suzuki and T.Ohtain, Acta Mater.(UK) 48,517(2000).
7. S.D.Lambade and G.G.Sahastrabudhe, Acoust.Lett.(UK) 22,51(1998).
8. R.R.Yadav and D.Singh, J.Phys.Soc.Jpn. 70,1825(2001).
9. F.S.Khan and P.B.Allen, Phys.Rev. B 35,1002(1987).
10. S.K.Kor, P.K.Mishra and R.P.Khare, Ind.J.Pure Appl.Phys. 16,127(1978).
11. G.G.Sahastrabudhe and S.D.Lambade, J.Acoust.Soc.Am. 104,81(1998).
12. M.Born and J.M.Mayer, Z.Phys. 75,1(1932).
13. K.Brugger, Phy. Rev.133,A1611(1964).
14. G.Leibfried and W.Ludwig, in Solid State Physics edited by F. Seitz and D. Turnbull (Academic Press, New York 1961),.Vol.12
15. G.Leibfried and H.Haln, Z.Phys. 150,497(1958).
16. P.B.Ghate , Phy. Rev. 139, A1966(1965).
17. S.Mori and Y.Hiki, J.Phys.Soc.Jpn. 45,1449(1978).
18. A.Akhiezer, J.Phys.(USSR) 1,277(1939).
19. H.E.Bömmel and K.Dransfeld,Phys.Rev. 117,245(1960).
20. W.P.Mason, Physical Acoustics, (Academic Press, New York 1965),.Vol IIIB, Chapter VI.
21. M.P.Tosi, in Solid State Physics edited by F Seitz and D. Turnbull (Academic Press, New York 1965), Vol 16.
22. R.W.G.Wyckoff, Crystal Structure, (Interscience Publishers, New York 1963), p. 85.
23. D.R.Lide edited, Handbook of Chemistry and Physics, (CRC Press, New York, 1998-99), 79th edition.

24. D.E.Gray edited, American Institute of Physics Handbook, (McGraw Hill Book Co., Inc. New York) 3rd edition.
25. Crystran wavesite, <http://www.crystran.co.uk/agcldata.htm> and <http://www.crystran.co.uk/lifdata.htm>
26. R.Truell, C.Elbaum and B.B.Chick, Ultrasonic Methods in Solid State Physics, (Academic Press, New York 1969),.p. 371.
27. R.C.Hanson, J.Phys.Chem.Solids 28,475(1967).
28. S.K.Kor, R.R.Yadav and Kailash,J.Phys.Soc.Jpn. 55,207(1986).
29. W.P.Mason and T.B Bateman, J.Acoust.Soc.Am. 40, 852 (1966).

CHAPTER-5

Ultrasonic Attenuation in Semiconductors

5.1 Introduction

A phonon-phonon interaction mechanism firstly proposed by Akhiezer [1], subsequently by Bömmel and Dransfeld [2] and Woodruff and Ehrenreich [3] and finally by Mason [4] to explain observed frequency and temperature dependence of ultrasonic attenuation in quartz, has been applied to losses in semiconductors [4]. Recently acoustic attenuation studies [5-11] has been made theoretically and experimentally in solids and liquids in different ways. In the preceding chapters, studies of ultrasonic attenuation have been done in metallic and dielectric crystals. Between the insulating and conducting crystals, the study of semiconducting crystal is also of great importance. In semiconducting crystal Ge and Si have been studied for elastic and inelastic properties and some other properties found unique. These crystals are available in pure form and are categorized by the low loss of ultrasound wave indicating their utility in microwave delay lines [12-14]. Several measurements [15-18] and calculations have been made for Ge and Si in previous years. Recently an attempt has been made in evaluating the parameter of normal valence semiconductors lead chalcogenides [19-20]. The sound wave modulates the equilibrium, thermal phonons distribution tends to relax back to equilibrium via phonon-phonon scattering mechanism. The relaxation process absorbs energy from sound wave and manifest as ultrasonic attenuation. The strength of coupling of thermal phonon modes is given by second- and third- order elastic constants, which is measure of the lattice anharmonicity.

In the present work nine semiconducting single crystals SnTe, EuSe, CdO, SmS, NpS, NpSe, PuS, PuSe and PuTe have been selected for the study of acoustical properties at the temperature range 100-300K along $\langle 100 \rangle$, $\langle 110 \rangle$ and $\langle 111 \rangle$ directions. It is well known that above selected semiconductors are having well-developed NaCl-type structure [21,22,30,31]. In this investigation some microstructural characteristics features well connected to ultrasonic parameters are discussed in SnTe, EuSe, CdO, SmS, NpS, NpSe, PuS, PuSe and PuTe. For the analysis SOEC and TOEC, ultrasonic velocities, Grüneisen parameter and ultrasonic absorption coefficient at the temperature range 100-300K are evaluated.

5.2 Theory

Theory is categorized into two phases, primary phase, temperature dependence of SOEC and TOEC has been discussed, while in the secondary phase the attenuation of ultrasound due to the phonon-viscosity mechanism i.e. Akhiezer mechanism and thermoelastic loss have been discussed.

5.2.1 Theory of second and third order elastic constants

Using Coulomb and Born-Mayer [23] potential $\phi(r_0) = A \exp.(-r_0/b)$, where r_0 is nearest neighbor distance and b -Born-Mayer parameter; and taking interaction effective to the second neighbor distance, SOEC and TOEC at absolute zero have been obtained following Brugger's definition [24] of elastic constants (Table 2.2 in chapter II). According to the anharmonic theory of lattice dynamics developed by Leibfried [25] and Mori [26]; lattice energy of the crystal changes with temperature, hence adding vibrational energy contribution to the elastic constants at absolute zero, one get SOEC and TOEC at desired temperatures;

$$C_{IJK} = C_{IJK}^0 + C_{IJK}^{Vib} \quad (5.1)$$

Where superscript 0 and Vib have used to denote SOEC and TOEC at 0⁰K and vibrational contribution respectively. Expressions for C_{IJK}^0 and C_{IJK}^{Vib} have been given in Tables 2.2-2.6 in chapter II.

5.2.2 Ultrasonic attenuation due to phonon-viscosity mechanism and thermoelastic loss:

Ultrasonic attenuation due to phonon-viscosity mechanism [4] is given as

$$\alpha = \frac{\omega^2 \tau_{th} E_0 D}{3\rho \bar{V}^3 (1 + \omega^2 \tau_{th}^2)} \quad (5.2)$$

above expression in Akhiezer regime ($\omega \tau_{th} \ll 1$) [1] reduces to equs. (2.78) and (2.79) in chapter II for longitudinal and shear waves respectively. Ultrasonic attenuation due to thermoelastic loss has been calculated using equ. (2.86) in chapter II.

5.3 Evaluations, results and discussions

Taking nearest neighbor distance [21,22,30,31] $r_0 = 3.157 \text{ \AA}^0, 3.095 \text{ \AA}^0, 2.347 \text{ \AA}^0, 2.985 \text{ \AA}^0, 2.780 \text{ \AA}^0, 2.921 \text{ \AA}^0, 2.801 \text{ \AA}^0, 2.910 \text{ \AA}^0$ and 3.100 \AA^0 for SnTe, EuSe, CdO, SmS, NpS, NpSe, PuS, PuSe and PuTe respectively and hardness parameter [27] $b = 0.315 \text{ \AA}^0, 0.303 \text{ \AA}^0, 0.311 \text{ \AA}^0, 0.302 \text{ \AA}^0, 0.303 \text{ \AA}^0, 0.313 \text{ \AA}^0, 0.311 \text{ \AA}^0, 0.292 \text{ \AA}^0, 0.298 \text{ \AA}^0$ and 0.302 \AA^0 for SnTe, EuSe, CdO, SmS, NpS, NpSe, PuS, PuSe and PuTe respectively; the second and third order

elastic constants (SOEC & TOEC) have been evaluated at temperature range 100-300K using expressions as given in Tables 2.2-2.6 in chapter II. SOEC and TOEC have been used to evaluate Grüneisen parameters along $\langle 100 \rangle$ direction for longitudinal wave over 39 pure modes & for shear wave over 18 modes; along $\langle 110 \rangle$ direction for longitudinal wave over 39 pure modes, for shear wave polarized along $\langle 001 \rangle$ over 14 modes & for shear wave polarized along $\langle 1\bar{1}0 \rangle$ over 20 modes and along $\langle 111 \rangle$ direction for longitudinal wave over 39 pure modes, for shear wave polarized along $\langle \bar{1}10 \rangle$ over 18 modes using Mason's Grüneisen Tables [4,28] (Appendix-A). The specific heat per unit volume (C_V) and crystal energy density (E_0) have been taken from the literature [29] as a function of (θ_D/T) at different temperatures. Non-linearity parameters (D_l and D_s) have been evaluated taking thermal conductivity and electrical resistivity [22,29,30,31] with the help of equ. (2.80) in chapter II. For the evaluation of thermal conductivity in NpS, NpSe, PuS, PuSe and PuTe; we have used the Wiedemann-Franz law. According to Wiedemann-Franz law, the ratio of thermal conductivity (K) to the electrical conductivity (σ) at any particular temperature is

constant, i.e. $\frac{K}{\sigma} = L_0 T$, where L_0 is the Lorentz number ($L_0 = \frac{\pi^2}{3} \left(\frac{k}{e} \right)^2$) where k is

Boltzman constant and e is the electronic charge and $\sigma = 1/R$ where R is the electrical resistivity. Ultrasonic attenuation due to Akhiezer loss (phonon-phonon interaction) have been evaluated using eqn.(5.2) and ultrasonic attenuation due to thermoelastic loss has been evaluated using eqn.(2.86) of chapter II. All the results have been evaluated by using our computer programme in C++ language.

It is obvious from the Tables 5.1-5.3 that the values of second and third order elastic constants are in agreement with that of NaCl and KCl [32-34]. It can be seen from the Tables 5.4-5.6 that the value of thermal relaxation time (τ_{th}) is of order of pico second in all semiconductors besides SnTe. The order of τ_{th} is of the order 10^{-11} sec. in SnTe. The behaviour of thermal relaxation time is much appreciable in CdO and SmS. The value of τ_{th} is decreasing with temperature in CdO and SmS, which is expected in metals [35]. One may give an expression for the temperature variation of thermal relaxation time as follows:

$$\tau_{th} = \tau_0 \exp(-T/\lambda)$$

Where τ_0 and λ are constants and T is the absolute temperature, Behaviour of relaxation time for SnTe, EuSe, NpS, NpSe, PuS, PuSe and PuTe is as for intermetallics [36].

The variation of 'D' with temperature is shown in Tables 5.7-5.12. Non-linearity constant ratio D_l/D_s along $\langle 100 \rangle$ direction lies between 8-16, D_l/D_{s1} along $\langle 110 \rangle$ direction and shear wave polarized along $\langle 001 \rangle$ is about 10-11 and D_{s2}/D_l along $\langle 110 \rangle$ direction and shear wave polarized along $\langle \bar{1}10 \rangle$ is about 1-1.5 and D_{s2}/D_l along $\langle 111 \rangle$ direction and shear wave polarized along $\langle \bar{1}10 \rangle$ is about 1-1.5 which are comparable with that in experimental value of NaCl-type LiF [37].

In the present investigation it is pointed out that the attenuation varies with temperature T in the following manner:

$$\alpha = \alpha_0 T^n$$

Where α_0 and n are constants. It is obvious from the Tables 5.13-5.18 and Figs. 5.1-5.10 that the value of ultrasonic attenuation due to phonon-phonon interaction $((\alpha/f^2)_l$ for longitudinal wave and $(\alpha/f^2)_s$ for shear wave) and due to thermoelastic loss $(\alpha/f^2)_{th}$ increases with temperature in all chosen semiconductors. The value of ultrasonic attenuation $(\alpha/f^2)_l$ is greater than the $(\alpha/f^2)_s$ along $\langle 100 \rangle$ direction and along $\langle 110 \rangle$ direction (shear wave polarized along $\langle 001 \rangle$ direction). While $(\alpha/f^2)_l$ is less than the $(\alpha/f^2)_s$ along $\langle 110 \rangle$ direction (shear wave polarized along $\langle \bar{1}10 \rangle$ direction) and along $\langle 111 \rangle$ direction (shear wave polarized along $\langle \bar{1}10 \rangle$ direction), which has been observed experimentally in semiconductors [38].

Contribution of $(\alpha/f^2)_{th}$ to total value of (α/f^2) at any temperature is intermediate to that of conducting and non conducting materials. This is due to fact that the thermal conduction and thermal expansion coefficient of semiconductors is intermediate between two.

Drastic increase in attenuation in PuTe at around room temperature is remained to explain.

The ultrasonic attenuation due to thermoelastic loss is negligible in comparison to the ultrasonic attenuation due to Akhiezer loss for all semiconducting single crystals in the temperature range 100-300K studied along $\langle 100 \rangle$, $\langle 110 \rangle$ and $\langle 111 \rangle$ directions.

Thus as concluding remark it can be said that these semiconducting crystal possess peculiar behaviour towards the attenuation due to thermoelastic mechanism is negligible in

comparison to the ultrasonic attenuation. The behaviour of temperature dependence of ultrasonic attenuation shows important microstructural features for these semiconducting materials applicable for material producing and processing industries.

Table 5.1 Calculated second and third order elastic constants (SOEC & TOEC) in 10^{11}Dyne/cm^2 of the semiconductors at the temperature range 100-300K

Semicon ductors	Temp. [K]	C_{11}	C_{12}	C_{44}	C_{111}	C_{112}	C_{123}	C_{144}	C_{166}	C_{456}
SnTe	100	3.879	0.849	0.921	-65.37	-3.417	1.138	1.588	-3.714	1.575
	200	4.032	0.781	0.925	-66.19	-3.138	0.701	1.600	-3.731	1.575
	300	4.189	0.713	0.928	-67.03	-2.858	0.263	1.613	-3.749	1.575
EuSe	100	4.351	0.911	0.990	-74.19	-3.647	1.211	1.718	-3.980	1.706
	200	4.520	0.835	0.994	-75.10	-3.332	0.716	1.731	-3.998	1.706
	300	4.692	0.760	0.998	-76.04	-3.017	0.222	1.744	-4.016	1.706
CdO	100	6.581	3.278	3.378	-95.00	-13.49	4.767	5.193	-13.80	5.158
	200	6.773	3.188	3.387	-95.74	-13.23	4.377	5.228	-13.85	5.158
	300	6.977	3.102	3.401	-96.58	12.97	3.987	5.263	-13.91	5.158

Table 5.2 Calculated second and third order elastic constants (SOEC & TOEC) in 10^{11}Dyne/cm^2 of the semiconductors at the temperature range 100-300K

Semicon ductors	Temp. [K]	C_{11}	C_{12}	C_{44}	C_{111}	C_{112}	C_{123}	C_{144}	C_{166}	C_{456}
SmS	100	4.811	1.074	1.160	-79.98	-4.329	1.477	1.987	-4.693	1.971
	200	4.943	0.998	1.163	-80.44	-4.029	0.983	2.001	-4.708	1.971
	300	5.106	0.919	1.168	-81.22	-3.714	0.489	2.016	-4.727	1.971
NpS	100	5.483	1.495	1.586	-87.44	-6.112	2.145	2.641	-6.476	2.620
	200	5.622	1.415	1.592	-87.88	-5.820	1.671	2.660	-6.496	2.620
	300	5.794	1.332	1.598	-88.65	-5.512	1.196	2.679	-6.521	2.620
NpSe	100	4.626	1.215	1.294	-74.69	-4.959	1.719	2.170	-5.271	2.153
	200	4.772	1.141	1.299	-75.29	-4.681	1.285	2.186	-5.291	2.153
	300	4.935	1.068	1.304	-76.08	-4.401	0.852	2.203	-5.314	2.153

Table 5.3 Calculated second and third order elastic constants (SOEC & TOEC) in 10^{11} Dyne/cm² of the semiconductors at the temperature range 100-300K

Semiconductors	Temp. [K]	C ₁₁	C ₁₂	C ₄₄	C ₁₁₁	C ₁₁₂	C ₁₂₃	C ₁₄₄	C ₁₆₆	C ₄₅₆
PuS	100	5.841	1.417	1.515	-96.52	-5.749	2.005	2.565	-6.156	2.546
	200	6.029	1.327	1.518	-96.86	-5.402	1.453	2.583	-5.402	2.546
	300	6.171	1.242	1.525	-96.85	-5.074	0.925	2.602	-6.198	2.546
PuSe	100	5.145	1.201	1.289	-85.28	-4.860	1.671	2.199	-5.221	2.182
	200	5.306	1.119	1.293	-85.98	-4.536	1.159	2.215	-5.240	2.182
	300	5.486	1.037	1.298	-86.88	-4.207	0.647	2.231	-5.262	2.182
PuTe	100	4.178	0.916	0.992	-70.21	-3.688	0.992	1.707	-4.003	1.695
	200	4.326	0.844	0.995	-70.92	-3.396	0.995	1.721	-4.019	1.695
	300	4.746	0.748	0.988	-77.23	-2.956	0.177	1.733	-3.974	1.695

Table 5.4 Thermal conductivity (K) in 10^5 erg/cm s, density (ρ) in g/cc, specific heat per unit volume (C_V) in 10^6 erg/cc K, energy density (E_0) in 10^9 erg/cc, ultrasonic velocities V_l in 10^5 cm/s for longitudinal wave and V_s in 10^5 cm/s for shear wave, Debye average velocity (\bar{V}) in 10^5 cm/s and thermal relaxation time (τ_{th}) in 10^{-11} sec of the semiconductors in the temperature range 100-300K.

Semiconductors	Temp. [K]	K	ρ	C_V	E_0	V_l	V_s	\bar{V}	τ_{th}
SnTe	100	5.321	6.700	6.257	0.410	2.406	1.172	1.302	1.500
	200	5.421	6.615	6.573	1.048	2.469	1.182	1.314	1.428
	300	6.511	6.504	6.551	1.686	2.538	1.195	1.329	1.686
EuSe	100	0.213	6.589	6.483	0.411	2.570	1.226	1.362	0.052
	200	0.211	6.501	6.870	1.077	2.637	1.236	1.375	0.053
	300	0.244	6.466	6.915	1.761	2.694	1.242	1.383	0.055
CdO	100	0.675	8.389	11.390	0.506	2.801	2.006	2.144	0.039
	200	0.689	8.348	14.800	1.872	2.847	2.014	2.157	0.030
	300	0.700	8.243	15.370	3.358	2.909	2.031	2.179	0.029

Table 5.5 Thermal conductivity (K) in 10^5 erg/cm s , density (ρ) in g/cc, specific heat per unit volume (C_V) in 10^6 erg/cc K , energy density (E_0) in 10^9 erg/cc , ultrasonic velocities V_l in 10^5 cm/s for longitudinal wave and V_s in 10^5 cm/s for shear wave, Debye average velocity (\bar{V}) in 10^5 cm/s and thermal relaxation time (τ_{th}) in 10^{-11} sec of the semiconductors in the temperature range 100-300K.

Semiconductors	Temp. [K]	K	ρ	C_V	E_0	V_l	V_s	\bar{V}	τ_{th}
SmS	100	4.116	5.752	6.856	0.396	2.892	1.420	1.576	0.725
	200	3.402	5.721	7.571	1.125	2.939	1.426	1.583	0.538
	300	3.360	5.695	7.681	1.879	2.994	1.432	1.591	0.518
NpS	100	0.142	10.538	8.651	0.514	2.281	1.227	1.354	0.027
	200	0.302	10.478	9.436	1.425	2.316	1.233	1.361	0.052
	300	0.490	10.398	9.546	2.373	2.361	1.240	1.370	0.082
NpSe	100	0.197	10.678	7.664	0.527	2.081	1.101	1.216	0.052
	200	0.446	10.629	8.194	1.435	2.119	1.105	1.222	0.109
	300	0.774	10.537	8.249	2.106	2.164	1.112	1.231	0.186

Table 5.6 Thermal conductivity (K) in 10^5 erg/cm s , density (ρ) in g/cc, specific heat per unit volume (C_V) in 10^6 erg/cc K , energy density (E_0) in 10^9 erg/cc , ultrasonic velocities V_l in 10^5 cm/s for longitudinal wave and V_s in 10^5 cm/s for shear wave, Debye average velocity (\bar{V}) in 10^5 cm/s and thermal relaxation time (τ_{th}) in 10^{-11} sec of the semiconductors in the temperature range 100-300K.

Semiconductors	Temp. [K]	K	ρ	C_V	E_0	V_l	V_s	\bar{V}	τ_{th}
PuS	100	0.057	10.637	8.642	0.527	2.343	1.194	1.322	0.011
	200	0.129	10.602	9.388	1.435	2.385	1.197	1.326	0.024
	300	0.272	10.440	9.340	2.360	2.431	1.209	1.340	0.049
PuSe	100	0.105	10.027	7.744	0.498	2.160	1.081	1.199	0.028
	200	0.244	10.992	8.291	1.308	2.197	1.085	1.204	0.061
	300	0.565	10.880	8.348	2.127	2.246	1.092	1.213	0.138
PuTe	100	2.453	10.575	7.116	0.470	1.988	0.968	1.075	0.089
	200	3.063	10.428	8.093	1.144	2.037	0.977	1.086	0.096
	300	1.470	10.355	6.929	1.815	2.141	0.977	1.088	0.537

Table 5.7 Average ultrasonic Grüneisen parameters $\langle \gamma_i^j \rangle_l$ for longitudinal wave, average square ultrasonic Grüneisen parameters ($\langle (\gamma_i^j)^2 \rangle_l$ for longitudinal wave , $\langle (\gamma_i^j)^2 \rangle_s$ for shear wave), non-linear parameters D_l for longitudinal wave and D_s for shear wave along $\langle 100 \rangle$ direction of the semiconductors at the temperature range 100-300K.]

Semiconductor	Temp.(K)	$\langle \gamma_i^j \rangle_l$	$\langle (\gamma_i^j)^2 \rangle_l$	$\langle (\gamma_i^j)^2 \rangle_s$	D_l	D_s
SnTe	100	0.520	2.309	0.134	19.544	1.202
	200	0.498	2.163	0.132	18.534	1.188
	300	0.479	2.034	0.130	17.504	1.170
EuSe	100	0.521	2.367	0.133	20.019	1.197
	200	0.500	2.220	0.131	19.023	1.179
	300	0.481	2.093	0.130	18.019	1.170
CdO	100	0.526	1.809	0.176	14.415	1.587
	200	0.533	1.785	0.195	14.720	1.755
	300	0.513	1.663	0.188	13.883	1.692
SmS	100	0.638	1.927	2.274	2.274	1.197
	200	0.613	1.773	2.188	18.124	1.188
	300	0.587	1.659	2.102	17.241	1.179

Table 5.8 Average ultrasonic Grüneisen parameters $\langle \gamma_i^j \rangle_l$ for longitudinal wave , average square ultrasonic Grüneisen parameters ($\langle (\gamma_i^j)^2 \rangle_l$ for longitudinal wave , $\langle (\gamma_i^j)^2 \rangle_s$ for shear wave), non-linear parameters D_l for longitudinal wave and D_s for shear wave along $\langle 100 \rangle$ direction of the semiconductors at the temperature range 100-300K.]

Semiconductor	Temp.(K)	$\langle \gamma_i^j \rangle_l$	$\langle (\gamma_i^j)^2 \rangle_l$	$\langle (\gamma_i^j)^2 \rangle_s$	D_l	D_s
NpS	100	0.516	2.073	0.140	17.306	1.257
	200	0.500	1.966	0.138	16.698	1.242
	300	0.484	1.861	0.136	15.901	1.224
NpSe	100	0.518	2.122	0.138	17.843	1.245
	200	0.500	1.999	0.137	17.037	1.229
	300	0.482	1.886	0.135	15.155	1.215
PuS	100	0.516	2.173	0.136	18.249	1.220
	200	0.500	2.072	0.134	17.671	1.206
	300	0.483	1.957	0.133	16.782	1.197
PuSe	100	0.518	2.233	0.135	19.435	1.201
	200	0.500	2.108	0.133	18.845	1.212
	300	0.482	1.993	0.132	18.021	1.199
PuTe	100	0.518	2.295	0.133	18.355	1.187
	200	0.498	2.157	0.132	17.116	1.188
	300	0.480	2.113	0.130	18.225	1.161

Table 5.9 Average ultrasonic Grüneisen parameters $\langle \gamma_i^j \rangle_1$ for longitudinal wave, average square ultrasonic Grüneisen parameters ($\langle (\gamma_i^j)^2 \rangle_1$ for longitudinal wave , $\langle (\gamma_i^j)^2 \rangle_{s1}$ for shear wave polarized along $\langle 001 \rangle$ direction, $\langle (\gamma_i^j)^2 \rangle_{s2}$ for shear wave polarized along $\langle 1\bar{1}0 \rangle$ direction), non-linear parameters D_1 for longitudinal wave, D_{s1} for shear wave polarized along $\langle 001 \rangle$ direction and D_{s2} for shear wave polarized along $\langle 1\bar{1}0 \rangle$ direction along $\langle 110 \rangle$ direction of the semiconductors at the temperature range 100-300K.]

Semiconductor	Temp.(K)	$\langle \gamma_i^j \rangle_1$	$\langle (\gamma_i^j)^2 \rangle_1$	$\langle (\gamma_i^j)^2 \rangle_{s1}$	$\langle (\gamma_i^j)^2 \rangle_{s2}$	D_1	D_{s1}	D_{s2}
SnTe	100	-0.794	2.396	0.219	3.479	18.678	1.970	31.311
	200	-0.749	2.159	0.191	3.313	17.320	1.723	29.817
	300	-0.707	1.960	0.170	3.163	15.892	1.530	28.467
EuSe	100	-0.793	2.432	0.196	3.589	18.912	1.764	32.301
	200	-0.748	2.198	0.173	3.422	17.641	1.557	30.798
	300	-0.707	2.003	0.155	3.219	16.255	1.395	29.466
CdO	100	-0.930	3.512	0.215	3.589	19.860	1.785	32.014
	200	-0.912	3.173	0.182	3.451	19.368	1.546	30.421
	300	-0.862	2.777	0.172	3.244	18.548	1.235	28.965
SmS	100	-0.786	2.339	0.229	3.365	17.842	2.061	30.285
	200	-0.750	2.142	0.206	3.234	17.013	1.854	29.124
	300	-0.713	1.959	0.184	3.102	15.761	1.656	27.918

Table 5.10 Average ultrasonic Grüneisen parameters $\langle \gamma_i^j \rangle_1$ for longitudinal wave, average square ultrasonic Grüneisen parameters ($\langle (\gamma_i^j)^2 \rangle_1$ for longitudinal wave , $\langle (\gamma_i^j)^2 \rangle_{s1}$ for shear wave polarized along $\langle 001 \rangle$ direction, $\langle (\gamma_i^j)^2 \rangle_{s2}$ for shear wave polarized along $\langle 1\bar{1}0 \rangle$ direction), non-linear parameters D_1 for longitudinal wave, D_{s1} for shear wave polarized along $\langle 001 \rangle$ direction and D_{s2} for shear wave polarized along $\langle 1\bar{1}0 \rangle$ direction along $\langle 110 \rangle$ direction of the semiconductors at the temperature range 100-300K.]

Semiconductor	Temp.(K)	$\langle \gamma_i^j \rangle_1$	$\langle (\gamma_i^j)^2 \rangle_1$	$\langle (\gamma_i^j)^2 \rangle_{s1}$	$\langle (\gamma_i^j)^2 \rangle_{s2}$	D_1	D_{s1}	D_{s2}
NpS	100	-0.805	2.318	0.415	3.007	17.590	3.736	27.065
	200	-0.769	2.120	0.364	2.892	16.729		26.030
	300	-0.734	1.934	0.317	2.774	15.448	2.844	24.966
NpSe	100	-0.805	2.336	0.366	3.103	18.003	3.297	27.924
	200	-0.765	2.115	0.316	2.967	16.808	2.846	26.928
	300	-0.727	1.920	0.275	2.838	15.417	2.475	25.542
PuS	100	-0.797	2.323	0.285	3.217	17.809	2.565	28.957
	200	-0.759	2.137	0.249	3.114	16.973	2.242	28.031
	300	-0.724	1.955	0.227	2.975	15.728	2.043	26.775
PuSe	100	-0.795	2.359	0.256	3.330	18.282	2.303	29.039
	200	-0.756	2.148	0.227	3.190	18.248	2.039	28.708
	300	-0.719	1.962	0.202	3.057	15.832	1.818	27.513
PuTe	100	-0.791	2.383	0.219	3.455	18.602	1.187	31.096
	200	-0.749	2.157	0.193	3.299	17.035	1.741	29.691

	300	-0.713	1.959	0.184	3.102	16.422	1.332	29.844
Table 5.11 Average ultrasonic Grüneisen parameters $\langle \gamma_i^j \rangle_1$ for longitudinal wave, average square ultrasonic Grüneisen parameters ($\langle (\gamma_i^j)^2 \rangle_1$ for longitudinal wave , $\langle (\gamma_i^j)^2 \rangle_s$ for shear wave), non-linear parameters D_1 for longitudinal wave and D_s for shear wave polarized along $\langle \bar{1}10 \rangle$ along $\langle 111 \rangle$ direction of the semiconductors at the temperature range 100-300K.]								
Semiconductor	Temp.(K)	$\langle \gamma_i^j \rangle_1$	$\langle (\gamma_i^j)^2 \rangle_1$	$\langle (\gamma_i^j)^2 \rangle_s$	D_1	D_s		
SnTe	100	-0.647	1.973	2.351	15.841	21.159		
	200	-0.615	1.788	2.242	14.667	20.178		
	300	-0.587	1.629	2.144	13.465	19.296		
EuSe	100	-0.651	2.004	2.427	16.024	21.843		
	200	-0.620	1.819	2.317	14.901	20.853		
	300	-0.592	1.661	2.220	13.710	19.980		
CdO	100	-0.619	1.959	1.448	15.822	21.845		
	200	-0.607	1.869	1.437	14.342	20.512		
	300	-0.562	1.785	1.386	14.121	19.012		
SmS	100	-0.515	2.244	0.134	15.229	20.466		
	200	-0.498	2.125	0.132	14.440	19.692		
	300	-0.480	2.010	0.131	13.393	18.918		

Table 5.12 Average ultrasonic Grüneisen parameters $\langle \gamma_i^j \rangle_1$ for longitudinal wave, average square ultrasonic Grüneisen parameters ($\langle (\gamma_i^j)^2 \rangle_1$ for longitudinal wave , $\langle (\gamma_i^j)^2 \rangle_s$ for shear wave), non-linear parameters D_1 for longitudinal wave and D_s for shear wave polarized along $\langle \bar{1}10 \rangle$ direction along $\langle 111 \rangle$ direction of the semiconductors at the temperature range 100-300K.]

Semiconductor	Temp.(K)	$\langle \gamma_i^j \rangle_1$	$\langle (\gamma_i^j)^2 \rangle_1$	$\langle (\gamma_i^j)^2 \rangle_s$	D_1	D_s
NpS	100	-0.628	1.870	2.028	14.658	18.256
	200	-0.604	1.728	1.953	14.106	17.573
	300	-0.580	1.593	1.875	13.215	17.271
NpSe	100	-0.633	1.895	2.096	15.182	18.844
	200	-0.606	1.734	2.004	14.207	18.038
	300	-0.579	1.589	1.919	13.124	17.271
PuS	100	-0.634	1.903	2.173	15.146	19.555
	200	-0.611	1.763	2.106	14.404	18.951
	300	-0.586	1.623	2.014	13.393	18.126
PuSe	100	-0.640	1.937	2.249	15.519	20.244
	200	-0.613	1.776	2.158	14.551	19.416
	300	-0.588	1.631	2.070	13.458	18.630
PuTe	100	-0.645	1.962	2.335	15.775	21.019
	200	-0.615	1.786	2.233	14.470	20.095
	300	-0.587	1.629	2.102	13.818	20.241

Table 5.13 Ultrasonic attenuation due to thermoelastic loss $(\alpha/f^2)_{th}$ and due to phonon-phonon interaction $((\alpha/f^2)_{Akh\ l}$ for longitudinal wave and $(\alpha/f^2)_{Akh\ s}$ for shear wave) of the semiconductors in the temperature range 100-300K in the unit 10^{-18} Np s²/cm along <100> direction.

Semiconductor	Temperature [K]	$(\alpha/f^2)_{th}$	$(\alpha/f^2)_{Akh\ l}$	$(\alpha/f^2)_{Akh\ s}$
SnTe	100	0.005	1.545	0.411
	200	0.008	3.343	0.976
	300	0.012	5.615	2.180
EuSe	100	0.014	4.623	1.273
	200	0.025	10.952	3.292
	300	0.033	16.403	5.432
CdO	100	0.023	1.837	0.275
	200	0.045	5.156	0.868
	300	0.058	7.927	1.419
SmS	100	0.017	4.663	1.250
	200	0.024	9.057	2.601
	300	0.031	13.178	4.118

Table 5.14 Ultrasonic attenuation due to thermoelastic loss $(\alpha/f^2)_{th}$ and due to phonon-phonon interaction $((\alpha/f^2)_{Akh\ l}$ for longitudinal wave and $(\alpha/f^2)_{Akh\ s}$ for shear wave) of the semiconductors in the temperature range 100-300K in the unit 10^{-18} Np s²/cm along <100> direction.

Semiconductor	Temperature [K]	$(\alpha/f^2)_{th}$	$(\alpha/f^2)_{Akh\ l}$	$(\alpha/f^2)_{Akh\ s}$
NpS	100	0.001	0.228	0.053
	200	0.004	1.135	0.280
	300	0.008	2.716	0.722
NpSe	100	0.002	0.570	0.134
	200	0.009	2.852	0.725
	300	0.019	7.097	1.965
PuS	100	0.0003	0.096	0.024
	200	0.001	0.497	0.134
	300	0.004	1.541	4.475
PuSe	100	0.001	0.286	0.073
	200	0.004	1.476	0.408
	300	0.011	4.898	1.477
PuTe	100	0.004	1.181	0.315
	200	0.007	2.754	0.807
	300	0.039	10.994	7.040

Table 5.15 Ultrasonic attenuation due to thermoelastic loss $(\alpha/f^2)_{th}$ and due to phonon-phonon interaction $((\alpha/f^2)_{Akh,l}$ for longitudinal wave, $(\alpha/f^2)_{Akh,S1}$ for shear wave polarized along $\langle 001 \rangle$ and $(\alpha/f^2)_{Akh,S2}$ for shear wave polarized along $\langle 1\bar{1}0 \rangle$ direction) of the semiconductors along $\langle 110 \rangle$ direction in the temperature range 100-300K in the unit 10^{-18} Np s²/cm.

Semiconductors	Temp.[K]	$(\alpha/f^2)_{th}$	$(\alpha/f^2)_{Akh,l}$	$(\alpha/f^2)_{Akh,S1}$	$(\alpha/f^2)_{Akh,S2}$
SnTe	100	0.011	1.476	0.673	10.697
	200	0.018	3.125	1.415	24.489
	300	0.026	5.098	2.352	43.621
EuSe	100	0.032	4.367	1.877	34.364
	200	0.059	10.156	4.347	85.990
	300	0.065	13.805	6.271	118.450
CdO	100	0.073	3.284	0.275	43.863
	200	0.132	8.516	8.681	84.213
	300	0.164	12.519	1.419	257.494
SmS	100	0.039	4.420	2.156	31.684
	200	0.055	8.502	4.059	63.767
	300	0.067	12.046	5.784	97.517

Table 5.16 Ultrasonic attenuation due to thermoelastic loss $(\alpha/f^2)_{th}$ and due to phonon-phonon interaction $((\alpha/f^2)_{Akh,l}$ for longitudinal wave, $(\alpha/f^2)_{Akh,S1}$ for shear wave polarized along $\langle 001 \rangle$ and $(\alpha/f^2)_{Akh,S2}$ for shear wave polarized along $\langle 1\bar{1}0 \rangle$ direction) of the semiconductors along $\langle 110 \rangle$ direction in the temperature range 100-300K in the unit 10^{-18} Np s²/cm.

Semiconductors	Temp.[K]	$(\alpha/f^2)_{th}$	$(\alpha/f^2)_{Akh,l}$	$(\alpha/f^2)_{Akh,S1}$	$(\alpha/f^2)_{Akh,S2}$
NpS	100	0.003	0.232	0.158	1.147
	200	0.009	1.137	0.890	5.874
	300	0.019	2.638	1.677	14.720
NpSe	100	0.005	0.575	0.356	3.014
	200	0.021	2.814	1.678	15.875
	300	0.044	6.773	4.003	41.307
PuS	100	0.001	0.093	0.051	0.574
	200	0.003	0.476	0.249	3.114
	300	0.009	1.445	0.764	10.009
PuSe	100	0.002	0.146	0.139	1.811
	200	0.003	0.277	0.694	9.767
	300	0.025	4.531	2.260	34.205
PuTe	100	0.008	1.130	0.518	8.169
	200	0.019	2.556	1.183	20.181
	300	0.085	18.918	8.077	180.971

Table 5.17 Ultrasonic attenuation due to thermoelastic loss $(\alpha/f^2)_{th}$ and due to phonon-phonon interaction $((\alpha/f^2)_{Akh,l}$ for longitudinal wave and $(\alpha/f^2)_{Akh,S}$ for shear wave polarized along $\langle \bar{1}10 \rangle$) of the semiconductors in the temperature range 100-300K in the unit 10^{-18} Np s^2/cm along $\langle 111 \rangle$ direction.

Semiconductor	Temperature [K]	$(\alpha/f^2)_{th}$	$(\alpha/f^2)_{Akh,l}$	$(\alpha/f^2)_{Akh,S}$
SnTe	100	0.007	1.252	7.229
	200	0.012	2.646	16.572
	300	0.018	4.320	29.664
EuSe	100	0.022	3.699	23.238
	200	0.039	8.579	58.223
	300	0.050	12.481	92.276
CdO	100	0.031	1.828	22.491
	200	0.061	5.543	64.453
	300	0.077	8.371	100.491
SmS	100	0.026	3.773	21.412
	200	0.037	7.216	43.116
	300	0.046	10.237	66.080

Table 5.18 Ultrasonic attenuation due to thermoelastic loss $(\alpha/f^2)_{th}$ and due to phonon-phonon interaction $((\alpha/f^2)_{Akh,l}$ for longitudinal wave and $(\alpha/f^2)_{Akh,S}$ for shear wave polarized along $\langle \bar{1}10 \rangle$ direction) of the semiconductors in the temperature range 100-300K in the unit 10^{-18} Np s^2/cm along $\langle 111 \rangle$ direction.

Semiconductor	Temperature [K]	$(\alpha/f^2)_{th}$	$(\alpha/f^2)_{Akh,l}$	$(\alpha/f^2)_{Akh,S}$
NpS	100	0.003	0.377	1.500
	200	0.006	0.959	3.966
	300	0.012	2.241	9.950
NpSe	100	0.003	0.485	2.034
	200	0.013	2.379	10.635
	300	0.028	5.766	27.931
PuS	100	0.001	0.079	0.387
	200	0.002	0.404	2.105
	300	0.057	1.230	6.776
PuSe	100	0.002	0.235	1.223
	200	0.006	1.192	6.606
	300	0.017	3.851	23.161
PuTe	100	0.006	0.959	5.522
	200	0.011	2.171	13.659
	300	0.061	15.917	122.739

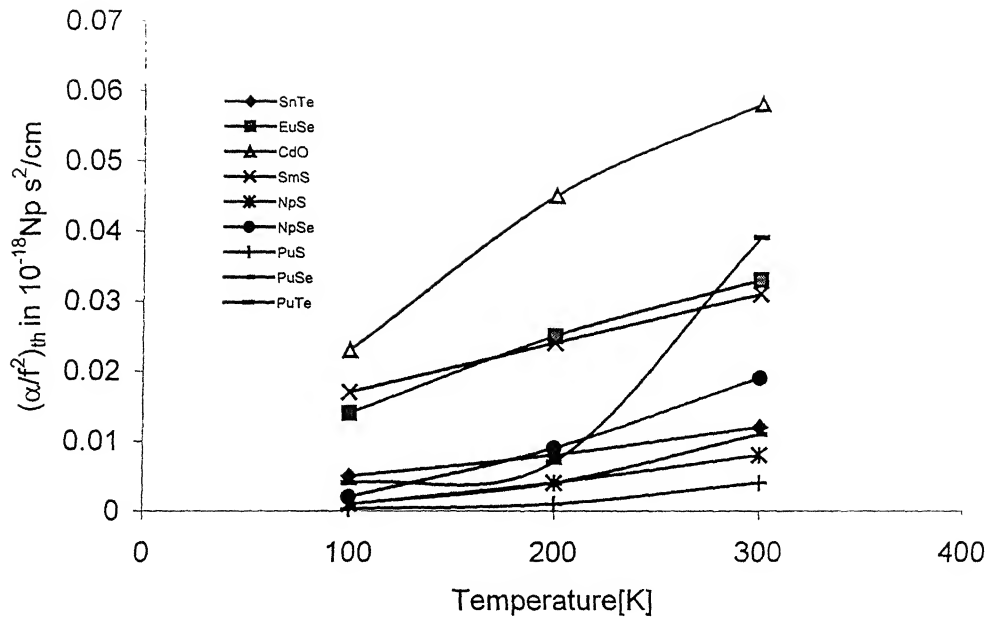


Fig.5.1 $(\alpha/f^2)_{th}$ vs. temperature along $\langle 100 \rangle$ direction

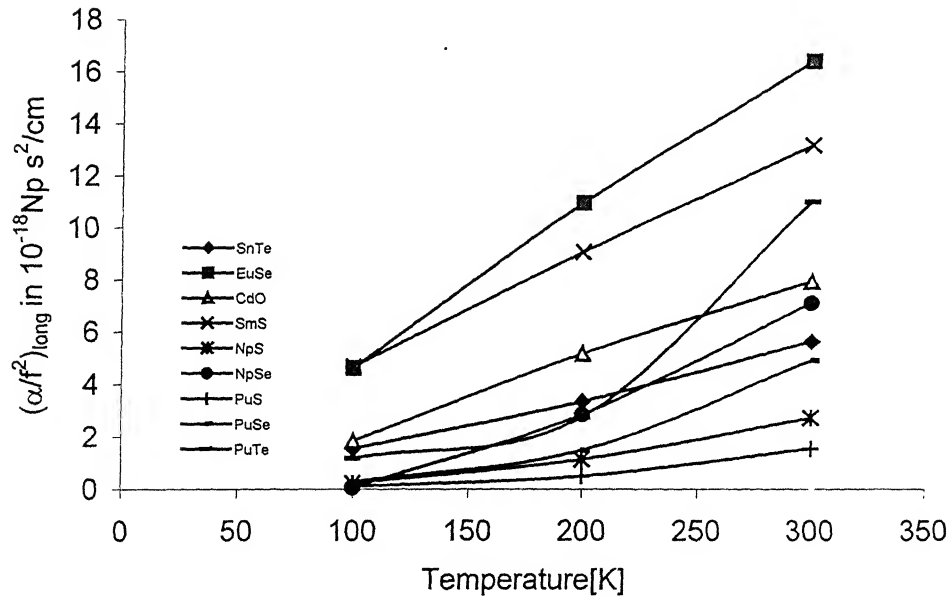


Fig.5.2 $(\alpha/f^2)_{long}$ vs. temperature along $\langle 100 \rangle$ direction

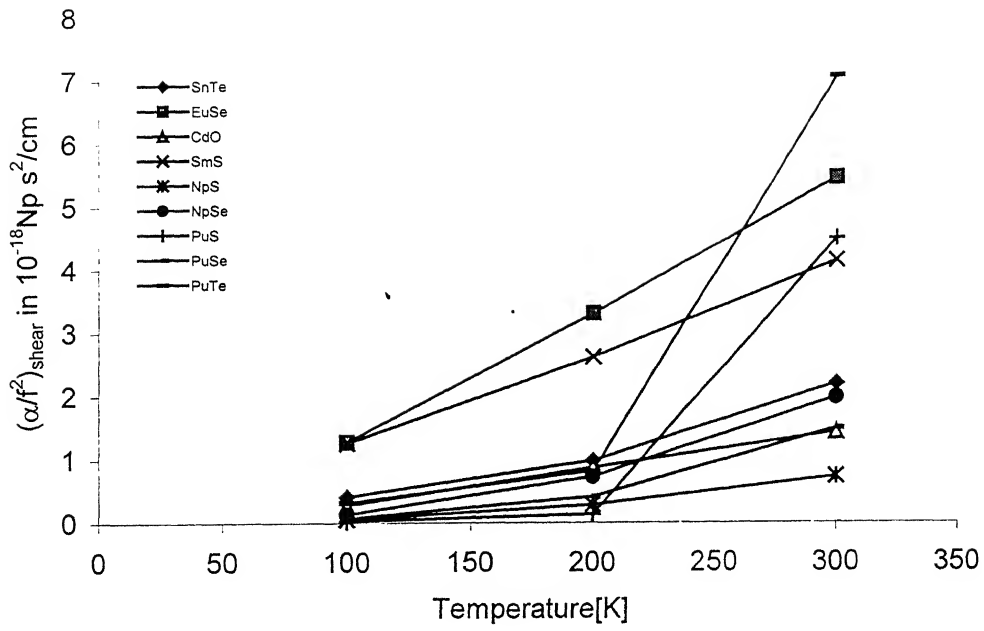


Fig.5.3 $(\alpha/f^2)_{\text{shear}}$ vs temperature along $\langle 100 \rangle$ direction

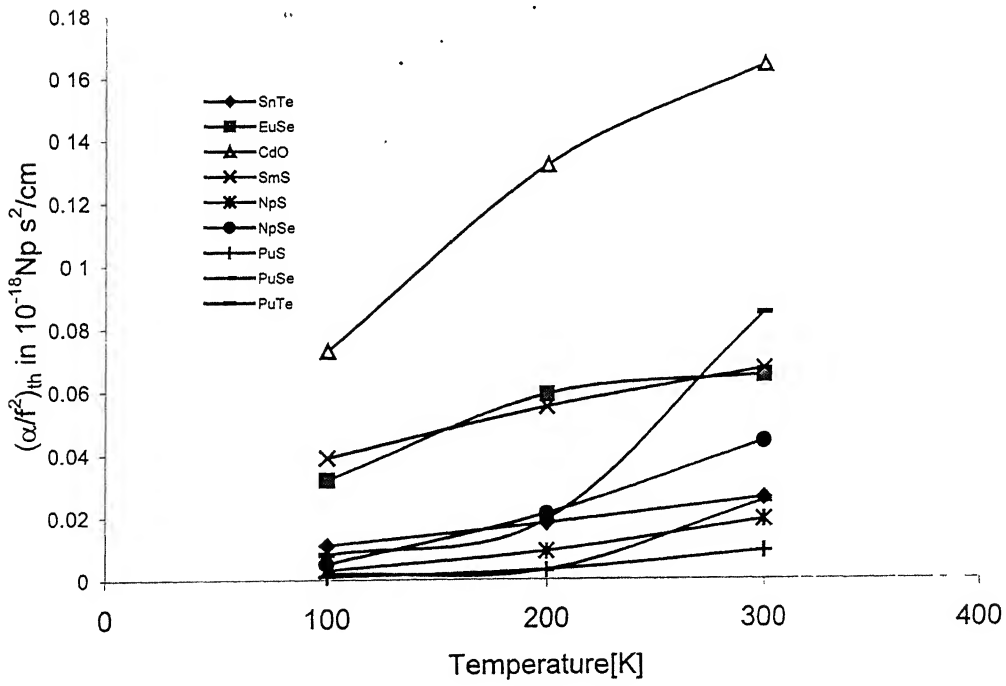


Fig.5.4 $(\alpha/f^2)_{\text{th}}$ vs. temperature along $\langle 110 \rangle$ direction

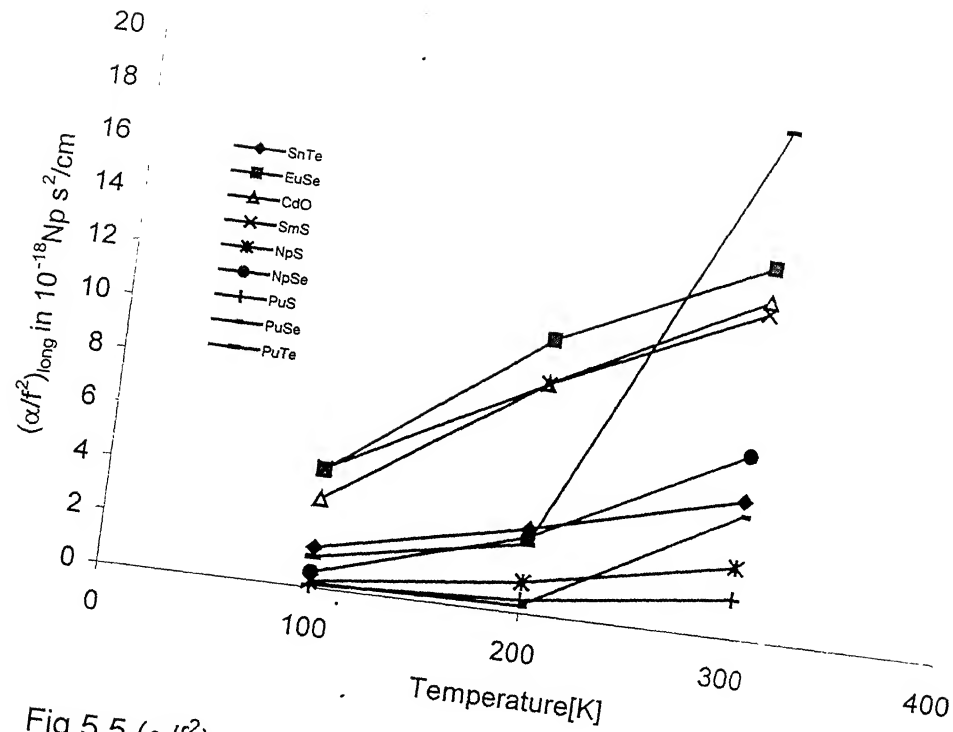


Fig.5.5 $(\alpha/f^2)_{\text{long}}$ vs. temperature along $\langle 110 \rangle$ direction

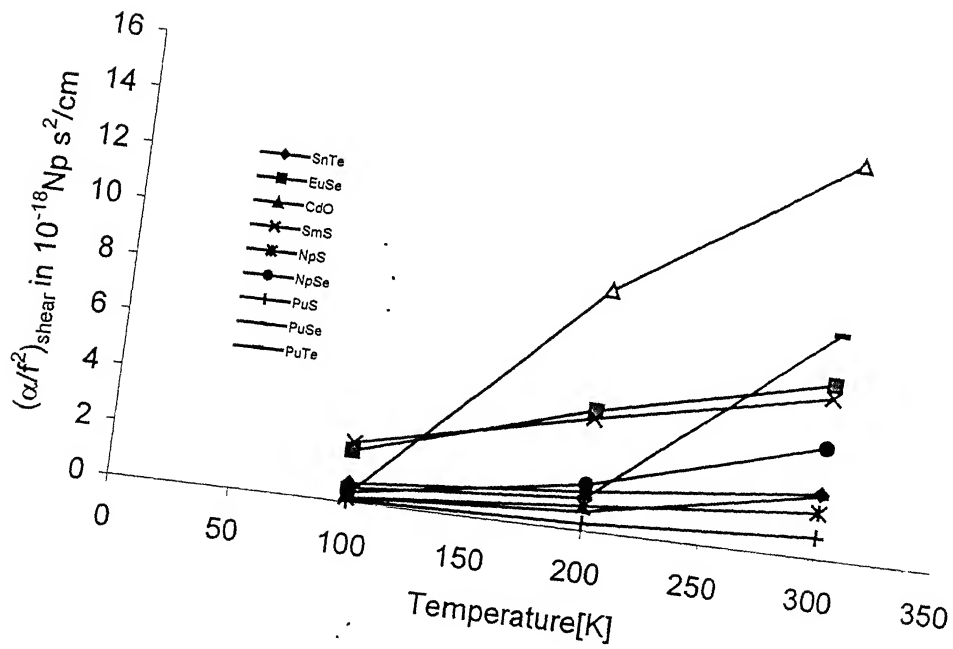


Fig.5.6 $(\alpha/f^2)_{\text{shear}}$ vs. temperature along $\langle 110 \rangle$ direction shear wave polarized along $\langle 001 \rangle$ direction

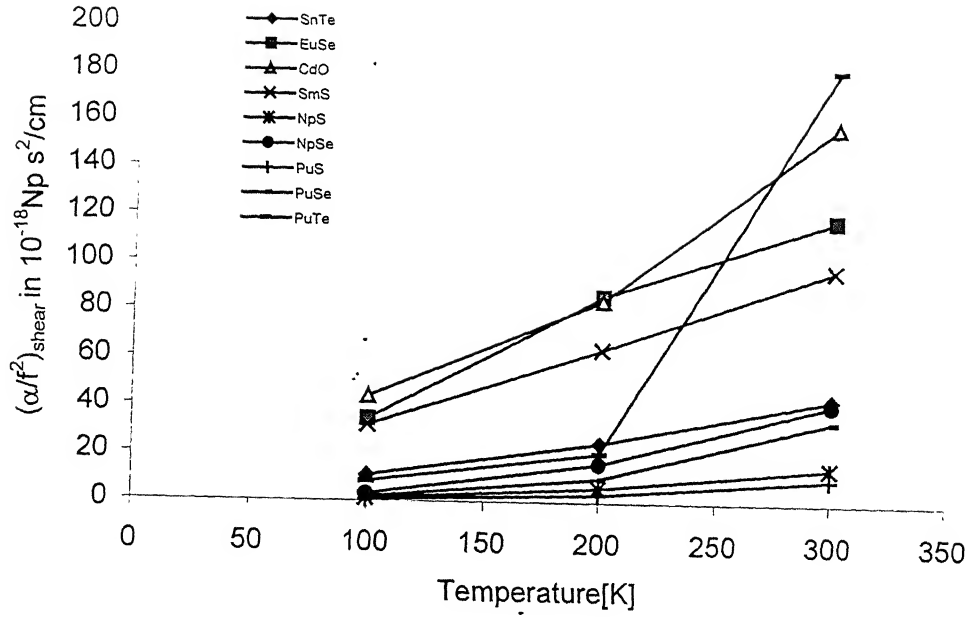


Fig.5.7 $(\alpha/f^2)_{\text{shear}}$ vs. temperature along $\langle 110 \rangle$ direction shear wave polarized along $\langle 1\bar{1}0 \rangle$ direction

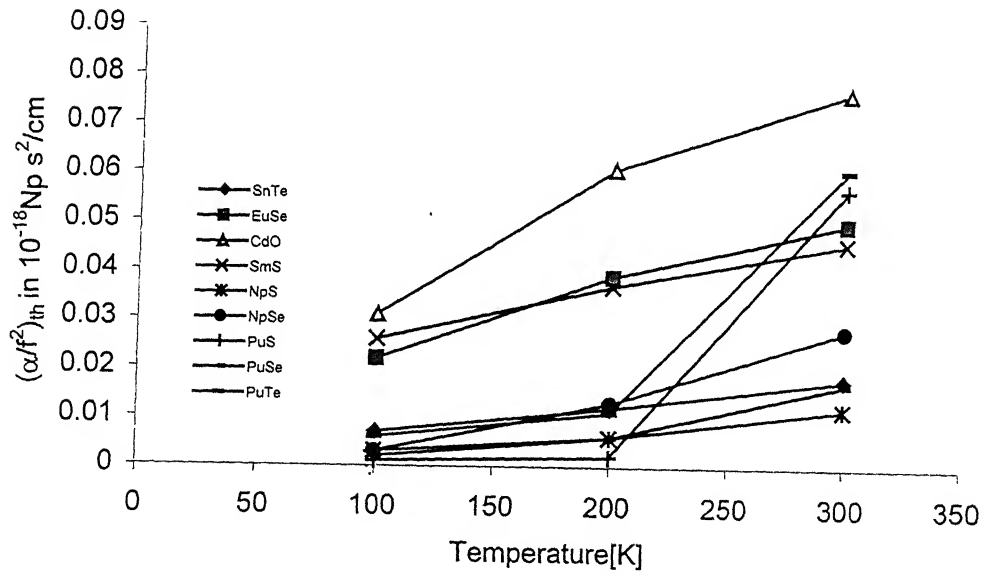


Fig.5.8 $(\alpha/f^2)_{\text{th}}$ vs. temperature along $\langle 111 \rangle$ direction

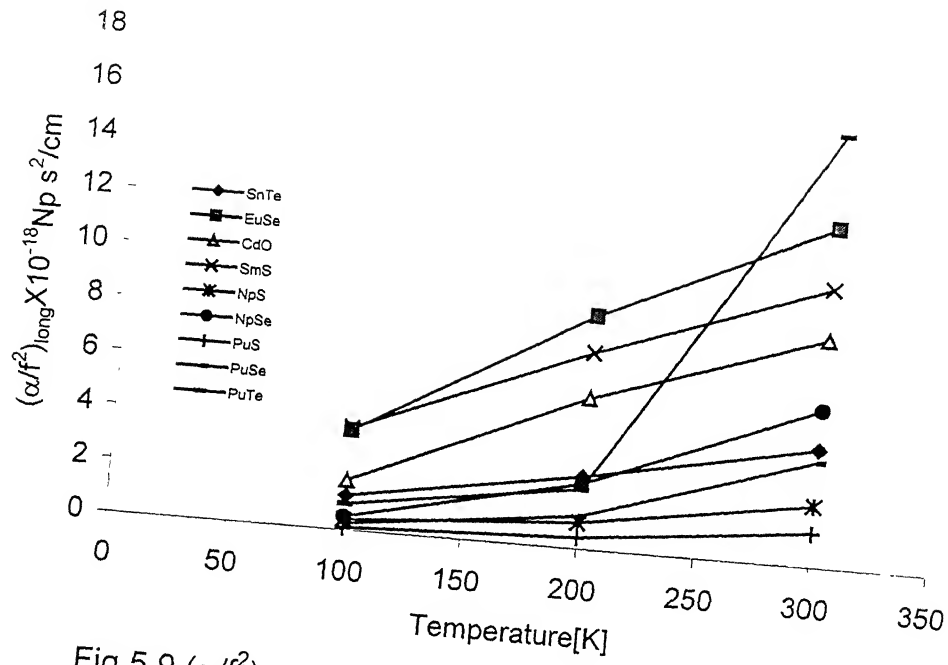


Fig.5.9 $(\alpha/f^2)_{\text{long}}$ vs. temperature along $\langle 111 \rangle$ direction

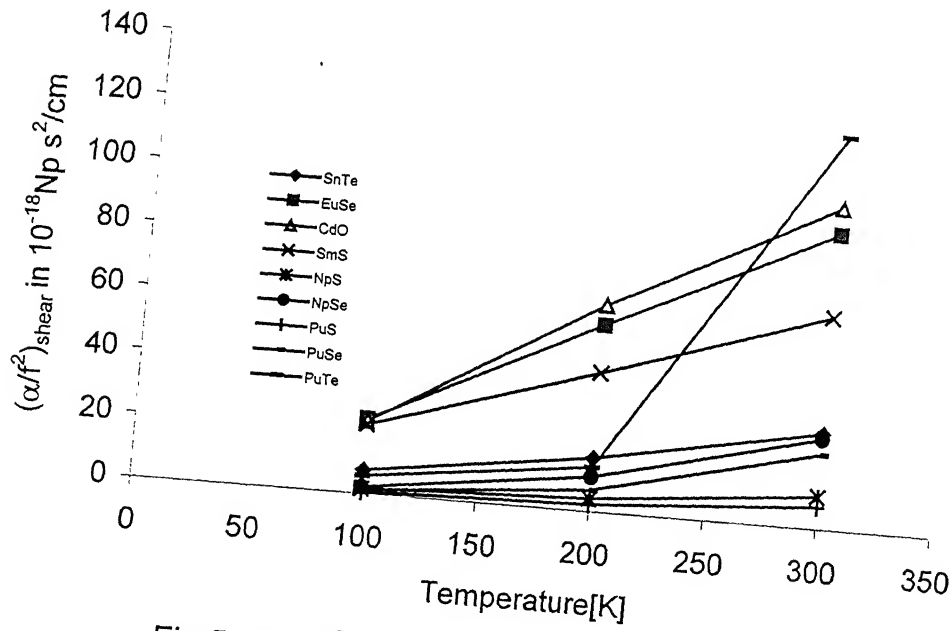


Fig.5.10 $(\alpha/f^2)_{\text{shear}}$ vs. temperature along $\langle 111 \rangle$ direction
shear wave polarized along $\langle \bar{1}10 \rangle$ direction

References

1. A.Akhiezer, J.Phys.(USSR) 1,277(1939).
2. H.E.Bömmel and K. Dransfeld, Phys. Rev. 117,1245(1960).
3. T.O.Woodruff and H.Ehrenreich, Phys. Rev. 123,1553(1961).
4. W.P.Mason, Physical Acoustics, (Academic Press, New York,1965), Vol. IIIB, Ch.-6.
5. J.R.Bae and S.Yun, Jpn.J.Appl.Phys.37,2801(1998).
6. R.E.Sirvent, B.Tan, I.Abdelraziq, S.S.Yun and F.B.Stumpf, J.Acost. Soc. Am. 93,819 (1993).
7. T.Stepinski and P.Wu, A.I.P.Conf. Proc. 497,431(1999).
8. J.A.Eiras, J.Alloy Compd.(Switzerland) 310,68(2000).
9. V.P.Matsokin and G.A.Petchenko, Low Temp.Phys. 26,517(2000).
10. H.Ogi, T.Hamaguchi and M.Hirao, Metall. Mater. Trans. A, Phys. Metall. Mater. Sc. (USA) 31A,1121(2000).
11. S.Ahmed, R.B.Thompson, Rev. of progress in quantative nondestructive evaluations, San Diego (A 27 July-1Aug.1997)(New York, NY USA, Plenum 1998) 2,1649(1998).
12. G.P.Rodrigue, Proc. IEEE 53,1428(1965).
13. W.Grofut, Microwave J. 10,65(1967).
14. R.W.Damon, IEEE spectrum 87(1967).
15. P.D. Southgate, Proc. Roy. Soc. (London) 76,385(1960).
16. J.Lamb, M.Redwood and Z.Stlinschlifer, Phys. Rev.Lett. 3,28(1959).
17. B.R.Dobbs, B.B.Chick and R.Trüll, Phys. Rev.Lett. 3,332(1959).
18. V.Celli, M.Kabber, T.Ninomeya and R. Thompson, Phys. Rev. 131,58(1963).
19. R.R.Yadav and K.Shanker, Ultrasonics International'93 conference proceedigs (p.459).
20. R.K.Singh, D.Phil. thesis submit to University of Allahabad on "Study of Ultrasonic Attenuation" (1993).
21. R.W.F.Wyckoff, Crystal Structure, (Interscience Publishers,New York, 2nd edition, 1963), 2nd edition.
22. P.Wachter, M.Filzmoser and J.Rebizant, Physica B293,199(2001).
23. M.Born and J.E.Mayer, Z.Phys. 75,1(1932).
24. K.Brugger, Phys. Rev. 133,A1611(1964).

25. G.Leibfried and W. Ludwig, in Solid State Physics, (edited by F.Seitz and D.Turnbull), Academic Press, New York,1961), Vol.12.
26. S.Mori and Y.Hiki, J.Phys. Soc. Jpn. 45,1449(1978).
27. M.P.Tosi, in Solid State Physics, (edited by F.Seitz and D.Turnbull), Academic Press, New York,1964), Vol.16.
28. W.P.Mason, J.Acoust. Soc. Am. 64,529(1978).
29. D.E.Gray (ed.), AIP Handbook, (McGraw Hill Book Company, New York), 3rd edition.
30. E.D. Debyatkova, V.P.Zhuze, A.V. Golubkov, V.M.Sergeeva and I.A. Smirnov, Soviet Physics-Solid State 6,343(1964).
31. V.P.Zhuze, A.V. Golubkov, E.V.Goncharova, T.I.Komarova and V.M.Sergeeva, Soviet Physics-Solid State 6,213(1964).
32. J.Shanker and G.D.Jain, Phys.Rev. B27,2515(1983).
33. U.C.Srivastava, Phys.Rev. B21,2602(1980).
34. D.S.Puri and M.P.Verma, Solid Stat. Commn. 18,1295(1976).
35. S.K.Kor and Kailash, Ind. J.Pure Appl. Phys. 24,179(1986).
36. R.R.Yadav and D.Singh, J.Phys.Soc.Jpn. 70,1825(2001).
37. R.C.Hanson, J.Phys. Chem. Solids 28,475(1967).
38. S.S.Shukla and S.S.Yun, J.Acoust.Soc.Am. 70,1723(1983).

CHAPTER-6

Effect of Concentration on Ultrasonic Attenuation in Metallic Alloys at Room Temperature

6.1 Introduction

In the preceding chapters ultrasonic attenuation has been studied in metallic, dielectric and semiconducting substances in wide temperature range along various crystallographic directions. Although the ultrasonic attenuation has been studied in different type materials by different methods recently [1-5]. Only few studies in alloys have been reported on the phonon-phonon interaction mechanism and thermoelastic loss mechanism causing ultrasonic attenuation.

In the present investigation metallic alloys $\text{Cu}_{100-x}\text{Pt}_x$, $\text{Ag}_{100-x}\text{Pt}_x$ and $\text{Au}_{100-x}\text{Pt}_x$ (where $x=1, 2, 3$ and 4) are taken for the study. The phonon viscosity and thermoelastic losses are obtained for longitudinal and shear waves along $\langle 100 \rangle$, $\langle 110 \rangle$ and $\langle 111 \rangle$ directions of propagation at room temperature. The investigation of Akhiezer damping (phonon-viscosity loss) and thermoelastic mechanism in metallic alloys $\text{Cu}_{100-x}\text{Pt}_x$, $\text{Ag}_{100-x}\text{Pt}_x$ and $\text{Au}_{100-x}\text{Pt}_x$ (where $x=1, 2, 3$ and 4) at room temperature lead to significant variation in the attenuation coefficient according to different composition of Pt in Cu, Ag and Au metals. The study is made starting with nearest neighbor distance and hardness parameter at room temperature over composition variation of Pt in Cu, Ag and Au metals.

6.2 Theory

6.2.1 Second and third order elastic constants (SOEC and TOEC)

The potential used for evaluation of SOEC and TOEC of the form

$$\phi(R) = \phi(c) + \phi(r) \quad (6.1)$$

Where $\phi(c)$ is electrostatic potential and $\phi(r)$ is the repulsive potential given as

$$\phi(c) = \pm e^2/r \quad \text{and} \quad \phi(r) = A \exp(-r/b) \quad (6.2)$$

Where e is the electronic charge, r is the nearest neighbor distance and A is a parameter, given as in eqn. (2.11) of chapter II.

Following Brugger [6] definition of elastic constants and starting from nearest neighbor distance and hardness parameter of the substance and taking interaction effective upto second nearest neighbor distance, SOEC and TOEC have been obtained at absolute zero of temperature using Tables (2.2) and (2.3) in chapter II. According to lattice dynamics developed by Leibfried and Ludwig [7], lattice energy changes with temperature, hence adding vibrational energy contribution to static elastic constants, one gets C_{IJ} and C_{IJK} at required temperature as

$$C_{IJ} = C_{IJ}^0 + C_{IJ}^{\text{Vib}} \quad (6.3)$$

$$C_{IJK} = C_{IJK}^0 + C_{IJK}^{\text{Vib}} \quad (6.4)$$

Where superscript 0 has been used to denote SOEC and TOEC at 0 K (static elastic constants) and superscript Vib has been used to denote temperature dependence SOEC and TOEC.

C_{IJ}^{Vib} and C_{IJK}^{Vib} are defined as

$$C_{IJ}^{\text{Vib}} = l_1 k \left(\frac{\partial C_{IJ}}{\partial r} \right)_{r=r_0} + \frac{f_{ij}^{\text{Vib}}}{TVc} \quad (6.5)$$

$$C_{IJK}^{\text{Vib}} = l_1 k \left(\frac{\partial C_{IJK}}{\partial r} \right)_{r=r_0} + \frac{f_{ijk}^{\text{Vib}}}{TVc} \quad (6.6)$$

where f_{IJ}^{Vib} and f_{IJK}^{Vib} are various constants, given as in Table 2.4 of chapter II. l_1 is the function of nearest neighbor distance and hardness parameters and for f.c.c. given as in equ.(2.25) in chapter II.

6.2.2 Ultrasonic attenuation

In the secondary phase of present evaluations Mason-Bateman [8] theory is still widely used successfully to study the ultrasonic attenuation at higher temperatures ($\cong 300\text{K}$) in solids. It is more reliable theory to study anharmonicity of the crystals as it involves elastic constants directly through non-linearity parameter 'D' in the evaluation of ultrasonic absorption coefficient (α).

The thermal relaxation time [8] for longitudinal wave is twice that of shear wave.

$$\tau_{th} = \tau_{sh} = \frac{1}{2} \tau_{long} = \frac{3K}{C_v \bar{V}^2} \quad (6.7)$$

K is thermal conductivity, C_v is specific heat per unit volume, \bar{V} is the Debye average velocity of ultrasonic wave as

$$\frac{3}{\bar{V}^3} = \frac{1}{V_l^3} + \frac{2}{V_s^3} \quad (6.8)$$

Thermoelastic loss [8] is obtained by

$$(\alpha/f^2)_{th} = \frac{4\pi^2 \langle \gamma_i^j \rangle^2 KT}{2\rho V_l^5} \quad (6.9)$$

$\langle \gamma_i^j \rangle$ is the average Gruneisen numbers; j is the direction of propagation and i is the mode of propagation. $\langle \gamma_i^j \rangle$ is related to SOEC and TOEC and are evaluated with the use of Mason's table for number of pure modes and then average is taken over total number of pure modes [8] and presented in Appendix A. ρ is the density of the material and T is the temperature in Kelvin scale.

For the Akhiezer loss (phonon-viscosity loss) ' α_{Akh} ', one has to evaluate the anharmonic parameter (acoustic coupling constant) 'D', which is the measure of the conversion of acoustic energy into thermal energy and is obtained by

$$D = 9 \langle (\gamma_i^j)^2 \rangle - (3 \langle \gamma_i^j \rangle^2 C_v T) / E_0 . \quad (6.10)$$

The ultrasonic absorption coefficient over frequency square $(\alpha/f^2)_{Akh}$ (Akhiezer type loss) is given by ($\omega\tau \leq 1$) [8]

$$(\alpha/f^2) = \frac{E_0 (D/3) 4\pi^2 \tau}{2\rho V^3} \quad (6.11)$$

By determining D_{long} and D_{shear} for longitudinal and shear wave; $(\alpha/f^2)_{Akhlong}$ and $(\alpha/f^2)_{Akh shear}$ can be obtained.

The ultrasonic absorption coefficient over frequency square $(\alpha/f^2)_{th}$ due to thermoelastic loss is given by

$$(\alpha/f^2)_{th} = \frac{4\pi^2 \langle \gamma_i^j \rangle^2 KT}{2\rho V_{long}^5} \quad (6.12)$$

where symbols are having their usual meanings.

6.3 Evaluations, results and discussion

The ultrasonic attenuation is evaluated with the computation of SOEC and TOEC from nearest neighbor distance (r_0) [9] ($\text{Cu}_{99}\text{Pt}_1=2.5621\text{\AA}^0$, $\text{Cu}_{98}\text{Pt}_2=2.5642\text{\AA}^0$, $\text{Cu}_{97}\text{Pt}_3=2.5663\text{\AA}^0$, $\text{Cu}_{96}\text{Pt}_4=2.5684\text{\AA}^0$, $\text{Ag}_{99}\text{Pt}_1=2.889^0$, $\text{Ag}_{98}\text{Pt}_2=2.880\text{\AA}^0$, $\text{Ag}_{97}\text{Pt}_3=2.89\text{\AA}^0$, $\text{Ag}_{96}\text{Pt}_4=2.885\text{\AA}^0$, $\text{Au}_{99}\text{Pt}_1=2.888\text{\AA}^0$, $\text{Au}_{98}\text{Pt}_2=2.887\text{\AA}^0$, $\text{Au}_{97}\text{Pt}_3=2.886\text{\AA}^0$, $\text{Au}_{96}\text{Pt}_4=2.885\text{\AA}^0$) and hardness parameter [9] $b=0.315 \text{\AA}^0$ for all the alloys. The SOEC and TOEC are presented in Table 6.1 for all metallic alloys. The Grüneisen parameter are evaluated along $\langle 100 \rangle$, $\langle 110 \rangle$ and $\langle 111 \rangle$ directions for longitudinal and shear wave using Grüneisen Tables (Appendix A). Specific heat (C_V), internal energy density (E_0) and density (ρ) of the alloys are taken from the literature [10]. The electrical resistivity data are taken from the literature [11,12]; the thermal conductivity at the given composition for the alloys have been evaluated by applying Wiedeman Franz law. All the values of primary physical constants like thermal conductivity (K), specific heat (C_V), internal energy density (E_0) and density (ρ) of the alloys are presented in Table 6.2. The thermal relaxation time (τ_{th}) has been evaluated taking thermal conductivity at requisite composition with the help of eqn.(6.7). The ultrasonic absorption coefficient over frequency square $\left(\alpha/f^2\right)$ due to phonon-phonon interaction and thermoelastic loss has been evaluated at room temperature using eqns. (6.11) and (6.12). The evaluated ultrasonic absorption coefficient over frequency square $\left(\alpha/f^2\right)$ due to phonon-phonon interaction $((\alpha/f^2)_l$ for longitudinal wave and $(\alpha/f^2)_s$ for shear wave) and thermoelastic loss $(\alpha/f^2)_{th}$ are presented in Tables 6.7, 6.8 and 6.9 along $\langle 100 \rangle$, $\langle 110 \rangle$ and $\langle 111 \rangle$ direction for longitudinal wave and shear wave polarized along $\langle 100 \rangle$, $\langle 001 \rangle$ & $\langle \bar{1}10 \rangle$ and $\langle \bar{1}10 \rangle$ directions respectively.

It is clear from Table 6.1 that the values of SOEC of these alloys is approximately half of that as reported by Giri [13] and Salama [14] for other alloys like Cu-Ni, Nb-Mo etc. It is obvious from the Table 6.6 that the thermal relaxation time (τ_{th}) decreases for all alloys as the percentage of platinum increases. From the Table 6.7, it is clear that values of non-linearity 'D' for all alloys do not vary much with the composition along $\langle 100 \rangle$, $\langle 110 \rangle$ and $\langle 111 \rangle$ directions of propagating wave. Hence variation is not much affected by 'D' values, but the change is due to the variation of thermal conductivity at different

composition. The ratio of D_l/D_s along $\langle 100 \rangle$ direction is about 10-14, D_l/D_{s1} along $\langle 110 \rangle$ direction shear wave polarized along $\langle 001 \rangle$ is approximately between 2.5-7.5, D_{s2}/D_l along $\langle 110 \rangle$ direction shear wave polarized along $\langle 1\bar{1}0 \rangle$ is approximately between 1.4-1.8 and D_s/D_l along $\langle 111 \rangle$ direction shear wave polarized along $\langle \bar{1}10 \rangle$ is approximately between 1.16-1.33. Which is very much similar to other metallic crystals and metallic alloys [15-18]. It is obvious from the Tables 6.8-6.10 and Figs. 6.1-6.10, that attenuation over frequency square $(\alpha/f^2)_{Akh}$. due to phonon-viscosity mechanism is found to contribute a vital part of the total attenuation as compared to the thermoelastic part. Both $(\alpha/f^2)_{Akh}$. and $(\alpha/f^2)_{th}$ go on decreasing as the composition of platinum increases in these alloys $Cu_{100-x}Pt_x$, $Ag_{100-x}Pt_x$ and $Au_{100-x}Pt_x$ (where $x=1,2,3$ and 4). As the case of other metals [16-18], the thermoelastic attenuation $(\alpha/f^2)_{th}$ is found negligible in comparison to Akhiezer loss $(\alpha/f^2)_{Akh}$ in all directions. Generally the values of attenuation obtained in the present work are comparable with the values available for the other metals [16,18]. Although these conclusion leads one to conclude that the behavior of alloys are similar to that of metallic crystals [16,18]. Values of non-linearity parameter 'D' and Ultrasonic attenuation ' (α/f^2) ' are found to be unequal in different directions with different compositions. The orders of different parameters are found to be unequal in $\langle 100 \rangle$, $\langle 110 \rangle$ and $\langle 111 \rangle$ crystallographic directions with different compositions. The orders of different parameters are found to be same as in Cu-Ni alloys [19]. However experimental value [16] in copper metal is $97 \times 10^{-17} \text{ Np s}^2/\text{cm}$, which is good agreement with evaluated value of attenuation ($59 \times 10^{-17} \text{ Np s}^2/\text{cm}$ for $Cu_{99}Pt_1$) along $\langle 100 \rangle$ direction for longitudinal waves. It is obvious from the Tables 6.7-6.9 and figs. 6.1-6.10 that the values of $(\alpha/f^2)_{Akh}$ for longitudinal wave is greater than shear wave attenuation along $\langle 100 \rangle$ and $\langle 110 \rangle$ (shear wave polarized along $\langle 001 \rangle$ direction) directions, while the same values are less than that along $\langle 110 \rangle$ (shear wave polarized along $\langle 1\bar{1}0 \rangle$ direction) and $\langle 111 \rangle$ (shear wave polarized along $\langle \bar{1}10 \rangle$ direction) directions. Although the experimental values for the absorption at different composition are not available in literature, but the trend of the present values are the same as expected.

On the basis of the obtained results in the present work, it is established that the process of study of ultrasonic attenuation in metals at room temperature can be extended

successfully to the various composition of the original metals and one may know about the composition of metallic alloys after the knowledge of ultrasonic attenuation values of those metallic alloys. Thus it is concluded that present theoretical approach for metals can be extended for metallic alloys.

The Ultrasonic study in this region in these alloys would be applicable in engineering and material science.

Table6.1 Second and third order elastic constants (SOEC & TOEC) of the metallic alloys at room temperature i.e. 300K($\times 10^{11}$ Dyne/cm).

Alloys	C_{11}	C_{12}	C_{44}	C_{111}	C_{112}	C_{123}	C_{144}	C_{166}	C_{456}
Cu ₉₉ Pt ₁	6.957	2.002	2.298	-100.5	-8.362	2.267	3.713	-9.447	3.632
Cu ₉₈ Pt ₂	6.784	1.995	2.285	-98.85	-8.344	2.254	3.699	-9.378	3.620
Cu ₉₇ Pt ₃	6.717	1.986	2.275	-98.21	-8.309	2.241	3.687	-9.332	3.608
Cu ₉₆ Pt ₄	6.679	1.978	2.265	-97.84	-8.273	2.229	3.675	-9.291	3.596
Ag ₉₉ Pt ₁	5.821	1.081	1.347	-90.57	-4.401	0.722	2.304	-5.471	2.253
Ag ₉₈ Pt ₂	5.694	1.078	1.346	-89.22	-4.372	0.719	2.301	-5.482	2.250
Ag ₉₇ Pt ₃	5.652	1.083	1.347	-88.76	-4.411	0.723	2.307	-5.473	2.256
Ag ₉₆ Pt ₄	5.632	1.085	1.349	-88.55	-4.419	0.729	2.310	-5.478	2.2590
Au ₉₉ Pt ₁	5.250	1.131	1.374	-79.41	-4.664	0.955	2.303	-5.619	2.250
Au ₉₈ Pt ₂	5.140	1.132	1.372	-78.29	-4.679	0.960	2.304	-5.604	2.251
Au ₉₇ Pt ₃	5.104	1.134	1.374	-77.92	-4.689	0.960	2.307	-5.608	2.555
Au ₉₆ Pt ₄	5.551	1.126	1.387	-82.35	-4.588	0.954	2.316	-5.693	2.258

Table 6.2 Thermal conductivity (K) in 10^7 erg/cm s K, specific heat (C_v) in 10^7 erg/cc K, density (ρ) in g/cc and energy density (E_0) in 10^9 erg/cc of the metallic alloys at room temperature.

Alloys	K	C_v	ρ	E_0
Cu ₉₉ Pt ₁	3.130	3.350	9.132	7.275
Cu ₉₈ Pt ₂	2.630	3.380	9.312	7.301
Cu ₉₇ Pt ₃	2.190	3.370	9.450	7.295
Cu ₉₆ Pt ₄	1.750	3.390	9.631	7.323
Ag ₉₉ Pt ₁	3.340	2.390	10.62	5.778
Ag ₉₈ Pt ₂	2.370	2.401	10.71	5.804
Ag ₉₇ Pt ₃	1.990	2.400	10.82	5.823
Ag ₉₆ Pt ₄	1.530	2.360	10.72	5.728
Au ₉₉ Pt ₁	2.160	2.420	19.30	6.187
Au ₉₈ Pt ₂	1.750	2.430	19.30	6.190
Au ₉₇ Pt ₃	1.470	2.431	19.32	6.202
Au ₉₆ Pt ₄	1.230	2.440	19.34	6.177

Table 6.3 Ultrasonic velocities (V_l for longitudinal wave, V_s for shear wave and \bar{V} - Debye average velocity) in 10^5 cm/s and thermal relaxation time (τ_{th}) in 10^{-11} sec of the alloys at room temperature.

Alloys	V_l	V_s	\bar{V}	τ_{th}
Cu ₉₉ Pt ₁	2.760	1.586	1.741	9.250
Cu ₉₈ Pt ₂	2.699	1.571	1.722	7.872
Cu ₉₇ Pt ₃	2.666	1.551	1.701	6.741
Cu ₉₆ Pt ₄	2.633	1.534	1.681	5.481
Ag ₉₉ Pt ₁	2.343	1.127	1.252	26.726
Ag ₉₈ Pt ₂	2.306	1.121	1.245	19.110
Ag ₉₇ Pt ₃	2.286	1.116	1.239	16.203
Ag ₉₆ Pt ₄	2.292	1.122	1.245	12.541
Au ₉₉ Pt ₁	1.649	0.844	0.934	30.670
Au ₉₈ Pt ₂	1.632	0.843	0.933	24.810
Au ₉₇ Pt ₃	1.625	0.843	0.933	20.843
Au ₉₆ Pt ₄	1.694	0.847	0.939	17.148

Table 6.4 Average of ultrasonic Grüneisen parameters ($\langle\gamma_l^j\rangle_l$ for longitudinal wave), average of square ultrasonic Grüneisen parameters ($\langle(\gamma_l^j)^2\rangle_{long}$ for longitudinal wave and $\langle(\gamma_l^j)^2\rangle_{shear}$ for shear wave) and acoustic coupling constants (D_l for longitudinal wave and D_s for shear wave) of the alloys at room temperature along $\langle 100 \rangle$ crystallographic direction.

Alloys	$\langle\gamma_l^j\rangle_l$	$\langle(\gamma_l^j)^2\rangle_{long}$	$\langle(\gamma_l^j)^2\rangle_{shear}$	D_l	D_s
Cu ₉₉ Pt ₁	0.479	1.671	0.144	14.086	1.298
Cu ₉₈ Pt ₂	0.485	1.707	0.146	14.381	1.314
Cu ₉₇ Pt ₃	0.487	1.720	0.147	14.495	1.319
Cu ₉₆ Pt ₄	0.488	1.728	0.147	14.556	1.321
Ag ₉₉ Pt ₁	0.472	1.920	0.130	16.451	1.171
Ag ₉₈ Pt ₂	0.477	1.949	0.131	16.688	1.181
Ag ₉₇ Pt ₃	0.480	1.958	0.132	16.769	1.184
Ag ₉₆ Pt ₄	0.480	1.962	0.132	16.805	1.186
Au ₉₉ Pt ₁	0.472	1.811	0.133	15.516	1.200
Au ₉₈ Pt ₂	0.478	1.839	0.134	15.747	1.212
Au ₉₇ Pt ₃	0.480	1.848	0.135	15.824	1.216
Au ₉₆ Pt ₄	0.459	1.736	0.131	14.872	1.177

Table 6.5 Average of ultrasonic Grüneisen parameters ($\langle\gamma_l^j\rangle_l$ for longitudinal wave), average of square ultrasonic Grüneisen parameters ($\langle(\gamma_l^j)^2\rangle_{long}$ for longitudinal wave,

$\langle(\gamma_i^j)^2\rangle_{\text{Shear1}}$ for shear wave polarized along $\langle 001 \rangle$ direction and $\langle(\gamma_i^j)^2\rangle_{\text{Shear2}}$ for shear wave polarized along $\langle 1\bar{1}0 \rangle$ direction) and acoustic coupling constants (D_l for longitudinal wave, D_{S1} for shear wave polarized along $\langle 001 \rangle$ direction and D_{S2} for shear wave polarized along $\langle 1\bar{1}0 \rangle$ direction) of the metallic alloys at room temperature along $\langle 110 \rangle$ crystallographic direction.

Alloys	$\langle\gamma_i^j\rangle_l$	$\langle(\gamma_i^j)^2\rangle_{\text{long}}$	$\langle(\gamma_i^j)^2\rangle_{\text{sh1}}$	$\langle(\gamma_i^j)^2\rangle_{\text{sh2}}$	D_l	D_{S1}	D_{S2}
Cu ₉₉ Pt ₁	-0.742	1.914	0.646	2.379	14.943	5.816	21.413
Cu ₉₈ Pt ₂	-0.755	1.981	0.709	2.426	15.452	6.3804	21.834
Cu ₉₇ Pt ₃	-0.760	2.004	0.728	2.445	15.632	6.552	22.004
Cu ₉₆ Pt ₄	-0.762	2.014	0.734	2.456	15.709	6.603	22.104
Ag ₉₉ Pt ₁	-0.699	1.878	0.191	2.941	15.080	1.715	26.467
Ag ₉₈ Pt ₂	-0.710	1.919	0.202	2.980	15.389	1.813	26.822
Ag ₉₇ Pt ₃	-0.714	1.932	0.206	2.993	15.501	1.853	26.852
Ag ₉₆ Pt ₄	-0.716	1.940	0.208	2.999	15.552	1.875	26.994
Au ₉₉ Pt ₁	-0.709	1.838	0.268	2.716	14.769	2.407	24.442
Au ₉₈ Pt ₂	-0.720	1.882	0.284	2.754	15.102	2.559	24.790
Au ₉₇ Pt ₃	-0.724	1.897	0.292	2.767	15.222	2.624	24.900
Au ₉₆ Pt ₄	-0.680	1.722	0.232	2.614	13.851	2.092	23.525

Table 6.6 Average of ultrasonic Grüneisen parameters ($\langle\gamma_i^j\rangle$) and acoustic coupling constants (D_l and D_s) of the alloys at room temperature along $\langle 111 \rangle$ crystallographic direction. (* shear wave polarized along $\langle 1\bar{1}10 \rangle$).

Alloys	$\langle\gamma_i^j\rangle$	$\langle(\gamma_i^j)^2\rangle_{\text{long}}$	$\langle(\gamma_i^j)^2\rangle_{\text{shear}}^*$	D_l	D_s^*
Cu ₉₉ Pt ₁	-0.563	1.526	1.603	12.417	14.428
Cu ₉₈ Pt ₂	-0.571	1.568	1.635	12.754	14.711
Cu ₉₇ Pt ₃	-0.574	1.583	1.647	12.876	14.826
Cu ₉₆ Pt ₄	-0.575	1.590	1.655	12.932	14.894
Ag ₉₉ Pt ₁	-0.574	1.565	1.993	12.856	17.936
Ag ₉₈ Pt ₂	-0.581	1.566	2.019	12.843	18.168
Ag ₉₇ Pt ₃	-0.583	1.607	2.027	13.204	18.245
Ag ₉₆ Pt ₄	-0.584	1.613	2.031	13.248	18.280
Au ₉₉ Pt ₁	-0.567	1.526	1.837	12.600	16.535
Au ₉₈ Pt ₂	-0.573	1.557	1.863	12.855	16.764
Au ₉₇ Pt ₃	-0.576	1.568	1.871	12.946	16.837
Au ₉₆ Pt ₄	-0.549	1.441	1.770	11.895	15.931

Table 6.7 Ultrasonic attenuation due to phonon-phonon interaction $[(\alpha/f^2)_{\text{Akh long}}$ for longitudinal wave and $(\alpha/f^2)_{\text{Akh shear}}$ for shear wave] and thermoelastic loss $(\alpha/f^2)_{\text{th}}$ of the alloys at room temperature along $\langle 100 \rangle$ in $10^{-17} \text{ Np s}^2/\text{cm}$.

Alloys	$(\alpha/f^2)_{\text{th}}$	$(\alpha/f^2)_{\text{Akh long}}$	$(\alpha/f^2)_{\text{Akh shear}}$
Cu ₉₉ Pt ₁	0.265	59.240	14.379
Cu ₉₈ Pt ₂	0.250	54.168	12.552
Cu ₉₇ Pt ₃	0.220	47.764	11.028
Cu ₉₆ Pt ₄	0.184	39.855	9.153
Ag ₉₉ Pt ₁	0.537	223.506	71.499
Ag ₉₈ Pt ₂	0.418	169.167	52.045
Ag ₉₇ Pt ₃	0.366	146.978	44.573
Ag ₉₆ Pt ₄	0.281	112.199	33.769
Au ₉₉ Pt ₁	1.107	408.082	117.891
Au ₉₈ Pt ₂	0.966	346.008	96.502
Au ₉₇ Pt ₃	0.833	295.939	81.424
Au ₉₆ Pt ₄	0.519	201.004	63.702

Table 6.8 Ultrasonic attenuation due to phonon-phonon interaction $[(\alpha/f^2)_{\text{Akh long}}$ for longitudinal wave and $(\alpha/f^2)_{\text{Akh shear}}$ for shear wave] and thermoelastic loss $(\alpha/f^2)_{\text{th}}$ of the alloys at room temperature along $\langle 110 \rangle$ in $10^{-17} \text{ Np s}^2/\text{cm}$.

Alloys	$(\alpha/f^2)_{\text{th}}$	$(\alpha/f^2)_{\text{Akh long}}$	$(\alpha/f^2)^*_{\text{Akh shear1}}$	$(\alpha/f^2)^{\#}_{\text{Akh shear2}}$
Cu ₉₉ Pt ₁	0.636	62.845	64.407	237.144
Cu ₉₈ Pt ₂	0.607	58.517	61.822	211.562
Cu ₉₇ Pt ₃	0.536	51.509	58.226	183.990
Cu ₉₆ Pt ₄	0.450	43.047	54.789	153.5167
Ag ₉₉ Pt ₁	1.176	204.877	104.635	1615.222
Ag ₉₈ Pt ₂	0.925	156.000	79.920	1182.336
Ag ₉₇ Pt ₃	0.813	134.752	69.733	1009.655
Ag ₉₆ Pt ₄	0.625	103.839	53.397	768.619
Au ₉₉ Pt ₁	2.491	388.440	236.432	2401.016
Au ₉₈ Pt ₂	2.081	320.628	202.937	1974.602
Au ₉₇ Pt ₃	1.899	284.688	175.782	1502.053
Au ₉₆ Pt ₄	1.137	187.201	113.206	1273.247

* shear wave polarized along $\langle 001 \rangle$ direction

shear wave polarized along $\langle 1\bar{1}0 \rangle$ direction

Table 6.9 Ultrasonic attenuation due to phonon-phonon interaction $[(\alpha/f^2)_{\text{Akh long}}$ for longitudinal wave and $(\alpha/f^2)_{\text{Akh shear}}$ for shear wave] and thermoelastic loss $(\alpha/f^2)_{\text{th}}$ of the alloys at room temperature along $\langle 111 \rangle$ in $10^{-17} \text{Np s}^2/\text{cm}$.

Alloys	$(\alpha/f^2)_{\text{th}}$	$(\alpha/f^2)_{\text{Akh long}}$	$(\alpha/f^2)^*_{\text{Akh shear}}$
Cu ₉₉ Pt ₁	0.366	52.223	159.592
Cu ₉₈ Pt ₂	0.347	48.302	142.545
Cu ₉₇ Pt ₃	0.306	42.430	123.969
Cu ₉₆ Pt ₄	0.256	35.410	103.220
Ag ₉₉ Pt ₁	0.794	174.662	1094.492
Ag ₉₈ Pt ₂	0.618	130.186	800.841
Ag ₉₇ Pt ₃	0.541	115.733	686.786
Ag ₉₆ Pt ₄	0.416	88.453	520.504
Au ₉₉ Pt ₁	1.592	331.392	1624.263
Au ₉₈ Pt ₂	1.391	282.461	1335.353
Au ₉₇ Pt ₃	1.200	242.117	1127.787
Au ₉₆ Pt ₄	0.743	160.767	862.242

* shear wave polarized along $\langle 1\bar{1}0 \rangle$ direction

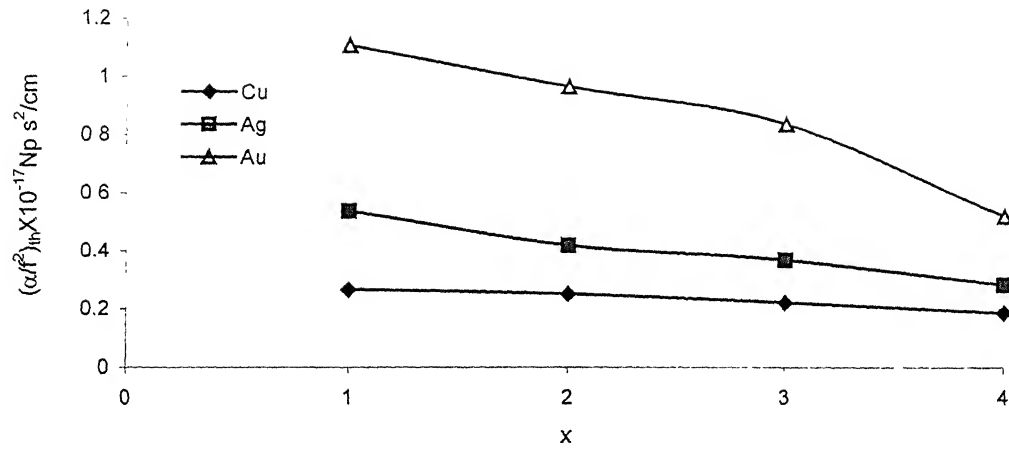


Fig. 6.1. $(\alpha/f^2)_{th}$ vs composition of Platinum(x) along $\langle 100 \rangle$ direction

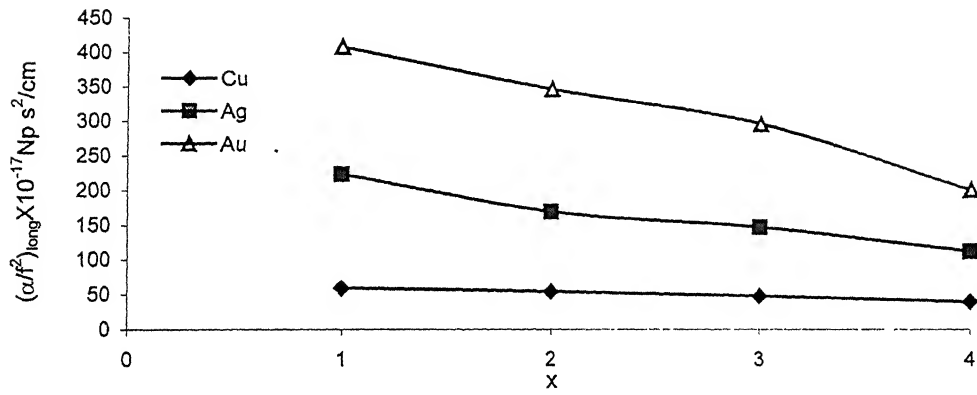


Fig. 6.2. $(\alpha/f^2)_{long}$ vs composition of Platinum(x) along $\langle 100 \rangle$ direction.

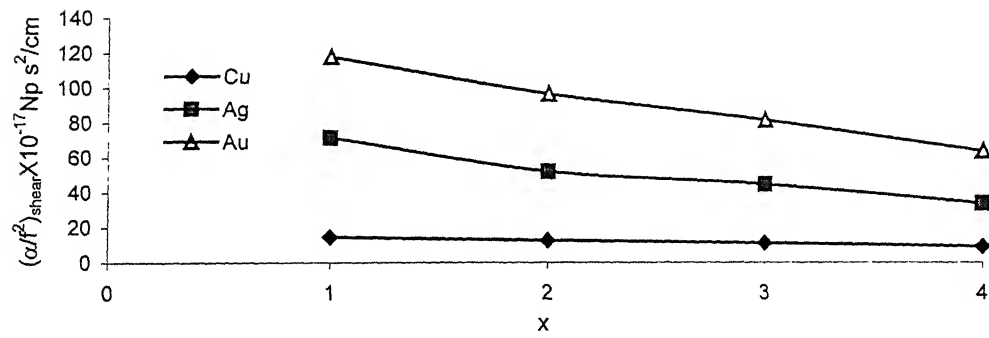


Fig. 6.3. $(\alpha/f^2)_{shear}$ vs composition of Platinum(x) along $\langle 100 \rangle$ direction.

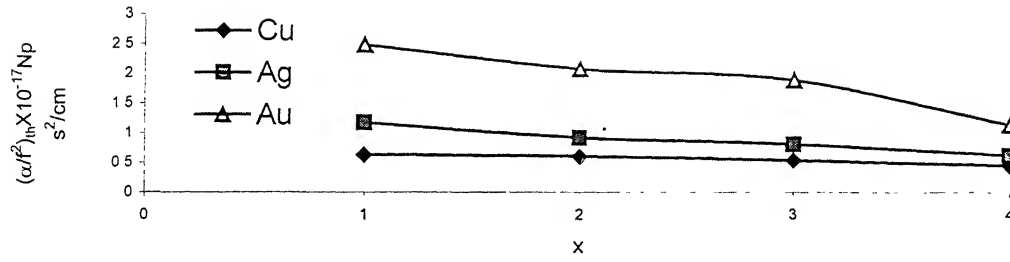


Fig. 6.4. $(\alpha/f^2)_{th}$ vs composition of Platinum(x) along $\langle 110 \rangle$ direction

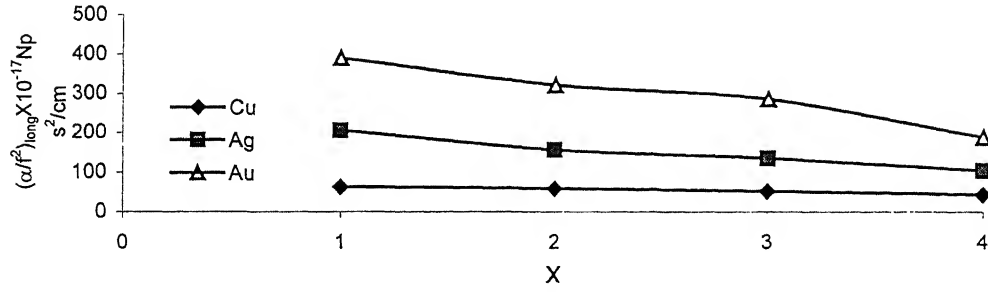


Fig. 6.5. $(\alpha/f^2)_{long}$ vs composition of Platinum(x) along $\langle 110 \rangle$ direction

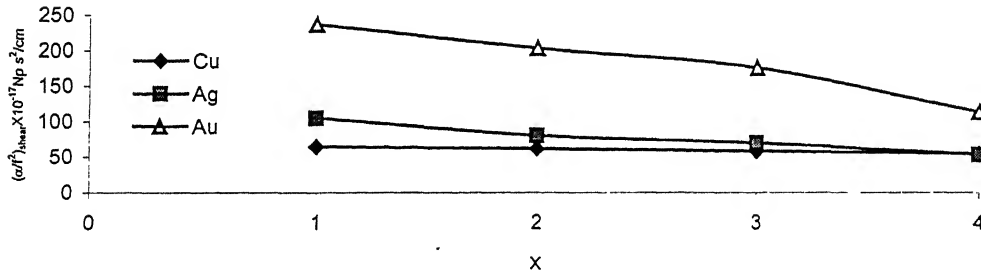


Fig. 6.6. $(\alpha/f^2)_{shear}$ vs composition of Platinum(x) along $\langle 110 \rangle$ direction shear wave polarized along $\langle 001 \rangle$ direction

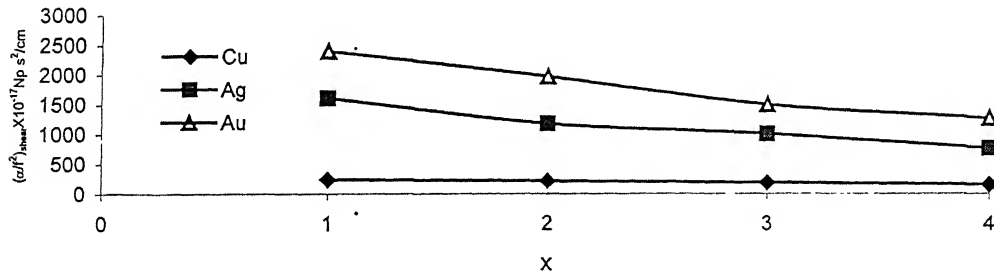


Fig. 6.7. $(\alpha/f^2)_{shear}$ vs composition of Platinum(x) along $\langle 110 \rangle$ direction shear wave polarized along $\langle 110 \rangle$ direction

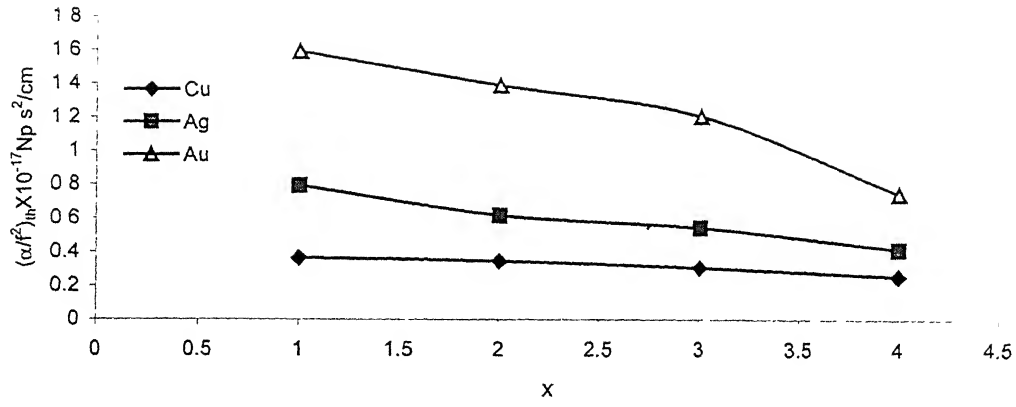


Fig. 6.8. $(\alpha/f^2)_{th}$ vs composition of Platinum(x) along <111> direction

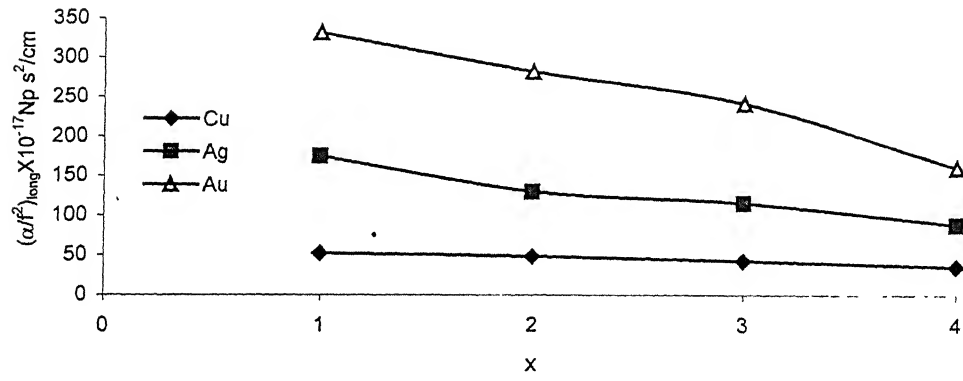


Fig. 6.9. $(\alpha/f^2)_{long}$ vs composition of Platinum(x) along <111> direction

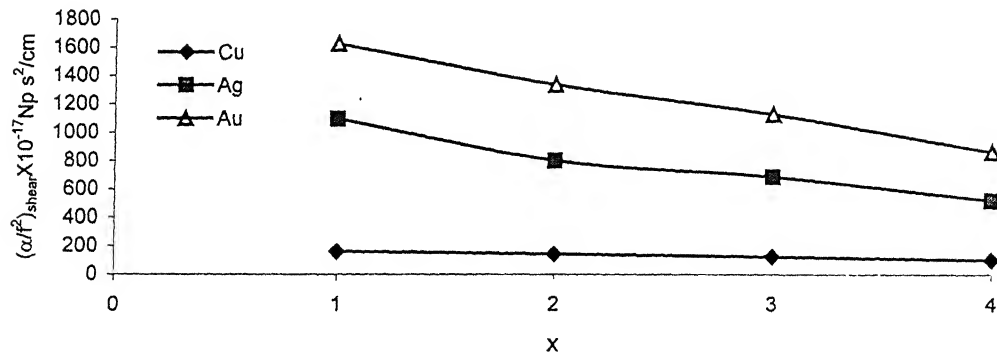


Fig. 6.10. $(\alpha/f^2)_{shear}$ vs composition of Platinum(x) along <111> direction shear wave polarized along <110> direction

References

1. C.A.Damianou, N.T.Sangvi, F.J.Fry, M.Moreno, J.Acoust. Soc. Am. 102,628(1997).
2. V.N.Kostur, J.K.Bhattacharjee and R.A.Ferrel. JETP Lett. 61,560(1995).
3. I.Vekhter, E.J.Nicol and J.P.Carbotte, Phys. Rev.B59,7123(1999).
4. .Bert, G.Bellessa, A.Quivy, Y.Calvayrae, Phys.Rev.B61,32(2000).
5. I.R.Abdelraziq, J.Acoust. Soc. Am. 107,788(2000).
6. K.Brugger, Phys.Rev.B133,1611(1964).
7. G.Leibfried and W.Ludwig, in Solid State Physics edited by F.Seitz and D.Turnbull, (Academic Press, New York,1961), Vol.12.
8. W.P.Mason, Physical Acoustics IIIB,(Academic Press, New York 1965), chapter .6.
9. M.P.Tosi, Solid State Physics edited by F.Seitz and D.Turnbull, (Academic Press, New York 1964) Vol.16.
10. D.E.Gray edited ,A.I.P.Hand book, McGraw Hill Company, Inc.; New York, IIIrd edition.
11. A.Goldsmith et al., Hand book of thermophysical properties of solid materials, Vol.II, The Macmillan Company, New York,1961.
12. F.A.Otte, J.Appl. Phys.27,197(1956).
13. A.K.Giri and G.B.Mitra, J.Mat.Sc.Lett.5,889(1986).
14. K.Salama and G.A.Alers, Phys. Stat. Solidi A41,241(1977).
15. S.K.Kor and R.P.Khare, Phys.Lett.A76,427(1980).
16. W.P.Mason, Low and high amplitude internal friction measurement in solids and their relation to imperfection in microplasticity (ed. C.J.McMohan Jr.), Interscience Publishers, Inc., New York,1968).
17. S.K.Kor U.S.Tandon and G.Rai, Phys. Rev. B6,2195(1972).
18. S.K.Kor P.K.Mishra and U.S.Tandon, Solid Stat.Commn.15,499(1974).
19. S.K.Kor and R.P.Khare, Acustica,56,280(1984).

CHAPTER-7

Ultrasonic Attenuation in Intermetallics

7.1. Introduction

Ultrasonic techniques are widely used for the determination of elastic properties and the characterization of the microstructure of materials. The elastic constants are determined by the measurement of velocities of the longitudinal and shear waves [1], while the microstructure (grain size, porosity.....) is generally evaluated by measuring their attenuation [2]. Ultrasonics also offers the possibility of measuring texture [3,4], phase changes and residual stresses [5]. Ultrasonic velocity and attenuation has been shown also to correlate in certain cases to fracture toughness and fatigue damage [6]. Recently ultrasonic velocity and attenuation [7-15] has been studied in various physical states and conditions.

In preceding chapters ultrasonic attenuation has been studied in metallics, dielectrics semiconducting crystals and metallic alloys in a wide temperature regions along various crystallographic directions. In the present chapter ultrasonic attenuation has been studied in intermetallic compounds or 'intermetallics'. They have received attention in recent years because of their technological promise as high temperature structural materials. The technical research has been accompanied by a programme of curiosity driven research, which has uncovered a number of novel physical features. Intermetallics have been known and studied since the late nineteenth century [16]. The British metallurgist Cecil Desch in 1914 wrote a monograph on intermetallic compounds [17] and declared that "attempt to form a theory of constitution of intermetallic compounds have been comparatively unsuccessful". When he returned to the subject 20 years later [18], he felt much more confident about the state of theory because in the mean time, William Hume-Rothery and Linus Pauling had introduced the concept of atomic size factor, electron per atom ratio, quantum theory of solids and electronegativity into the interpretation of formulation of intermetallic compounds. A recent detailed account of the crystal chemistry and physical metallurgy of these compounds by Ferro and Saccone [19] ; it is very different indeed from Desch's mystified view in 1914.

One of the oldest applications of intermetallics is for superconducting magnet winding: the favoured intermetallics for this purpose are Nb_3Sn , V_3Ga and Nb_3Al all of them with the A-15 crystal structure. Nb_3Al is particularly widely used, and discovery of ceramic superconductors has not dented the use of the metallic superconductors. Apart from the

subtle methods that must be used to prepare multifilaments of intermetallics such as Nb₃Al, there are also some purely physical issues such as effect of partial destruction of long range atomic order on the critical temperature for superconduction and on the critical current and related issue of non-stoichiometry and the consequent antisite atoms in the structure. These matters have spawned an extensive literature. A comprehensive review of niobium aluminide superconductor by Glowacki in Cambridge, has recently appeared [20] and the reader can be confidently referred to this source.

Perhaps the newest application of an intermetallics is the use of ZrCo as a selective hybridizing agent in order to separate the three hydrogen isotopes, hydrogen, deuterium and tritium from the mixture by a selective decomposition of the mixed isotropic hydrides. This was demonstrated by Naik et al. in Bombay [21]. The method exploits the differential pressure composition isotherms in the range 296 to 673K and also the differing kinetics of absorption desorption of three isotopes. There is scope much consequential research on the characteristic of other intermetallics and the theoretical basis for the isotopic differences.

In the present chapter the study of ultrasonic attenuation due to e-p interaction (Akhiezer loss) in Lanthanum Monochalcogenides (LaS, LaSe and LaTe) at the temperature range 5K-80K, due to p-p interaction and thermoelastic loss in Lanthanum Monochalcogenides (LaS, LaSe and LaTe) from 100K to 450K, in Praseodymium Monochalcogenides (PrS, PrSe and PrTe) from 100K to 500K, in Cerium Monochalcogenides (CeS, CeSe and CeTe) and Neodymium Monochalcogenides (NdS, NdSe and NdTe) at room temperature have been made along $\langle 100 \rangle$, $\langle 110 \rangle$ and $\langle 111 \rangle$ crystallographic directions for longitudinal and shear wave polarized along $\langle 100 \rangle$, $\langle 001 \rangle$ & $\langle 1\bar{1}0 \rangle$ and $\langle \bar{1}10 \rangle$ crystallographic directions respectively.

These monochalcogenides were synthesized by V.P.Zhuze et al.[22-25] using the Ivandelli's method [26]. All compounds obtained have a metallic lusture. The sulfides are golden yellow, selenides from golden yellow to copper red and tellurides from violet blue to blue. The phase composition of the samples was checked by X-ray diffraction. It was shown that all the materials have well formed NaCl-type structure. All materials are extensively used in carbon lighting application especially by the motion picture industry for studio lighting and projection. To make them more useful for the industries a study of behaviour of ultrasonic attenuation have been studied as the function of different physical conditions. Ultrasonic Grüneisen parameters and non-linearity constants have also been evaluated in these intermetallics.

6.2 Theory

6.2.1 Theory of SOEC and TOEC

SOEC and TOEC have evaluated following Brugger's definition [27] of elastic constants at absolute zero using Born-Mayer potential [28]. The SOEC and TOEC at different temperature are obtained by the method developed by Leibfried and Hahn [29], Leibfried and Ludwig [30], Ghate [31] and finally by Mori and Hiki [32] for NaCl-type crystals. The explicit expression for temperature dependence SOEC and TOEC have been presented in Tables 2.2-2.6 in chapter II.

6.2.2 Ultrasonic attenuation due to electron-phonon interaction

At lower temperatures the mean free path of the conduction electrons are comparable with acoustical phonons. Thus the coupling between electrons and propagating ultrasonic waves will lead to the dissipation of energy and viscous loss occurs [15].

The attenuation caused by energy loss due to compressional and shear viscosities of lattice [15] at the temperature range 5-80K are given as in eqs.(2.43) and (2.44) in chapter II.

6.2.3 Ultrasonic attenuation due to phonon-phonon interaction and thermoelastic loss

An effort has been made to establish the theory of ultrasonic absorption over frequency square (α/f^2) in these intermetallic compounds due to phonon-phonon interaction and thermoelastic loss. Akhiezer [33] first proposed the ultrasonic attenuation due to phonon-phonon interaction; which was modified by Woodruff and Ehrenreich [34], Bömmel and Dransfeld [35] and finally by Mason [36]. In the present investigation $(\alpha/f^2)_{th}$, $(\alpha/f^2)_{Akh.long}$ and $(\alpha/f^2)_{Akh.shear}$ are evaluated using the eqns. (2.86),(2.78) and (2.79) in chapter II.

6.3 Evaluations, Results and Discussions:

The theory is tested for intermetallics, rock-salt type structure. Starting with the nearest neighbor distance r_0 [22-25,37], for LaS=2.894A⁰, LaSe= 3.032A⁰ and LaTe=3.211 A⁰; PrS=2.855A⁰, PrSe=2.960A⁰ and PrTe=3.140 A⁰; CeS=2.889A⁰, CeSe=2.991A⁰ and CeTe=3.173 A⁰ and NdS=2.8405A⁰, NdSe=2.879A⁰ and NdTe=3.1245A⁰ and repulsive parameters (Born parameter) [38] LaS, LaSe & LaTe=0.313 A⁰, PrS, PrSe & PrTe=0.313 A⁰; CeS=0.303 A⁰; CeSe=0.313 A⁰ & CeTe=0.311 A⁰ and NdS=0.299 A⁰, NdSe= 0.315A⁰& NdTe=0.298 A⁰. SOEC and TOEC are evaluated by means of Tables 2.2-2.6 of chapter II. The values of SOEC and velocities (V_l for longitudinal wave and V_s for shear wave) are presented in Tables 7.1 (for Lanthanum Monochalcogenides in the temperature range 5-

80K), We have evaluated ultrasonic absorption (α/f^2) due to electron-phonon interaction in LaS, LaSe and LaTe for the temperature range 5K-80K according to the eqns (2.43) and (2.44) in chapter II and using evaluated second order elastic constants (SOEC) as presented in Tables 7.1. The values of electrical resistivity (R), evaluated values of viscosity (η_e) and ultrasonic attenuation due to e-p interaction [$(\alpha/f^2)_{\text{long}}$ for longitudinal wave and $(\alpha/f^2)_{\text{shear}}$ for shear wave) are presented in Tables 7.2. For the evaluation, we have used the resistivity data calculated according to Wiedemann-Franz Law [39], utilizing the thermal conductivity values taken from the literature [25]. The evaluated values of SOEC and TOEC elastic constants are presented in Tables 7.3-7.5 (for Lanthanum Monochalcogenides in the temperature range 100-450K), Tables 7.6-7.8 (for Praseodymium Monochalcogenides in the temperature range 100-500K) and Tables 7.9 (for Cerium and Neodymium Monochalcogenides at room temperature). The SOEC and TOEC give the Grüneisen parameters along $\langle 100 \rangle$, $\langle 110 \rangle$ and $\langle 111 \rangle$ direction for longitudinal wave and shear wave polarized along $\langle 100 \rangle$, $\langle 001 \rangle$ & $\langle 1\bar{1}0 \rangle$ and $\langle \bar{1}10 \rangle$ directions respectively as given in Appendix-A. The values of C_V and E_0 evaluated as a function of (θ_D/T) [θ_D and T being Debye and Kelvin temperatures respectively) are taken from literature [39]. τ_{th} is calculated by eqn. (2.65) in chapter II using density and thermal conductivity data. The values of density (ρ), thermal conductivity (K), specific heat per unit volume (C_V), energy density (E_0), V_l for longitudinal velocity, V_s for shear wave, Debye average velocity (\bar{V}) and thermal relaxation time (τ_{th}) are presented in Tables 7.10-7.16 Lanthanum Monochalcogenides, Praseodymium Monochalcogenides and Cerium & Neodymium Monochalcogenides respectively in their temperature range. The non-linearity coupling constants (D) are computed using average Grüneisen parameters are presented in Tables 7.17-7.25 along $\langle 100 \rangle$, $\langle 110 \rangle$ and $\langle 111 \rangle$ crystallographic direction for Lanthanum Monochalcogenides, Praseodymium Monochalcogenides and Cerium & Neodymium Monochalcogenides respectively in their temperature range. Finally ultrasonic attenuation due to the phonon-viscosity and thermoelastic loss are evaluated using the eqns. 2.78, 2.79 and 2.86 in chapter II along $\langle 100 \rangle$, $\langle 110 \rangle$ and $\langle 111 \rangle$ directions. The values of ultrasonic attenuation $(\alpha/f^2)_{\text{th}}$, $(\alpha/f^2)_{\text{Akh, long}}$ and $(\alpha/f^2)_{\text{Akh shear}}$ are presented in Tables 7.26-7.34 and Figs. 7.5-7.7, 7.11-7.14 and 7.17-7.29 for La and Pr Monochalcogenides.

SOEC and TOEC were evaluated using the Coulomb and Born-Mayer potential. Born parameter in Born-Mayer potential $\phi(r_0)=A \exp(-r_0/b)$ is determined as follows [32,38]:

Total free energy of a crystal in equilibrium condition should be minimum. In cubic crystal for equilibrium condition:

$$-(e^2/r_0)S_3^{(1)}-(2r_0/b)\phi(r_0)-(4\sqrt{2}r_0/b)\phi(\sqrt{2}r_0)+(h\omega_0/4)G_1\coth x=0$$

a set of 'b' which satisfies this relation and also minimize $\sum(C_{ij}^{cal}-C_{ij}^{exp})$ is chosen as the most probable one, where C_{ij}^{cal} are SOEC calculated and C_{ij}^{exp} are experimental SOEC at room temperature. C_{ij}^{exp} are not available for us in literature. Therefore we have chosen 'b' values as in other family compounds in literature [32]. Ghate [31] used two values ($b=0.333A^0$ and $0.288A^0$) of Born-parameter for NaCl-type crystal[38].

It is further assumed that the value of 'b' is independent of temperature. For other family members LiF, KCl; Mori and Hiki [32] used Born parameters $0.270A^0$ and $0.298A^0$ and calculated TOEC. Calculated values were good agreement with experimental values of those determined by Drabble and Strathen [40], thus our choice of 'b' for all intermetallics is justified. The values of SOEC are good agreement with experimental one [41] of light tellurides; these are also Rock-salt type structure materials. In the case of Palladium metal, these is good agreement between attenuation values using C_{11} and C_{44} calculated with present method [42] and that using C_{11} values by Hsu [43]. Positive temperature dependence of C_{11} was also found in the case of Tungston in the work of Stathis [44].

On the other chalcogenide system, the bulk modulus $(C_{11}+2C_{12})/3$ of SmS, SmSe, SmTe, UTe, NpTe, PuTe, AmTe and a rock salt type ZrC are 47.6GPa [45], 40GPa, 40GPa [46], 45 GPa, 65GPa, 34GPa, 15GPa [41,47,48] and 23 GPa [49,50] respectively. These values are approximately in the same order as in the evaluated 25GPa, 23GPa and 20GPa for the chosen monochalcogenides (La,Pr,Ce,Nd-chalcogenides) in present investigation. There are no experimental data for the chosen chalcogenides, therefore the direct comparison could not be made. Thus with the above conclusions the theory for the evaluation of SOEC and TOEC at different temperatures for these chalcogenides is being established. However, full account of many interactions and Vander Wall's interaction between ions and also consideration of the non-linearity of the material upto some extent may further improve the calculated results of TOEC [51]

It can be seen from the Tables 7.2 and Figs.7.1-7.2, that the values of ultrasonic attenuation at the temperature range 5K-80K in LaS, LaSe and LaTe are smaller than the values of attenuation in metallic compounds as found in literatures [52-53]. This is due to higher electrical resistivity values of Lanthanum Monochalcogenides ($\cong 10^{-5}\Omega cm$) in

comparison to the electrical resistivity values of metals ($\cong 10^{-7} \Omega \text{cm}$). According to previous workers [52-53] the attenuation in metals at lower temperatures decreases very sharply with the increase in temperature, but in these intermetallic compounds the attenuation decreases gradually with increase in temperature as the variation of the resistivity with the temperatures. Although experimental data for ultrasonic attenuation in LaS, LaSe and LaTe at 5K-80K are not available in literature for comparison, however the values of (α_l/α_s) for La-Monochalcogenides becomes $\cong 4.5$ like in metals [54]. Thus the overall behavior of ultrasonic attenuation due to e-p interaction in LaS, LaSe and LaTe at temperature range 5-80K provides some different characteristic feature for these intermetallic compounds in comparison to that of metals available in the literatures [54,42].

As one has mentioned that all monochalcogenides are compound with metallic bonding possessed well-developed structure of NaCl-type [22-25,37]. The evaluated thermal relaxation time (τ_{th}) is of the same order of 10^{-11} sec for all these intermetallics, which is as expected as in NaCl-type crystals [55]. It is obvious from the eqn. (2.65) of chapter II that τ_{th} is directly proportional to the thermal conductivity values.

The variation of non-linearity parameter (D) with temperature is shown in Tables 7.17-7.25 and Figs. 7.3-7.4, 7.8-7.10 and 7.15-7.16 for La and Pr-monochalcogenides. The non-linearity constant (Acoustic coupling constant) 'D' is decreasing with very small values as the temperature increases. This behaviour of 'D' is observed in previously NaCl-type crystals. Therefore it does not affect much the temperature dependence of ultrasonic attenuation in La and Pr-chalcogenides for both longitudinal and shear wave. It is clear from the Tables 7.17-7.25 and Figs. 7.3 and 7.4 that the value of 'D' increases with increasing molecular weight of these materials. It is obvious from the Tables 7.17 and 7.19 that the values of D_l/D_s is about 12-15 which is expected between 3 to 16 as previous studies in dielectric crystals [55] along $\langle 100 \rangle$ crystallographic direction.

It is seen from the Tables 7.20-7.22 that the ratio of D_l/D_{s1} for longitudinal wave along $\langle 110 \rangle$ direction and shear wave polarized along $\langle 001 \rangle$ direction is larger than that of other NaCl-type material [55,56]. In the case of Lanthanum Monochalcogenides it varies from 18-58, while in the other Monochalcogenides it varies from 4-12, which is very similar with experimental result 3.8 of rocksalt type material LiF reported by Hanson [56]. The ratio of D_{s2}/D_l (shear wave along $\langle 110 \rangle$ direction and polarized along $\langle 1\bar{1}0 \rangle$) is almost in the same order for all the substances and its numerical value range is from 1.3-1.9, these are also

very much similar with experimental results in LiF [56] in all the rare earth Monochalcogenides.

It is clear from Tables 7.23-7.25 that the values of D_{shear} is more than D_{long} for all the rare-earth monochalcogenides when the waves are propagating along $\langle 111 \rangle$ direction for longitudinal and shear wave polarized along $\langle \bar{1}10 \rangle$ direction. The ratio of D_s/D_l (shear wave polarized along $\langle 1\bar{1}0 \rangle$ direction) is almost in the same order as that of other NaCl-type crystals [55,56]. The numerical value of D_s/D_l varies from 1.3-1.9 in all rare earth monochalcogenides is very much similar with experimental result of LiF [56] i.e.1.9.

It is obvious from the Tables 7.26-7.34 and Figs. 7.5-7.7,7.11-7.14 and 7.17-7.29 that the ultrasonic absorption over frequency square due to p-p interaction (Akhiezer type damping) for all intermetallic compounds along $\langle 100 \rangle$, $\langle 110 \rangle$ and $\langle 111 \rangle$ directions for longitudinal and shear waves increases with temperatures from 100-500K. Also, the values of ultrasonic attenuation in Ce and Nd-monochalcogenides are appreciable at room temperature having the same order as in other intermetallic compounds evaluated by us. It can be seen from the Table 7.35, the experimental values of ultrasonic absorption coefficient in LiF (NaCl-type) at 900MHz at room temperature is comparable with our evaluated values ultrasonic absorption in these intermetallics studied in this chapter at room temperature.

However due to lack of experimental value in whole temperature range, the comparison could not possible for different temperatures. If we compare the quantum of attenuation in lead chalcogenides with rare-earth monochalcogenides, we find that attenuation values are much higher than those of rare-earth monochalcogenides, but order is nearly same [58] (comparison for $\langle 100 \rangle$ only). However in the case of lanthanum monochalcogenides, the values of ultrasonic attenuations are much larger than that of lead chalcogenide systems.

As discussed, the non-linearity parameter 'D' (Acoustic coupling constants) does not much affect the temperature dependence of the attenuation. The behavior of temperature dependence of $(\alpha/f^2)_{\text{th}}$ and $(\alpha/f^2)_{\text{Akh}}$ is the same as that of total thermal conductivity of these intermetallics from 100-450K for La-monochalcogenides, 100-500K for Pr-monochalcogenides. A distinct peculiarity of rare-earth intermetallic compounds is their lower electronic thermal conductivity with anomalous temperature dependence. The electronic thermal conductivity of these compounds decreases with temperatures as in the case of La & Pr-monochalcogenides [24,25]. Therefore the attenuation in these compounds is

mainly due to lattice part of the thermal conductivity and it directly affects the temperature dependence of the attenuation in these materials.

The ultrasonic attenuation over frequency due to thermoelastic loss is negligible due to low values of thermal conductivity as expected, since the order is the same as for other NaCl-type crystals [53,55,56].

It was confirmed by measurements that for temperatures below 500K, the attenuation is independent of the dislocation count and it has not been considered here [59]. With the many experimental and theoretical studies it is well established that p-p interaction mechanism is the dominating cause for attenuation in solids at higher temperatures \approx room temperature [33-36,53,55,57] and electron-phonon is the cause for the attenuation at lower temperature below 80K where free electrons are available in the metallic, intermetallics and semimetallics [42,52,60]. In the theory employing phonon-phonon interaction several approximations are made, which are valid at higher temperature [61,62]. One of them is that $E_0 = nE_i$, n is the number of modes and E_i is the thermal energy of i^{th} mode given by

$$E_i = \left(3hN_i / v_{qi}^3 \right) \int_0^{v_{qi}} \left\{ v^3 dv / (\exp(hv/kT) - 1) \right\}$$

Where N_i is the total numbers of modes in the sector i v_{qi} is the cut off frequency (limiting) supported by lattice.

Therefore, on the basis of above experimentally and theoretical established fact, we have evaluated ultrasonic attenuation in these materials at different temperatures establishing Mason-Bateman approach observing the effect of lattice thermal conductivity values at different higher temperatures. It is clear from the plotting graphs that the attenuation takes appreciable values at lower temperature (below 100K) due to possible e-p interaction and appreciable values at higher temperature (>100K) due to possible p-p interaction. The behavior proves the fact that attenuation due to p-p interaction mechanism occurs mainly at room temperature and above and it goes down at 100K. Since whole the computation is dependent of nearest neighbor distance and hardness parameter (Born parameter), one may state that ultrasonic attenuation in these rare-earth intermetallics is very important characteristic property of the materials and it is also concluded that Mason theory is still good for the evaluation of ultrasonic attenuation due to e-p interaction at low temperature and due to phonon-phonon interaction and thermoelastic loss near to room temperature value for these rare-earth intermetallics.

Table 7.1 Calculated second order elastic constants (in 10^{11} Dyne/cm²), density (ρ) [in g/cc], V_l and V_s (in 10^5 cm/s) at the temperature range 5-80K.

Substance	Temp.K→	5	10	20	40	60	80
LaS	C_{11}	4.6499	4.6499	4.6498	4.6512	4.6611	4.6791
	C_{44}	1.3435	1.3435	1.3434	1.3436	1.3441	1.3448
	V_l	2.7862	2.7885	2.7932	2.7983	2.8060	2.8161
	V_s	1.4976	1.4989	1.5014	1.5040	1.5068	1.5098
LaSe	C_{11}	4.1990	4.1990	4.2000	4.2055	4.2233	4.2475
	C_{44}	1.0941	1.0941	1.0942	1.0944	1.0950	1.0957
	V_l	2.5243	2.5261	2.5309	2.5358	2.5358	2.5373
	V_s	1.2805	1.2895	1.2915	1.2936	1.2919	1.2984
LaTe	C_{11}	3.7151	3.7150	3.7153	3.7251	3.7455	3.7708
	C_{44}	0.8514	0.8514	0.8514	0.8517	0.8522	0.8527
	V_l	2.3408	2.3425	2.3443	2.3509	2.3609	2.3724
	V_s	1.1206	1.1214	1.1223	1.1241	1.1261	1.1283

Table 7.2 Electrical resistivity(R) in 10^{-5} Ω cm, viscosity(η_e) in 10^{-3} poise and the ultrasonic attenuation due to e-p interaction [$(\alpha/f^2)_l$ for longitudinal wave and $(\alpha/f^2)_s$ for shear wave] in 10^{-19} Nps²/cm, at the temperature range 5-80K.

Substance	Temp.K→	5	10	20	40	60	80
LaS	R	1.000	1.040	1.170	1.420	1.670	1.830
	η_e	1.1167	1.121	0.994	0.814	0.693	0.631
	$(\alpha/f^2)_l$	2.342	2.247	1.990	1.632	1.378	1.245
	$(\alpha/f^2)_s$	10.044	10.017	8.869	7.278	6.161	5.5951
LaSe	R	2.170	2.250	2.330	2.501	2.670	2.750
	η_e	0.469	0.489	0.469	0.421	0.395	0.381
	$(\alpha/f^2)_l$	1.195	1.151	1.147	1.026	0.958	0.912
	$(\alpha/f^2)_s$	6.222	5.990	5.968	5.350	5.023	4.820
LaTe	R	1.420	1.580	1.710	2.000	2.330	2.500
	η_e	0.663	0.595	0.550	0.469	0.402	0.374
	$(\alpha/f^2)_l$	1.983	1.779	1.640	1.392	1.181	1.086
	$(\alpha/f^2)_s$	12.511	11.225	10.225	8.816	7.535	6.991

Table-7.3 Second and Third Order Elastic Constants (SOEC & TOEC) in 10^{11} Dyne/cm² of LaS at Temperature range 100K-450K

SOEC & TOEC	100K	200K	300K	400K	450K
C ₁₁	4.700	4.845	5.007	5.173	5.266
C ₁₂	1.261	1.184	1.106	1.034	0.985
C ₄₄	1.346	1.351	1.356	1.362	1.365
C ₁₁₁	75.516	-76.129	-76.905	-77.727	-78.13
C ₁₁₂	-5.191	-4.929	-4.665	-4.401	-4.249
C ₁₂₃	1.764	1.296	0.828	0.361	0.052
C ₁₄₄	2.248	2.266	2.283	2.300	2.311
C ₁₆₆	-5.486	-5.507	-5.530	-5.555	-5.569
C ₄₅₆	2.231	2.231	2.231	2.231	2.231

Table-7.4 Second and Third Order Elastic Constants (SOEC & TOEC) of LaSe 10^{11} Dyne/cm² at temperature range 100K-450K .

SOEC & TOEC	100K	200K	300K	400K	450K
C ₁₁	4.280	4.430	4.592	4.757	4.839
C ₁₂	1.021	0.950	0.879	0.808	0.772
C ₄₄	1.097	1.102	1.106	1.111	1.113
C ₁₁₁	-70.631	-71.382	-72.222	-73.085	-73.52
C ₁₁₂	-4.143	-3.860	-3.577	-3.294	-3.152
C ₁₂₃	1.413	0.972	0.532	0.092	-0.128
C ₁₄₄	1.868	1.882	1.897	1.911	1.918
C ₁₆₆	-4.448	-4.467	-4.487	-4.508	-4.518
C ₄₅₆	1.853	1.853	1.853	1.853	1.853

Table-7.5 Second and Third Order Elastic Constants (SOEC&TOEC) 10^{11} Dyne/cm² of LaTe at temperature range 100K-450K

SOEC & TOEC	100K	200K	300K	400K	450K
C ₁₁	3.800	3.950	4.106	4.264	4.342
C ₁₂	0.780	0.710	0.640	0.569	0.534
C ₄₄	0.854	0.857	0.861	0.864	0.865
C ₁₁₁	-64.825	-65.602	-66.442	-67.298	-67.73
C ₁₁₂	-3.125	-2.837	-2.550	-2.262	-2.119
C ₁₂₃	1.002	0.531	0.061	-0.410	-0.645
C ₁₄₄	1.484	1.496	1.508	1.519	1.525
C ₁₆₆	-3.429	-3.445	-3.461	-3.477	-3.485
C ₄₅₆	1.472	1.472	1.472	1.472	1.472

Table-7.6 Second and Third Order Elastic Constants (SOEC & TOEC) [10^{11} Dyne/cm²] of PrS at temperature range 100K-500K

Temp(K)	100	200	300	400	500
C ₁₁	4.757	4.905	5.069	5.237	5.409
C ₁₂	1.352	1.279	1.205	1.132	1.058
C ₄₄	1.432	1.438	1.443	1.450	1.456
C ₁₁₁	-75.576	-76.191	-76.972	-77.800	-78.686
C ₁₁₂	-5.543	-5.272	-4.999	-4.726	-4.453
C ₁₂₃	1.936	1.515	1.095	0.675	0.255
C ₁₄₄	2.374	2.392	2.411	2.429	2.447
C ₁₆₆	-5.849	-5.871	-5.896	-5.922	-5.949
C ₄₅₆	2.355	2.355	2.355	2.355	2.355

Table-7.5 Second and Third Order Elastic Constants (SOEC&TOEC) 10^{11} Dyne/cm² of LaTe at temperature range 100K-450K

SOEC & TOEC	100K	200K	300K	400K	450K
C ₁₁	3.800	3.950	4.106	4.264	4.342
C ₁₂	0.780	0.710	0.640	0.569	0.534
C ₄₄	0.854	0.857	0.861	0.864	0.865
C ₁₁₁	-64.825	-65.602	-66.442	-67.298	-67.73
C ₁₁₂	-3.125	-2.837	-2.550	-2.262	-2.119
C ₁₂₃	1.002	0.531	0.061	-0.410	-0.645
C ₁₄₄	1.484	1.496	1.508	1.519	1.525
C ₁₆₆	-3.429	-3.445	-3.461	-3.477	-3.485
C ₄₅₆	1.472	1.472	1.472	1.472	1.472

Table-7.6 Second and Third Order Elastic Constants (SOEC & TOEC) [10^{11} Dyne/cm²] of PrS at temperature range 100K-500K

Temp(K)	100	200	300	400	500
C ₁₁	4.757	4.905	5.069	5.237	5.409
C ₁₂	1.352	1.279	1.205	1.132	1.058
C ₄₄	1.432	1.438	1.443	1.450	1.456
C ₁₁₁	-75.576	-76.191	-76.972	-77.800	-78.686
C ₁₁₂	-5.543	-5.272	-4.999	-4.726	-4.453
C ₁₂₃	1.936	1.515	1.095	0.675	0.255
C ₁₄₄	2.374	2.392	2.411	2.429	2.447
C ₁₆₆	-5.849	-5.871	-5.896	-5.922	-5.949
C ₄₅₆	2.355	2.355	2.355	2.355	2.355

Table-7.7 Second and Third Order Elastic Constants (SOEC & TOEC) [10^{11} Dyne/cm²] of PrSe at temperature range 100K-500K

Temp(K)	100	200	300	400	500
C ₁₁	4.550	4.651	4.741	4.945	5.104
C ₁₂	1.142	1.074	1.001	0.931	0.859
C ₄₄	1.224	1.228	1.231	1.237	1.242
C ₁₁₁	-73.102	-73.331	-73.375	-74.639	-75.418
C ₁₁₂	-4.639	-4.396	-4.118	-3.848	-3.572
C ₁₂₃	1.609	1.185	0.758	0.332	0.095
C ₁₄₄	2.056	2.071	2.087	2.103	2.119
C ₁₆₆	-4.990	-5.002	-5.013	-5.042	-5.064
C ₄₅₆	2.039	2.039	2.039	2.039	2.039

Table-7.8 Second and Third Order Elastic Constants (SOEC & TOEC) [10^{11} Dyne/cm²] of PrTe at temperature range 100K-500K

Temp(K)	100	200	300	400	500
C ₁₁	4.002	4.120	4.263	4.413	4.567
C ₁₂	0.870	0.803	0.734	0.666	0.597
C ₄₄	0.944	0.947	0.951	0.955	0.959
C ₁₁₁	-66.779	-67.205	-67.897	-68.67	-69.484
C ₁₁₂	3.499	-3.232	-2.954	-2.674	-2.395
C ₁₂₃	1.173	0.737	0.300	0.136	-0.573
C ₁₄₄	1.623	1.635	1.648	1.661	1.673
C ₁₆₆	-3.816	-3.829	-3.846	-3.863	-3.880
C ₄₅₆	1.610	1.610	1.610	1.610	1.610

Table 7.9 Second and third order elastic constants (in 10^{11} Dyne/cm²) of other monochalcogenides at room temperature

Material→	CeS	CeSe	CeTe	NdS	NdSe	NdTe
C ₁₁	5.401	4.723	4.261	5.728	4.998	4.762
C ₁₂	1.094	0.943	0.684	1.180	1.155	0.708
C ₄₄	1.349	1.174	0.904	1.446	1.391	0.952
C ₁₁₁	-84.295	-73.703	-68.830	-89.306	-76.204	-78.259
C ₁₁₂	-4.481	-3.859	-2.717	-4.834	-4.783	-2.767
C ₁₂₃	0.799	0.641	0.172	0.901	1.013	0.069
C ₁₄₄	2.298	2.001	1.580	2.458	2.331	1.678
C ₁₆₆	-5.487	-4.770	-3.641	-5.881	-5.680	-3.815
C ₄₅₆	2.246	1.955	1.544	2.404	2.278	1.642

Table 7.10 Density (ρ) in g/cc, thermal conductivity (K) in 10^5 erg/cm s K, specific heat (C_V) in 10^8 erg/cc deg. internal energy (E₀) in 10^8 erg/cc, longitudinal and shear velocities (V_l and V_s) in 10^5 cm/s, Debye average velocity (\bar{V}) in 10^5 cm/s and thermal relaxation time (τ_{th}) in 10^{-11} sec of LaS at the temperature range 100-450K

Temp.K→	100	200	300	400	450
ρ	5.86	5.80	5.78	5.77	5.75
K	20.929	25.115	28.463	29.301	28.882
C _V	0.063	0.073	0.083	0.084	0.084
E ₀	2.903	10.206	18.301	26.647	30.832
V _l	2.832	2.890	2.943	2.997	3.026
V _s	1.515	1.526	1.532	1.538	1.541
\bar{V}	2.084	2.103	2.114	2.126	2.132
τ_{th}	2.309	2.161	2.308	2.317	2.263

Table 7.11 Density (ρ) in g/cc, thermal conductivity (K) in 10^5erg/cm s K , specific heat (C_V) in 10^8erg/cc deg , internal energy (E_0) in 10^8erg/cc , longitudinal and shear velocities (V_l and V_s) in 10^5cm/s , Debye average velocity (\bar{V}) in 10^5cm/s and thermal relaxation time (τ_{th}) in 10^{-11}sec of LaSe at the temperature range 100-450K

Temp.K→	100	200	300	400	450
ρ	6.45	6.31	6.23	6.13	6.12
K	15.906	19.673	22.185	24.278	24.068
C_V	0.059	0.070	0.072	0.073	0.073
E_0	2.993	9.583	16.722	23.957	27.707
V_l	2.560	2.650	2.715	2.790	2.812
V_s	1.304	1.321	1.333	1.346	1.349
\bar{V}	1.805	1.833	1.852	1.873	1.878
τ_{th}	2.485	2.519	2.688	2.844	2.795

Table 7.12 Density (ρ) in g/cc, thermal conductivity (K) in 10^5erg/cm s K , specific heat (C_V) in 10^8erg/cc deg , internal energy (E_0) in 10^8erg/cc , longitudinal and shear velocities (V_l and V_s) in 10^5cm/s , Debye average velocity (\bar{V}) in 10^5cm/s and thermal relaxation time (τ_{th}) in 10^{-11}sec of LaTe at the temperature range 100-450K

Temp.K→	100	200	300	400	450
ρ	6.68	6.56	6.44	6.32	6.30
K	14.860	18.627	20.929	22.185	21.975
C_V	0.055	0.061	0.062	0.062	0.062
E_0	3.150	8.996	15.092	21.092	24.491
V_l	2.385	2.432	2.479	2.526	2.550
V_s	1.131	1.133	1.135	1.137	1.139
\bar{V}	1.577	1.582	1.588	1.593	1.596
τ_{th}	3.289	3.687	4.036	4.221	4.153

Table 7.13 Density (ρ) in g/cc, thermal conductivity (K) in 10^5erg/cm s K , specific heat (C_V) in 10^8erg/cc deg , internal energy (E_0) in 10^8erg/cc , longitudinal and shear velocities (V_l and V_s) in 10^5cm/s , Debye average velocity (\bar{V}) in 10^5cm/s and thermal relaxation time (τ_{th}) in 10^{-11}sec of PrS at the temperature range 100-450K

Temp.K→	100	200	300	400	500
ρ	6.225	6.201	6.173	6.160	6.154
K	8.400	11.574	13.813	15.400	15.464
C_V	7.300	8.430	8.710	8.770	8.670
E_0	3.800	11.850	20.397	29.101	37.888
V_l	2.764	2.813	2.866	2.916	2.965
V_s	1.517	1.523	1.529	1.534	1.538
\bar{V}	1.671	1.679	1.689	1.695	1.701
τ_{th}	1.237	1.444	1.671	1.834	1.849

Table 7.14 Density (ρ) in g/cc, thermal conductivity (K) in 10^5erg/cm s K , specific heat (C_V) in 10^8erg/cc deg , internal energy (E_0) in 10^8erg/cc , longitudinal and shear velocities (V_l and V_s) in 10^5cm/s , Debye average velocity (\bar{V}) in 10^5cm/s and thermal relaxation time (τ_{th}) in 10^{-11}sec of PrSe at the temperature range 100-450K

Temp.K→	100	200	300	400	500
ρ	7.205	7.102	7.042	6.932	6.812
K	5.413	7.280	8.960	9.520	9.927
C_V	7.010	7.760	7.871	7.812	7.573
E_0	3.942	11.357	19.055	26.546	33.799
V_l	2.513	2.559	2.595	2.671	2.737
V_s	1.303	1.315	1.322	1.336	1.350
\bar{V}	1.442	1.455	1.464	1.481	1.498
τ_{th}	1.115	1.329	1.594	1.668	1.753

Table 7.15 Density (ρ) in g/cc, thermal conductivity (K) in 10^5erg/cm s K , specific heat (C_V) in 10^8erg/cc deg , internal energy (E_0) in 10^8erg/cc , longitudinal and shear velocities (V_l and V_s) in 10^5cm/s , Debye average velocity (\bar{V}) in 10^5cm/s and thermal relaxation time (τ_{th}) in 10^{-11}sec of PrTe at the temperature range 100-450K

Temp.K→	100	200	300	400	500
ρ	7.40	7.305	7.204	7.101	7.015
K	4.667	6.347	7.653	8.400	8.973
C_V	6.191	6.624	6.631	6.583	6.500
E_0	3.777	10.162	16.608	22.925	29.199
V_l	2.324	2.375	2.433	2.493	2.552
V_s	1.129	1.139	1.152	1.160	1.169
\bar{V}	1.254	1.265	1.280	1.291	1.302
τ_{th}	1.440	1.800	2.113	2.299	2.443

Table 7.16 Density (ρ) in g/cc, thermal conductivity (K) in 10^5erg/cm s K , specific heat (C_V) in 10^8erg/cc deg , internal energy (E_0) in 10^8erg/cc , longitudinal and shear velocities (V_l and V_s) in 10^5cm/s , Debye average velocity (\bar{V}) in 10^5cm/s and thermal relaxation time (τ_{th}) in 10^{-11}sec of other materials at room temperature.

Material→	CeS	CeSe	CeTe	NdS	NdSe	NdTe
ρ	5.928	6.797	6.957	6.386	7.765	7.398
K	8.600	6.720	5.461	10.084	33.602	5.074
C_V	8.456	7.662	6.450	8.900	8.592	6.481
E_0	2.065	1.921	1.660	2.155	2.128	1.338
V_l	3.018	2.636	2.475	2.995	2.537	2.537
V_s	1.509	1.314	1.140	1.505	1.338	1.134
\bar{V}	1.672	1.455	1.269	1.667	1.479	1.264
τ_{th}	1.091	1.239	1.576	1.222	5.365	1.468

Table 7.17 Average of ultrasonic Grüneisen parameters ($\langle\gamma_i^j\rangle_l$ for longitudinal wave), average of square ultrasonic Grüneisen parameters ($\langle(\gamma_i^j)^2\rangle_{\text{long}}$ for longitudinal wave and $\langle(\gamma_i^j)^2\rangle_{\text{Shear}}$ for shear wave) and acoustic coupling constants (D_l for longitudinal wave and D_s for shear wave) of the intermetallics at their temperature range along $\langle 100 \rangle$ crystallographic direction.

Material	Temp.[K]	$\langle\gamma_i^j\rangle$	$\langle(\gamma_i^j)^2\rangle_l$	$\langle(\gamma_i^j)^2\rangle_s$	D_l	D_s
LaS	100	0.519	2.104	0.139	17.192	1.251
	200	0.501	1.983	0.138	17.264	1.243
	300	0.484	1.871	0.136	16.523	1.223
	400	0.467	1.773	0.134	15.754	1.200
	450	0.457	1.717	0.133	15.281	1.970
LaSe	100	0.519	2.213	0.135	18.332	1.221
	200	0.499	2.082	0.134	18.191	1.203
	300	0.481	1.962	0.132	17.361	1.190
	400	0.464	1.857	0.131	16.512	1.170
	450	0.456	1.809	0.130	16.123	1.170
LaTe	100	0.519	2.367	0.132	19.904	1.192
	200	0.502	2.243	0.131	19.170	1.182
	300	0.482	2.107	0.129	18.111	1.163
	400	0.464	1.991	0.128	17.172	1.151
	450	0.451	1.919	0.124	16.571	1.123

Table 7.18 Average of ultrasonic Grüneisen parameters ($\langle\gamma_i^j\rangle_l$ for longitudinal wave), average of square ultrasonic Grüneisen parameters ($\langle(\gamma_i^j)^2\rangle_{\text{long}}$ for longitudinal wave and $\langle(\gamma_i^j)^2\rangle_{\text{Shear}}$ for shear wave) and acoustic coupling constants (D_l for longitudinal wave and D_s for shear wave) of the intermetallics at their temperature range along $\langle 100 \rangle$ crystallographic direction.

Material	Temp.[K]	$\langle\gamma_i^j\rangle$	$\langle(\gamma_i^j)^2\rangle_l$	$\langle(\gamma_i^j)^2\rangle_s$	D_l	D_s
PrS	100	0.519	2.064	0.142	17.024	1.278
	200	0.501	1.942	0.140	16.394	1.260
	300	0.483	1.833	0.138	15.600	1.242
	400	0.462	1.740	0.137	14.888	1.233
	500	0.452	1.648	0.134	14.131	1.206
PrSe	100	0.511	2.094	0.136	17.453	1.224
	200	0.496	1.992	0.135	16.919	1.215
	300	0.482	1.900	0.134	16.236	1.206
	400	0.464	1.790	0.132	15.349	1.188
	500	0.448	1.703	0.131	14.650	1.178
PrTe	100	0.514	2.260	0.133	19.041	1.197
	200	0.496	2.135	0.132	18.253	1.188
	300	0.478	2.014	0.130	17.305	1.170
	400	0.461	1.909	0.129	16.449	1.161
	500	0.446	1.815	0.128	15.674	1.152

Table 7.19 Average of ultrasonic Grüneisen parameters ($\langle\gamma_i^j\rangle_l$ for longitudinal wave), average of square ultrasonic Grüneisen parameters ($\langle(\gamma_i^j)^2\rangle_{\text{long}}$ for longitudinal wave and $\langle(\gamma_i^j)^2\rangle_{\text{shear}}$ for shear wave) and acoustic coupling constants (D_l for longitudinal wave and D_s for shear wave) of the intermetallics at room temperature along $\langle 100 \rangle$ crystallographic direction.

Material	$\langle\gamma_i^j\rangle$	$\langle(\gamma_i^j)^2\rangle_l$	$\langle(\gamma_i^j)^2\rangle_s$	D_l	D_s
CeS	0.482	1.933	0.133	11.142	1.197
CeSe	0.481	1.931	0.133	11.168	1.197
CeTe	0.479	2.078	0.129	17.900	1.170
NdS	0.482	1.930	0.133	16.567	1.197
NdSe	0.483	1.846	0.137	15.467	1.233
NdTe	0.480	2.161	0.129	18.445	1.170

Table 7.20 Average of ultrasonic Grüneisen parameters ($\langle\gamma_i^j\rangle_l$ for longitudinal wave), average of square ultrasonic Grüneisen parameters ($\langle(\gamma_i^j)^2\rangle_{\text{long}}$ for longitudinal wave, $\langle(\gamma_i^j)^2\rangle_{\text{shear1}}$ for shear wave polarized along $\langle 001 \rangle$ direction and $\langle(\gamma_i^j)^2\rangle_{\text{shear2}}$ for shear wave polarized along $\langle 1\bar{1}0 \rangle$ direction) and acoustic coupling constants (D_l for longitudinal wave, D_{s1} for shear wave polarized along $\langle 001 \rangle$ direction and D_{s2} for shear wave polarized along $\langle 1\bar{1}0 \rangle$ direction) of the intermetallics at their temperature range along $\langle 110 \rangle$ crystallographic direction.

Material	Temp.[K]	$\langle\gamma_i^j\rangle$	$\langle(\gamma_i^j)^2\rangle_l$	$\langle(\gamma_i^j)^2\rangle_{s1}$	$\langle(\gamma_i^j)^2\rangle_{s2}$	D_l	D_{s1}	D_{s2}
LaS	100	-0.808	2.905	0.135	4.020	21.924	1.212	36.181
	200	-0.767	2.625	0.31	3.649	20.897	1.222	33.115
	300	-0.731	2.433	0.126	3.474	19.719	1.135	31.270
	400	-0.696	2.199	0.122	3.262	17.960	1.094	29.357
	450	-0.678	2.094	0.119	3.080	17.149	1.072	27.717
LaSe	100	-0.798	2.937	0.082	4.092	22.485	0.735	36.823
	200	-0.756	2.646	0.078	3.938	21.321	0.703	35.440
	300	-0.716	2.413	0.075	3.559	21.714	0.672	32.027
	400	-0.681	2.224	0.072	3.334	18.319	0.645	30.005
	450	-0.665	2.133	0.070	3.245	17.620	0.633	29.208
LaTe	100	-0.794	3.030	0.046	3.598	23.995	0.411	32.385
	200	-0.748	2.737	0.044	3.426	22.771	0.393	30.830
	300	-0.706	2.531	0.042	3.252	22.789	0.379	29.271
	400	-0.657	2.237	0.041	3.122	18.617	0.365	28.101
	450	-0.626	2.095	0.040	3.078	17.514	0.359	27.704

Table 7.21 Average of ultrasonic Grüneisen parameters ($\langle\gamma_l^j\rangle_l$ for longitudinal wave), average of square ultrasonic Grüneisen parameters ($\langle(\gamma_l^j)^2\rangle_{\text{long}}$ for longitudinal wave, $\langle(\gamma_l^j)^2\rangle_{\text{Shear1}}$ for shear wave polarized along $\langle 001 \rangle$ direction and $\langle(\gamma_l^j)^2\rangle_{\text{Shear2}}$ for shear wave polarized along $\langle 1\bar{1}0 \rangle$ direction) and acoustic coupling constants (D_l for longitudinal wave, D_{S1} for shear wave polarized along $\langle 001 \rangle$ direction and D_{S2} for shear wave polarized along $\langle 1\bar{1}0 \rangle$ direction) of the intermetallics at their temperature range along $\langle 110 \rangle$ crystallographic direction.

Material	Temp.[K]	$\langle\gamma_l^j\rangle$	$\langle(\gamma_l^j)^2\rangle_l$	$\langle(\gamma_l^j)^2\rangle_{S1}$	$\langle(\gamma_l^j)^2\rangle_{S2}$	D_l	D_{S1}	D_{S2}
PrS	100	-0.788	2.262	0.319	3.081	17.045	2.871	27.729
	200	-0.755	2.082	0.286	2.970	16.401	2.574	26.730
	300	-0.725	1.921	0.260	2.870	15.335	2.340	25.830
	400	-0.686	1.721	0.225	2.737	14.017	2.025	24.633
	500	-0.655	1.604	0.203	2.633	13.438	1.287	26.001
PrSe	100	-0.788	2.262	0.319	3.081	17.045	2.871	27.729
	200	-0.755	2.082	0.286	2.970	16.401	2.574	26.730
	300	-0.725	1.921	0.260	2.870	15.335	2.340	25.830
	400	-0.686	1.742	0.225	2.737	14.017	2.025	24.633
	500	-0.655	1.604	0.203	2.633	13.438	1.287	26.001
PrTe	100	-0.783	2.338	0.215	3.403	18.028	1.935	30.627
	200	-0.744	2.134	0.193	3.264	17.043	1.737	29.376
	300	-0.706	1.944	0.173	3.124	15.705	1.577	28.116
	400	-0.670	1.783	0.156	3.001	14.501	1.404	27.009
	500	-0.638	1.645	0.143	2.889	13.446	1.289	26.011

Table 7.22 Average of ultrasonic Grüneisen parameters ($\langle\gamma_l^j\rangle_l$ for longitudinal wave), average of square ultrasonic Grüneisen parameters ($\langle(\gamma_l^j)^2\rangle_{\text{long}}$ for longitudinal wave, $\langle(\gamma_l^j)^2\rangle_{\text{Shear1}}$ for shear wave polarized along $\langle 001 \rangle$ direction and $\langle(\gamma_l^j)^2\rangle_{\text{Shear2}}$ for shear wave polarized along $\langle 1\bar{1}0 \rangle$ direction) and acoustic coupling constants (D_l for longitudinal wave, D_{S1} for shear wave polarized along $\langle 001 \rangle$ direction and D_{S2} for shear wave polarized along $\langle 1\bar{1}0 \rangle$ direction) of the intermetallics at room temperature along $\langle 110 \rangle$ crystallographic direction.

Material	$\langle\gamma_l^j\rangle$	$\langle(\gamma_l^j)^2\rangle_l$	$\langle(\gamma_l^j)^2\rangle_{S1}$	$\langle(\gamma_l^j)^2\rangle_{S2}$	D_l	D_{S1}	D_{S2}
CeS	-0.722	1.934	0.234	2.936	15.485	2.106	26.424
CeSe	-0.719	1.923	0.229	2.940	15.451	2.061	24.460
CeTe	-0.704	1.984	0.154	3.253	16.132	1.386	29.277
NdS	-0.724	1.939	0.241	2.925	15.503	2.169	26.325
NdSe	-0.732	1.920	0.2325	2.750	15.333	2.925	24.751
NdTe	-0.703	2.047	0.136	3.415	16.269	1.260	30.735

Table 7.23 Average of ultrasonic Grüneisen parameters ($\langle\gamma_i^j\rangle_l$ for longitudinal wave), average of square ultrasonic Grüneisen parameters ($\langle(\gamma_i^j)^2\rangle_{\text{long}}$ for longitudinal wave and $\langle(\gamma_i^j)^2\rangle_{\text{Shear}}$ for shear wave) and acoustic coupling constants (D_l for longitudinal wave and D_s for shear wave) of the intermetallics at their temperature range along $\langle 111 \rangle$ crystallographic direction. (* shear wave polarized along $\langle \bar{1}10 \rangle$)

Material	Temp.[K]	$\langle\gamma_i^j\rangle$	$\langle(\gamma_i^j)^2\rangle_l$	$\langle(\gamma_i^j)^2\rangle_s$	D_l	D_s
LaS	100	-0.654	1.522	2.065	18.586	18.586
	200	-0.626	1.397	1.977	10.753	17.793
	300	-0.602	1.285	1.893	10.095	17.036
	400	-0.581	1.202	1.855	9.602	16.698
	450	-0.566	1.144	1.815	9.112	16.335
LaSe	100	-0.650	1.995	2.621	15.761	23.582
	200	-0.616	1.796	2.500	14.633	22.501
	300	-0.589	1.641	2.394	13.490	21.547
	400	-0.561	1.496	2.301	12.363	20.711
	450	-0.551	1.440	2.217	11.916	19.951
LaTe	100	-0.646	1.523	2.222	10.550	20.000
	200	-0.617	1.387	2.126	10.155	19.130
	300	-0.568	1.267	2.034	10.155	18.308
	400	-0.566	1.165	1.953	9.326	17.578
	450	-0.554	1.119	1.916	8.975	17.245

Table 7.24 Average of ultrasonic Grüneisen parameters ($\langle\gamma_i^j\rangle_l$ for longitudinal wave), average of square ultrasonic Grüneisen parameters ($\langle(\gamma_i^j)^2\rangle_{\text{long}}$ for longitudinal wave and $\langle(\gamma_i^j)^2\rangle_{\text{Shear}}$ for shear wave) and acoustic coupling constants (D_l for longitudinal wave and D_s for shear wave) of the intermetallics at their temperature range along $\langle 111 \rangle$ crystallographic direction. (* shear wave polarized along $\langle \bar{1}10 \rangle$)

Material	Temp.[K]	$\langle\gamma_i^j\rangle$	$\langle(\gamma_i^j)^2\rangle_l$	$\langle(\gamma_i^j)^2\rangle_s$	D_l	D_s
PrS	100	-0.630	1.883	2.005	14.659	18.045
	200	-0.603	1.723	1.918	13.955	17.262
	300	-0.578	1.581	1.837	12.945	16.533
	400	-0.549	1.463	1.796	12.077	16.164
	500	-0.533	1.348	1.695	11.157	15.255
PrSe	100	-0.625	1.848	2.080	14.548	18.720
	200	-0.602	1.713	2.007	13.931	18.063
	300	-0.581	1.592	1.942	13.073	17.478
	400	-0.555	1.455	1.855	12.008	16.695
	500	-0.533	1.348	1.787	11.174	16.083
PrTe	100	-0.639	2.452	2.300	20.061	20.700
	200	-0.612	1.768	2.210	14.448	19.890
	300	-0.585	1.616	2.118	13.314	19.062
	400	-0.560	1.486	2.038	12.264	18.342
	500	-0.538	1.372	1.965	11.382	17.685

Table 7.25 Average of ultrasonic Grüneisen parameters ($\langle \gamma_l^j \rangle_l$ for longitudinal wave), average of square ultrasonic Grüneisen parameters ($\langle (\gamma_l^j)^2 \rangle_{\text{long}}$ for longitudinal wave and $\langle (\gamma_l^j)^2 \rangle_{\text{shear}}$ for shear wave) and acoustic coupling constants (D_l for longitudinal wave and D_s for shear wave) of the intermetallics at room temperature along $\langle 111 \rangle$ crystallographic direction. (* shear wave polarized along $\langle \bar{1}10 \rangle$)

Material	$\langle \gamma_l^j \rangle$	$\langle (\gamma_l^j)^2 \rangle_l$	$\langle (\gamma_l^j)^2 \rangle_s$	D_l	D_s
CeS	-0.583	1.606	1.987	13.202	17.883
CeSe	-0.582	1.598	1.990	13.166	17.910
CeTe	-0.590	1.646	2.206	13.600	19.854
NdS	-0.584	1.609	1.979	13.213	17.820
NdSe	-0.578	1.581	1.859	13.015	16.731
NdTe	-0.600	1.691	2.316	13.665	20.844

Table 7.26 Ultrasonic attenuation due to phonon-phonon interaction [$(\alpha/f^2)_{\text{Akh long}}$ for longitudinal wave and $(\alpha/f^2)_{\text{Akh shear}}$ for shear wave] and due to thermoelastic loss $(\alpha/f^2)_{\text{th}}$ of the intermetallics at their temperature range along $\langle 100 \rangle$ in $10^{-18} \text{ Np s}^2/\text{cm}$.

Crystal	Temp.(K)	$(\alpha/f^2)_{\text{th}}$	$(\alpha/f^2)_{\text{Akh long}}$	$(\alpha/f^2)_{\text{Akh shear}}$
LaS	100	0.482	11.392	2.712
	200	1.432	34.571	8.716
	300	1.612	59.934	16.333
	400	2.021	79.182	27.381
	450	2.114	84.622	42.921
LaSe	100	0.684	16.572	4.172
	200	1.482	47.752	13.132
	300	2.241	79.482	28.851
	400	2.913	107.742	35.216
	450	3.112	116.391	39.651
LaTe	100	1.192	29.941	8.401
	200	2.851	88.724	26.931
	300	4.421	147.912	49.532
	400	5.801	199.003	73.181
	450	6.102	212.372	80.881

Table 7.27 Ultrasonic attenuation due to phonon-phonon interaction [$(\alpha/f^2)_{\text{Akh long}}$ for longitudinal wave and $(\alpha/f^2)_{\text{Akh shear}}$ for shear wave] and due to thermoelastic loss $(\alpha/f^2)_{\text{th}}$ of the intermetallics at their temperature range along $\langle 100 \rangle$ in $10^{-18} \text{Np s}^2/\text{cm}$.

Crystal	Temp.(K)	$(\alpha/f^2)_{\text{th}}$	$(\alpha/f^2)_{\text{Akh long}}$	$(\alpha/f^2)_{\text{Akh shear}}$
PrS	100	0.035	7.301	1.659
	200	0.096	24.400	5.907
	300	0.146	43.917	11.510
	400	0.186	62.411	17.744
	500	0.202	74.095	22.640
PrSe	100	0.035	8.048	2.023
	200	0.083	25.747	6.814
	300	0.136	48.096	13.501
	400	0.157	61.742	19.097
	500	0.172	74.563	24.996
PrTe	100	0.044	13.360	3.665
	200	0.102	40.873	12.069
	300	0.154	70.256	22.399
	400	0.188	94.565	33.150
	500	0.211	115.151	44.006

Table 7.28 Ultrasonic attenuation due to phonon-phonon interaction [$(\alpha/f^2)_{\text{Akh long}}$ for longitudinal wave and $(\alpha/f^2)_{\text{Akh shear}}$ for shear wave] and due to thermoelastic loss $(\alpha/f^2)_{\text{th}}$ of the intermetallics at room temperature along $\langle 100 \rangle$ in $10^{-18} \text{Np s}^2/\text{cm}$.

Material	$(\alpha/f^2)_{\text{th}}$	$(\alpha/f^2)_{\text{Akh long}}$	$(\alpha/f^2)_{\text{Akh shear}}$
CeS	0.0723	18.481	7.953
CeSe	0.097	25.625	11.081
CeTe	0.105	53.299	17.826
NdS	0.083	30.410	8.693
NdSe	0.519	170.375	45.375
NdTe	0.081	35.997	12.793

Table 7.29 Ultrasonic attenuation due to phonon-phonon interaction $[(\alpha/f^2)_{\text{Akh long}}$ for longitudinal wave and $(\alpha/f^2)_{\text{Akh shear}}$ for shear wave] and due to thermoelastic loss $(\alpha/f^2)_{\text{th}}$ of the intermetallics at their temperature range along $\langle 110 \rangle$ in $10^{-18} \text{Np s}^2/\text{cm}$.

Crystal	Temp.(K)	$(\alpha/f^2)_{\text{th}}$	$(\alpha/f^2)_{\text{Akh long}}$	$(\alpha/f^2)^*_{\text{Akh shear1}}$	$(\alpha/f^2)^{\#}_{\text{Akh shear2}}$
LaS	100	1.170	14.526	2.621	78.226
	200	2.450	43.303	8.532	223.065
	300	3.687	74.374	15.177	418.260
	400	4.478	93.978	21.230	569.587
	450	4.652	98.823	23.395	604.949
LaSe	100	1.617	10.250	2.514	125.905
	200	3.399	57.686	7.666	386.662
	300	4.699	102.991	13.486	642.531
	400	6.286	123.943	19.346	899.618
	450	6.616	131.958	21.489	991.604
LaTe	100	2.841	36.091	2.900	228.547
	200	6.323	105.363	9.001	705.360
	300	9.490	186.062	16.139	1245.39
	400	11.655	215.798	23.152	1784.56
	450	11.705	224.477	25.821	1993.66

* shear wave polarized along $\langle 001 \rangle$ direction

shear wave polarized along $\langle 1\bar{1}0 \rangle$ direction

Table 7.30 Ultrasonic attenuation due to phonon-phonon interaction $[(\alpha/f^2)_{\text{Akh long}}$ for longitudinal wave and $(\alpha/f^2)_{\text{Akh shear}}$ for shear wave] and due to thermoelastic loss $(\alpha/f^2)_{\text{th}}$ of the intermetallics at their temperature range along $\langle 110 \rangle$ in $10^{-18} \text{Np s}^2/\text{cm}$.

Crystal	Temp.(K)	$(\alpha/f^2)_{\text{th}}$	$(\alpha/f^2)_{\text{Akh long}}$	$(\alpha/f^2)^*_{\text{Akh shear1}}$	$(\alpha/f^2)^{\#}_{\text{Akh shear2}}$
PrS	100	0.0100	7.448	5.667	34.736
	200	0.228	24.961	17.547	121.335
	300	0.339	42.937	29.359	226.780
	400	0.408	59.125	42.611	343.738
	500	0.443	68.049	45.451	422.725
PrSe	100	0.084	7.860	4.744	45.820
	200	0.192	24.959	14.436	149.912
	300	0.307	45.426	26.195	289.154
	400	0.342	56.379	32.551	395.965
	500	0.347	68.394	27.285	551.239
PrTe	100	0.103	12.646	5.925	93.787
	200	0.229	38.161	17.647	298.451
	300	0.336	64.015	30.116	543.829
	400	0.397	83.647	40.089	771.194
	500	0.433	98.783	49.163	993.222

* shear wave polarized along $\langle 001 \rangle$ direction

shear wave polarized along $\langle 1\bar{1}0 \rangle$ direction

Table 7.31 Ultrasonic attenuation due to phonon-phonon interaction $[(\alpha/f^2)_{\text{Akh long}}$ for longitudinal wave and $(\alpha/f^2)_{\text{Akh shear}}$ for shear wave] and due to thermoelastic loss $(\alpha/f^2)_{\text{th}}$ of the intermetallics at their temperature range along $\langle 110 \rangle$ in $10^{-18} \text{Np s}^2/\text{cm}$.

Material	$(\alpha/f^2)_{\text{th}}$	$(\alpha/f^2)_{\text{Akh long}}$	$(\alpha/f^2)^*_{\text{Akh shear1}}$	$(\alpha/f^2)^{\#}_{\text{Akh shear2}}$
CeS	0.163	29.351	25.684	175.559
CeSe	0.217	35.453	19.079	244.947
CeTe	0.226	48.035	21.117	446.054
NdS	0.185	28.561	15.752	191.185
NdSe	1.191	165.692	107.641	910.805
NdTe	0.174	31.750	5.555	185.924

* shear wave polarized along $\langle 001 \rangle$ direction

[#] shear wave polarized along $\langle 1\bar{1}0 \rangle$ direction

Table 7.32 Ultrasonic attenuation due to phonon-phonon interaction $[(\alpha/f^2)_{\text{Akh long}}$ for longitudinal wave and $(\alpha/f^2)_{\text{Akh shear}}$ for shear wave] and due to thermoelastic loss $(\alpha/f^2)_{\text{th}}$ of the intermetallics at their temperature range along $\langle 111 \rangle$ in $10^{-18} \text{Np s}^2/\text{cm}$.

Crystal	Temp.(K)	$(\alpha/f^2)_{\text{th}}$	$(\alpha/f^2)_{\text{Akh.long}}$	$(\alpha/f^2)^*_{\text{Akh shear}}$
LaS	100	0.077	0.724	4.019
	200	0.163	2.228	12.523
	300	0.250	3.622	22.787
	400	0.312	5.024	31.393
	450	0.325	5.251	35.653
LaSe	100	0.106	0.508	6.838
	200	0.227	2.747	20.872
	300	0.312	4.817	36.731
	400	0.434	6.309	52.703
	450	0.459	6.722	58.547
LaTe	100	0.190	2.371	16.642
	200	0.429	6.771	51.481
	300	0.661	11.018	91.678
	400	0.850	12.363	131.525
	450	0.907	15.272	143.579

* shear wave polarized along $\langle \bar{1}10 \rangle$ direction

Table 7.33 Ultrasonic attenuation due to phonon-phonon interaction $[(\alpha/f^2)_{\text{Akh long}}$ for longitudinal wave and $(\alpha/f^2)_{\text{Akh shear}}$ for shear wave] and due to thermoelastic loss $(\alpha/f^2)_{\text{th}}$ of the intermetallics at their temperature range along $\langle 111 \rangle$ in $10^{-17} \text{Np s}^2/\text{cm}$.

Crystal	Temp.(K)	$(\alpha/f^2)_{\text{th}}$	$(\alpha/f^2)_{\text{Akh long}}$	$(\alpha/f^2)^{\bullet}_{\text{Akh shear}}$
PrS	100	0.060	6.287	23.427
	200	0.139	21.016	81.885
	300	0.209	36.442	153.216
	400	0.257	50.627	232.612
	500	0.281	58.502	286.378
PrSe	100	0.053	6.708	30.933
	200	0.122	21.200	101.304
	300	0.197	38.726	195.658
	400	0.224	48.298	268.365
	500	0.243	56.873	340.971
PrTe	100	0.068	14.075	63.388
	200	0.155	32.352	202.076
	300	0.231	54.270	368.703
	400	0.277	70.677	523.722
	500	0.308	83.617	675.556

[•] shear wave polarized along $\langle \bar{1}10 \rangle$ direction

Table 7.34 Ultrasonic attenuation due to phonon-phonon interaction $[(\alpha/f^2)_{\text{Akh long}}$ for longitudinal wave and $(\alpha/f^2)_{\text{Akh shear}}$ for shear wave] and due to thermoelastic loss $(\alpha/f^2)_{\text{th}}$ of the intermetallics at room temperature along $\langle 111 \rangle$ in $10^{-17} \text{Np s}^2/\text{cm}$.

Material	$(\alpha/f^2)_{\text{th}}$	$(\alpha/f^2)_{\text{Akh long}}$	$(\alpha/f^2)^{\bullet}_{\text{Akh shear}}$
CeS	0.073	18.481	7.953
CeSe	0.097	25.625	11.081
CeTe	0.105	53.299	17.826
NdS	0.083	30.410	8.693
NdSe	0.519	170.375	45.375
NdTe	0.081	35.997	12.793

• shear wave polarized along $\langle \bar{1}10 \rangle$ direction

Table 7.35 Comparison of ultrasonic absorption coefficient (α) in dB/ μ sec of intermetallics with LiF at room temperature at 900MHz

Material	$\langle 100 \rangle_l$	$\langle 100 \rangle_s$	$\langle 110 \rangle_l$	$\langle 110 \rangle_{s1}$	$\langle 110 \rangle_{s2}$	$\langle 111 \rangle_l$	$\langle 111 \rangle_{s3}$
LiF(exp.)	3.5	0.8	1.3	0.8	10.0	0.8	5.0
LaS	1.3	0.2	1.5	0.2	4.5	0.1	0.3
LaSe	1.5	0.3	2.0	0.1	6.0	0.1	0.4
LaTe	2.6	0.4	3.3	0.1	10.0	0.2	0.8
PrS	0.9	0.1	0.9	0.3	2.5	0.7	1.7
PrSe	0.9	0.1	0.8	0.3	2.7	0.7	1.8
PrTe	1.2	0.2	1.0	0.3	4.4	1.5	3.0
CeS	0.5	0.1	0.6	0.3	1.9	0.5	1.3
CeSe	0.5	0.1	0.7	0.2	2.3	0.6	0.6
CeTe	1.0	0.2	0.8	0.2	3.6	0.7	2.4
NdS	0.2	0.1	0.6	0.2	2.0	0.1	0.1
NdSe	3.0	0.4	3.0	1.0	8.6	1.3	5.8
NdTe	0.6	0.1	0.6	0.1	0.01	0.1	0.01

Where subscripts having meaning in following manner with their crystallographic directions:

l-stands for longitudinal wave,

s- stands for shear wave,

s1- stands for shear wave polarized along $\langle 001 \rangle$ direction

s2- stands for shear wave polarized along $\langle 1\bar{1}0 \rangle$ direction

s3- stands for shear wave polarized along $\langle \bar{1}10 \rangle$ direction

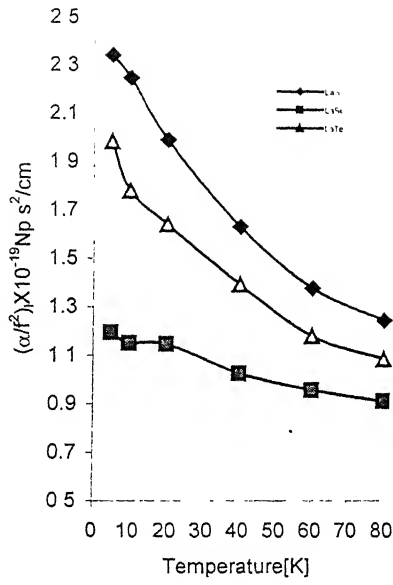


Fig.7.1 $(\alpha/f^2)_{\text{long}}$ vs temperature

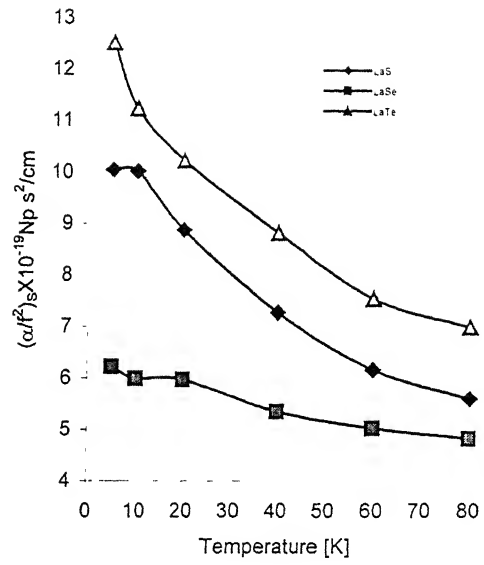


Fig.7.2 $(\alpha/f^2)_{\text{shear}}$ vs temperature

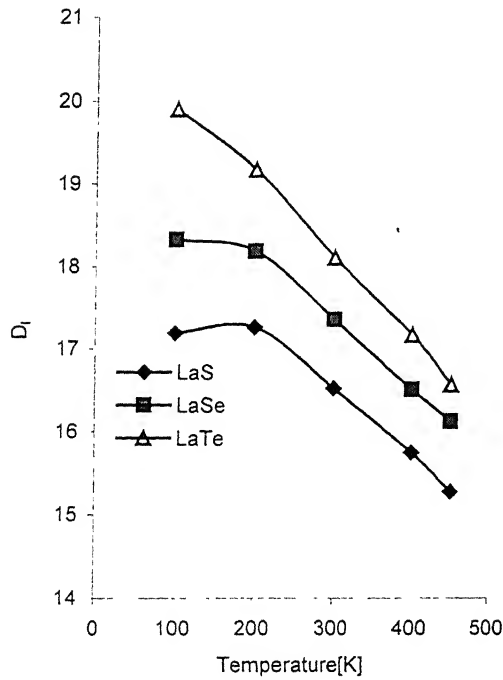


Fig.7.3 D_l vs. temperature along $\langle 100 \rangle$ direction

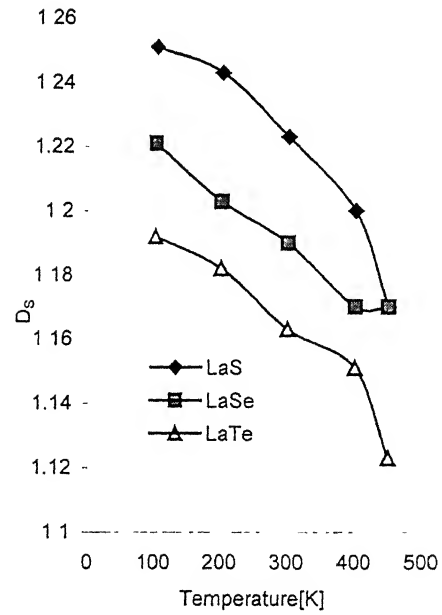


Fig.7.4 D_s vs. temperature along $\langle 100 \rangle$ direction

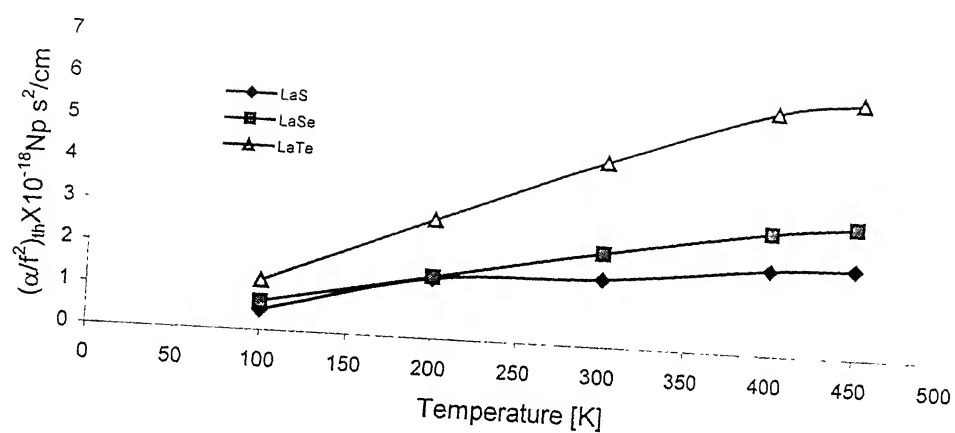


Fig.7.5 $(\alpha/f^2)_{th}$ vs. temperature along $\langle 100 \rangle$ direction

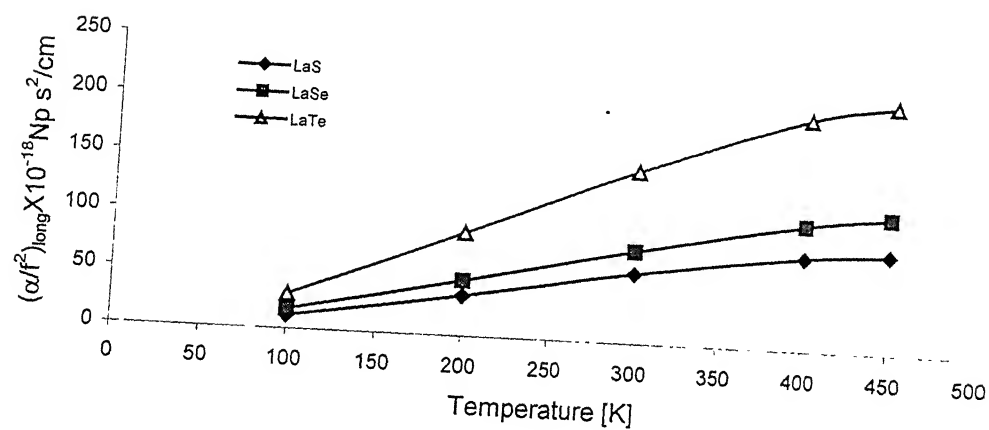


Fig.7.6 $(\alpha/f^2)_{long}$ vs. temperature along $\langle 100 \rangle$ direction

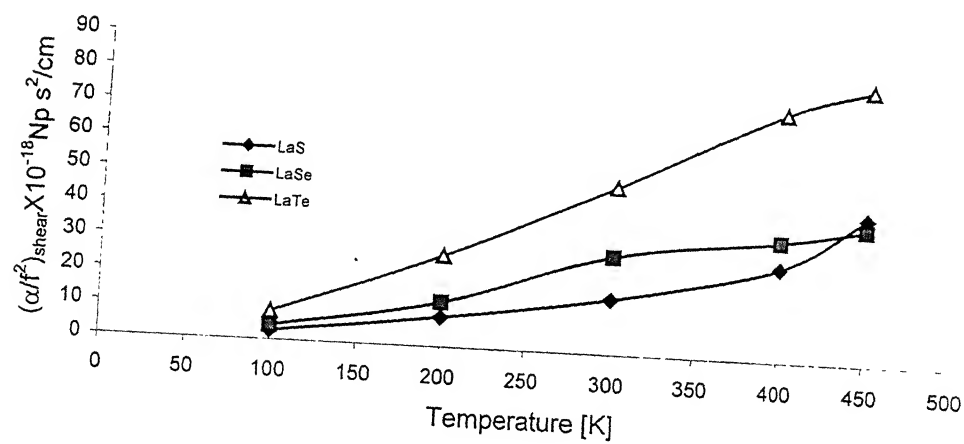


Fig.7.7 $(\alpha/f^2)_{shear}$ vs. temperature along $\langle 100 \rangle$ direction

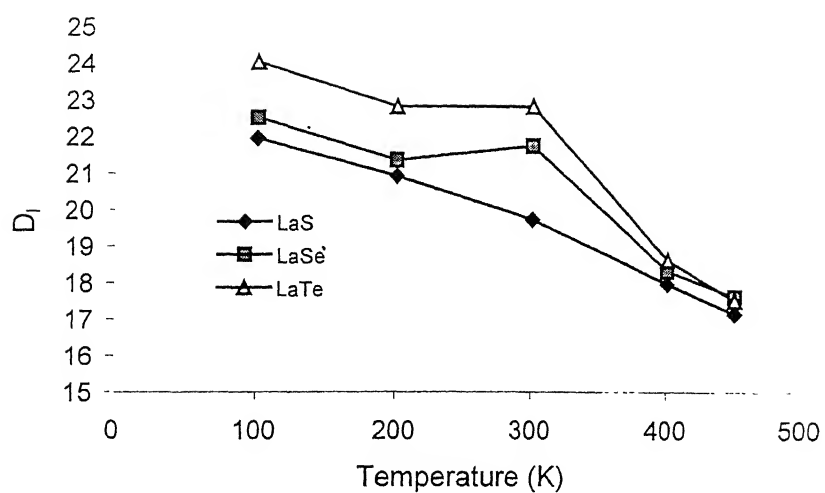


Fig.7.8 D_1 vs. temperature along $\langle 110 \rangle$ direction

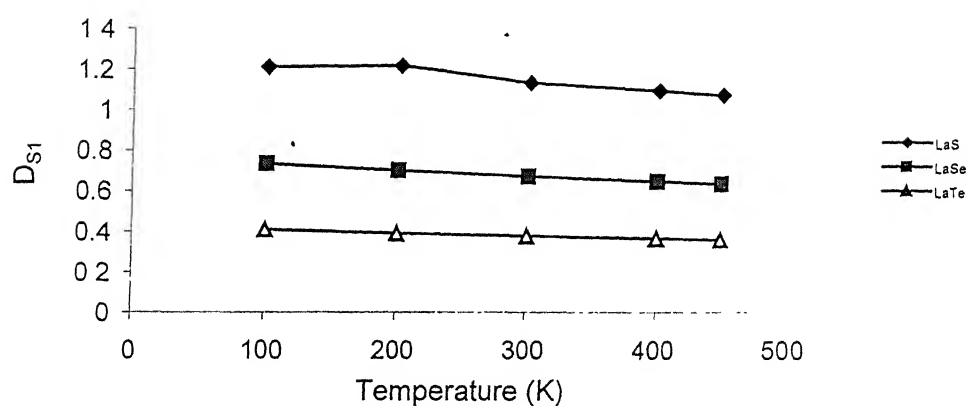


Fig.7.9 D_{S1} vs. temperature along $\langle 110 \rangle$ direction with polarized along $\langle 001 \rangle$ direction.

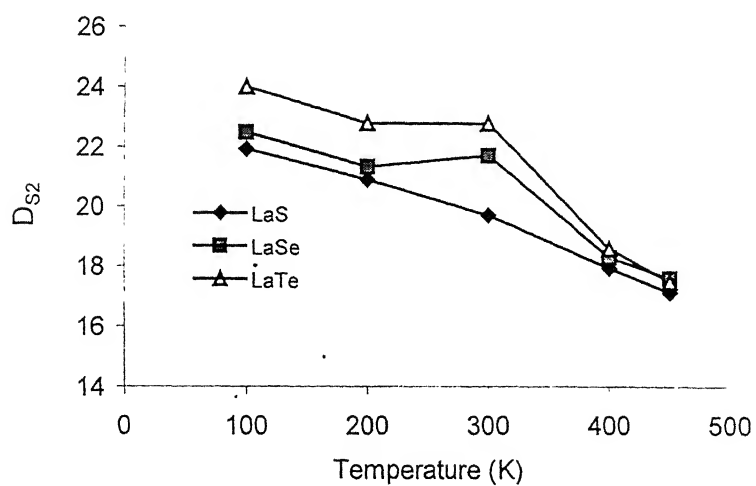


Fig.7.10 D_{S2} vs. temperature along $\langle 110 \rangle$ direction polarized along $\langle 110 \rangle$ direction.

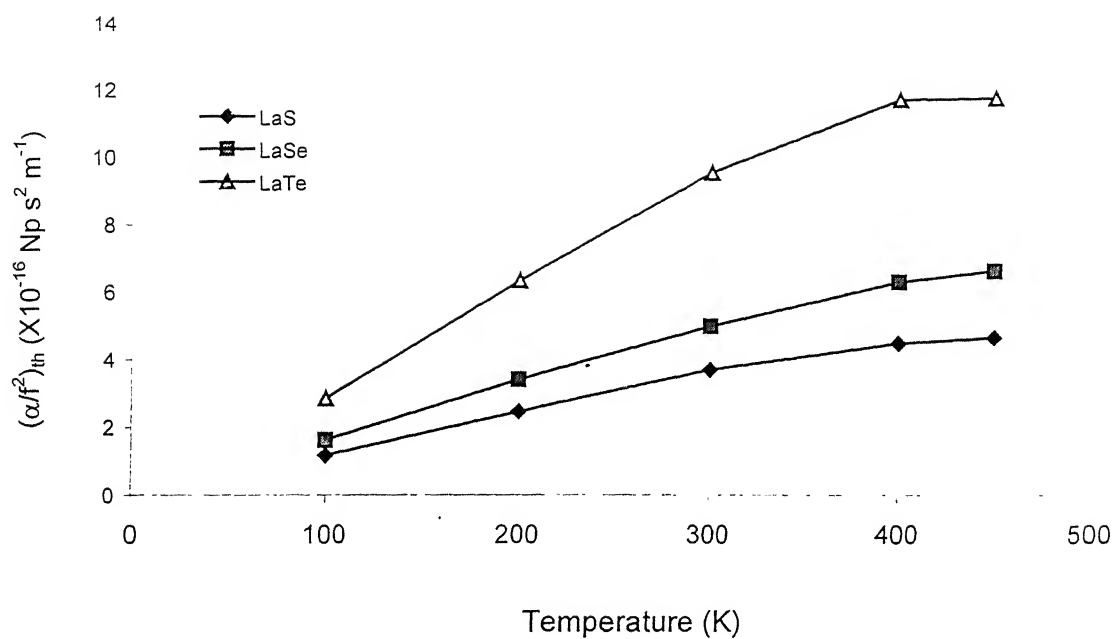


Fig.7.11 $(\alpha/f^2)_{th}$ vs. temperature along $\langle 110 \rangle$ direction.

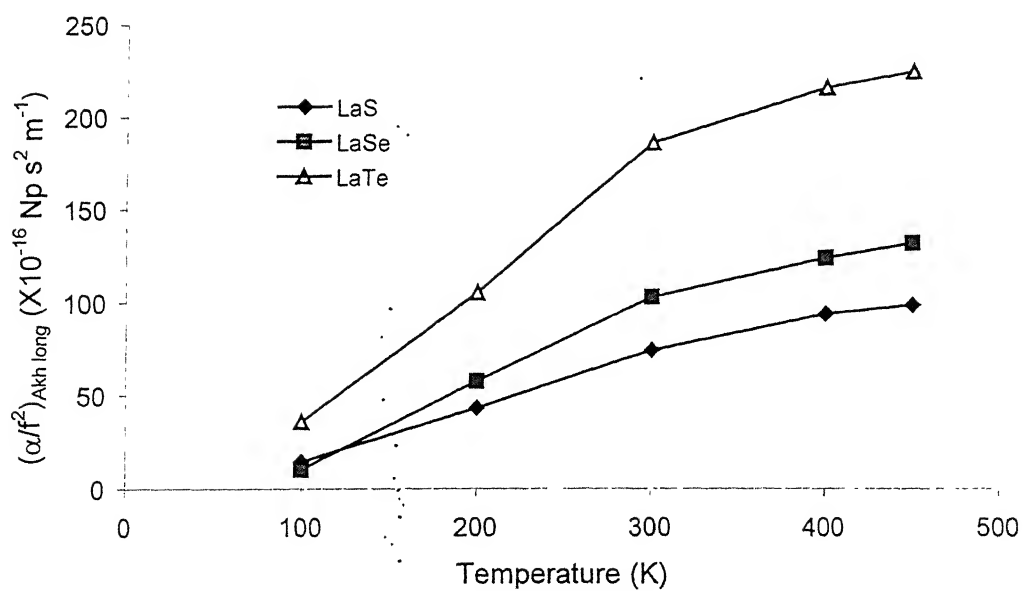


Fig.7.12 $(\alpha/f^2)_{Akh \text{ long}}$ vs. temperature along $\langle 110 \rangle$ direction

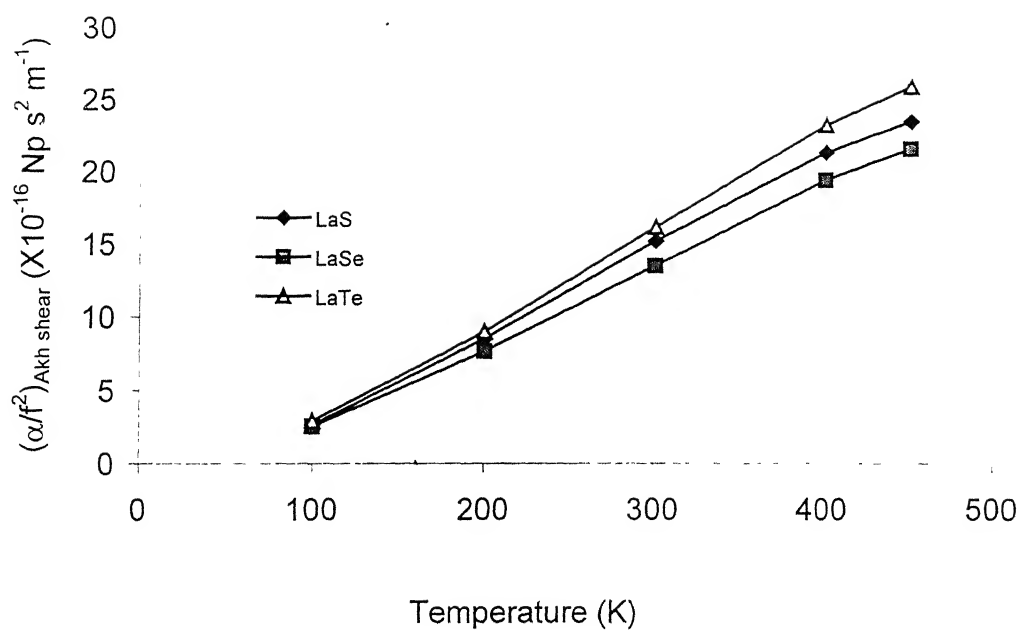


Fig.7.13 $(\alpha/f^2)_{\text{Akh,shear}}$ vs. temperature along $\langle 110 \rangle$ direction polarized along $\langle 001 \rangle$ direction.

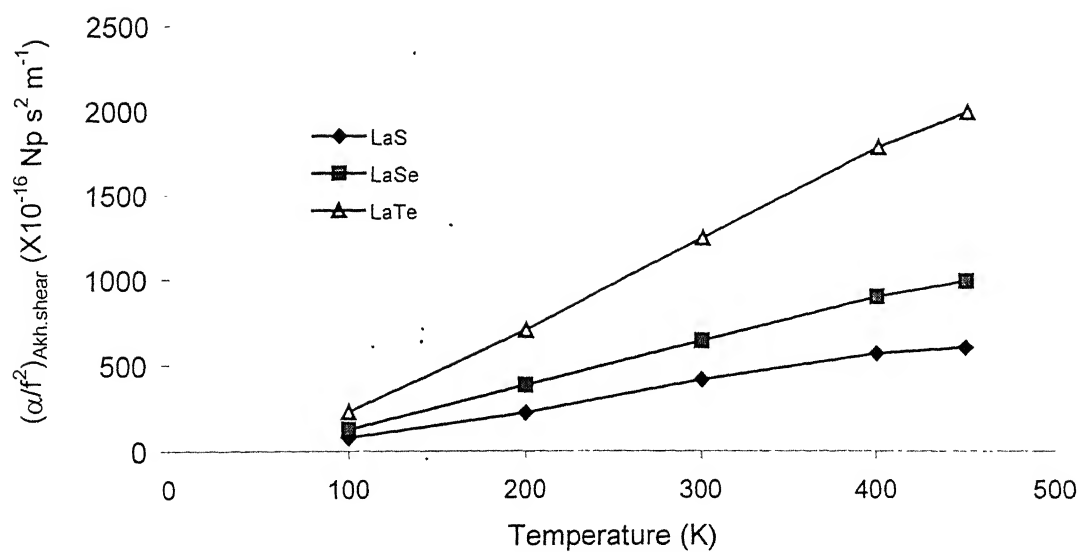


Fig.7.14 $(\alpha/f^2)_{\text{Akh,shear}}$ vs. temperature along $\langle 110 \rangle$ direction polarized along $\langle 1\bar{1}0 \rangle$ direction.

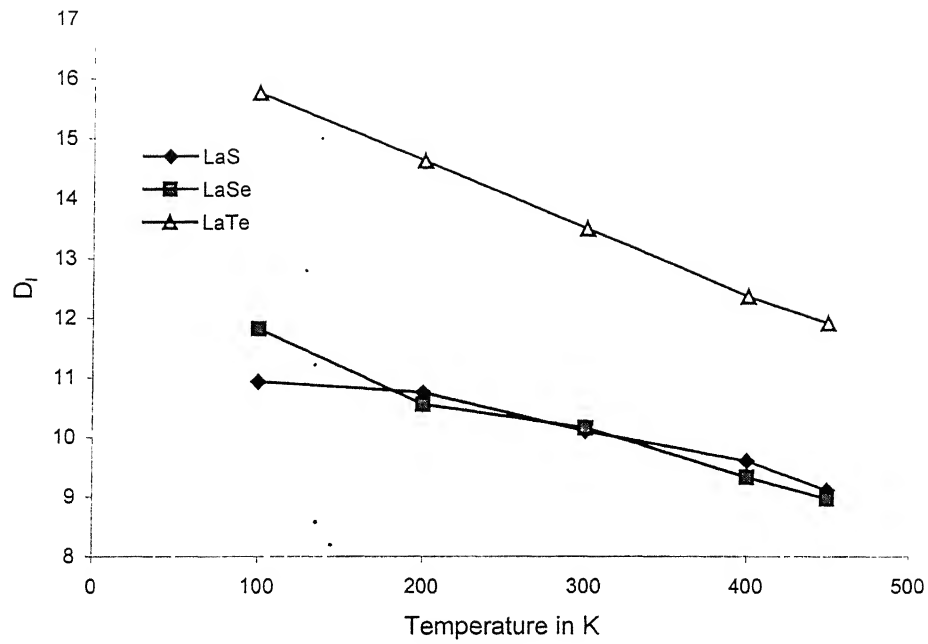


Fig.7.15 D_l vs temperature for longitudinal wave along $\langle 111 \rangle$ direction

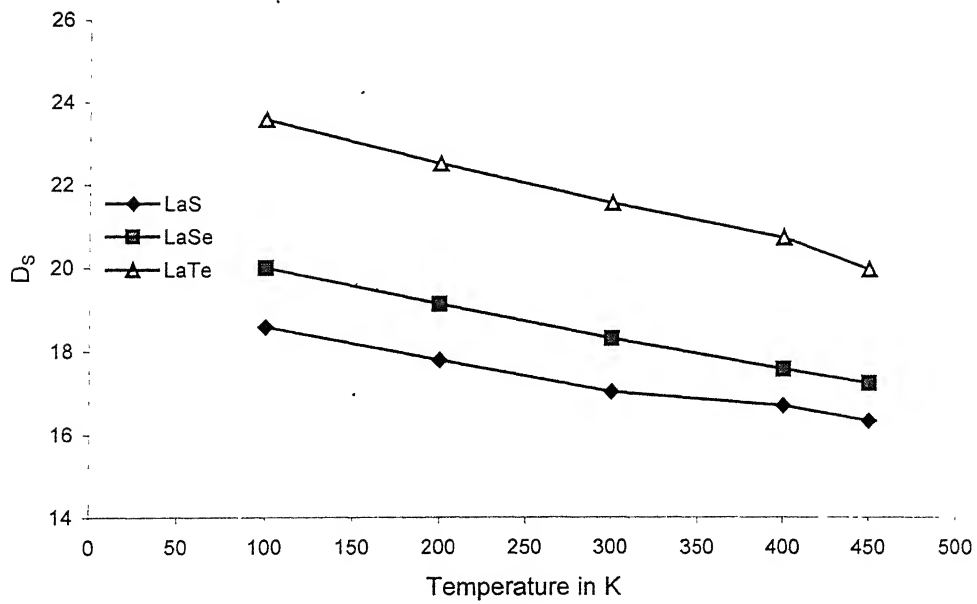


Fig.7.16 D_s vs. temperature for shear wave along $\langle 111 \rangle$ direction and shear wave polarized along $\langle \bar{1}10 \rangle$ direction

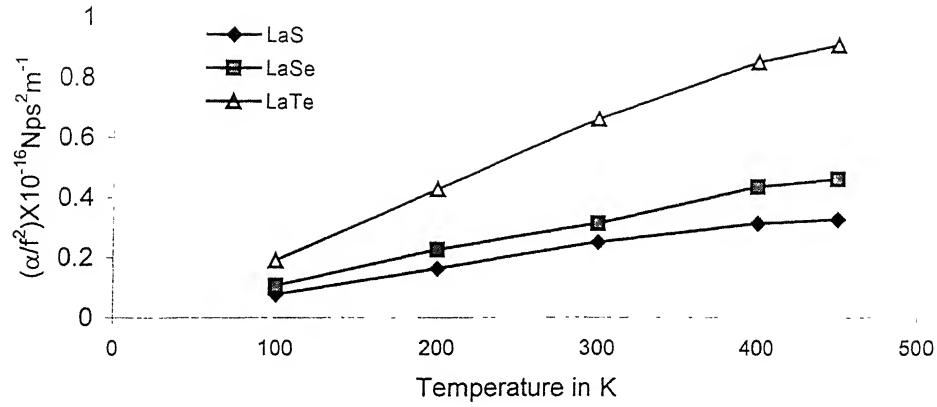


Fig. 7.17 $(\alpha/f^2)_{th}$ vs. temperature along $\langle 111 \rangle$ direction

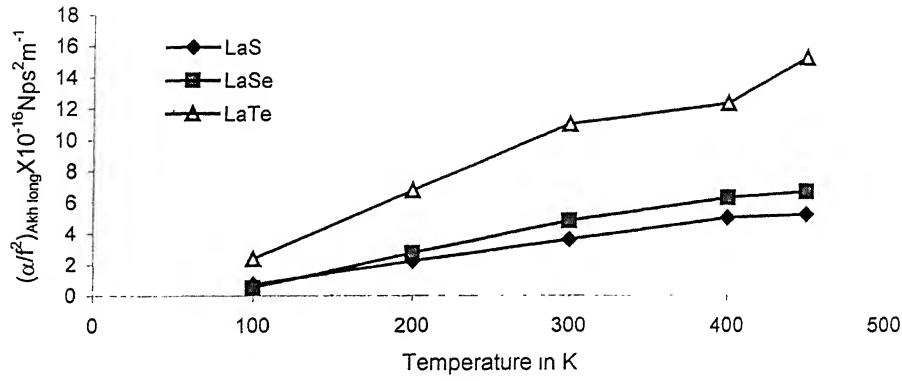


Fig. 7.18 $(\alpha/f^2)_{Akh \text{ long}}$ vs. temperature along $\langle 111 \rangle$ direction

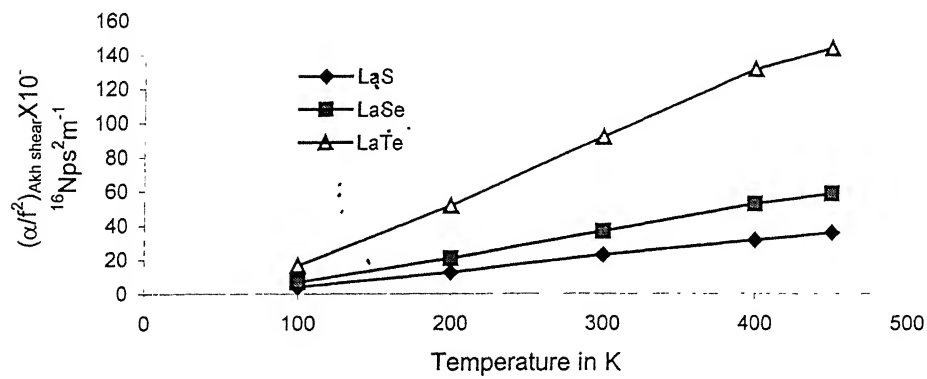


Fig. 7.19 $(\alpha/f^2)_{Akh \text{ shear}}$ vs. temperature along $\langle 111 \rangle$ direction polarized along $\langle \bar{1}10 \rangle$ direction

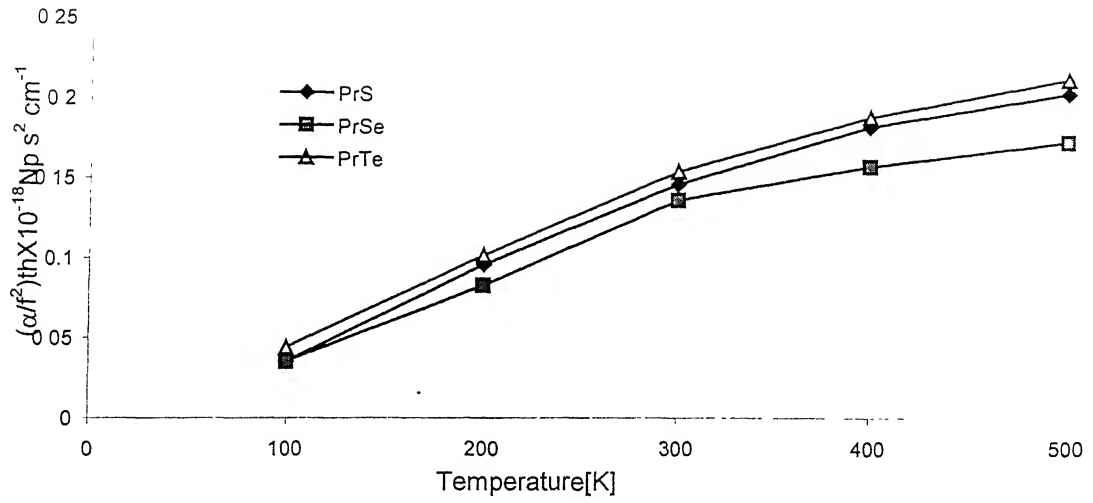


Fig.7.20 $(\alpha/f^2)_{th}$ vs. temperature along <100> direction

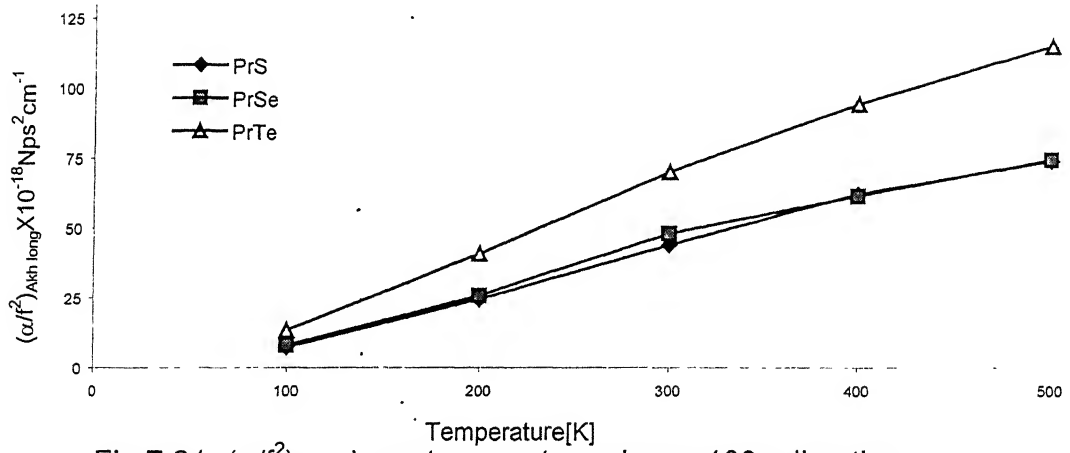


Fig.7.21 $(\alpha/f^2)_{Akh.long}$ vs temperature along <100> direction

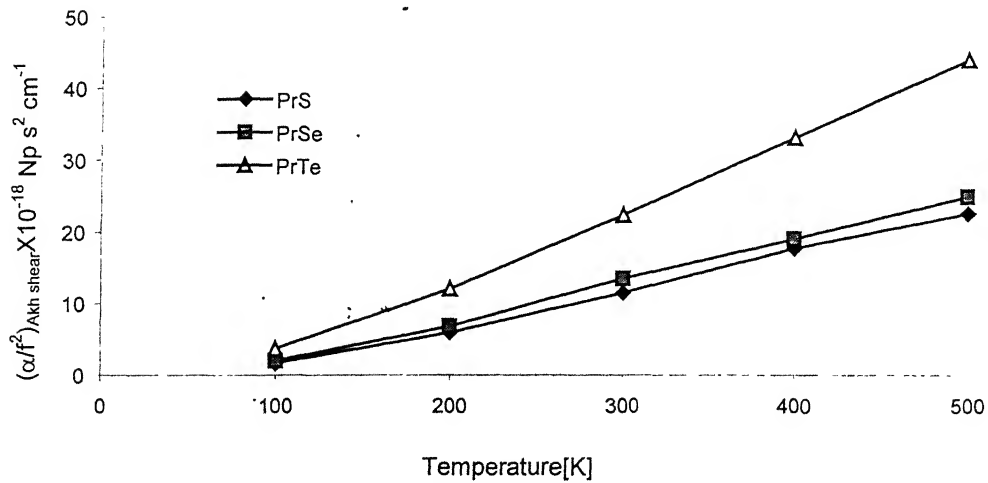


Fig. 7.22 $(\alpha/f^2)_{Akh.shear}$ vs. temperature along <100> direction

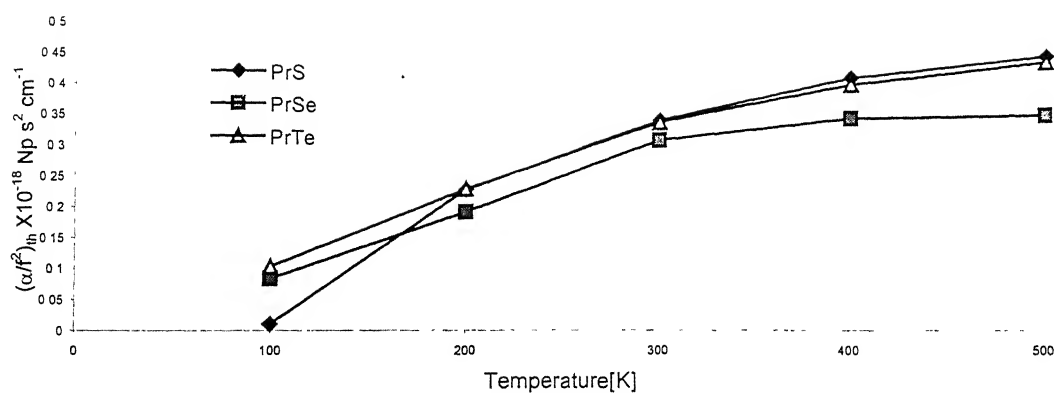


Fig.7.23 $(\alpha/f^2)_{th}$ vs. temperature along $\langle 110 \rangle$ direction

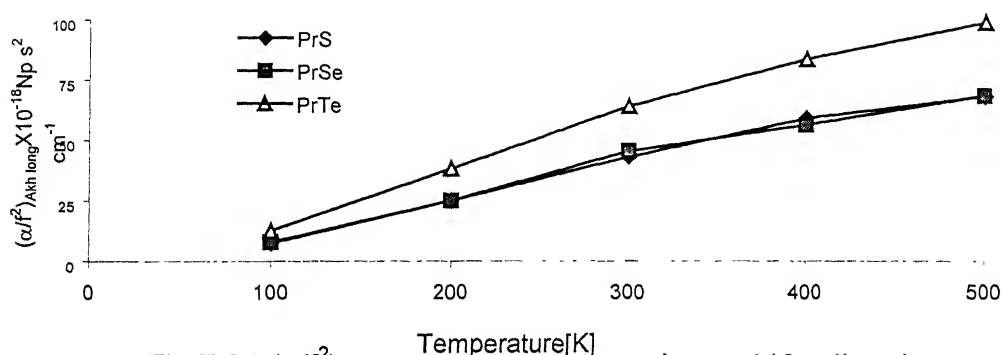


Fig.7.24 $(\alpha/f^2)_{Akh \text{ long.}}$ vs temperature along $\langle 110 \rangle$ direction

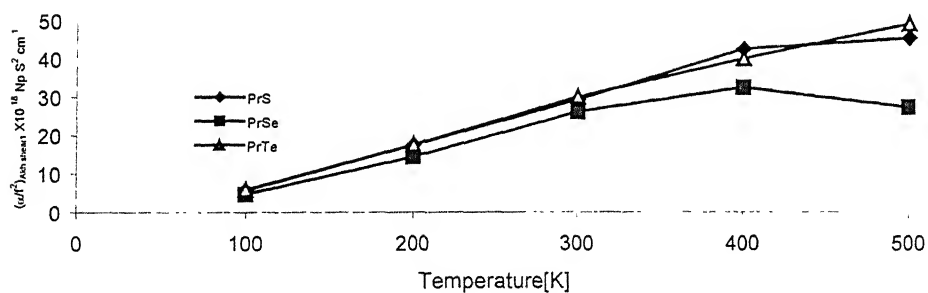


Fig.7.25 $(\alpha/f^2)_{Akh \text{ shear1}}$ vs temperature along $\langle 110 \rangle$ direction polarized along $\langle 001 \rangle$ direction

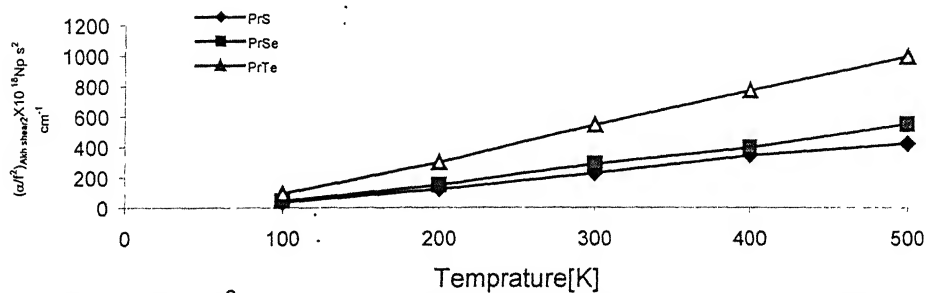


Fig.7.26 $(\alpha/f^2)_{Akh.shear2}$ vs. temperature along $\langle 110 \rangle$ direction polarized along $\langle 110 \rangle$

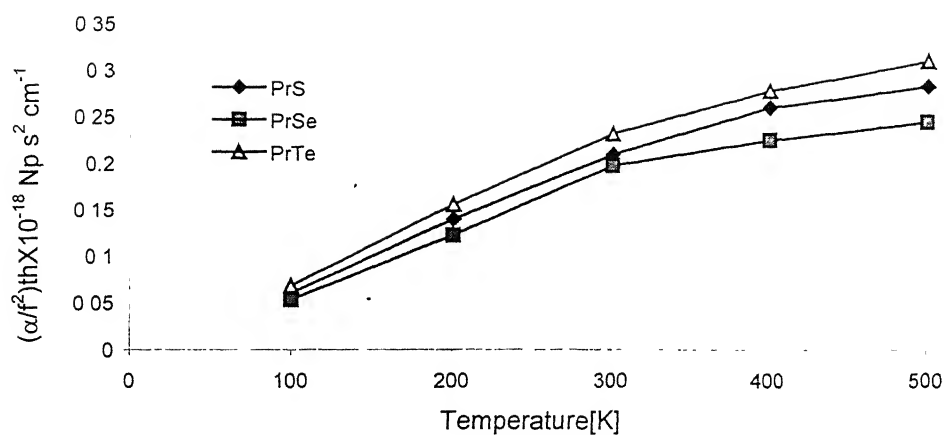


Fig.7.27 $(\alpha/f^2)_{th}$ vs temperature along $\langle 111 \rangle$ direction

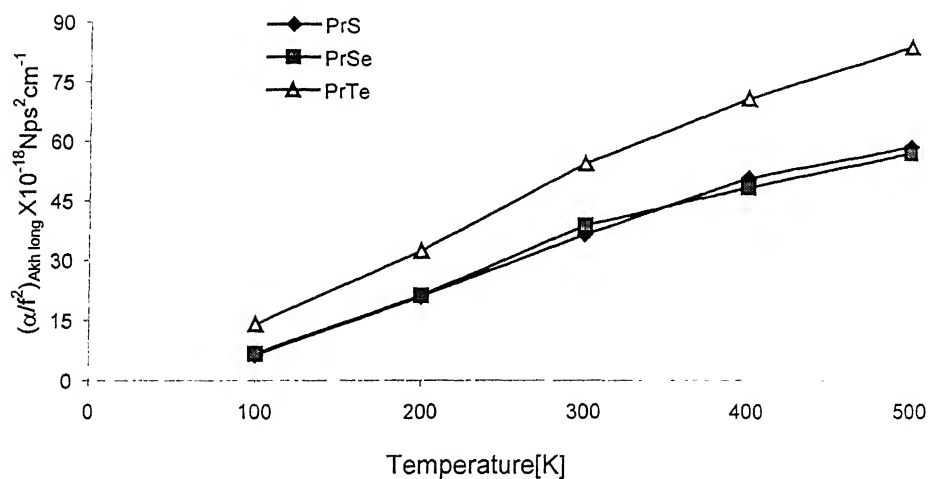


Fig.7.28 $(\alpha/f^2)_{Akh.long}$ vs temperature along $\langle 111 \rangle$ direction

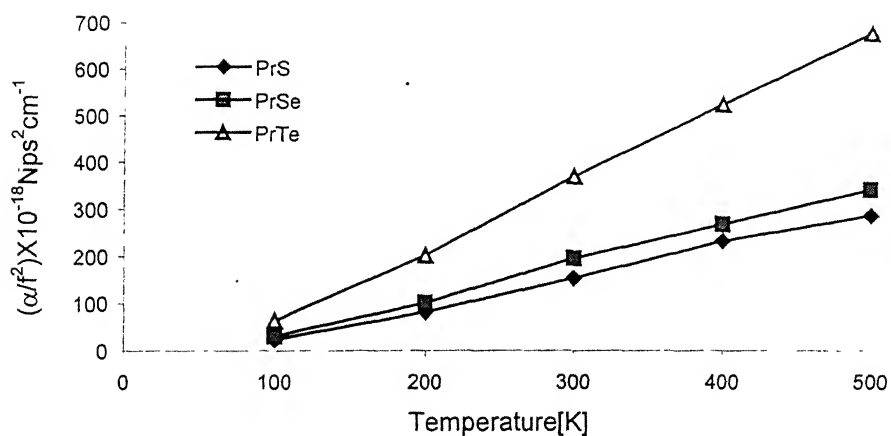


Fig.7.29 $(\alpha/f^2)_{Akh.shear}$ vs temperature along $\langle 111 \rangle$ direction polarized along $\langle \hat{1}10 \rangle$ direction

References

1. E.Schreiber, O.Anderson, N.Soga, Elastic constants and their measurements. (McGraw Hill, New York 1973).
2. E.P.Papadakis, J.Testing Eval. 12,273(1984).
3. D.Daniel, K.Sakata, J.J.Jonas, I.Mararow and J.F.Bussiere, Material Res.Soc. Symposium Proc. 142,77(1989).
4. Y.Li and R.B.Thomson, Material Res.Soc. Symposium Proc. 142,83(1989).
5. D.R.Allen, W.H.B.Copper, C.M.Sayer and M.G.Silk, in Research techniques in nondestructing Testing, edited by R.S.Sharpe, (Academic Press, New York, 1982), Vol. VI pp.151-209.
6. A.Vary, in Research techniques in nondestructing Testing, edited by R.S.Sharpe, (Academic Press, New York, 1982), Vol. VI pp.151-209.
7. A.P.Shatilo, C.Saundergeld and C.S,Rai, The Society of Exploration Geophysicist, Geoarchieve, March-April (1998).
8. M.B.Walker,M.P.Smith and K.V.Samaklin, Phys.Rev. B65,014517(2002).
9. K.Foster, R.G.Leisure and J.B.Shakare, Phys.Rev. B61,241(2000).
10. C.A.Damianon, N.T.Sanghvi,F.J.Fry and M.Moreno, J.Acoust. Soc. Am., 102, 628 (1997).
11. T.Gupta and D.M.Gatonde, Mod.Phys.Lett. B15,269(2001).
12. J.Wang, Q.F.Fang and Z.G.Zue, Phys.Stat.Solidi (Germany) A165,389(1998).
13. C.Zhu and R.Zheng, J.Appl.Phys. 87,3579(2000).
14. S.Ahmed, R.B.Thomson, Rev.of Progress in Quantative non destructive evaluation, San Diego, CA, 27July-1Aug.1997(New York, N Y, USA, Plenum 1998), Vol.2, pp.1649-1655.
15. W.P.Mason, Piezoelectric crystals and their applications to ultrasonics, D.Van Nostrand Co.Inc.Princeton, New Jersey, (1950) p.479.
16. R.W.Cahn, Contempory Physics 42,365(2001).
17. C.H.Desch, Intermetallic Compounds (Longmans Green, London),1914.
18. C.H.Desch,The Chemistry of Solids, (Cornell University Press, Ithaca, New York 1934) pp.153-160.
19. R.Ferro and A.Saccone, Physical Metallurgy, , edited by R.W.Cahn and P.Haasen, Amsterdam, North Holland 1996) 4th edition p.205.
20. B.A.Glowacki, Intermetallics 7,117(1999).

21. Y.Naik, G.A.Rama Rao and V.Venugopal, *Intermetallics* 9,309(2001).
22. V.P.Zhuze, A.V.Golubkov, E.V.Goncharova and V.M.Sergeeva , *Soviet Physics-Solid State* 6,205(1964).
23. V.P.Zhuze, A.V.Golubkov, E.V.Goncharova, T.I.Komarova and V.M.Sergeeva , *Soviet Physics-Solid State* 6,213(1964).
24. E.D.Debyatkova, V.P.Zhuze, A.V.Golubkov, V.M.Sergeeva and I.A.Smirnov, *Soviet Physics-Solid State* 6,343(1964).
25. A.V.Golubkov, E.D.Debyatkova, V.P.Zhuze, V.M.Sergeeva and I.A.Smirnov, *Soviet Physics-Solid State* 8,1403(1966).
26. A.Iandelli, *Gazz.Chim.Ital.* 85,881(1955).
27. K.Brugger, *Phys.Rev.* A133,1611(1964).
28. M.Born and J.B.Mayer, *Z.Phys.* 75,1(1931).
29. G.Leibfried and H.Haln, *Z.Phys.* 150, 497(1958).
30. G.Leibfried and W.Ludwig, in *Solid State Physics* edited by F.Seitz and D. Turnbull (Academic Press, New York 1964), Vol.12.
31. P.B.Ghate, *Phys.Rev.* 139,A1666(1965).
32. S.Mori and Y.Hiki, *J.Phys.Soc.Jpn.* 45,1449(1978).
33. A.Akhiezer, *J.Phys.(USSR)* 1,277(1939).
34. T.O.Woodruff and H.Ehrenreich, *Phys.Rev.* 123,1553(1961).
35. H.E.Bömmel and K.Dransfeld, *Phys.Rev.* 117,245(1960).
36. W.P.Mason, *Physical Acoustics* (Academic Press,New York 1965), Vol.IIIB p.237.
37. R.W.F.Wyckoff, *Crystal Structure*,Inter Science Publsheers,New York, (1948).
38. M.P.Tosi, in *Solid State Physics* edited by F.Seitz and D. Turnbull (Academic Press, New York 1965), Vol.16.
39. D.E.Gray edited, *AIP Handbook* (McGraw Hill Company, Inc., New York, 1978).
40. J.R.Drabble and R.E.W.Strathern, *Proc. Phys,Soc.* 92,1553(1970).
41. P.Wachter,M.Filzmoser and J.Rebizant, *Physica B*293,199(2001).
42. S.K.Kor and R.R.Yadav, *J.Pure Appl.Ultrason.* 8,90(1986).
43. D.K.Hsu and R.G.Leiser, *Phys.Rev.* B20(1979).
44. H.James Stathis and D.I.Bolef, *J.Appl.Phys.* 9,51(1980).
45. E.Kaldes and P.Wachter, *Solid State Comm.* 11,907(1972).
46. A.Chatterjee, A.K.Singh and A.Jayaraman,*Phys.Rev.* B6,2285(1972).

47. U.Benedict, W.B.Holzapfel, in K.A.Gschneidner jr, L.Eyring, G.H.Lander. G.R. Choppin (eds.). Handbook on the Physics and chemistry of Rare-earth, Lanthanides/Actinides: Physics I, (Elsevier Science, Amsterdam 1993), Vol.17, chapter 113,p.245.
48. M.Mendic, P.Wachter, J.C.Spirlet and J.Rebizent, Physica B,186-188,678(1993).
49. W.Frank,C.Elässer and M.Fähnle, Phy.Rev.Lett. 74,1791(1995).
50. P.T.Jochyme and K.Parlinski, Eur.Phys.J. B15,265(2000).
51. D.S.Puri, Solid State Commn. 18,1295(1976).
52. S.K.Kor, Kailash, K.Shanker and P.Mehrotra, J.Phys.Soc.Jpn. 56,2428(1987).
53. S.K.Kor and P.K.Mishra, Acustica 34,249(1976).
54. M.Levy, R.Kagiwada and I.Rudnick, Phys.Rev. 132,2039(1963).
55. S.K.Kor, R.R.Yadav and Kailash, J.Phys.Soc.Jpn. 55,207(1986).
56. R.C.Hanson, J.Phys.Chem.Solids 28,475(1967).
57. L.G.Merkulov, R.V.Kovalenkov and E.V.Konovodchenko,Soviet Physics-Solid State 11, 2241(1970).
58. R.R.Yadav and K.Shanker, "Ultrasonics International Conference'93" proc.pp.459-462.
59. L.Lamb, M.Redwood and Z.Steirschlifier, Phys.Rev.Lett. 3,332(1959).
60. R.R.Yadav and D.Singh, Intermetallics 9,189(2001).
61. S.D.Lambade, G.G.Sahasrabudhe and S.Rajgopalan, Phys.Rev. B51,15861(1995).
62. S.K.Kor and Kailash, Ind.J.Pure Appl.Phys. 24,179(1986).

CHAPTER-8

Ultrasonic Attenuation in Semi-Metallic Single Crystals

8.1 Introduction

Ultrasonic absorption coefficient can be used for non-destructive testing technique to characterize the materials [1-7]. A review [8] of these studies shows that the ultrasonic attenuation varies from substance to substance in different crystallographic directions and temperatures. At room temperature ($\approx 300\text{K}$) and above, the phonon-phonon interaction is the most dominant factor contributing to ultrasonic attenuation in almost all type of solids viz. metallic, dielectric and semiconducting materials. In the low temperature region in metals the most important factor contributing to ultrasonic attenuation is the electron-phonon interaction. In the low temperature region, the electron mean free path increases and is of the same magnitude as the mean free path of acoustic phonons at high frequency.

Although a number of studies have been made in metallic, dielectric and semiconducting crystals due to electron-phonon interaction, phonon-phonon interaction and thermoelastic loss at higher temperatures. An attempt has been made in semi-metallic single crystals rare-earth Gadolinium Monopnictides GdX ($\text{X}=\text{P}, \text{As}, \text{Sb}$ and Bi) and Neptunium telluride (NpTe) in the present investigation.

The rare-earth monopnictides RX ($\text{X}=\text{N}, \text{P}, \text{As}, \text{Sb}$ and Bi) are quite interesting as the observed anomalous physical properties of these semimetals have been attracted much attention in recent years [9-12], because they are the typical low carrier, strongly correlated system with simple NaCl structure. A weak overlap between the bottom of the conduction band and top of the valence band is sufficient to turn these materials into semimetals with low carrier concentration [13,14]. Gd monopnictides are the simplest series, because Gd is located in the centre of the rare-earth metals in the periodic table of the elements; the Gd^{+3} ion appearing in GdX has $4f^7$ configuration and is an ion with spin $7/2$ and no orbital momentum. The crystalline electric field effect in GdX is considered to be fairly worked. NpTe has been associated with semimetallic behaviour. In NpTe the

resistivity decreases towards lower temperatures below a small maximum near 30K, which is typical for a metal and due to phonons. According to the Luttinger theorem [16] (as interpreted by Martin and Allen [17]) the sum of f and d electrons is even. This statement has been checked and verified for 50 compounds [18]. For NpTe this sum is odd, either $5f^5$ or $5f^46d^1$ or anything in between. Thus in spite of f-d hybridization and possibility of hybridization gap, in NpTe the Fermi level will not be in this gap, and indeed NpTe has no activated resistivity behaviour.

The behaviour of ultrasonic attenuation in GdP, GdAs, GdSb, GdBi and NpTe single crystals have been studied in the present work .

Behaviour of ultrasonic attenuation due to electron-phonon interaction in these semi-metals has been studied from 2K to 80K. Ultrasonic attenuation due to phonon-phonon interaction and due to thermoelastic loss in these materials have been studied at the temperature range 100K-300K along $\langle 100 \rangle$, $\langle 110 \rangle$ and $\langle 111 \rangle$ orientations.

8.2 Theory

8.2.1 Temperature dependence of second and third order elastic constants

The second and third order elastic constants are obtained at 0K following Brugger's [19] definition starting with hardness parameter and nearest neighbor distance and assuming Coulomb and Born-Mayer potential (article 2.2 in chapter II). The anharmonic theory of lattice dynamics is supplied for such derivation. The approach developed by Leibfried and Hahn [20] and Mori and Hiki [21] is used here (article 2.2 in chapter II). Formula for Various elastic constants are found as

$$\begin{aligned} C_{ij} &= C_{ij}^0 + C_{ij}^{\text{Vib}} \\ C_{ijk} &= C_{ijk}^0 + C_{ijk}^{\text{Vib}} \end{aligned} \quad (8.1)$$

C_{ij}^{Vib} and C_{ijk}^{Vib} are shown in Table 2.4-2.6 in chapter II.

All the evaluated elastic constants are presented in Tables 2.2 and 2.3 in chapter II).

8.2.2 Theory of ultrasonic attenuation

It is well established that the ultrasonic attenuation is the temperature dependent property (as in preceding chapters). At low temperature e-p interaction is most dominating in metals, while phonon-phonon interaction is the most effective at higher

temperatures in all type materials. The expressions for attenuation in different temperature region are discussed in Article 2.4 of chapter II.

- (i) At low temperatures (2K-80K) the ultrasonic absorption coefficient over frequency square (α/f^2) is given as:

$$(\alpha/f^2)_{\text{long}} = \frac{2\pi^2}{\rho V_l^3} \left(\frac{4}{3} \eta_e + \chi \right) \quad \text{for longitudinal wave} \quad (8.2)$$

$$(\alpha/f^2)_{\text{shear}} = \frac{2\pi^2}{\rho V_s^3} \eta_e \quad \text{for shear wave} \quad (8.3)$$

- (ii) At higher temperature (100-300K)) the ultrasonic absorption coefficient over frequency square (α/f^2) is given as:

- (a) due to Akhiezer loss

$$(\alpha/f^2)_{\text{long}} = \frac{2\pi^2 E_0 (D/3) \tau_l}{2\rho V_l^3} \quad \text{for longitudinal wave} \quad (8.4)$$

$$(\alpha/f^2)_{\text{shear}} = \frac{2\pi^2 E_0 (D/3) \tau_s}{2\rho V_s^3} \quad \text{for shear wave} \quad (8.5)$$

- (b) due to thermoelastic loss

$$(\alpha/f^2)_{\text{th}} = \frac{2\pi^2 <(\gamma_i^j)^2> KT}{\rho V_l^5} \quad (8.6)$$

where symbols have their meaning given in section B of chapter II.

8.3 Evaluations, results and discussions:

The ultrasonic absorption due to electron-phonon interaction, phonon-phonon interaction and thermoelastic relaxation is evaluated using nearest neighbor distance and hardness parameter for these semi-metallics GdP, GdAs, GdSb, GdBi and NpTe in the temperature range 2-300K. Proceeding with first part C_{IJ} and C_{IJK} at different temperatures are evaluated from nearest neighbor distance [22,23,24] $r_0=2.8545\text{\AA}^0$, 2.9532\AA^0 , 3.1095\AA^0 , 3.1475\AA^0 and 3.125\AA^0 for GdP, GdAs, GdSb, GdBi and NpTe and hardness parameter[25] $b=0.302\text{ A}^0$ for Gadolinium Monopnictides (GdX) and $b=0.311\text{ A}^0$ for NpTe. The SOEC and TOEC have been evaluated at different temperatures using the expressions as given in Tables 2.2,-2.6 of chapter II. SOEC at low temperatures using from 5K to 80K are presented in Tables 8.1-8.5 for GdP, GdAs, GdSb , GdBi and NpTe

respectively. The ultrasonic velocities for longitudinal and shear waves is evaluated with eqn.(2.39) in chapter II.

The evaluated V_l and V_s and ρ are presented in Tables 8.6-8.10. Electronic viscosity (η_e) has been calculated with the eqn. (2.42) in chapter II using electrical resistivity from the literature [22,24,15]. Ultrasonic absorption coefficient due to electron-phonon interaction has been calculated at temperature range 2K-80K using the eqns. (8.2) and (8.3). The values of electrical resistivity (R), electronic viscosity (η_e) and ultrasonic absorption coefficient over frequency square $[(\alpha/f^2)_{long}$ for longitudinal wave and $(\alpha/f^2)_{shear}$ for shear wave] are presented in Tables 8.11-8.15 Fig. 8.1-8.10. SOEC and TOEC of these semimetals at 100K, 200K and 300K are presented in Tables 8.16. Which have been used to obtain Grüneisen parameters [8] $\langle \gamma_i^j \rangle$ and $\langle (\gamma_i^j)^2 \rangle$ along $\langle 100 \rangle$ direction for longitudinal wave over 39 modes and for shear wave over 18 modes; along $\langle 110 \rangle$ direction for longitudinal wave over 39 pure mode, for shear wave polarized along $\langle 001 \rangle$ direction over 14 modes & for shear wave polarized along $\langle \bar{1}10 \rangle$ direction over 20 modes and along $\langle 111 \rangle$ direction for longitudinal wave over 39 pure mode & for shear wave polarized along $\langle \bar{1}\bar{1}0 \rangle$ direction over 14 modes using Grüneisen Table [8] presented in Appendix A. The thermal conductivity is evaluated with resistivity data [22,24 and 27] using Wiedeman-Franz law [26]. Thermal relaxation time (τ_{th}) has been evaluated taking thermal conductivity with eqn.(2.65) as in the chapter II. Specific heat per volume (C_v), energy density (E_0) of the materials have been evaluated as a function of θ_D/T from AIP Hand book [27], where θ_D is Debye temperature and T is the Kelvin temperature. The evaluated values of ρ , K , C_v , E_0 , V_l , V_s , \bar{V} and τ_{th} are presented in Table 8.17. The acoustic coupling constants (D_l for longitudinal wave and D_s for shear wave) have been calculated using Grüneisen parameters $\langle \gamma_i^j \rangle$, $\langle (\gamma_i^j)^2 \rangle_l$ and $\langle (\gamma_i^j)^2 \rangle_s$ with eqn. (2.80) in chapter II. The evaluated values of Grüneisen parameters $\langle \gamma_i^j \rangle$, $\langle (\gamma_i^j)^2 \rangle_l$ and $\langle (\gamma_i^j)^2 \rangle_s$ and non-linearity parameters (acoustic coupling constants) (D_l for longitudinal wave and D_s for shear wave) are presented in Tables 8.18-8.20 along $\langle 100 \rangle$, $\langle 110 \rangle$ and $\langle 111 \rangle$ crystallographic directions respectively. The ultrasonic absorption coefficient over frequency square due to Akhiezer loss $[(\alpha/f^2)_{long}$ for longitudinal wave and $(\alpha/f^2)_{shear}$ for

shear wave] is evaluated using eqns.(8.4) and (8.5). The ultrasonic absorption coefficient over frequency square due to thermoelastic loss $(\alpha/f^2)_{th}$ is evaluated using eqn.(8.6). The values of $(\alpha/f^2)_{th}$, $(\alpha/f^2)_{long}$ and $(\alpha/f^2)_{shear}$ are presented in Tables 8.21,8.22 and 8.23 along $\langle 100 \rangle$, $\langle 110 \rangle$ and $\langle 111 \rangle$ crystallographic directions.

It is obvious from the Tables 8.1-8.5 and 8.16 that the order of second and third order elastic constants in these materials is the same as other NaCl-type single crystals Lanthanum Monochalcogenides [28]. In NpTe one may compare the results of SOEC and TOEC with the Table 8.24. Although present results of C_{11} and C_{12} are very low in comparison to the results obtained by ultrasonic measurement [24]. The value of bulk modulus of NpTe ($B = \frac{1}{3}(C_{11} + 2C_{12})$) is also low in comparison to results obtained by ultrasonic measurement [24] and the bulk modulus derived from X-ray data under pressure [27]. But the orders of all elastic constants are same as expected for NaCl-type single crystals.

It is obvious from the eqn.(2.42), that the electronic viscosity (η_e) is inversely proportional to resistivity (R). As the semimetallic materials GdP, GdAs, GdSb, GdBi and NpTe have fewer carrier electrons, the electrical resistivity values are quite high and evaluated η_e is small in general for all semimetallic materials GdP, GdAs, GdSb, GdBi and NpTe. The ultrasonic attenuation for both longitudinal and shear waves is directly proportional to η_e . Thus, ultrasonic attenuation in these semimetals is very low in comparison to pure metals, as expected due to large values of resistivity of these materials. Due to the smaller number of free carrier electrons available, the ultrasonic attenuation arising from electron-phonon interaction in these Gadolinium monophosphides and Neptunium telluride is very small in general. The ten curves (Figs. 8.1-8.10) for ultrasonic absorption coefficients over frequency square as a function of temperature ($\cong 80K$) are quantitatively similar. At low temperatures the ultrasonic absorption coefficient, firstly decreases rapidly with increasing temperature and show a kink at just above Neel temperature T_N . (Figs. 8.1-8.10). At higher temperature the ultrasonic attenuation is linear with temperature except in case of NpTe. It is clear from the Table 8.15 and Figs. 8.5 and 8.10 that the value of ultrasonic attenuation due to e-p interaction in NpTe is decreased upto Neel temperature and then increased. The Neel temperature as

determined from the derivative $\frac{\partial \rho}{\partial T}$ are found to be 15.9K, 18.7K, 23.4K, 25.8K and 30K for GdP, GdAs, GdSb, GdBi and NpTe respectively. Although for GdP and GdAs electrical resistivity kinks in the curve of R vs. T appears exactly at the Neel temperature T_N (15.9K and 18.7K)[22], in plots of ultrasonic attenuation vs. temperature kinks appear just above the Neel temperature, approximately at 20K (Figs.8.1-8.4) because of the elastic behavior as shown with values of SOEC in Table-8.1 and Table 8.2. It can be understood with Tables 8.11-8.15 that the shear wave attenuation $(\alpha/f^2)_S$ in GdX and NpTe is greater than ultrasonic attenuation for longitudinal waves $(\alpha/f^2)_L$. For GdP and GdAs the metal like behavior of curves (Figs. 8.1-8.4) $[(\alpha/f^2) \text{ vs. temperature } (T)]$ appears above $T_L \approx 70K$ and $65K$ respectively. In the temperature range between T_N and T_L , $\alpha(T)$ deviate from the linear behavior. For GdSb, GdBi and NpTe however, the linear behaviour of $\alpha(T)$ remains even when T is decreased near to T_N , i.e. $T_L \approx T_N$. Although the attenuation in these Gadolinium Monopnictides GdX (X=P, As, Sb and Bi) and Neptunium Telluride (NpTe) is smaller than the pure metals, yet the trend of temperature dependence of (α) is the same nature as for metals, except for some anomalous kinks due to anomalous physical parameters observed in the rare-earth materials.

It is clear from the Table 8.17 that the evaluated thermal relaxation time (τ_{th}) is of the order of 10^{-11} sec. for Gd-monopnictides and picosecond for Np-telluride, which is expected as in previous NaCl-type materials. All the semimetallics GdP, GdAs, GdSb, GdBi and NpTe are materials with metallic bonding possessed well-developed structure of NaCl-type [22,24].

The variation of acoustic coupling constant (D) with temperature is shown in Tables 8.18-8.20 for all these materials. The acoustic coupling constants (i.e. non-linearity parameter) 'D' is decreasing with very small values as the temperature increases. The value of 'D' does not vary much with temperature. Therefore it does not affect very much the temperature dependence of ultrasonic attenuation in these semimetallics. The value of acoustic coupling constant for longitudinal wave (D_L) is more than acoustic coupling constant for shear wave (D_S) for all semimetallics along $\langle 100 \rangle$ and $\langle 110 \rangle$ (in which shear wave polarized along $\langle 001 \rangle$ direction) crystallographic directions, while the value of acoustic coupling constant for longitudinal wave (D_L) is less than acoustic coupling

constant for shear wave (D_s) for all semimetals along $\langle 110 \rangle$ (shear wave polarized along $\langle 1\bar{1}0 \rangle$ and $\langle 110 \rangle$ in which shear wave polarized along $\langle \bar{1}10 \rangle$ direction) crystallographic directions. The ratio D_l / D_s along $\langle 100 \rangle$ is about 13-15 and D_l / D_{s1} along $\langle 110 \rangle$ (in which shear wave polarized along $\langle 001 \rangle$ direction) is about 10-14 for all semimetals. The ratio D_{s2} / D_l along $\langle 110 \rangle$ (in which shear wave polarized along $\langle 1\bar{1}0 \rangle$ direction) is about 1.2-1.5 and D_s / D_l along $\langle 111 \rangle$ (in which shear wave polarized along $\langle \bar{1}10 \rangle$ direction) is about 1.3-1.5 for all semimetals, which is expected as other rock-salt type materials [28,29].

It is clear from the Tables 8.21-8.23 and Figs. 8.11-8.20, that the ultrasonic attenuation due to phonon-phonon interaction $(\alpha/f^2)_{Akh}$ increases with temperature. An appreciable higher value appears at room temperature, it goes down near 100K, where the phonon-phonon interaction ceases. No experimental data are available for the comparison of these results directly. So the results are compared with NaCl-type materials. The values of ultrasonic absorption coefficient over frequency square due to Akhiezer loss for longitudinal and shear waves in these semi-metallic compounds, are compared with NaCl, KCl and KBr in Table 8.25. From the Table 8.25 it is very clear that results of present investigation of the semimetals is very similar the experimental results obtained by Merkulov et al. [30] using pulse-echo technique at room temperature for NaCl, KCl and KBr at 100MHz.

It is clear from the Tables 8.21-8.23 and Figs 8.11-8.20, the ultrasonic attenuation due to thermoelastic relaxation $(\alpha/f^2)_{th}$ increases with temperature also, but $(\alpha/f^2)_{th}$ is negligible as compared to $(\alpha/f^2)_{Akh}$, and order of $(\alpha/f^2)_{th}$ is same as in intermetallics [28].

Thus our present theoretical approach is valid for the study of behaviour of ultrasonic absorption and other related parameters in the semimetals at different temperatures and along different orientations.

Table 8.1 Calculated second order elastic constants(SOEC)(10^{11} Dyne/cm²) of GdP at temperature range 2-80K

Temperature(K)	C ₁₁	C ₁₂	C ₄₄
2	5.149	1.370	1.407
5	5.149	1.370	1.407
10	5.149	1.370	1.407
20	5.149	1.370	1.407
30	5.149	1.368	1.407
40	5.150	1.365	1.407
50	5.157	1.359	1.408
60	5.160	1.352	1.408
70	5.169	1.345	1.408
80	5.180	1.338	1.408

Table 8.2 Calculated second order elastic constants(SOEC)(10^{11} Dyne/cm²) of GdAs at temperature range 2-80K

Temperature(K)	C ₁₁	C ₁₂	C ₄₄
2	4.825	1.225	1.250
5	4.825	1.225	1.250
10	4.825	1.225	1.250
20	4.825	1.225	1.250
30	4.826	1.220	1.250
40	4.831	1.214	1.250
50	4.839	1.207	1.251
60	4.850	1.199	1.251
70	4.862	1.191	1.252
80	4.876	1.184	1.252

Table 8.3 Calculated second order elastic constants(SOEC)(10^{11} Dyne/cm²) of GdSb at temperature range 2-80K

Temperature(K)	C ₁₁	C ₁₂	C ₄₄
2	4.041	0.842	0.861
5	4.041	0.842	0.861
10	4.041	0.841	0.861
20	4.042	0.840	0.861
30	4.045	0.835	0.861
40	4.052	0.828	0.861
50	4.062	0.821	0.861
60	4.074	0.813	0.861
70	4.087	0.806	0.862
80	4.101	0.799	0.863

Table 8.4 Calculated second order elastic constants(SOEC)(10^{11} Dyne/cm²) of GdBi at temperature range 2-80K

Temperature(K)	C ₁₁	C ₁₂	C ₄₄
2	4.123	0.900	0.917
5	4.123	0.900	0.917
10	4.122	0.900	0.917
20	4.123	0.898	0.917
30	4.124	0.889	0.917
40	4.134	0.885	0.917
50	4.143	0.878	0.918
60	4.154	0.871	0.918
70	4.166	0.863	0.918
80	4.179	0.856	0.919

Table 8.5 Calculated second order elastic constants(SOEC)(10^{11} Dyne/cm²) of NpTe at temperature range 2-80K

Temperature(K)	C ₁₁	C ₁₂	C ₄₄
2	3.972	0.940	0.956
5	3.972	0.940	0.956
10	3.972	0.939	0.956
20	3.972	0.938	0.956
30	3.976	0.932	0.956
40	3.985	0.926	0.956
50	3.995	0.919	0.957
60	4.007	0.912	0.957
70	4.020	0.905	0.957
80	4.034	0.898	0.958

Table 8.6 Ultrasonic velocity V_l for longitudinal wave , V_s for shear wave and density (ρ) of GdP at temperature range 2-80K.

Temperature(K)	V _l (10 ⁵ cm/s)	V _s (10 ⁵ cm/s)	ρ (g/cc)
2	2.765	1.445	6.733
5	2.765	1.445	6.733
10	2.765	1.445	6.733
20	2.765	1.445	6.733
30	2.765	1.445	6.732
40	2.766	1.446	6.731
50	2.768	1.446	6.727
60	2.772	1.447	6.725
70	2.773	1.447	6.723
80	2.776	1.448	6.723

Table 8.7 Ultrasonic velocity V_l for longitudinal wave , V_s for shear wave and density (ρ) of GdAs at temperature range 2-80K.

Temperature(K)	$V_l(10^5\text{cm/s})$	$V_s(10^5\text{cm/s})$	$\rho(\text{g/cc})$
2	2.509	1.277	7.662
5	2.509	1.277	7.662
10	2.5093	1.277	7.662
20	2.509	1.277	7.662
30	2.509	1.277	7.661
40	2.511	1.278	7.660
50	2.513	1.278	7.659
60	2.516	1.278	7.658
70	2.523	1.279	7.657
80	2.523	1.279	7.656

Table 8.8 Ultrasonic velocity V_l for longitudinal wave , V_s for shear wave and density (ρ) of GdSb at temperature range 2-80K.

Temperature(K)	$V_l(10^5\text{cm/s})$	$V_s(10^5\text{cm/s})$	$\rho(\text{g/cc})$
2	2.288	1.056	7.719
5	2.288	1.056	7.719
10	2.288	1.056	7.719
20	2.288	1.056	7.719
30	2.289	1.056	7.718
40	2.291	1.056	7.717
50	2.294	1.056	7.716
60	2.297	1.056	7.715
70	2.301	1.057	7.713
80	2.306	1.057	7.712

Table 8.9 Ultrasonic velocity V_l for longitudinal wave , V_s for shear wave and density (ρ) of GdBi at temperature range 2-80K.

Temperature(K)	$V_l(10^5\text{cm/s})$	$V_s(10^5\text{cm/s})$	$\rho(\text{g/cc})$
2	2.055	0.969	9.760
5	2.056	0.969	9.760
10	2.055	0.969	9.760
20	2.055	0.969	9.759
30	2.055	0.969	9.758
40	2.058	0.969	9.757
50	2.060	0.967	9.755
60	2.063	0.970	9.753
70	2.066	0.970	9.751
80	2.070	0.970	9.750

Table 8.10 Ultrasonic velocity V_l for longitudinal wave , V_s for shear wave and density (ρ) of NpTe at temperature range 2-80K.

Temperature(K)	$V_l(10^5\text{cm/s})$	$V_s(10^5\text{cm/s})$	$\rho(\text{g/cc})$
2	1.943	0.963	10.512
5	1.944	0.954	10.501
10	1.970	0.966	10.231
20	1.973	0.968	10.202
30	1.977	0.969	10.166
40	1.980	0.970	10.016
50	1.997	0.977	10.015
60	2.002	0.978	9.991
70	2.006	0.979	9.985
80	2.015	0.981	9.935

Table 8.11 Electrical resistivity (R) in $10^{-6}\Omega$ cm, viscosity (η_e) in 10^{-3} g/cm s, $(\alpha/f^2)_l$ for longitudinal wave in 10^{-17} Np s²/cm and $(\alpha/f^2)_s$ for shear wave in 10^{-17} Np s²/cm of GdP at the temperature range 2-80K.

Temperature(K)	R	η_e	$(\alpha/f^2)_l$	$(\alpha/f^2)_s$
2	8.667	1.542	0.028	0.149
5	10.333	1.294	0.023	0.125
10	14.167	0.943	0.017	0.091
20	22.000	0.607	0.011	0.058
30	23.333	0.573	0.010	0.055
40	24.667	0.541	0.010	0.052
50	26.000	0.514	0.009	0.049
60	27.333	0.488	0.008	0.047
70	32.500	0.411	0.007	0.039
80	35.000	0.381	0.0065	0.036

Table 8.12 Electrical resistivity (R) in $10^{-6}\Omega$ cm, viscosity (η_e) in 10^{-3} g/cm s, $(\alpha/f^2)_l$ for longitudinal wave in 10^{-17} Np s²/cm and $(\alpha/f^2)_s$ for shear wave in 10^{-17} Np s²/cm of GdAs at the temperature range 2-80K.

Temperature(K)	R	η_e	$(\alpha/f^2)_l$	$(\alpha/f^2)_s$
2	4.75	2.667	0.057	0.329
5	6.33	2.002	0.043	0.247
10	8.33	1.521	0.033	0.188
20	13.50	0.938	0.020	0.116
30	15.30	0.817	0.017	0.101
40	17.50	0.724	0.015	0.089
50	18.75	0.675	0.014	0.083
60	21.50	0.589	0.012	0.072
70	25.00	0.506	0.010	0.065
80	28.75	0.440	0.009	0.054

Table 8.13 Electrical resistivity (R) in $10^{-6}\Omega$ cm, viscosity (η_e) in 10^{-3} g/cm s, $(\alpha/f^2)_l$ for longitudinal wave in 10^{-17} Np s²/cm and $(\alpha/f^2)_s$ for shear wave in 10^{-17} Np s²/cm of GdSb at the temperature range 2-80K.

Temperature(K)	R	η_e	$(\alpha/f^2)_l$	$(\alpha/f^2)_s$
2	0.333	33.833	0.962	7.343
5	0.667	16.892	0.480	3.666
10	1.000	11.267	0.320	2.445
20	4.000	2.816	0.080	0.611
30	6.000	1.877	0.053	0.407
40	7.333	1.536	0.043	0.333
50	8.667	1.299	0.036	0.281
60	10.000	1.126	0.031	0.244
70	12.500	0.901	0.025	0.195
80	13.750	0.818	0.022	0.177

Table 8.14 Electrical resistivity (R) in $10^{-6}\Omega$ cm, viscosity (η_e) in 10^{-3} g/cm s, $(\alpha/f^2)_l$ for longitudinal wave in 10^{-17} Np s²/cm and $(\alpha/f^2)_s$ for shear wave in 10^{-17} Np s²/cm of GdBi at the temperature range 2-80K.

Temperature(K)	R	η_e	$(\alpha/f^2)_l$	$(\alpha/f^2)_s$
2	0.333	21.979	1.029	7.323
5	0.667	16.476	0.510	3.659
10	1.000	8.325	0.258	1.849
20	3.500	3.139	0.097	0.697
30	5.500	1.997	0.062	0.443
40	6.250	1.758	0.054	0.390
50	7.750	1.417	0.043	0.314
60	8.750	1.255	0.038	0.278
70	10.000	1.156	0.035	0.256
80	12.500	1.071	0.031	0.224

Table 8.15 Electrical resistivity (R) in $10^{-4}\Omega$ cm. viscosity (η_e) in 10^{-5} g/cm s, $(\alpha/f^2)_l$ for longitudinal wave in 10^{-21} Np s²/cm and $(\alpha/f^2)_s$ for shear wave in 10^{-20} Np s²/cm of NpTe at the temperature range 2-80K.

Temperature(K)	R	η_e	$(\alpha/f^2)_l$	$(\alpha/f^2)_s$
2	6.048	1.063	3.581	2.099
5	6.129	1.048	3.529	2.069
10	6.290	1.004	3.335	1.955
20	6.452	0.977	3.240	1.900
30	6.935	0.906	2.997	1.760
40	7.258	0.866	2.853	1.680
50	7.099	0.877	2.857	1.687
60	6.935	0.896	2.903	1.722
70	6.774	0.917	2.956	1.761
80	6.452	0.959	3.069	1.837

Table 8.16 Second and third order elastic constants (SOEC and TOEC) of the semi-metallics at the temperature range 100-300K in the unit of 10^{11} Dyne/cm².

Material	Temp (K)	C ₁₁	C ₁₂	C ₄₄	C ₁₁₁	C ₁₁₂	C ₁₂₃	C ₁₄₄	C ₁₆₆	C ₄₅₆
GdP	100	5.200	1.322	1.409	-84.62	-5.39	1.872	2.375	-5.73	2.357
	200	5.360	1.242	1.415	-85.30	-5.08	1.386	2.393	-5.75	2.357
	300	5.538	1.161	1.420	-86.17	-4.76	0.901	2.411	-5.78	2.357
GdAs	100	4.936	1.185	1.263	-81.55	-4.81	1.653	2.160	-5.15	2.143
	200	5.106	1.105	1.274	-82.37	-4.49	1.163	2.176	-5.17	2.143
	300	5.286	1.026	1.279	-83.30	-4.18	0.673	2.192	-5.19	2.143
GdSb	100	4.344	0.889	0.969	-74.37	-3.55	1.173	1.687	-3.89	1.674
	200	4.509	0.814	0.973	-75.23	-3.24	0.672	1.699	-3.91	1.674
	300	4.680	0.738	0.976	-76.17	-2.92	0.172	1.172	-3.93	1.674
GdBi	100	4.230	0.841	0.919	-72.94	-3.35	1.092	1.607	-3.68	1.595
	200	4.395	0.766	0.922	-73.83	-3.03	0.589	1.619	-3.70	1.595
	300	4.565	0.691	0.926	-74.78	-2.71	0.086	1.630	-3.72	1.595
NpTe	100	4.084	0.884	0.957	-68.17	-3.55	1.186	1.654	-3.87	1.641
	200	4.231	0.813	0.962	-69.52	-3.27	0.962	1.666	-3.88	1.641
	300	4.389	0.743	0.966	-70.36	-2.98	0.276	1.679	-3.90	1.641

Table 8.17 Density(ρ) in (g/cc), thermal conductivity(K) in 10^5 erg/cm sec K, specific heat (C_v) in 10^7 erg/cc K, internal energy density (E_0) in 10^9 erg/cc, longitudinal velocity (V_l) in (10^5 cm/s), shear velocity (V_s) in (10^5 cm/s). Debye average velocity (\bar{V}) in (10^5 cm/s) and thermal relaxation time (τ_{th}) in 10^{-11} sec of the semimetallics at temperature range 100K-300K.

Material	Temp(K)	ρ	K	C_v	E_0	V_l	V_s	\bar{V}	τ_{th}
GdP	100	6.721	6.596	0.777	44.870	2.782	1.448	1.601	0.994
	200	6.708	7.795	0.861	127.92	2.827	1.452	1.607	1.052
	300	6.696	8.575	0.874	214.20	2.876	1.456	1.613	1.131
GdAs	100	7.653	7.795	0.739	46.087	2.540	1.288	1.427	1.556
	200	7.639	8.575	0.803	122.66	2.585	1.292	1.492	1.563
	300	7.626	8.647	0.811	204.94	2.633	1.295	1.437	1.579
GdSb	100	7.710	15.591	0.644	43.801	2.374	1.121	1.247	4.671
	200	7.696	16.333	0.678	110.74	2.421	1.124	1.251	4.618
	300	7.683	16.078	0.684	178.69	2.468	1.180	1.288	5.856
GdBi	100	9.745	21.439	0.627	43.977	2.083	0.971	1.081	8.780
	200	9.723	21.438	0.655	108.27	2.126	0.974	1.085	8.832
	300	9.701	23.386	0.658	173.90	2.169	0.977	1.089	8.996
NpTe	100	10.512	0.376	0.656	0.422	1.971	0.955	1.061	0.152
	200	10.056	0.891	0.674	1.063	2.051	0.978	1.088	0.335
	300	9.919	1.633	0.685	1.751	2.537	1.134	1.264	0.602

Table 8.18 Average ultrasonic Grüneisen parametrs $\langle \gamma_i^j \rangle_l$ for longitudinal wave . average square ultrasonic Grüneisen parametrs ($\langle (\gamma_i^j)^2 \rangle_l$ for longitudinal wave , $\langle (\gamma_i^j)^2 \rangle_s$ for shear wave), non-linear parameters (D_l for longitudinal wave and D_s for shear wave) along $\langle 100 \rangle$ direction of the semi-metallics at the temperature range 100-300K.

Material	Temp.[K]	$\langle \gamma_i^j \rangle$	$\langle (\gamma_i^j)^2 \rangle_l$	$\langle (\gamma_i^j)^2 \rangle_s$	D_l	D_s
GdP	100	0.519	2.155	0.137	17.999	1.235
	200	0.500	2.034	0.136	17.292	1.220
	300	0.483	1.922	0.134	16.440	1.204
GdAs	100	0.520	2.221	0.136	18.685	1.220
	200	0.500	2.089	0.134	17.819	1.205
	300	0.482	1.972	0.132	16.921	1.190
GdSb	100	0.520	2.387	0.132	20.285	1.191
	200	0.499	2.240	0.131	19.248	1.178
	300	0.480	2.113	0.130	18.219	1.166
GdBi	100	0.521	2.424	0.132	20.654	1.188
	200	0.499	2.274	0.131	19.556	1.175
	300	0.480	2.143	0.129	18.504	1.163
NpTe	100	0.518	2.307	0.133	19.513	1.199
	200	0.498	2.168	0.132	18.563	1.185
	300	0.479	2.043	0.130	17.591	1.170

Table 8.19 Average ultrasonic Grüneisen parametrs $\langle \gamma_i^j \rangle_1$ for longitudinal wave , average square ultrasonic Grüneisen parametrs ($\langle (\gamma_i^j)^2 \rangle_1$ for longitudinal wave , $\langle (\gamma_i^j)^2 \rangle_{s1}$ for shear wave polarized along $\langle 001 \rangle$ direction, $\langle (\gamma_i^j)^2 \rangle_{s2}$ for shear wave polarized along $\langle 1\bar{1}0 \rangle$ direction, non-linear parameters (D_1 for longitudinal wave, D_{s1} for shear wave polarized along $\langle 001 \rangle$ direction and D_{s2} for shear wave polarized along $\langle 1\bar{1}0 \rangle$ direction) along $\langle 110 \rangle$ direction of the semi-metallics at the temperature range 100-300K.]

Material	Temp.[K]	$\langle \gamma_i^j \rangle$	$\langle (\gamma_i^j)^2 \rangle_1$	$\langle (\gamma_i^j)^2 \rangle_{s1}$	$\langle (\gamma_i^j)^2 \rangle_{s2}$	D_1	D_{s1}	D_{s2}
GdP	100	-0.803	2.344	0.329	3.170	17.75	2.959	28.53
	200	-0.763	2.129	0.287	3.034	16.81	2.584	27.31
	300	-0.726	1.941	0.252	2.907	15.53	2.268	26.16
GdAs	100	-0.801	2.369	0.277	3.304	18.26	2.495	29.74
	200	-0.759	2.143	0.242	3.150	17.03	2.178	28.35
	300	-0.721	1.952	0.214	3.015	15.72	2.003	27.13
GdSb	100	-0.790	2.440	0.186	3.629	19.21	1.675	32.66
	200	-0.746	2.209	0.165	3.463	17.84	1.488	31.17
	300	-0.730	1.997	0.125	3.209	16.13	1.126	28.89
GdBi	100	-0.789	2.464	0.175	3.702	19.51	1.570	33.32
	200	-0.744	2.231	0.155	3.533	18.07	1.398	31.79
	300	-0.704	2.034	0.139	3.382	16.62	1.259	30.43
NpTe	100	-0.790	2.388	0.212	3.480	18.58	1.911	31.32
	200	-0.747	2.161	0.188	3.322	17.33	1.689	29.90
	300	-0.707	1.967	0.167	3.178	15.97	1.503	28.60

Table 8.20 Average ultrasonic Grüneisen parametrs $\langle \gamma_i^j \rangle_1$ for longitudinal wave , average square ultrasonic Grüneisen parametrs ($\langle (\gamma_i^j)^2 \rangle_1$ for longitudinal wave , $\langle (\gamma_i^j)^2 \rangle_s$ for shear wave polarized along $\langle \bar{1}10 \rangle$ direction), non-linear parameters (D_1 for longitudinal wave and D_s for shear wave polarized along $\langle \bar{1}10 \rangle$ direction) along $\langle 111 \rangle$ direction of the semi-metallics at the temperature range 100-300K.

Material	Temp.[K]	$\langle \gamma_i^j \rangle$	$\langle (\gamma_i^j)^2 \rangle_1$	$\langle (\gamma_i^j)^2 \rangle_s$	D_1	D_s
GdP	100	-0.635	1.909	2.140	15.083	19.256
	200	-0.609	1.750	2.050	14.256	18.452
	300	-0.584	1.909	1.967	13.228	17.702
GdAs	100	-0.642	1.944	2.232	15.514	20.090
	200	-0.612	1.770	2.130	14.453	19.170
	300	-0.586	1.622	2.041	13.377	18.372
GdSb	100	-0.652	2.012	2.454	16.231	20.088
	200	-0.622	1.828	2.345	15.029	21.105
	300	-0.607	1.661	2.173	13.677	19.555
GdBi	100	-0.655	2.032	2.504	16.450	22.534
	200	-0.624	1.844	2.393	15.180	21.535
	300	-0.595	1.682	2.294	13.930	20.643
NpTe	100	-0.645	1.967	2.353	15.764	21.174

200	-0.616	1.790	2.249	14.665	20.241
300	-0.588	1.634	2.154	13.506	19.386

Table 8.21 Ultrasonic attenuation due to thermoelastic loss $(\alpha/f^2)_{th}$ and due to phonon-phonon interaction $[(\alpha/f^2)_l$ for longitudinal wave and $(\alpha/f^2)_s$ for shear wave] of the semimetals along $\langle 100 \rangle$ direction at the temperature range 100-300K (in the unit of $10^{-18} \text{Np s}^2/\text{cm}$).

Material	Temperature (K)	$(\alpha/f^2)_{th}$	$(\alpha/f^2)_l$	$(\alpha/f^2)_s$
GdP	100	0.029	6.637	1.619
	200	0.058	18.437	4.796
	300	0.082	30.012	8.467
GdAs	100	0.047	12.818	3.209
	200	0.088	31.061	8.424
	300	0.113	46.312	13.383
GdSb	100	0.131	48.295	13.459
	200	0.229	108.216	33.060
	300	0.285	198.584	101.145
GdBi	100	0.274	108.584	30.829
	200	0.456	226.559	70.790
	300	0.624	350.736	120.695
NpTe	100	0.006	1.875	0.506
	200	0.022	9.149	2.692
	300	0.050	24.092	7.759

Table 8.22 Ultrasonic attenuation due to thermoelastic loss $(\alpha/f^2)_{th}$ and due to phonon-phonon interaction $[(\alpha/f^2)_l$ for longitudinal wave, $(\alpha/f^2)_{s1}$ for shear wave (polarized along $\langle 001 \rangle$ direction) and $(\alpha/f^2)_{s2}$ for shear wave (polarized along $\langle 1\bar{1}0 \rangle$ direction)] of the semimetals along $\langle 100 \rangle$ direction at the temperature range 100-300K (in the unit of $10^{-18} \text{Np s}^2/\text{cm}$).

Material	Temperature (K)	$(\alpha/f^2)_{th}$	$(\alpha/f^2)_l$	$(\alpha/f^2)_{s1}$	$(\alpha/f^2)_{s2}$
GdP	100	0.068	6.969	4.533	37.408
	200	0.135	20.166	13.895	107.232
	300	0.186	28.354	15.950	183.974
GdAs	100	0.112	12.636	6.670	53.079
	200	0.201	29.677	15.225	198.211
	300	0.251	43.034	22.112	312.011
GdSb	100	0.302	45.742	18.931	369.188
	200	0.512	101.215	42.753	873.341
	300	0.658	133.975	49.080	1259.46
GdBi	100	0.628	102.594	40.781	864.855
	200	1.013	209.618	84.403	1919.681
	300	1.342	314.828	130.490	3154.629
NpTe	100	0.014	1.785	0.807	13.235
	200	0.049	8.539	3.838	67.934
	300	0.110	21.870	9.968	189.688

Table 8.23 Ultrasonic attenuation due to thermoelastic loss $(\alpha/f^2)_{th}$ and due to phonon-phonon interaction $[(\alpha/f^2)_l$ for longitudinal wave and $(\alpha/f^2)_s$ for shear wave(polarized along $\langle \bar{1}10 \rangle$ direction)] of the semimetallics along $\langle 111 \rangle$ direction at the temperature range 100-300K (in the unit of $10^{-18} \text{Np s}^2/\text{cm}$).

Material	Temperature (K)	$(\alpha/f^2)_{th}$	$(\alpha/f^2)_l$	$(\alpha/f^2)_s$
GdP	100	0.043	5.580	25.251
	200	0.086	15.187	72.459
	300	0.120	24.154	124.476
GdAs	100	0.071	10.653	53.290
	200	0.131	25.188	134.025
	300	0.166	36.619	211.269
GdSb	100	0.205	38.655	249.659
	200	0.355	84.429	591.393
	300	0.454	133.975	852.623
GdBi	100	0.433	86.488	584.981
	200	0.711	176.137	1300.272
	300	0.961	263.845	2139.829
NpTe	100	0.009	1.515	8.946
	200	0.033	7.228	45.985
	300	0.075	18.498	128.568

Table 8.24 Comparison of experimental SOEC and bulk modulus (B) of NpTe at room temperature (all in GPa).

Author	C_{11}	C_{12}	C_{44}	B	Ref.no.
Benedikt et al.	-	-	-	62.00	27
Wachter et al.	129.00	37.00	10.60	67.00	24
Present work	43.90	8.00	10.00	20.00	-

Table 8.25 Comparable data for ultrasonic absorption coefficient (α) in dB/ μ sec.(attenuation) in semimetallics at room temperature ($f=100\text{MHz}$).

Propagation direction	Polarization	NaCl (exp)[30]	KCl (exp)[30]	KBr (exp.)[30]	GdP	GdAs	GdSb	GdBi	NpTe
$\langle 100 \rangle$	long.	0.21	0.43	0.40	0.75	1.06	4.26	7.52	0.54
$\langle 100 \rangle$	Shear	0.03	0.06	0.06	0.04	0.15	0.86	1.02	0.09
$\langle 110 \rangle$	long.	0.14	0.34	0.27	0.71	0.98	2.87	5.93	0.48
$\langle 110 \rangle$	shear $\langle \bar{1}10 \rangle$	0.03	0.06	0.06	0.20	0.25	0.42	1.11	0.12
$\langle 110 \rangle$	shear $\langle \bar{1}10 \rangle$	0.40	0.45	0.40	2.33	3.51	10.72	26.77	2.21
$\langle 111 \rangle$	long.	0.09	0.25	0.19	0.61	0.84	2.87	4.97	0.41
$\langle 111 \rangle$	shear $\langle \bar{1}10 \rangle$	0.20	0.25	0.30	1.57	2.38	7.26	18.16	1.49

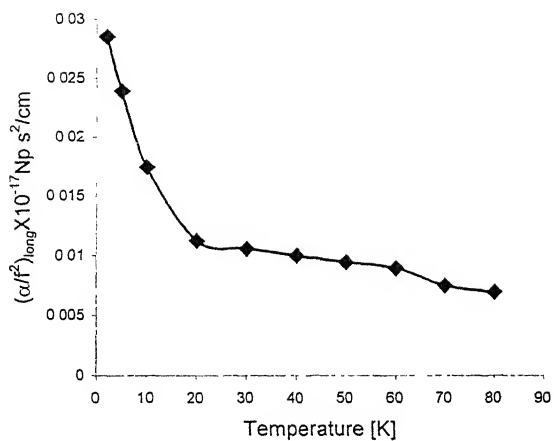


Fig.8.1 $(\alpha/f^2)_{\text{long}}$ vs temperature of GdP

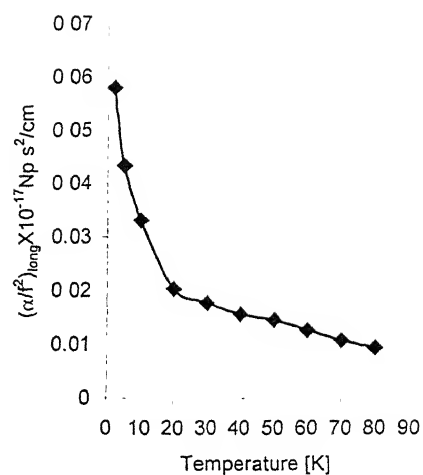


Fig.8.2 $(\alpha/f^2)_{\text{long}}$ vs. temperature of GdAs

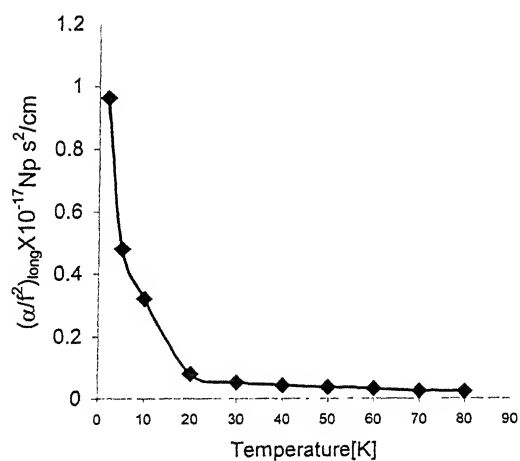


Fig.8.3 $(\alpha/f^2)_{\text{long}}$ vs. temperature of GdSb.

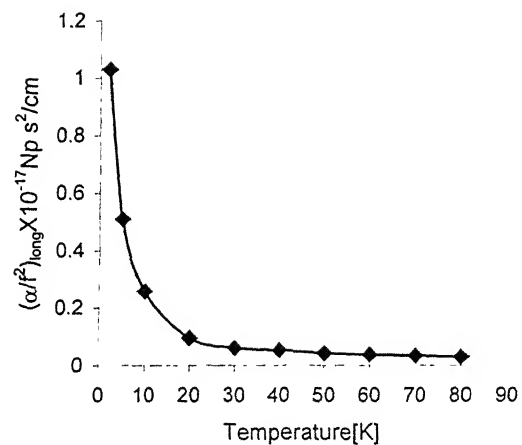


Fig.8.4 $(\alpha/f^2)_{\text{long}}$ vs. temperature of GdBi

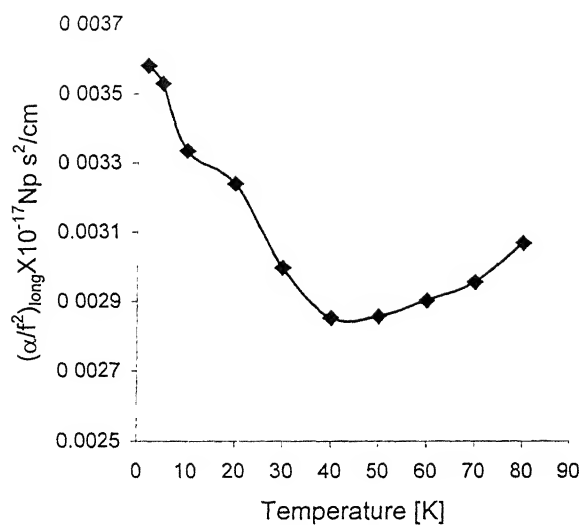


Fig.8.5 $(\alpha/f^2)_{\text{long}}$ vs. temperature of NpTe

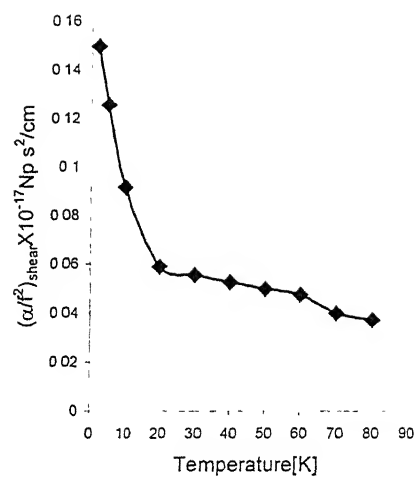


Fig.8.6 $(\alpha/f^2)_{\text{shear}}$ vs. temperature of GdP

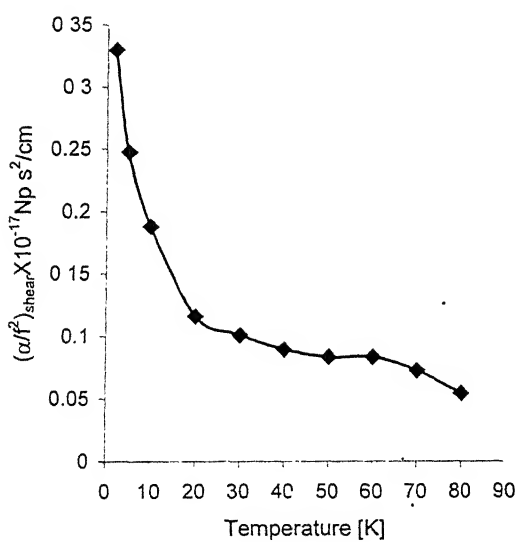


Fig.8.7 $(\alpha/f^2)_{\text{shear}}$ vs. temperature of GdAs

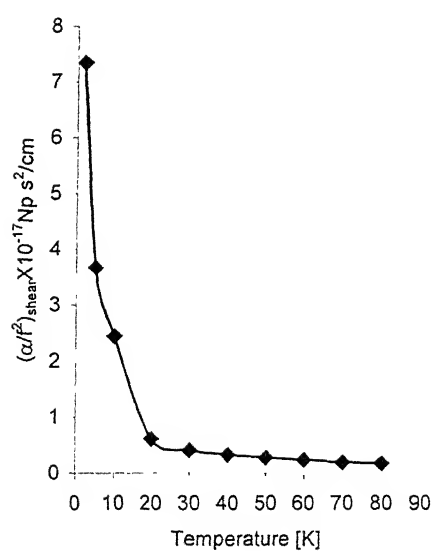


Fig.8.8 $(\alpha/f^2)_{\text{shear}}$ vs. temperature of GdSb

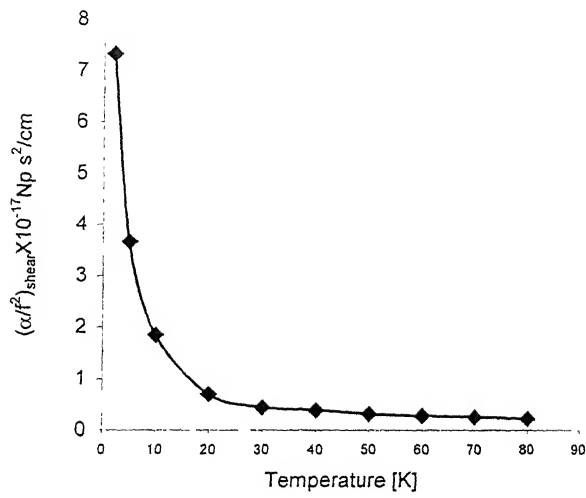


Fig.8.9 $(\alpha/f^2)_{\text{shear}}$ vs. temperature of GdBi

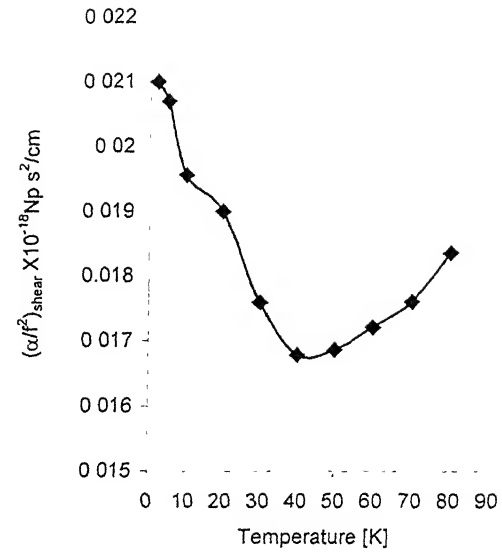


Fig.8.10 $(\alpha/f^2)_{\text{shear}}$ vs. temperature of NpTe

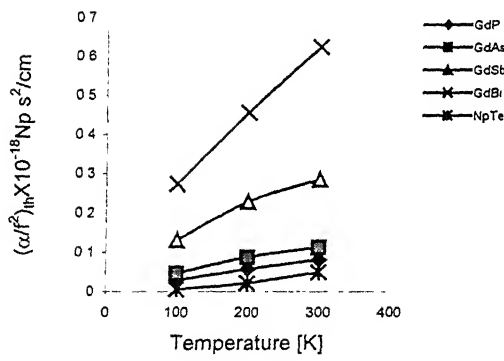


Fig.8.11 $(\alpha/f^2)_{\text{th}}$ vs temperature of the semimetals along <100> direction

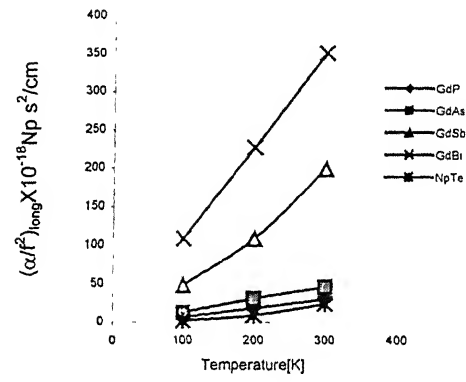


Fig.8.12 $(\alpha/f^2)_{\text{long}}$ vs temperature of the semimetals along <100> direction

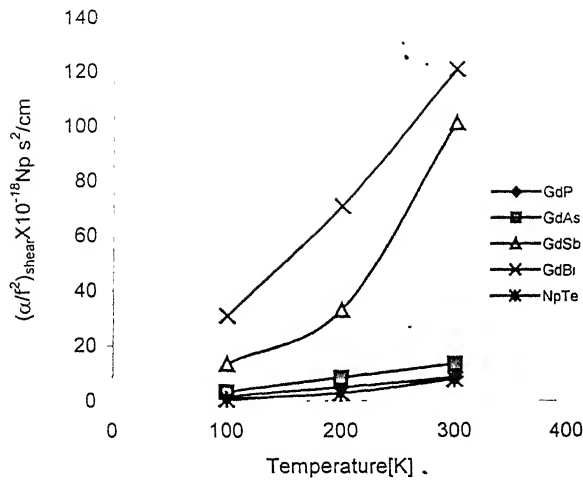


Fig.8.13 $(\alpha/f^2)_{\text{shear}}$ vs temperature of the semimetallics along $\langle 100 \rangle$ direction

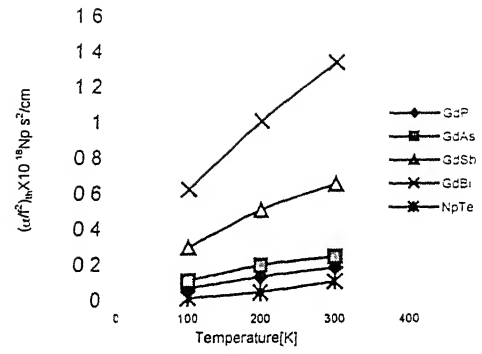


Fig.8.14 $(\alpha/f^2)_{\text{th}}$ vs temperature of the semimetallics along $\langle 110 \rangle$ direction

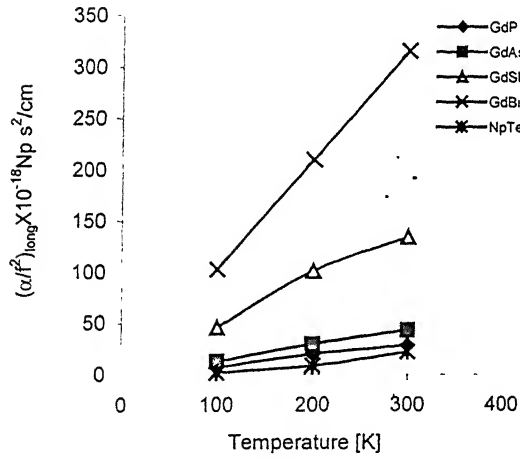


Fig.8.15 $(\alpha/f^2)_{\text{long}}$ vs temperature of the semimetallics along $\langle 110 \rangle$ direction

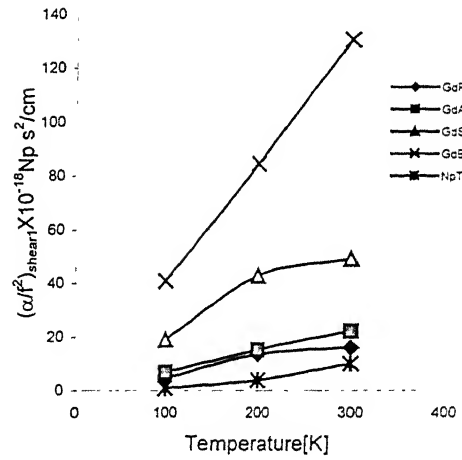


Fig.8.16 $(\alpha/f^2)_{\text{shear1}}$ vs temperature of the semimetallics along $\langle 110 \rangle$ direction shear wave polarized along $\langle 001 \rangle$ direction

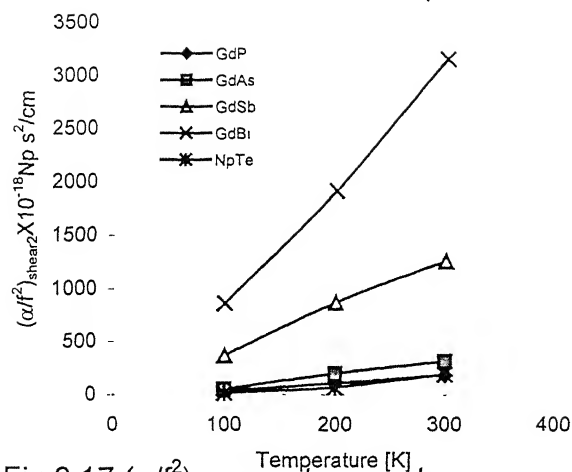


Fig.8.17 $(\alpha/f^2)_{\text{shear}_2}$ vs temperature of the semimetals along $\langle 110 \rangle$ direction shear wave polarized along $\langle 110 \rangle$ direction

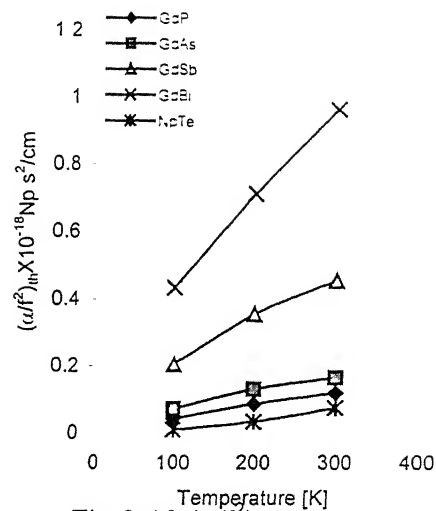


Fig.8.18 $(\alpha/f^2)_{\text{th}}$ vs temperature of the semimetals along $\langle 111 \rangle$ direction

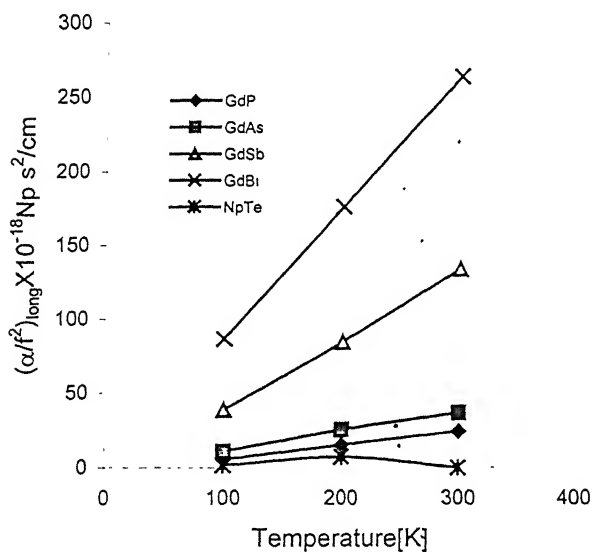


Fig.8.19 $(\alpha/f^2)_{\text{long}}$ vs temperature of the semimetals along $\langle 111 \rangle$ direction

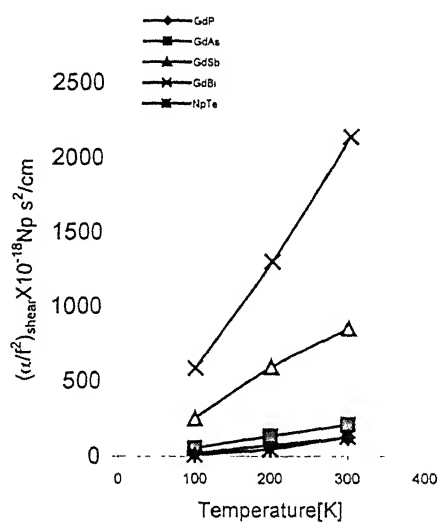


Fig.8.20 $(\alpha/f^2)_{\text{shear}}$ vs temperature of the semimetals along $\langle 111 \rangle$ direction shear wave polarized along $\langle 110 \rangle$ direction

References

1. M.B. Walker, M.F.Smith and K.V.Samokhin, Phys. Rev. B65,014517(2002).
2. T.Gupta and D.M.Gaintonde, Mod. Phys. Lett. B15, 269(2001).
3. K.Foster, R.G.Leisure, J.B.Shaklee, J.Y.Kim and K.F.Kelton, Phys. Rev. B61,241 (2000).
4. V.P.Matsokin and G.A.Petchenko, Low Temp. Phys.(USA), 26,517(2000).
5. N.Chelliah and R.Sabesan, Ind.J.Pure Appl.Phys. 32,315(1994).
6. M.A.Sidkey, J.Pure Appl.Ultrason. 18,91(1996).
7. C.A.Damianau, N.T.Sanghvi, F.J.Fry, J.Moreno, J.Acoust.Soc.Am. 102,628(1997).
8. W.P.Mason, Physical Acoustics , (Academic Press, New York,1965). Vol IIIB Chapter 6
9. T.Suzuki, Jpn.J.Appl.Phys.Series 8,267(1993).
10. T.Suzuki, Physica B 186 & 188,347(1993).
11. T.Kasuya, T.Suzuki and Y.Haga, J.Phys.Soc.Jpn. 62,2549(1993).
12. D.X.Li, Y.Haga, H.Shida, T.Suzuki, T.Koide and G.Kido, Phys.Rev. B53, 8473(1996).
13. A.Hasegava and A.Yanase, J.Phys.Soc.Jpn 42,9(1987).
14. T.Kasuya, O.Sakai, J.Tanaka, H.Kitazava and T.Suzuki, J.Magn.Magn. Mater. 63 & 64,9(1987).
15. J.M. Fournier and E. Graze: K.A.Gschneidner Jr., L.Eyring, G.H.Lander, G.R.Choppin (Eds.) Handbook on the Physics and Chemistry of Rare earths, Vol.17, Lanthanides/Actinides: Physics I, North-Holland, Amsterdam,p.409(1993).
16. L.M.Luttinger, Phys.Rev. 119,1153(1960).
17. R.M.Martin and J.W.Allen, J.Appl.Phys. 50,7561(1979).
18. P.Wachter, in Handbook on the Physics and Chemistry of Rareearths, Vol.19, Lanthanides/Actinides: Physics II, K.A.Gschneidner Jr., L.Eyring, G.H.Lander, G.R.Choppin (Eds.) Elsevier Science, Amsterdam,chapter 132, p.177(1994).
19. K.Brugger, Phys.Rev. A133,1611(1963).
20. G.Leibfried and H.Haln, Z.Phys. 150,497(1958).
21. S.Mori and Y.Hiki, J.Phys.Soc.Jpn 45,1449(1978).
22. D.X.Li, Y.Haga, H.Shida, T.Suzuki and Y.S.Kwon, Phys.Rev. B54,10483(1996).

23. O.Vogt and K.Mattenberger, J.Alloys Compounds. 223,226(1995).
24. P.Wachter, M.Filzmoser and J.Rebizant. Physica B293,199(2001).
25. M.P.Tosi, in Solid State Physics edited by F. Seitz and D. Turnbull),(Academic Press, New York, Vol.16 (1964).
26. C.Kittel, Introduction to Solid State Physics, Seventh edition, (John Wiley & Sons, Inc. New York,1996) 7Th Edition, p. 166.
27. U.B.Benedict, W.B.Holzapfel, in: K.A.Gschneidner Jr., L.Eyring, G.H.Lander, G.R.Choppin (Eds.) Handbook on the Physics and Chemistry of Rareearths, Vol.17, Lanthanides/Actinides: Physics I, Elsevier Science Amsterdam chapter 113 ,p.245(1993).
28. R.R.Yadav and D.Singh, J.Phys.Soc.Jpn. 70,1825(2001).
29. S.K.Kor, R.R.Yadav and Kailash, J.Phys.Soc.Jpn. 55,207(1986).
30. L.G.Merkulov, R.V.Kovalenok and E.V. Konovodchenko, Soviet Physics-Solid State, 11,2241(1970).

CHAPTER-9

Application of Morse potential to Evaluate the Ultrasonic Attenuation in Semi-metallic GdX Single Crystals (X=P, As, Sb and Bi) in the Temperature Range 10 to 300K.

9.1 Introduction

Ultrasonics, because of its wide range applications in almost every field has been studied in detail. Ultrasonic velocity and attenuation studies have been made in solids, liquids and liquid crystals. A number of books, review articles are available which give the experimental techniques and theoretical interpretations of results [1-10].

In solids [11,12,13], there are several causes of ultrasonic attenuation, the most important being the electron-phonon (e-p) interaction below 80K [13,14] and phonon-phonon (p-p) interaction above 100K [15,16]. Several potentials [17,18,19] have been used to evaluate second- and third-order elastic constants (SOEC and TOEC). The first principal methods [20] are available for the evaluation of SOEC and TOEC. Morse potential which is most appropriate one for studying the physical properties of the metals [18] and the results of several metallic crystals the SOEC and TOEC as evaluated are very good agreement with experimental values [18]. The physical properties of semi-metallic crystal [21] are more or less of the same type as the metallic crystal. As such the Morse potential has been used to evaluate SOEC and TOEC of semi-metallic crystals GdX (X=P, As, Sb and Bi) as the Morse potential gives clear picture of the process taking place. Also in the same semi-metallic crystals ultrasonic results are available in chapter VIII using Coulomb and Born-Mayer potential for the evaluation of SOEC and TOEC.

In the present investigation ultrasonic attenuation studies have been made in semi-metallic crystals GdX (X=P, As, Sb and Bi), due to the e-p interaction from 10-80K and due to p-p interaction between 100-300K along $\langle 100 \rangle$, $\langle 110 \rangle$ and $\langle 111 \rangle$ crystallographic directions. The substance chosen have been studied with reference to the other properties by several authors [22,23] because they are typical carrier strongly correlated system with simple f.c.c structure. The results are quite interesting particularly at Neel temperature and have been discussed.

8.2. Theory

8.2.1 SOEC and TOEC by Morse potential

The interaction energy $\phi(r_{ij})$ of two atoms separated by a distance r_{ij} according to Morse is given by [18] :

$$\phi(r_{ij}) = D [e^{-2\alpha(r_{ij} - r_o)} - 2e^{-\alpha(r_{ij} - r_o)}] \quad (9.1)$$

Where α and D are constants with dimensions of reciprocal distance and energy respectively and r_o is the equilibrium distance of approach of two atoms. Since, $\phi(r_o) = -D$, D is the dissociation energy. For Morse parameters, the following equations are introduced:

$$d\phi/da = 0 \text{ at } a = a_o \quad (9.2)$$

Bulk modulus is written as:

$$\text{Bulk Modulus (B)} = (1/18Na_o) (d^2\phi/da^2)_{a=a_o} \quad (9.3)$$

and

$$r_j = [m_j^2 + n_j^2 + l_j^2]^{1/2} a = M_j a \quad (9.4)$$

Where: m_j , n_j and l_j are the position coordinates of any atom in terms of half the lattice parameter a .

$$\beta = e^{\alpha a_o} \quad (9.5)$$

The potential energy of a large crystal is obtained by choosing one atom in the lattice as origin, calculating its interaction with all other atoms in the crystal and then multiplying by $N/2$, where N is the total number of atoms under consideration. The range of interatomic potential has been taken upto 10th shell consisting of 176 atoms in f.c.c.. Thus the total energy is:

$$\phi = (1/2) ND \sum_j [e^{-2\alpha(r_j - r_o)} - 2e^{-\alpha(r_j - r_o)}] \quad (9.6)$$

r_j is the distance of the j^{th} atom from origin in the lattice. At absolute zero, a_o is the value of a , $\phi(a_o)$ is the energy of cohesion. $\phi(a_o) = u_o(a_o)$ is the energy of sublimation at zero temperature. $[d\phi/da]_{a=a_o}$ vanishes and $[d^2\phi(a)/da^2]_{a=a_o}$ is related to bulk modulus, given by eqn (9.3) Also:

$$[d\phi(a)/da]_{a=a_o} \text{ gives } \beta = \frac{\sum_j M_j e^{-\alpha a_o M_j}}{\sum_j e^{-2\alpha a_o M_j}} \quad (9.7)$$

and $\phi(a_o) = u_o(a_o)$ gives:

$$D = \frac{u_o(a_o)}{[\beta^2 \sum_j e^{-2\alpha a_o M_j}] - \beta \sum_j e^{-\alpha a_o M_j}} \quad (9.8)$$

Where β is given by eqn. (9.7).

The bulk modulus is given by eqn (9.3) from which:

$$D = \frac{18Ba_o}{2\alpha^2\beta^2 \sum_j M_j^2 e^{-2\alpha a_o M_j} - \alpha^2\beta \sum_j e^{-\alpha a_o M_j}} \quad (9.9)$$

Eqns (9.8) and (9.9) are satisfied for unique set of values of α and D. To solve these two equations for a general range of α and arrive at two different values of D, say D_1 and D_2 . Unfortunately, one cannot arrive at a value of α for which $D_1 \sim D_2 = 0$. One therefore settles for a value of α for which $D_1 \sim D_2$ is of the order of 10^{-24} . The values of α obtained by this approximation are correct and tallies exactly with other materials studied earlier [18]. Since β is known from eqn. (9.7), knowing α , r_o is obtained from eqn. (9.5). The calculations and computer program have been tested for several metallic crystals and values of α , r_o and D are exactly same as obtained for Cu, Ag, Au etc. [18]. From these values SOEC and TOEC are obtained as follows:

The expression for SOEC (C_{11}^0) is as follows:

$$\begin{aligned} C_{11}^0 = & \frac{2Da^2\alpha^2\beta^2}{V} \sum \frac{m_j^4 e^{-2\alpha a M_j}}{M_j^2} - \frac{2Da^2\alpha^2\beta}{V} \sum \frac{m_j^4 e^{-\alpha a M_j}}{M_j^2} \\ & + \frac{Da\alpha\beta^2}{V} \sum \frac{m_j^4 e^{-2\alpha a M_j}}{M_j^3} - \frac{Da\alpha\beta}{V} \sum \frac{m_j^4 e^{-\alpha a M_j}}{M_j^3} \end{aligned} \quad (9.10)$$

The expression for C_{12}^0 is obtained by replacing m_j^4 by $m_j^2 n_j^2$ in eqn (9.10) above and V is the atomic volume, which is equal to $2a^3$ in the present case.

The expression for TOEC (C_{111}^0) is as follows:

$$\begin{aligned} C_{111}^0 = & -\frac{4Da^3\alpha^3\beta^2}{V} \sum \frac{m_j^6 e^{-2\alpha a M_j}}{M_j^3} - \frac{6Da^2\alpha^2\beta}{V} \sum \frac{m_j^6 e^{-2\alpha a M_j}}{M_j^4} \\ & - \frac{3Da\alpha\beta^2}{V} \sum \frac{m_j^6 e^{-2\alpha a M_j}}{M_j^5} + \frac{Da^3\alpha^3\beta}{V} \sum \frac{m_j^6 e^{-\alpha a M_j}}{M_j^3} \\ & + \frac{3Da^2\alpha^2\beta}{V} \sum \frac{m_j^6 e^{-\alpha a M_j}}{M_j^4} + \frac{3Da\alpha\beta}{V} \sum \frac{m_j^6 e^{-\alpha a M_j}}{M_j^5} \end{aligned} \quad (9.11)$$

The expression for $C_{112}^0 (=C_{166}^0)$ is obtained by replacing m_j^6 by $m_j^4 n_i^2$ in all summations in eqn. (9.11). Also, the expression for C_{123}^0 which is equal to $C_{456}^0 = C_{166}^0$ is obtained by replacing m_j^6 by $m_j^2 n_j^2 l_j^2$ in all summations in eqn. (9.11). The summations are for the coordinates of atoms upto 10^{th} shell.

In the central force model, the elastic constants obey Cauchy relations at absolute zero:

$$C_{12}^0 = C_{44}^0; \quad C_{112}^0 = C_{166}^0 \quad \text{and} \quad C_{123}^0 = C_{456}^0 = C_{166}^0 \quad (9.12)$$

Thus, we have only two and three independent SOEC and TOEC respectively. However, experimentally these relations are not true.

9.2.2 Temperature dependence of SOEC and TOEC

According to the lattice dynamics developed by Leibfried et al. [24,25] lattice energy changes with temperature, hence adding its vibrational energy contribution to elastic constants at absolute zero one gets C_{ij} and C_{ijk} (SOEC and TOEC) at the required temperature.

$$C_{ij} = C_{ij}^0 + C_{ij}^{\text{vib}} \quad (9.13)$$

$$C_{ijk} = C_{ijk}^0 + C_{ijk}^{\text{vib}} \quad (9.14)$$

Where the superscript has been used to denote SOEC and TOEC at absolute zero.. The C_{ij}^{vib} and C_{ijk}^{vib} are vibrational contributions and are functions of various G 's which are functions of r_0 and b presented in Tables 2.4-2.6 in chapter II.

9.2.3 Ultrasonic attenuation due to e-p interaction

In metals at low temperatures, mean free path of the electron becomes comparable to the wavelength of the acoustical phonons. The coupling of the conduction electrons with the propagating ultrasonic wave causes dissipation of energy of the wave and thus viscous loss occurs [11]. The attenuation caused by the energy loss due to compressional and shear viscosities of the lattice at low temperature are as given in eqns. (2.43) and (2.44) in chapter II.

9.2.4 Ultrasonic attenuation due to phonon-phonon interaction

At higher temperature (above 100K), Ultrasonic attenuation occurs due to phonon viscosity mechanism. Akhiezer [27] was first to propose the phonon viscosity mechanism which was improved by Bömmel and Dransfeld [28]. Finally Mason [11,12] used the Grüneisen numbers in the Akhiezer region ($\omega\tau_{\text{th}} \ll 1$) to evaluate the ultrasonic attenuation. Although there are several methods for evaluation of the ultrasonic attenuation, the one proposed by Mason [12], has been

used [14,15] and results are quite good as some of the earlier results are in agreement with experimental values.

The ultrasonic attenuation due to p-p interaction $[(\alpha/f^2)_{\text{long}} \text{ and } (\alpha/f^2)_{\text{shear}}]$ for longitudinal and shear waves respectively] and due to thermoelastic loss $(\alpha/f^2)_{\text{th}}$ has been evaluated using eqns. (2.78), (2.79) and (2.80) respectively.

9.3 Evaluations, results and discussions

The experimental values of lattice parameter, bulk modulus and cohesive energy are used to evaluate the Morse parameters D , α and r_0 using the eqns. 9.1-9.4. the Morse parameters D , α and r_0 are presented in Table 9.1. These parameters are used to evaluate second and third order elastic constants (SOEC and TOEC) at absolute zero using eqns. (9.5) and (9.6). The values of SOEC and TOEC at absolute zero are presented in Table 9.2. These values of SOEC and TOEC at absolute zero were added with vibrational contribution (which is given as in the Tables 2.7-2.9 in chapter II). The evaluated values of temperature dependence of SOEC are presented in Table 9.3. By utilization of SOEC from the Table 9.3, the ultrasonic velocities (V_l for longitudinal wave and V_s for shear wave) are evaluated. The viscosity of electron gas has been evaluated with eqn.(2.42) with electrical resistivity (R) [21]. The values of viscosity (η_e) with electrical resistivity (R) values are presented in Tables 8.11-8.14 in chapter VIII. Eqns. (2.43) and (2.44) [in chapter II) have been used to evaluate ultrasonic attenuation due to electron-phonon interaction for longitudinal and shear waves respectively. The values of ultrasonic attenuation due to electron-phonon interaction are presented in Table 9.4 for longitudinal and shear waves.

The values of SOEC and TOEC of these semi-metallics at 100,200 and 300K are presented in Table 9.5. Which have been used to obtain average Grüneisen numbers $\langle \gamma_i^I \rangle$ and $\langle (\gamma_i^I)^2 \rangle$ along $\langle 100 \rangle$, $\langle 110 \rangle$ and $\langle 111 \rangle$ crystallographic directions using Grüneisen Tables [12] (Appendix A). Thermal conductivity is evaluated with resistivity data available in literature[27] using Weidemann-Franz law. The thermal relaxation time (τ_{th}) has been evaluated taking thermal conductivity with eqn. (2.65) as in chapter II. Specific heat per unit volume (C_v), energy density (E_0) of these materials have been evaluated as a function of θ_D/T from the AIP Handbook [29], where θ_D is Debye temperature. Primary physical constants like K , C_v , E_0 etc. are presented in Table 8.17 of chapter VIII. The values of ultrasonic velocities (V_l for longitudinal wave, V_s for shear wave and \bar{V} -Debye average velocity) and thermal relaxation time (τ_{th}) are presented in

Table 9.6. The nonlinear parameters (D_l for longitudinal wave and D_s for shear wave) are calculated using average Grüneisen numbers $\langle \gamma_l^I \rangle$ and $\langle (\gamma_l^I)^2 \rangle$ with eqn. (2.36) in chapter II. The evaluated average Grüneisen numbers $\langle \gamma_l^I \rangle$ and $\langle (\gamma_l^I)^2 \rangle$ and nonlinear parameters (D_l for longitudinal wave and D_s for shear wave) are presented in Tables 9.7-9.9 along $\langle 100 \rangle$, $\langle 110 \rangle$ and $\langle 111 \rangle$ crystallographic directions respectively. The values of ultrasonic attenuation due to thermoelastic loss $(\alpha/f^2)_{th}$ and due to phonon-phonon interaction $[(\alpha/f^2)_{long}$ for longitudinal wave and $(\alpha/f^2)_{shear}$ for shear wave] have been evaluated with eqns. (2.86), (2.78) and (2.79) of chapter II. The evaluated values of ultrasonic attenuation due to thermoelastic loss $(\alpha/f^2)_{th}$ and due to phonon-phonon interaction $[(\alpha/f^2)_{long}$ for longitudinal wave and $(\alpha/f^2)_{shear}$ for shear wave] are presented in Tables 9.8-9.10 and Figs. 9.9-9.18.

The Morse parameters D , α and r_0 for GdX ($X=P, As, Sb$ and Bi) are of the same order of magnitude as for metallic crystals. It is clear from the Table 9.4 and Figs.9.1-9.8 that the ultrasonic attenuation due to e-p interaction falls rapidly as the temperature increases from 10K-80K and of the same nature as for other metallic crystals. It is obvious from the Figs 9.1-9.8 show that the ultrasonic attenuation due to e-p interaction is smooth except at Neel temperature, where there is a small kink in attenuation. Ultrasonic attenuation values in semi-metallics are less than that of the metallic compounds due to e-p interaction as the resistivity of semi-metallic compounds are more than the metallic crystals. The Morse potential can be safely used in semi-metallic compounds GdX ($X=P, As, Sb$ and Bi) for evaluation of SOEC and TOEC as the physical properties of these materials are more or less of the same nature as metallic crystals.

It is obvious from the Tables 9.3-9.5 that the evaluated values of SOEC and TOEC by Morse potential are very less in comparison to evaluated values of SOEC and TOEC by Coulomb and Born-Mayer potential as presented in Table 8.1-8.4 and 8.16. It is obvious from the Tables 9.7-9.9 that the values of non-linearity constant 'D' are different from the evaluated values of the same in previous chapter, because the values of SOEC and TOEC are quite different in both cases.

It is obvious from the Table 9.10-9.12 and Figs. 9.10-9.18 that the values of ultrasonic attenuation due to phonon-phonon interaction $[(\alpha/f^2)_{long}$ for longitudinal wave and $(\alpha/f^2)_{shear}$ for shear wave] increases with temperature, but the values of these materials are more than the those values presented in Table 8.21–8.23 .in previous chapter VIII (using Coulomb and Born-Mayer

potential). The values of ultrasonic attenuation due to thermoelastic loss $((\alpha/f^2)_{th})$ is negligible in comparison to the values of ultrasonic attenuation due to phonon-phonon interaction $[(\alpha/f^2)_{long}]$ for longitudinal wave and $(\alpha/f^2)_{shear}$ for shear wave] and also increases with temperature.

The obtained results confirm in semi-metallics also that the major cause of ultrasonic attenuation are due to electron-phonon interaction, phonon-phonon interaction and thermoelastic loss and also confirms that the Morse potential can be safely used in semi-metallics like in metals to produce SOEC and TOEC. Hence the present approach is valid to study the microstructural properties of the material, which may be utilized in material science and technology.

Table 9.1 The Morse parameters D , α and r_0 for the GdX (X=P, As, Sb and Bi)

Matrial	D (in 10^{-14} ergs)	α in $(10^{-8}\text{cm})^{-1}$	r_0 in (10^{-8}cm)
GdP	17.73	1.70	4.07
GdAs	16.99	1.70	4.18
GdSb	14.37	1.70	4.43
GdBi	15.10	1.70	4.48

Table 9.2 The second- and third order elastic constants (SOEC and TOEC)at 0K for GdX (X=P, As, Sb and Bi) all in 10^{11}Dyne/cm^2

Crystals	C_{11}^0	$C_{12}^0 = C_{44}^0$	C_{111}^0	$C_{112}^0 = C_{123}^0$	$C_{123}^0 = C_{144}^0 = C_{456}^0$
GdP	3.64	2.04	-42.27	-23.74	0.251
GdAs	3.45	1.92	-40.89	-22.75	0.209
GdSb	2.85	1.55	-35.31	-19.29	0.127
GdBi	2.84	1.55	-36.05	-19.76	0.125

Table 9.3 The second order elastic constants (SOEC) for GdX(X=P,As,Sb and Bi) all in 10^{11} Dyne/cm² at the temperature range 10-80K for GdX(X=P,As,Sb and Bi).

Material	SOEC	10	20	30	40	50	60	70	80	Neel Temp
GdP	C ₁₁	1.41	2.82	3.29	3.53	3.67	3.76	3.83	3.88	2.71
	C ₁₂	-0.88	0.534	1.01	1.24	1.38	1.48	1.54	1.59	0.50
	C ₄₄	2.06	2.06	2.06	2.06	2.06	2.06	2.06	2.06	2.06
GdAs	C ₁₁	2.51	3.19	3.41	3.53	3.59	3.64	3.68	3.70	3.18
	C ₁₂	0.49	1.17	1.39	1.51	1.57	1.62	1.65	1.67	1.16
	C ₄₄	1.92	1.92	1.92	1.92	1.92	1.92	1.92	1.92	1.92
GdSb	C ₁₁	2.48	2.79	2.90	2.95	2.98	3.01	3.06	3.08	2.82
	C ₁₂	0.88	1.19	1.29	1.35	1.38	1.40	1.42	1.45	1.26
	C ₄₄	1.55	1.55	1.55	1.55	1.55	1.55	1.55	1.55	1.55
GdBi	C ₁₁	2.32	2.74	2.89	2.96	3.00	3.03	3.06	3.08	2.88
	C ₁₂	0.85	1.08	1.22	1.29	1.33	1.36	1.38	1.40	1.20
	C ₄₄	1.56	1.56	1.56	1.56	1.56	1.56	1.56	1.56	1.55

Table 9.4 Ultrasonic attenuation due to e-p interaction $(\alpha/f^2)_L$ and $(\alpha/f^2)_S$ L and S for longitudinal and shear waves respectively (all in 10^{-17} Nps²/m); (T_N is the Neel temperature for the compound).

Temp. (in K)	GdP		GdAs		GdSb		GdBi	
	$(\alpha/f^2)_L$	$(\alpha/f^2)_S$	$(\alpha/f^2)_L$	$(\alpha/f^2)_S$	$(\alpha/f^2)_L$	$(\alpha/f^2)_S$	$(\alpha/f^2)_L$	$(\alpha/f^2)_S$
10	11.4	48.3	5.37	9.80	91.7	110.0	83.0	126.0
15.7(T_N)	3.71	3.71						
			3.96	6.17				
18.9(T_N)								
20	2.6	3.1	3.70	6.00	15.9	27.8	19.9	36.0
23.4(T_N)					12.9	16.5		
25.8(T_N)							15.5	29.0
30	1.9	2.90	2.98	5.34	9.8	18.0	11.9	22.9
40	1.6	2.77	2.48	4.60	7.7	15.8	10.2	20.0
50	1.47	2.60	2.20	4.30	6.4	12.8	8.10	16.0
60	1.35	2.50	1.90	3.8	5.5	11.0	7.10	14.0
70	1.1	2.10	1.60	3.3	4.3	8.4	6.10	12.6
80	1.0	1.95	1.40	2.8	3.9	8.0	4.80	10.0

Table 9.5 Second and third order elastic constants (SOEC and TOEC) of the semimetallics at the temperature range 100-300K in the unit of 10^{11} Dyne/cm².

Material	Temp [K]	C ₁₁	C ₁₂	C ₄₄	C ₁₁₁	C ₁₁₂	C ₁₂₃	C ₁₄₄	C ₁₆₆	C ₂₂₅
GdP	100	3.959	1.664	2.058	-38.96	-20.38	-0.115	0.247	-23.77	0.251
	200	4.193	1.790	2.061	-44.34	-22.15	-0.665	0.249	-23.82	0.251
	300	4.405	1.811	2.065	-47.51	-22.89	-1.209	0.249	-23.85	0.251
GdAs	100	3.751	1.704	1.920	-40.60	-21.10	-0.745	0.209	-22.78	0.209
	200	3.959	1.749	1.923	-44.26	-22.09	-1.034	0.199	-20.90	0.209
	300	4.172	1.741	1.927	-46.95	-22.53	-1.939	0.209	-22.85	0.209
GdSb	100	3.118	1.413	1.562	-35.93	-18.22	-0.346	0.127	-19.32	0.128
	200	3.314	1.429	1.562	-39.08	-18.93	-0.885	0.127	-19.34	0.128
	300	3.518	1.412	1.568	-41.62	-19.26	-1.413	0.127	-19.36	0.128
GdBi	100	3.482	1.421	1.821	-38.41	-20.11	-0.118	0.219	-22.19	0.125
	200	3.592	1.432	1.839	-42.41	-20.42	-0.618	0.218	-21.22	0.125
	300	3.613	1.443	1.868	-45.00	-21.32	-1.389	0.220	-22.82	0.215

Table 9.6 Longitudinal velocity (V_l) in 10^5 cm/sec, shear velocity (V_s) in 10^5 cm/sec, Debye average velocity (\bar{V}) in 10^5 cm/sec and thermal relaxation time (τ_{th}) in 10^{-11} sec of the semimetallics at temperature range 100-300K.

Material	Temperature (K)	V_l	V_s	\bar{V}	τ_{th}
GdP	100	2.427	1.750	1.892	0.711
	200	2.499	1.752	1.902	0.750
	300	2.565	1.756	1.913	0.805
GdAs	100	2.214	1.584	1.714	1.077
	200	2.276	1.587	1.724	1.078
	300	2.339	1.590	1.733	1.065
GdSb	100	2.011	1.423	1.543	3.050
	200	2.075	1.426	1.552	3.004
	300	1.904	1.271	1.390	4.195
GdBi	100	1.780	1.262	1.367	5.485
	200	1.838	1.264	1.376	5.179
	300	1.897	1.267	1.385	4.225

Table 9.7 Average of ultrasonic Grüneisen parameters $\langle \gamma_i^j \rangle_l$ for longitudinal waves, average of square of ultrasonic Grüneisen parameters $\langle (\gamma_i^j)^2 \rangle_l$ for longitudinal waves, average of square of ultrasonic Grüneisen parameters $\langle (\gamma_i^j)^2 \rangle_s$ for shear waves, non-linear parameters D_l for longitudinal waves, D_s for shear wave and ratio of non linearity parameters (D_l / D_s) of the semimetals at the temperature range 100-300K along $\langle 100 \rangle$ crystallographic directions.

Material	Temp.[K]	$\langle \gamma_i^j \rangle_l$	$\langle (\gamma_i^j)^2 \rangle_l$	$\langle (\gamma_i^j)^2 \rangle_s$	D_l	D_s	D_l / D_s
GdP	100	12.136	7.308	4.119	71.344	37.067	1.924
	200	12.219	7.688	3.862	78.917	34.755	2.271
	300	10.517	5.703	3.643	73.710	32.789	2.248
GdAs	100	19.582	1.928	14.778	166.968	133.000	1.255
	200	18.627	5.659	13.995	145.418	125.953	1.155
	300	17.749	5.460	13.174	140.291	118.566	1.183
GdSb	100	15.411	10.073	4.583	94.264	41.283	2.283
	200	15.157	9.964	4.271	99.856	38.441	2.598
	300	14.727	9.633	3.978	104.250	37.415	2.786
GdBi	100	16.834	11.116	4.940	103.960	44.460	2.338
	200	16.407	10.855	4.587	100.228	41.279	2.632
	300	15.909	10.459	4.270	102.546	42.548	2.400

Table 9.8 Average of ultrasonic Grüneisen parameters $\langle \gamma_i^j \rangle_l$ for longitudinal waves, average of square of ultrasonic Grüneisen parameters $\langle (\gamma_i^j)^2 \rangle_l$ for longitudinal waves, average of square of

ultrasonic Grüneisen parameters $\langle(\gamma_i^j)^2\rangle_{s1}$ for shear waves (polarized along $\langle 001 \rangle$ direction), average of square of ultrasonic Grüneisen parameters $\langle(\gamma_i^j)^2\rangle_{s2}$ for shear waves (polarized along $\langle 1\bar{1}0 \rangle$ direction), non-linear parameters D_l for longitudinal waves, D_{s1} for shear wave (polarized along $\langle 001 \rangle$ direction), D_{s2} for shear wave (polarized along $\langle 1\bar{1}0 \rangle$ direction), ratio of non linearity parameters (D_l / D_{s1}) and (D_{s2}/D_l) of the semimetals at the temperature range 100-300K along $\langle 110 \rangle$ crystallographic directions.

Material	Temp [K]	$\langle\gamma_i^j\rangle_l$	$\langle(\gamma_i^j)^2\rangle_l$	$\langle(\gamma_i^j)^2\rangle_{s1}$	$\langle(\gamma_i^j)^2\rangle_{s2}$	D_l	D_{s1}	D_{s2}	D_l / D_{s1}	D_{s2}/D_l
GdP	100	10.58	7.785	25.93	10.38	54.90	233.3	93.40	0.235	1.701
	200	11.39	8.329	25.59	9.663	68.85	230.3	86.97	0.298	1.263
	300	7.131	5.656	25.21	10.69	43.41	226.9	96.24	0.191	2.217
GdAs	100	8.955	1.933	41.29	60.64	71.29	376.7	545.8	0.189	7.655
	200	13.55	6.259	40.39	42.70	97.35	363.5	384.3	0.268	3.948
	300	12.52	5.925	39.03	39.84	91.61	351.3	358.6	0.261	3.914
GdSb	100	14.70	11.02	30.05	13.45	83.72	270.4	13.45	0.310	1.446
	200	14.18	10.81	29.54	12.86	87.96	265.8	12.86	0.331	1.316
	300	13.29	10.31	28.98	12.19	86.97	271.4	13.21	0.320	1.512
GdBi	100	16.35	12.22	32.36	14.68	94.84	291.2	132.1	0.326	1.393
	200	15.48	11.80	31.71	13.86	96.41	285.4	124.7	0.338	1.293
	300	14.43	11.21	31.11	13.01	97.41	290.6	128.4	0.334	1.319

Table 9.9 Average of ultrasonic Grüneisen parameters $\langle\gamma_i^j\rangle_l$ for longitudinal waves, average of square of ultrasonic Grüneisen parameters $\langle(\gamma_i^j)^2\rangle_l$ for longitudinal waves, average of square of ultrasonic Grüneisen parameters $\langle(\gamma_i^j)^2\rangle_s$ for shear waves (polarized along $\langle 1\bar{1}0 \rangle$ direction), non-linear parameters D_l for longitudinal waves, D_s for shear wave (polarized along $\langle 1\bar{1}0 \rangle$ direction) and ratio of non linearity parameters (D_l / D_s) of the semi-metals at the temperature range 100-300K along $\langle 100 \rangle$ crystallographic directions.

Material	Temp.[K]	$\langle\gamma_i^j\rangle_l$	$\langle(\gamma_i^j)^2\rangle_l$	$\langle(\gamma_i^j)^2\rangle_s$	D_l	D_s	D_l / D_s
GdP	100	13.971	7.841	6.196	85.107	55.761	1.526
	200	15.910	8.675	5.701	108.151	51.311	2.108
	300	14.967	7.158	9.182	108.421	82.636	1.312
GdAs	100	10.026	1.063	41.382	85.122	372.441	0.228
	200	15.608	6.732	28.899	114.027	260.091	0.438
	300	15.043	6.638	27.327	111.739	245.944	0.454
GdSb	100	19.356	11.508	7.847	123.420	70.888	1.741
	200	20.174	11.745	7.605	138.475	68.445	2.023
	300	20.610	11.656	7.350	139.754	69.514	2.014
GdBi	100	21.134	12.703	8.596	135.879	77.364	1.756
	200	21.734	12.759	8.208	149.251	73.873	2.024
	300	22.111	12.604	7.910	150.24	71.186	2.111

Table 9.10 $(\alpha/f^2)_{th}$ due to thermoelastic loss, $(\alpha/f^2)_l$ for longitudinal wave and $(\alpha/f^2)_s$ for shear wave of the semimetallics along $\langle 100 \rangle$ direction at the temperature range 100-300K (in the unit of $10^{-18} \text{Np s}^2/\text{cm}$).

Material	Temperature (K)	$(\alpha/f^2)_{th}$	$(\alpha/f^2)_l$	$(\alpha/f^2)_s$
GdP	100	0.017	31.262	21.669
	200	0.018	95.261	60.849
	300	0.013	148.096	102.701
GdAs	100	0.007	131.437	143.059
	200	0.021	281.064	359.430
	300	0.017	413.067	556.054
GdSb	100	0.122	264.595	163.329
	200	0.109	636.468	377.689
	300	0.195	1315.415	788.384
GdBi	100	0.270	600.579	360.958
	200	0.225	1323.685	775.836
	300	0.203	2015.140	1450.123

Table 9.11 $(\alpha/f^2)_{th}$ due to thermoelastic loss, $(\alpha/f^2)_l$ for longitudinal wave, $(\alpha/f^2)_{s1}$ for shear wave (polarized along $\langle 001 \rangle$ direction) and $(\alpha/f^2)_{s2}$ for shear wave (polarized along $\langle 1\bar{1}0 \rangle$ direction) of the semimetallics along $\langle 100 \rangle$ direction at the temperature range 100-300K (in the unit of $10^{-18} \text{Np s}^2/\text{cm}$).

Material	Temperature (K)	$(\alpha/f^2)_{th}$	$(\alpha/f^2)_l$	$(\alpha/f^2)_{s1}$	$(\alpha/f^2)_{s2}$
GdP	100	0.018	24.058	136.403	54.601
	200	0.020	83.104	403.161	152.262
	300	0.013	87.222	710.547	301.424
GdAs	100	0.007	56.121	405.146	584.027
	200	0.023	188.513	1037.409	1096.636
	300	0.019	269.725	1647.563	1681.663
GdSb	100	0.133	234.993	1069.934	478.867
	200	0.118	560.654	2611.899	1136.982
	300	0.195	987.212	4615.112	5023.214
GdBi	100	0.297	547.888	2364.358	1072.585
	200	0.244	1179.178	5364.619	2343.742
	300	0.245	2156.321	9844.221	5981.234

Table 9.12 $(\alpha/f^2)_{th}$ due to thermoelastic loss. $(\alpha/f^2)_l$ for longitudinal wave and $(\alpha/f^2)_s$ for shear wave(polarized along $\langle \bar{1}10 \rangle$ direction) of the semimetallics along $\langle 111 \rangle$ direction at the temperature range 100-300K (in the unit of $10^{-18} \text{Np s}^2 \text{ cm}$).

Material	Temperature (K)	$(\alpha/f^2)_{th}$	$(\alpha/f^2)_l$	$(\alpha/f^2)_s$
GdP	100	0.018	37.293	32.596
	200	0.020	130.550	89.836
	300	0.016	217.835	258.826
GdAs	100	0.004	67.008	400.607
	200	0.024	220.392	742.215
	300	0.021	329.001	1153.430
GdSb	100	0.140	346.435	280.455
	200	0.128	882.618	672.493
	300	0.221	1556.125	1156.231
GdBi	100	0.309	784.978	628.091
	200	0.265	1825.420	1388.451
	300	0.245	2456.231	1825.623

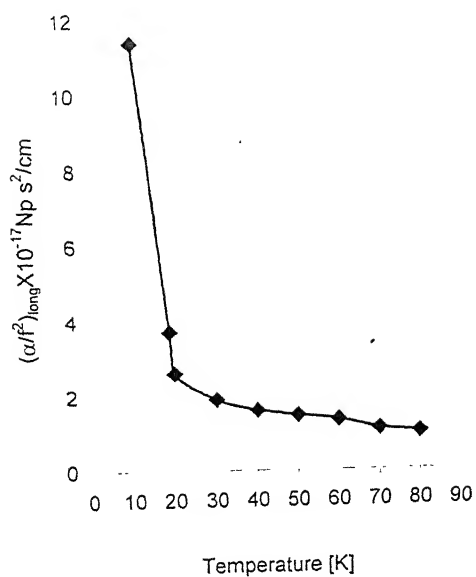


Fig 9.1 $(\alpha/f^2)_{\text{long}}$ vs. temperature of GdP

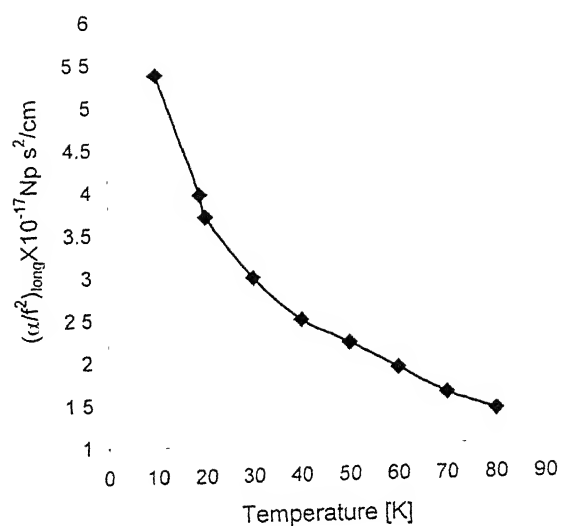


Fig 9.2 $(\alpha/f^2)_{\text{long}}$ vs temperature of GdAs

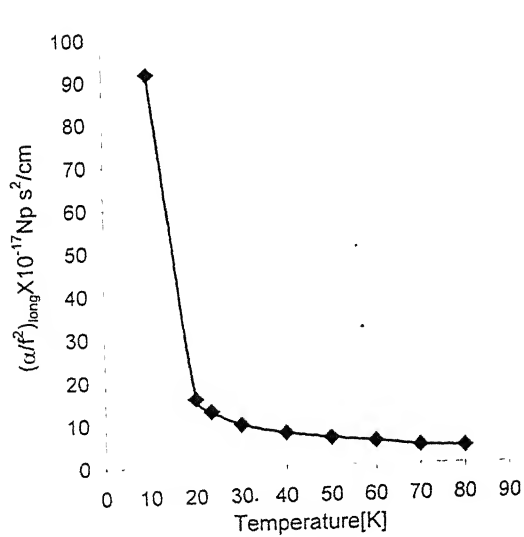


Fig 9.3 $(\alpha/f^2)_{\text{long}}$ vs temperature of GdSb

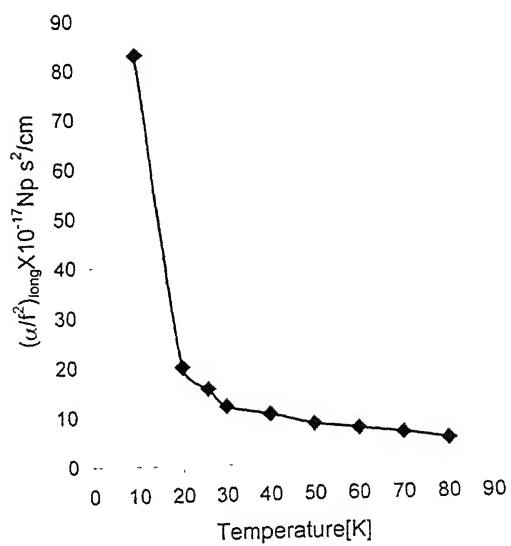


Fig 9.4 $(\alpha/f^2)_{\text{long}}$ vs temperature of GdBi

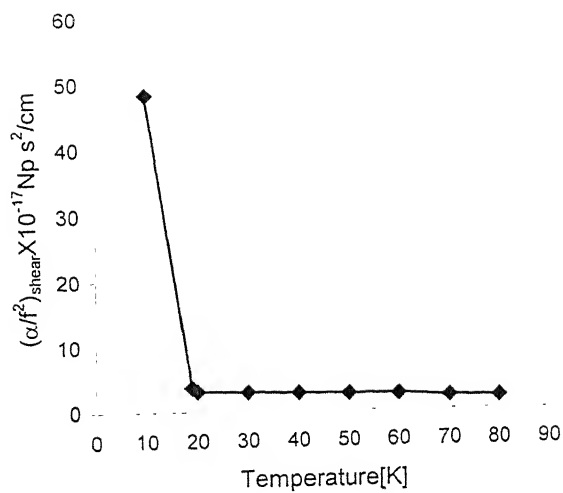


Fig. 9.5 $(\alpha/f^2)_{\text{shear}}$ vs. temperature
GdP

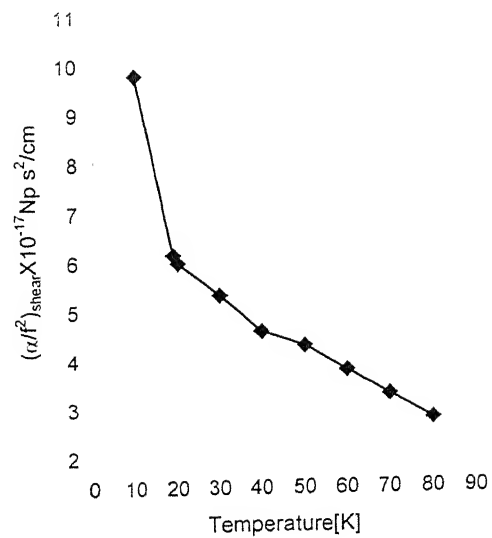


Fig. 9.6 $(\alpha/f^2)_{\text{shear}}$ vs. temperature
GdAs

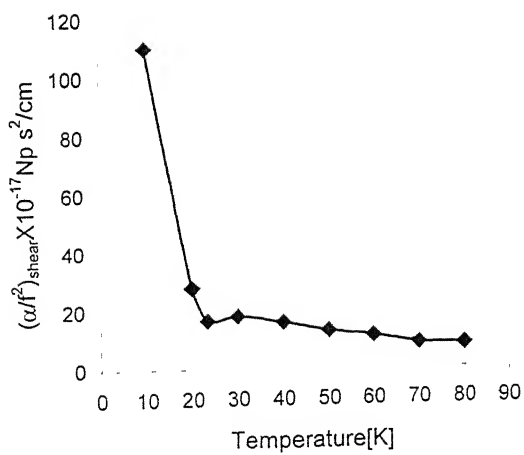


Fig. 9.7 $(\alpha/f^2)_{\text{shear}}$ vs. temperature
GdSb

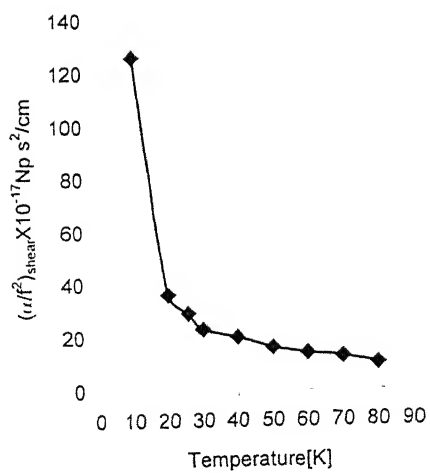


Fig. 9.8 $(\alpha/f^2)_{\text{shear}}$ vs. temperature
GdBi

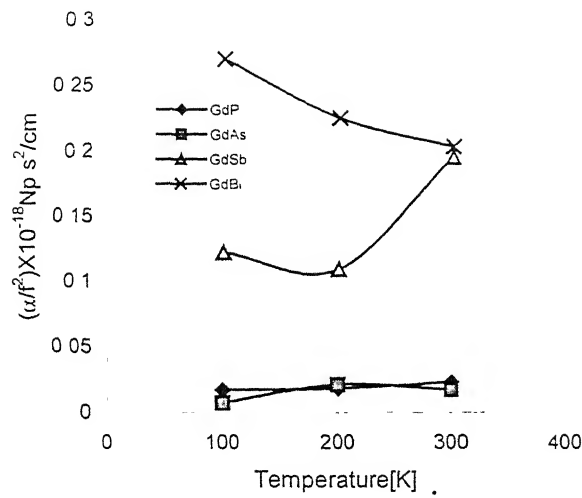


Fig.9.9 $(\alpha/f^2)_{th}$ vs temperature of the semimetals along <100> direction

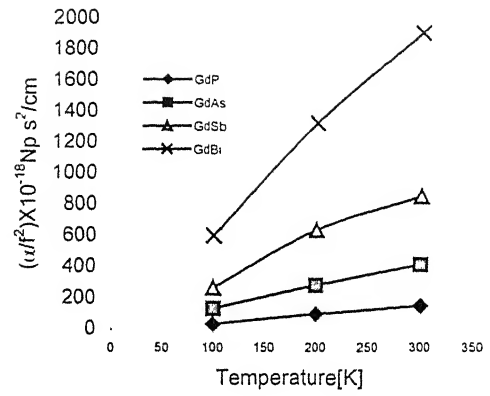


Fig.9.10 $(\alpha/f^2)_{long}$ vs temperature of the semimetals along <100> direction

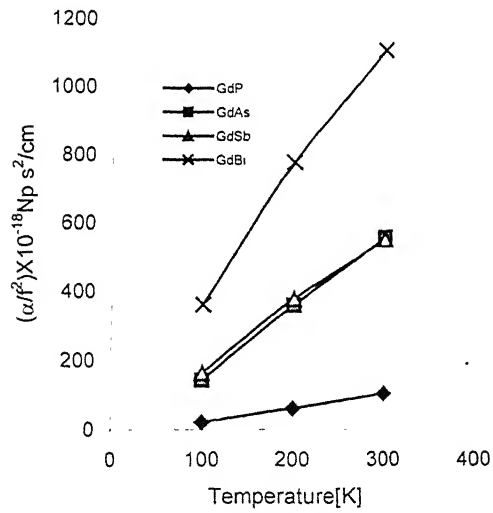


Fig.9.11 $(\alpha/f^2)_{shear}$ vs temperature of the semimetals along <100> direction

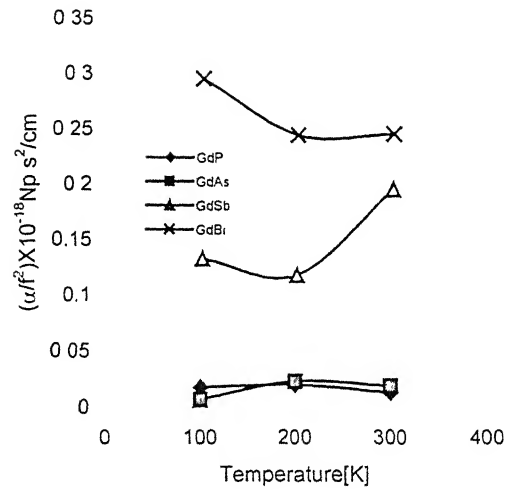


Fig.9.12 $(\alpha/f^2)_{th}$ vs temperature of the semimetals along <110> direction

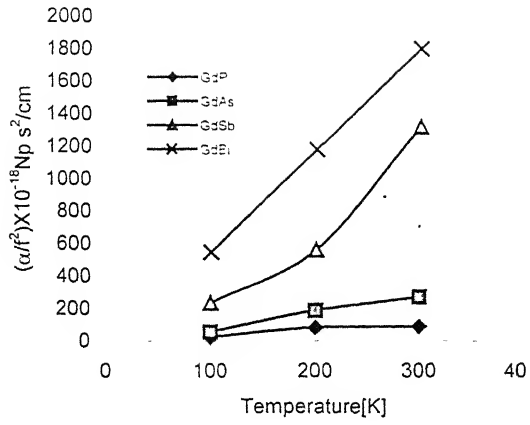


Fig.9.13 $(\alpha/f^2)_{\text{long}}$ vs temperature of the semimetals along $\langle 110 \rangle$ direction

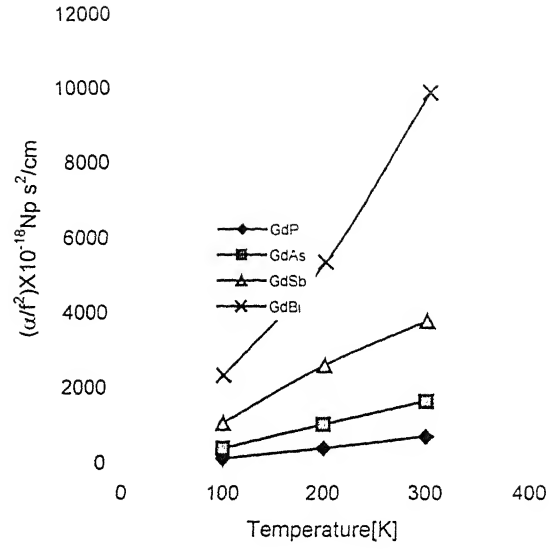


Fig.9.14 $(\alpha/f^2)_{\text{shear}}$ vs temperature of the semimetals along $\langle 110 \rangle$ direction shear wave polarized along $\langle 001 \rangle$ direction

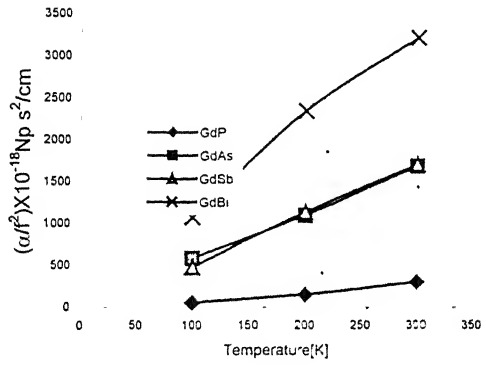


Fig.9.15 $(\alpha/f^2)_{\text{shear}}$ vs temperature of the semimetals along $\langle 110 \rangle$ direction shear wave polarized along $\langle 110 \rangle$ direction

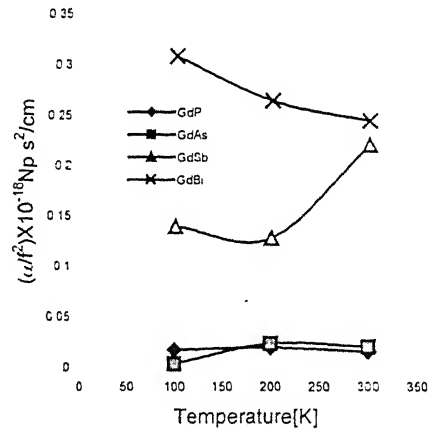


Fig.9.16 $(\alpha/f^2)_{\text{th}}$ vs temperature of the semimetals along $\langle 111 \rangle$ direction

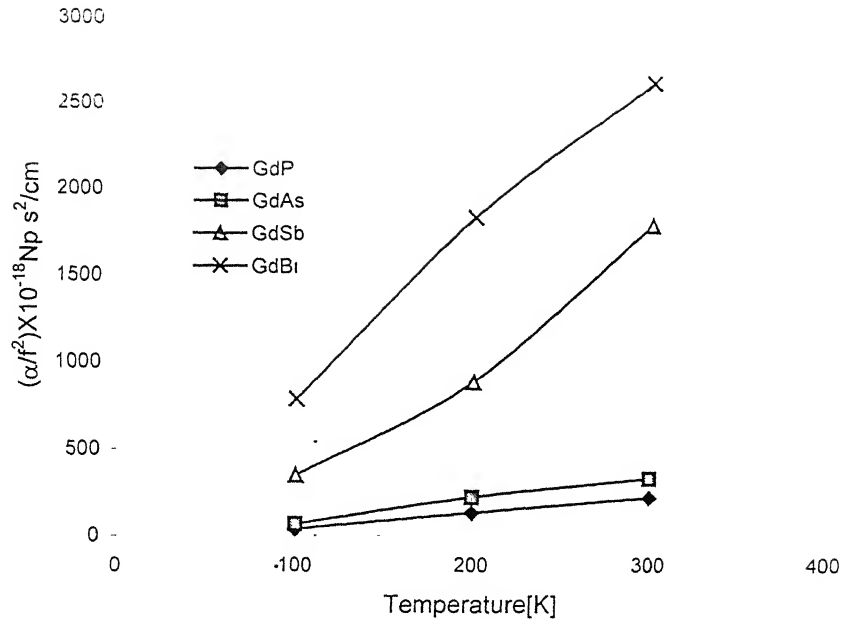


Fig.9.17 $(\alpha/f^2)_{\text{long}}$ vs temperature of the semimetals along

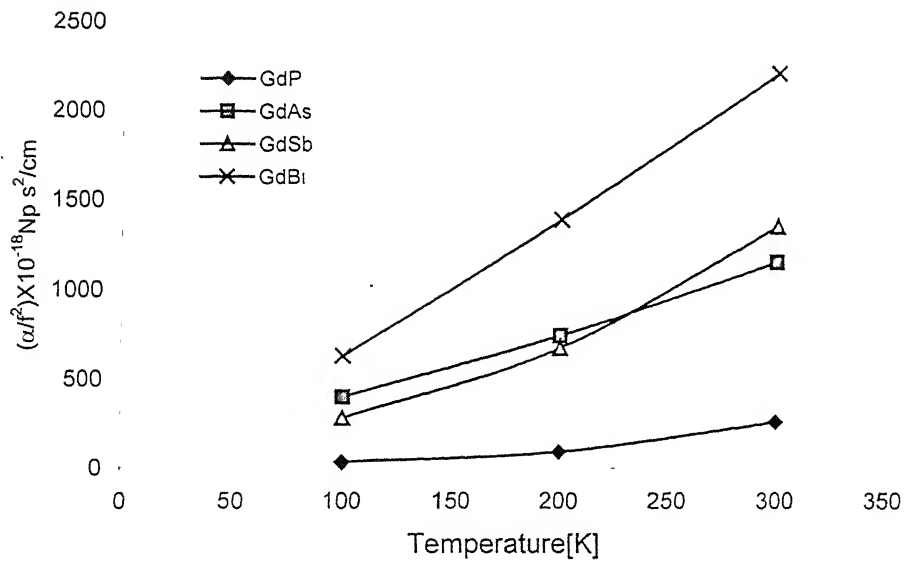


Fig.9.18 $(\alpha/f^2)_{\text{th}}$ vs temperature of the semimetals along $\langle 111 \rangle$ direction shear wave polarized along $\langle \bar{1}10 \rangle$ direction

References

1. R.P.Singh and G.S.Verma, Phys.Rev. 171,838(1968).
2. A.Paul, A.Maiti and C.Basu. Ind.J.Phys. 74A,139(2000).
3. K.Kawashima, D.Naito and Shimiza, A.I.P.Conf.Proc.(USA) 509B,1121(2000).
4. R.T.Beyer and S.V.Letcher, Physical Ultrasonics, (Academic Press, New York 1969).
5. Y.Xie and J.Beanith, Czech.J.Phys. 18,91(1996).
6. C.A.Damianou, N.T.Sanghvi, F.J.Fry and M.Moreno, J.Acoust.Soc.Am. 102,628(1997).
7. A.P.Cracknell, Ultrasonics, (Wykeham Publications Ltd, London 1980).
8. T.Gupta and D.M.Gaitonde, Mod.Phys.Lett. B15,269(2001).
9. J.R.Bae and S.Yun, Jpn.J.Phys. 37,2801(1998)
10. M.S.Ojha, G.C.Rout and S.N.Behera, Basu, Ind.J.Phys. 76A,79(2002).
11. W.P.Mason, Piezoelectric Crystals and their applications to Ultrasonics, (D.Van Nortrand Co.,Inc.,Princeton1950) pp. 479-481.
12. W.P.Mason, Physical Acoustics, (Academic Press New York 1965) Vol.IIIB pp.237-285.
13. S.K.Kor, Kailash, K.Shanker, and P.Mehrotra, J.Phys.Soc.Jpn. 56, 2428(1987).
14. S.K.Kor and P.K.Mishra.Acustica 34, 249(1976).
15. S.K.Kor, U.S. Tandon and Gulshan Rai, Phys. Rev. B5, 4143(1972).
16. S.K.Kor, P.K.Mishra and U.S.Tandon, Sol.Stat. Comm. 15, 499(1974).
17. M.Born and J.B..Mayer, Z.Phys. 75,1(1931).
18. L.A.Garifalco and V.G.Weizer, Phys. Rev. 114,687(1959).
19. B.R.K.Gupta, U.Kawald, H.Johausmann et al., J.Phys.(Condensed Matter) 4,6879(1992).
20. J.Sörgel and U.Scherz, Eur.Phys.J. B5,45(1998).
21. D.X.Li, Y.Haga.H. Shida, T.Suzuki and Y.S,Kwon, Phys.Rev. B54,10483(1996).
22. N.H.Anderson and H.Smith, Phys.Rev. B19,384(1979).
23. T.Kasuya, Prog.Theor.Phys. 16,58(1956)
24. G.Leibfried and H.Hahn, Z.Phys. 150, 497(1958).
25. G.Leibfried and W.Ludwig, in Solid State Physics edited by F.Seitz and D.Turnbull, (Academic Press,New York, 1964) Vol.12.
26. W.P Mason. and A Rosenberg, J. Acoust. Soc. Am. 45, 470(1969).
27. A.Akhiezer, J.Phys.(USSR) 1, 277(1939)
28. H.E.Bömmel and K.Dransfeld,Phys. Rev. 117, 1245(1960)

29. Dwight E. Gray, American Institute of Physics Handbook, (McGraw Hill Book Company, Inc. New York) ,Third Edition.

CHAPTER-10

Behaviour of Acoustical Phonons in BCC Metals in Low Temperature Region using Morse Potential

10.1 Introduction

In the present chapter, temperature dependence of ultrasonic attenuation using Morse potential has been studied in transition metals (d-block elements of the Periodic Table) viz. Vanadium (V), Niobium (Nb) and Tantalum (Ta) from the 5-80K due to electron-phonon interaction for longitudinal and shear waves. It is well known that the chosen metals V, Nb and Ta possessed b.c.c. structure and having following interesting properties:

Vanadium ($Z=23$), Niobium ($Z=41$) and Tantalum ($Z=73$) are the transition elements of group VB in b.c.c. phase with outer configuration $3d^34s^2$, $4d^35s^2$ and $5d^36s^2$ respectively, high melting points ($V=1900^\circ\text{C}$, $Nb=2500^\circ\text{C}$, $Ta=3000^\circ\text{C}$) and exhibit variable valency. Also, the density (ρ) of transition metals of group VB increases significantly from the Vanadium ($\rho=6.1\text{g/cc}$) to Niobium ($\rho=8.6\text{g/cc}$), then to Tantalum ($\rho=16.6\text{g/cc}$). Further, because of lanthanide contraction, the covalent and ionic radii of Nb and Ta are almost identical with the value of 1.34\AA . Consequently, these two elements have very similar properties, occur together and are very difficult to separate. Vanadium forms many different +ive ions, but Niobium and Tantalum are metals (highly unreactive and resistant to acid except HF), their compounds in the (+5) state are mostly covalent, volatile and readily hydrolyzed properties associated with non metals. Finally it is worthwhile to mention that the Vanadium is seldom used on its own, but it is used in metal alloys and acts like an important catalyst in oxidation reactions. Niobium is used in chromium nickel stainless steel. Because it is unreactive and is not rejected by the human body, tantalum is used for making metal plates, screws and wires for replacing badly fractured bone.

10.2 Theory

Theory has been completed in two parts. In the first part discussion has been made about the temperature variation of SOEC and in the next part about the ultrasonic attenuation due to e-p interaction. A theory is evolved to evaluate second-order elastic constants of body centred cubic structure transition metals using Morse potential. Morse parameters are determined from the experimental values of lattice parameter, bulk modulus and cohesive energy at absolute zero

temperature. Temperature dependence of SOEC has been evaluated using the anharmonic theory of lattice dynamics.

10.2.1 Theory of the second order elastic constants:

Girifalco and Weizer [1] used Morse potential to calculate the the second order elastic constants at absolute zero for a number of cubic metals. They came to conclusion that the Morse potential can be used to study of atomic properties of metals.

According to the Morse potential, the interaction energy $\phi(r_{ij})$ between the two atoms i and j separated by a distance r_{ij} is given by

$$\phi(r_{ij}) = D[e^{-2\alpha(r_{ij}-r_0)} - 2e^{-\alpha(r_{ij}-r_0)}] \quad (10.1)$$

The average energy per atom is given by

$$\phi = (1/2)ND \sum_j [e^{-2\alpha(r_j-r_0)} - 2e^{-\alpha(r_j-r_0)}] \quad (10.2)$$

r_j is the distance of the j^{th} atom from origin in the lattice. The summation goes to 168 neighbouring atoms for b.c.c. metals. ϕ is defined as the average cohesive energy per atom. It is convenient to introduce the following quantities:

$$\beta = e^{\alpha r_0} \quad (10.3)$$

$$r_j = [m_j^2 + n_j^2 + l_j^2]^{1/2} a = M_j a \quad (10.4)$$

Where: m_j , n_j and l_j are the position coordinates of any atom in terms of half the lattice parameter “a”. The volume V is $4a^3$ for b.c.c. metals, The equilibrium condition is that

$$d\phi/da = 0 \text{ at } a = a_0 \quad (10.5)$$

So the lattice is in equilibrium at the observed lattice parameters. Bulk modulus (B) can be expressed as:

$$\text{Bulk Modulus (B)} = (a^3/9V) (d^2\phi/da^2)_{a=a_0} \quad (10.6)$$

For a cubic crystal there are three independent second order elastic constants at absolute zero namely C_{11} , C_{12} and C_{44} . In this investigation Brugger's[2] definition of second order elastic constants have been used.

In the central force model, the elastic constants. Cauchy relations:

$$C_{12}^0 = C_{44}^0$$

Hence only two independent SOEC at absolute zero have been used here

The expression of the SOEC at absolute zero are given below when Morse potential is used:

$$C_{11}^0 = \frac{2Da^2 \alpha^2 \beta^2}{V} \sum \frac{m_i^4 e^{-2\alpha a M_i}}{M_i^2} - \frac{2Da^2 \alpha^2 \beta}{V} \sum \frac{m_i^4 e^{-\alpha a M_i}}{M_i^2} + \frac{Da\alpha\beta^2}{V} \sum \frac{m_i^4 e^{-2\alpha a M_i}}{M_i^3} - \frac{Da\alpha\beta}{V} \sum \frac{m_i^4 e^{-\alpha a M_i}}{M_i^3} \quad (10.7)$$

$$C_{12}^0 = C_{44}^0 = \frac{2Da^2 \alpha^2 \beta^2}{V} \sum \frac{m_j^2 n_j^2 e^{-2\alpha a M_j}}{M_j^2} - \frac{2Da^2 \alpha^2 \beta}{V} \sum \frac{m_j^2 n_j^2 e^{-\alpha a M_j}}{M_j^2} + \frac{Da\alpha\beta^2}{V} \sum \frac{m_j^2 n_j^2 e^{-2\alpha a M_j}}{M_j^3} - \frac{Da\alpha\beta}{V} \sum \frac{m_j^2 n_j^2 e^{-\alpha a M_j}}{M_j^3} \quad (10.8)$$

Applying the anharmonic theory of lattice dynamics developed by Leibfried et al.[3,4], SOEC at different temperatures are obtained. Vibrational energy of the crystal changes with temperature, therefore adding vibrational energy contribution to the elastic constant at absolute zero temperature one gets

$$C_{IJ} = C_{IJ}^0 + C_{IJ}^{Vib} \quad (10.9)$$

and thus SOEC at required temperature are found, the C_{IJ}^{Vib} 's are given as

$$C_{11}^{Vib} = f^{(1,1)} G_1^2 + f^{(2)} G_2 \quad (10.10)$$

$$C_{12}^{Vib} = f^{(1,1)} G_1^2 + f^{(2)} G_{1,1} \quad (10.11)$$

$$C_{44}^{Vib} = f^{(2)} G_{1,1} \quad (10.12)$$

Various $f^{(n)}$'s and G_n 's are given as

$$f^{(2)} = \frac{3\sqrt{3}}{32} \frac{\eta\omega_0}{r_0^3} \coth\left(\frac{\eta\omega_0}{2kT}\right) \quad (10.13)$$

$$f^{(2)} = \frac{3\sqrt{3}}{32} \frac{\eta\omega_0}{r_0^3} \left[\frac{\eta\omega_0}{2kT \sinh^2\left(\frac{\eta\omega_0}{2kT}\right)} + \coth\left(\frac{\eta\omega_0}{2kT}\right) \right] \quad (10.14)$$

$$G_1 = [(8/9)\phi(r_1)(2\rho_1 + 2\rho_1^2 - \rho_1^3) + (1/2)\phi(r_2)(2\rho_2 + 2\rho_2^2 - \rho_2^3)]H \quad (10.15)$$

$$G_2 = [(8/27)\phi(r_1)(-6\rho_1 - 6\rho_1^2 - \rho_1^3 + \rho_1^4) + (1/2)\phi(r_2)(-6\rho_2 - 6\rho_2^2 - \rho_2^3 + \rho_2^4)]H \quad (10.16)$$

$$G_{11} = [(8/27)\phi(r_1)(-6\rho_1 - 6\rho_1^2 - \rho_1^3 + \rho_1^4)]H \quad (10.17)$$

$$\text{where } H = [(4/9)\phi(r_1)(\rho_1^2 - 2\rho_1) + (1/4)\phi(r_2)(\rho_2^2 - 2\rho_2)]^{-1} \quad (10.18)$$

$$\text{and } r_1 = r_0\sqrt{3}, r_2 = 2r_0, \rho_1 = r_1/b \text{ and } \rho_2 = r_2/b \quad (10.19)$$

$$\text{and } \phi(r_1) = A \exp(-r_1/b) \text{ and } \phi(r_2) = A \exp(-r_2/b) \quad (10.20)$$

$$\text{where } A = 1.74756 b \left(\frac{e^2}{r_0^2}\right) [8\sqrt{3} \exp(-\frac{r_0\sqrt{3}}{b}) + 12 \exp(-\frac{2r_0}{b})]^{-1} \quad (10.21)$$

r_0 is related to nearest neighbor distance r_1 and next nearest neighbor distance r_2 as in eqn. (10.19), b is hardness parameter. η is planck's constants divided 2π and M_1 being mass of single ion. The procedure discussed in chapter II (part A) for obtaining vibrational contribution to elastic constants of f.c.c. crystals has been used to obtain vibrational contribution in the present chapter taking crystal symmetry into account.

10.2.2 Theory used in ultrasonic attenuation due to electron-phonon interaction

Debye's theory of specific heat concludes that the energy exchanges occur between free electron and lattice vibration (acoustical phonon). Analysis of thermal conductivity were only the method by which above effect could be visualized, until the measurements on ultrasonic attenuation in metals by Bömmel [5] and MckMinnon [6]. Their study has shown that ultrasonic attenuation provides an additional tool for observing such interactions, since at low temperatures, electrons are responsible for the major contribution to the ultrasonic attenuation. Not only this the investigations of the electron-phonon interactions are also of great interest, as the character of these interactions can be controlled with an external electric field. Hence if the carrier drift velocity in the external field exceeds the propagation velocity of the elastic waves, then the latter are not attenuated but amplified [7]

At low temperature in pure metals [8], where the mean free path of electron becomes large and is comparable to wavelength of the acoustical phonon. The momentum given to it by vibrating lattice is not returned to the lattice at once and viscous loss occurs.

The attenuation of ultrasonic waves caused by the energy loss due to compresional and shear viscosities of the lattice [9] at low temperature are as given by eqns. (2.43) and (2.44) in chapter II.

10.3 Evaluations, results and discussions:

The Morse parameters D , α and r_0 have been determined by using eqns. (10.2) to (10.6) and experimental values of lattice parameter, bulk modulus and cohesive energy of these metals. The

values of lattice parameter, bulk modulus and cohesive energy of these metals have been taken from the literature [10]. The values of D , α and r_0 are presented in Table 10.1, these values of D , α and r_0 have been used to evaluate SOEC at absolute zero as eqns.(10.7) and (10.8).

For vibrational contribution, the values of nearest neighbor distance [10] $r_0 = 2.62\text{\AA}$, 2.86\AA and 2.86\AA for Vanadium, Niobium and Tantalum respectively and hardness parameter [11] $b=0.303\text{\AA}$ for all metals. Using the theory discussed above, SOEC at different temperatures have been computed and presented in Table 10.2. Taking resistivity values [12,13] and temperature variation density [14], the temperature dependence of ultrasonic attenuation due to electron-phonon interaction $[(\alpha/f^2)_{\text{long}}$ and $(\alpha/f^2)_{\text{shear}}$ for longitudinal and shear waves respectively] have been evaluated using eqns. (2.37) and (2.38) in chapter II. The temperature variation of ultrasonic attenuation for longitudinal and shear waves for the transition metals are presented in Tables 10.3, 10.4 and 10.5 (Values of ultrasonic velocities V_l and V_s , electronic viscosity (η_e) and resistivity (R) are also presented in these Tables) and figs. 10.1 to 10.2.

The order of elastic constants at lower temperature is same as presented in the literatures [10, 15-19] for these metals. The ultrasonic attenuation values from 5K to 80K in the metallic crystal Vanadium, Niobium and Tantalum obtained, are shown in figs. 10.1 to 10.6 from 5K to 80K for longitudinal and shear waves. Present study shows that the attenuation of sound waves decreases rapidly as temperature increases and it becomes negligible small at 60K as compared to low temperature value for these transition metals. Thus e-p interaction in these b.c.c. metals almost ceases at 45K. Ultrasonic attenuation for shear wave $(\alpha/f^2)_{\text{shear}}$ is greater than ultrasonic attenuation for longitudinal wave $(\alpha/f^2)_{\text{long}}$ in case of Vanadium and Tantalum, while ultrasonic attenuation for shear wave $(\alpha/f^2)_{\text{shear}}$ is smaller than ultrasonic attenuation for longitudinal wave $(\alpha/f^2)_{\text{long}}$ in case of Niobium. Thus the behavior in all metals of ultrasonic attenuation due to electron-phonon interaction is the same as presented by Kor and Mishra [19]. The values of $(\alpha/f^2)_{\text{long}}$ and $(\alpha/f^2)_{\text{shear}}$ for longitudinal and shear waves does not vary much because of values of C_{11} and C_{44} . The values of $(\alpha/f^2)_{\text{long}}$ and $(\alpha/f^2)_{\text{shear}}$ for longitudinal and shear waves are decreasing with temperature as studied in previous studies [17,18]. Although values of $(\alpha/f^2)_{\text{long}}$ and $(\alpha/f^2)_{\text{shear}}$ for longitudinal and shear waves are very low using Morse potential. But the variation is the same as observed previously.

Hence present study confirms the validity of present approach employing Morse potential for the ultrasonic attenuation due to e-p interaction in these metals.

Table 10.1 The Morse parameters D , α and r_0 for the transition metals V, Nb and Ta

Matrrial	D (in 10^{-14} ergs)	α in $(10^{-8}\text{cm})^{-1}$	r_0 in (10^{-8}cm)
V	12.321	1.5413	2.367
Nb	18.051	1.3535	2.518
Ta	19.819	1.3215	2.519

Table 10.2 Second order elastic constants (SOEC) of the metals in the unit of 10^{12} Dyne/cm. at the temperature range 5-80K

Metal	SOEC	5	10	20	30	40	50	60	70	80
V	C_{11}	2.425	2.425	2.425	2.425	2.425	2.425	2.425	2.426	2.426
	C_{12}	1.143	1.143	1.143	1.143	1.142	1.142	1.142	1.142	1.142
	C_{44}	0.521	0.521	0.520	0.521	0.522	0.522	0.522	0.523	0.523
Nb	C_{11}	2.622	2.622	2.622	2.622	2.621	2.622	2.623	2.623	2.623
	C_{12}	1.256	1.256	1.256	1.256	1.255	1.255	1.255	1.255	1.254
	C_{44}	0.442	0.442	0.442	0.443	0.443	0.443	0.443	0.443	0.444
Ta	C_{11}	2.714	2.714	2.713	2.714	2.715	2.715	2.715	2.716	2.716
	C_{12}	1.504	1.504	1.504	1.503	1.503	1.503	1.502	1.502	1.502
	C_{44}	0.973	0.973	0.973	0.973	0.973	0.973	0.974	0.974	0.974

Table 10.3 Ultrasonic velocities (V_l for longitudinal wave and V_s for shear wave) in the unit of 10^5 cm/s, electrical resistivity (R) in the unit of $10^{-6}\Omega$ cm, viscosity (η_e) in the unit of cp, $(\alpha/f^2)_l$ for longitudinal wave in the unit of 10^{-17} Np s²/cm and $(\alpha/f^2)_s$ for shear wave in the unit of 10^{-17} Np s²/cm of Vanadium at the temperature range 2-80K.

Temp.(K)	V_l	V_s	R	η_e	$(\alpha/f^2)_l$	$(\alpha/f^2)_s$
5	6.285	2.913	0.013	2.753	4.695	32.657
10	6.286	2.913	0.014	2.556	4.358	30.322
20	6.288	2.913	0.037	0.967	1.647	11.477
30	6.289	2.913	0.014	0.098	0.981	3.035
40	6.290	2.913	0.380	0.094	0.160	1.118
50	6.293	2.913	0.750	0.048	0.081	0.566
60	6.292	2.913	1.270	0.028	0.048	0.334
70	6.293	2.914	1.900	0.019	0.032	0.223
80	6.295	2.914	2.650	0.013	0.023	0.160

Table 10.4 Ultrasonic velocities (V_l for longitudinal wave and V_s for shear wave) in the unit of 10^5 cm/s, electrical resistivity (R) in the unit of $10^{-6}\Omega$ cm, viscosity (η_e) in the unit of cp, $(\alpha/f^2)_l$ for longitudinal wave in the unit of 10^{-17} Np s²/cm and $(\alpha/f^2)_s$ for shear wave in the unit of 10^{-17} Np s²/cm of Niobium at the temperature range 2-80K.

Temp.(K)	V_l	V_s	R	η_e	$(\alpha/f^2)_l$	$(\alpha/f^2)_s$
5	5.414	2.223	0.020	1.424	2.608	26.073
10	5.415	2.223	0.030	0.949	1.738	17.384
20	5.415	2.223	0.080	0.356	0.652	6.518
30	5.416	2.223	0.250	0.114	0.209	2.086
40	5.416	2.224	0.560	0.051	0.093	0.931
50	5.416	2.224	0.970	0.029	0.054	0.537
60	5.417	2.224	1.500	0.019	0.035	0.348
70	5.417	2.224	2.070	0.014	0.026	0.258
80	5.418	2.225	2.680	0.011	0.019	0.195

Table 10.5 Ultrasonic velocities (V_l for longitudinal wave and V_s for shear wave) in the unit of 10^5cm/s , electrical resistivity (R) in the unit of $10^{-6}\Omega\text{ cm}$, viscosity (η_e) in the unit of cp. $(\alpha/f^2)_l$ for longitudinal wave in the unit of $10^{-17}\text{Np s}^2/\text{cm}$ and $(\alpha/f^2)_s$ for shear wave in the unit of $10^{-17}\text{Np s}^2/\text{cm}$ of Tantalum at the temperature range 2-80K.

Temp.(K)	V_l	V_s	R	η_e	$(\alpha/f^2)_l$	$(\alpha/f^2)_s$
5	4.020	2.407	0.003	1.111	26.475	85.412
10	4.020	2.407	0.003	1.046	25.647	82.737
20	4.020	2.407	0.051	0.675	1.609	5.918
30	4.020	2.407	0.230	0.149	0.357	1.151
40	4.020	2.407	0.540	0.064	0.152	0.490
50	4.020	2.407	0.950	0.036	0.086	0.279
60	4.021	2.407	1.430	0.024	0.057	0.185
70	4.021	2.407	1.960	0.017	0.042	0.135
80	4.021	2.407	2.500	0.014	0.033	0.106

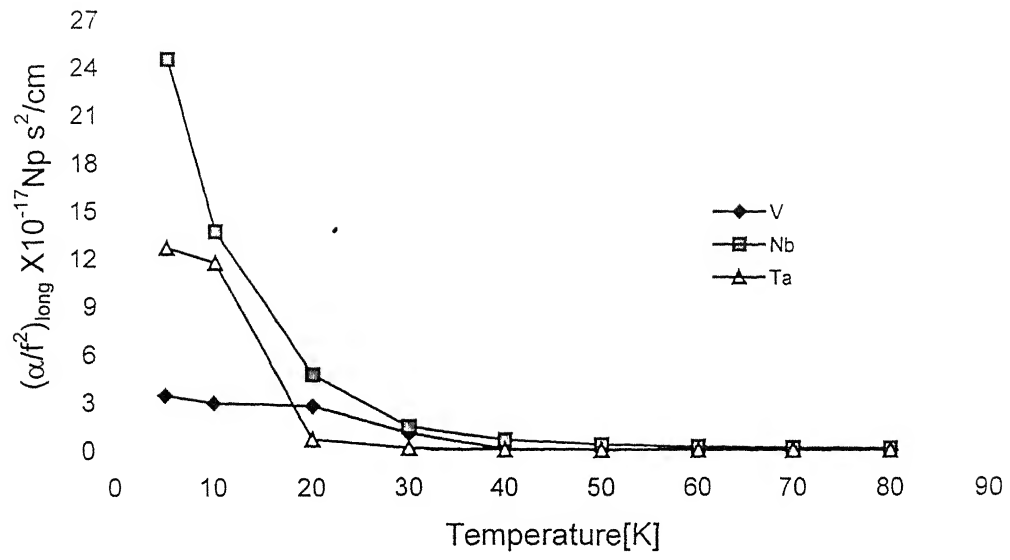


Fig.10.1 $(\alpha/f^2)_{\text{long}}$ vs. temperature

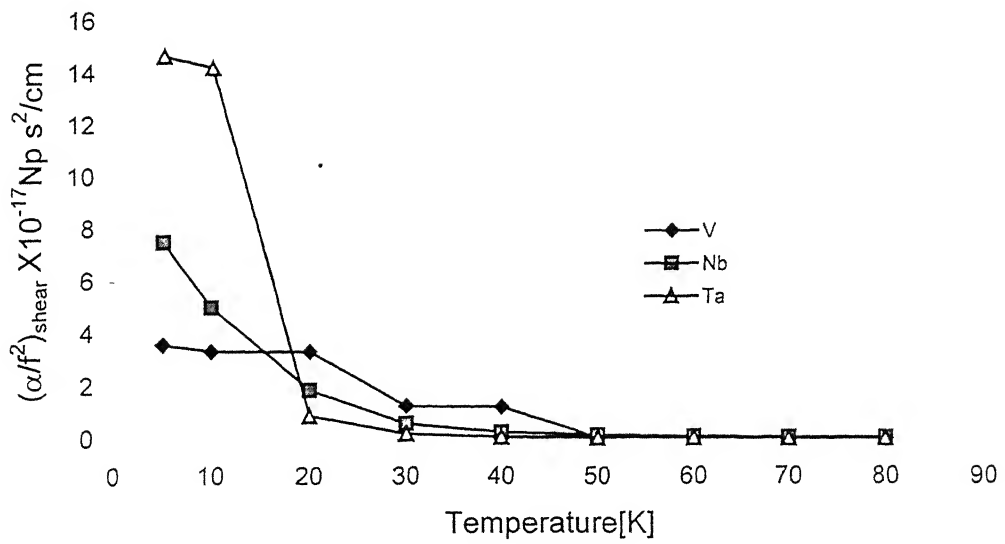


Fig.10.2 $(\alpha/f^2)_{\text{shear}}$ vs. temperature

References:

1. R.C.Lincon, K.M.Koliwad and P.B.Ghate, Phys. Rev. 157,463(1967).
2. K.Brugger, Phys.Rev. 113, A1611(1964).
3. G.Leibfried and H.Haln, Z.Phys.150,497(1958).
4. G.Leibfried and W.Ludwig, in Solid State Physics edited by F.Seitz and D.Turnbull. (Academic Press, New York 1961) p.275, Vol.12.
5. H.E.Bömmel, Phys.Rev. 96,220(1954).
6. L.McKMinnon, Phys.Rev. 98,1210(1955).
7. D.L.White, J.Appl.Phys.33,2547(1962).
8. W.P.Mason, Phys.Rev. 97,555(1955).
9. W.P.Mason, Piezoelectric Crystals and their applications to Ultrasonics, (D.Van Nostrand and Co., Priceton 1950) p.478.
10. C. Kittel, Introduction to Solid State Physics, (John Wiley and Sons, Inc., New York, 1996), 7th edition.
11. M.P.Tosi, in Solid State Physics edited by F.Seitz and D.Turnbull, (Academic Press, New York 1965) Vol.16.
12. Y.S.Touloukian, Thermophysical Properties of Matter, Thermophysical Properties Research Centre (TPRC) data series, (IFI/Plenum New York 1970), Vol.1, pp.245,355 and 411.
13. M.Cox, Phys.Rev. 64,241(1943).
14. D.E.Gray edited, AIP Handbook, McGraw Hill Co.Inc.New York,(1981).
15. A.Verma, M.L.Verma and R.P.S.Rathore, Acta Phys.Pol.A90,547(1996).
16. M.L.Verma, A.Verma and R.P.S.Rathore, Ind.J.Phys.76A,165(2002).
17. G.A.Alers, Phys. Rev. 119,1532(1960).
18. J.Carol Keith, J.Appl.Phys. 36,3689(1965).
19. O.Eriksson, J.M.Wills and A.M.Boring, Phys. Rev. B48,5844(1993).
20. R.K.Singh, Ph.D. Thesis submitted to University of Allahabad (1993).

CHAPTER-11A

Experimental Techniques and Methodology

11a.1 Introduction

A number of experimental techniques are available now a day for precise determination ultrasonic absorption in different media. The choice and use of an individual technique obviously depend upon (a) whether the medium is solid, liquid or gas and (b) the desired external conditions (frequency, temperature, concentration etc.) and accuracy of measurements.

Different available techniques can be categorized under the following two heads:

- (i) Standing wave technique
- (ii) Progressive wave technique

The standing wave techniques work well for measurements below 1MHz, but at higher frequencies progressive wave methods are decidedly more suitable.

Standing wave technique

These techniques make use of the fact that the energy of stationary sound wave between the boundaries of a test fluid, decays exponentially according to the law

$$E_t = E_0 \exp(-2\delta t) \quad (11A.1)$$

Where E_t and E_0 , respectively stand for the acoustic energies at time $t=t$ and $t=0$ and $\delta = \alpha c$ (α being the absorption and c the velocity of sound in fluid)

The decay constant is highly sensitive to boundary losses, which increase with frequency and cause limitations to use standing wave techniques at high frequencies. The reverberation method [1-3], the resonance technique [4-7] and the tuning fork technique [8] are the representatives of standing wave technique.

Progressive wave technique

The intensity of plane progressive waves in a medium falls off exponentially with distance travelled, according to relation

$$I_x = I_0 \exp(-2\alpha x) \quad (11A.2)$$

Where I_x and I_0 represent the intensity of acoustic waves at a distance x from the source and incident intensity respectively. In progressive wave techniques use of eqn. (11a.2), typically, the intensity verses distance plot directly gives the absorption

coefficient. This technique is particularly useful for high frequency measurement. At low frequencies, they need a large fluid column for considerable absorption, which is inconvenient to handle with. Moreover very large transmitters are required to give a proper directivity of the sound beam.

Methods based on the progressive wave technique are classified in the following three groups

1. Mechanical technique
2. Optical technique and
3. Electrical technique

Electrical methods

Under this there are three general methods for the measurement of ultrasonic attenuation and velocity in fluids based upon the progressive wave technique.

- (a) Interferometric technique,
- (b) Direct technique and
- (c) Pulse technique.

The choice of experimental techniques employed for measuring ultrasonic absorption in fluids is governed principally by the range of frequency over which the studies are to be carried on and volume of fluid available. In liquid crystal since even large volumes can be procured, one may choose the method only on the basis of frequency considerations. It is found that the following methods are most suitable in frequency regions noted against [9] in Table 11a.1

Table 11a.1: Various techniques with frequency range

Technique	Frequency range
Tuning fork technique	100-300Hz
Resonant sphere technique	5KHz-1.5MHZ
Reverberation technique	50KHz-1MHz
Streaming technique	150KHz-2MHz
Optical (Debye-shear's) technique	1.5MHz-100MHz
Pulse technique	1.5MHz-200MHz

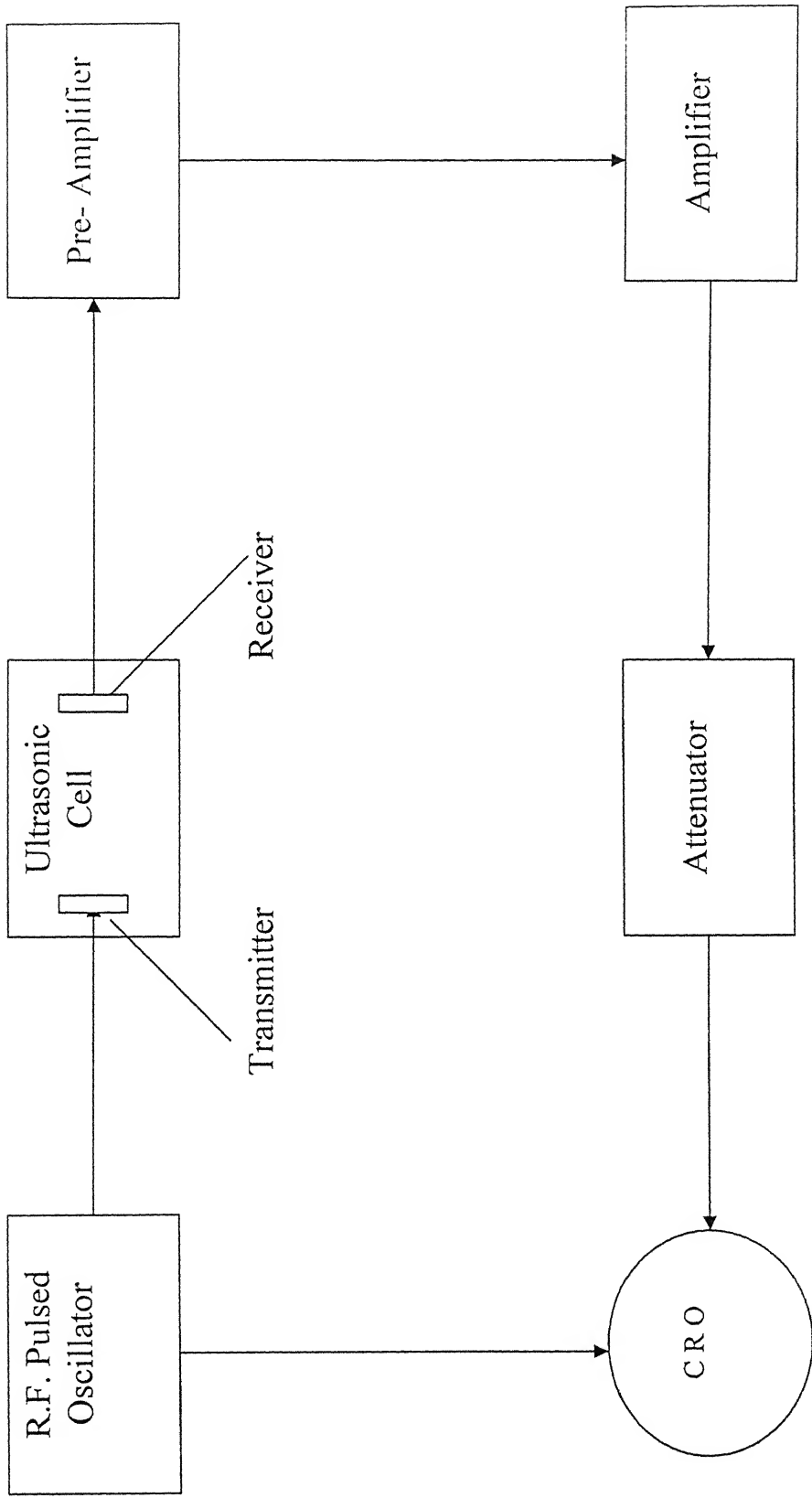


Fig 11a.1 Block diagram of experimental set up used for ultrasonic absorption measurement.

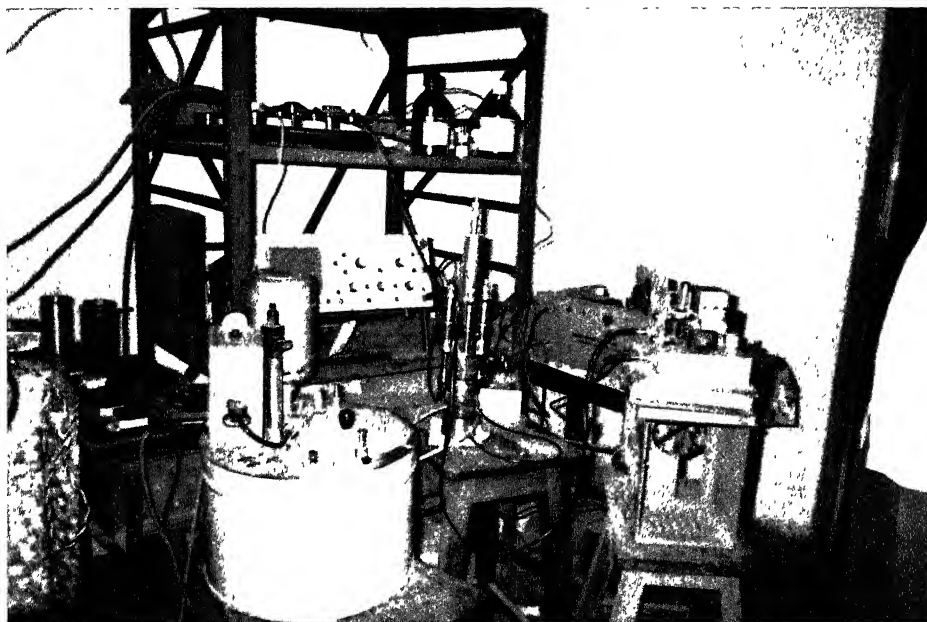


Fig. 11a.2 Photograph of experimental set up used for ultrasonic absorption measurement

The upper frequency limit of pulse technique has been increased upto 650MHz. In the present investigation pulse technique is used for ultrasonic absorption measurement in the frequency region 5MHz-55MHz.

11b.2 Pulse technique

This technique was first initially applied by Pellam and Galt [10] and Pinkerton [11] in ultrasonic measurements and further modified by Atkinson et al.[12]. Pulse technique is the most suitable technique extensively used these days. Before starting a detailed consideration of this method let us discuss the inevitable limitations of progressive wave methods, because these methods use continuous waves, the following defects may creep in

- (1) Use of considerably high power source, necessary for making measurement at high frequencies leads to appreciable heating of the test fluid and a consequent change in the intrinsic absorption.
- (2) The phenomenon of condition, which involves the formation, and subsequent collapse of gas bubbles, leads to scattering of sound energy and thus affecting the absorption.
- (3) The phenomenon of scattering or d.c flow of the test fluid causes an error in the measured absorption.
- (4) The fourth practical source of error is introduced in setting up the standing waves.

All these defect are virtually removed by the pulse technique. The arrangement consists of a quartz transducer and a polished reflector like variable path interferometer method. Short pulses of radio frequency are used to excite the transmitting crystal. The corresponding acoustic pulse is reflected and picked up by the same transducer now acting as receiver. By the use of suitable electronic equipment and initial and reflected pulses may be compared on an oscilloscope. In the present technique two quartz crystals were used one as transmitter and other receiver. The transmitter crystal is smaller than the receiver crystal

The present experimental set up as represented in the block diagram of Fig. 11a.1 (and the photograph of the experimental set up is shown in Fig. 11a.2) consists of the following electronic and mechanical units.

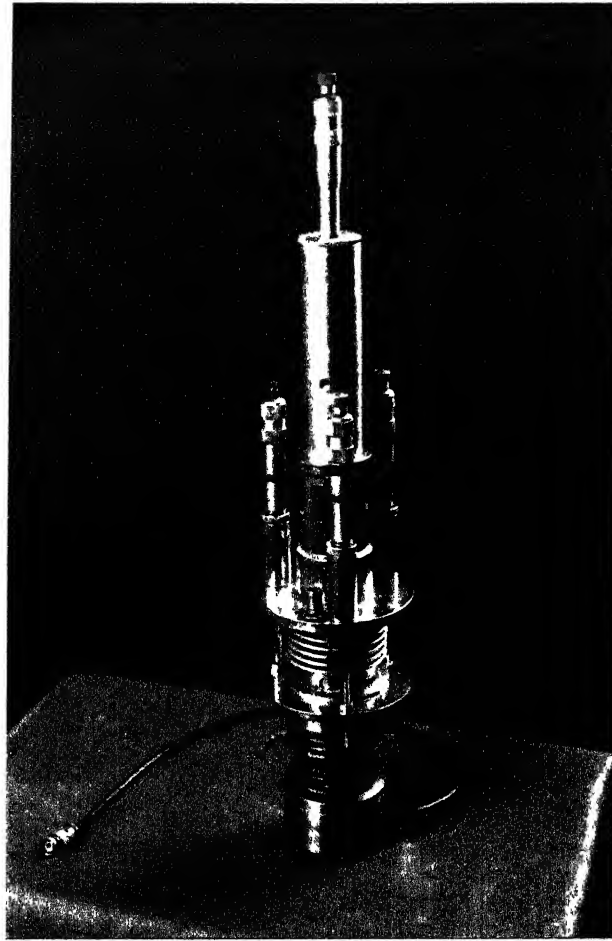


Fig. 11a.3 Photograph of measuring cell (Darwari Cell) used for ultrasonic absorption measurement

- (a) Ultrasonic cell
- (b) Pre-amplifier
- (c) Pulse receiver (amplifier)
- (d) Attenuator and
- (e) Oscilloscope

(a) Pulse Transmitter

This is of the Chesapeake model U-100. The pulser works for frequencies between 1-210MHz and pulses of 1, 1.5 and 6 microseconds width are obtainable within this range. The output of pulser can be varied upto 1000 Watts with the help of potentiometer device. A variable capacitor and a set of twelve plug in coils can produce pulses in different frequency regions. The rise time of the pulser is 0.5 microseconds. The pulser repetition rate can also be varied from 50 to as high as 70000 pulses per second. If needed, the pulse can also be used to trigger some other unit.

(b) Ultrasonic Cell

It is locally designed metallic vessel, which can be leveled with three screws. Water is circulated through a narrow tube wrapped on the surface of the cell. The temperature is controlled by ultra thermostat (model: NBE 12953). The accuracy of thermostat is $\pm 0.5^{\circ}\text{C}$. The X-cut quartz crystal is fixed at the bottom of the cell and works as receiver, while another crystal held vertically above and parallel to receiver work as transmitter and can be moved up and down within an accuracy of ± 0.001 cm. The ultrasonic cell is essentially the same as assembled by Darwari [13] (shown in Fig.11a.3). The photograph of the cell is designed with the following considerations:

- (i) The transmitter crystal is smaller than the receiver crystal.
- (ii) Very good adjustment can be made for crystal parallelism and for that reason very high frequency (Upto 300MHz).
- (iii) This can be kept in the vessel not open to air and therefore, will not change the concentration of the solution even if kept for a long time.
- (iv) The whole cell can be immersed in a constant temperature bath and can be used for temperature variation.
- (v) The cell is made of stainless steel.

- (vi) The movable crystal can be moved continuously and distance can be read upto third decimal place of a cm.

(c) Pre-amplifier

Arenberg PA 620B tuned preamplifier is used to receive the signal after travelling the substance. This is small unit and is placed near the receiving transducer. The preamplifier covers 5-60 MHz frequency range in ten steps with a gain approximately equal to 35 dB. Input tuning is achieved with the help of inductance coil.

(d) Pulse Receiver

Arenberg wideband amplifier model WA 600 D is used as receiver. This amplifier covers a range of frequencies 1-65 MHz with an overall gain of 65 dB. The input impedance is 93Ω and the video bandwidth of the amplifier is 3 MHz. Maximum output detected is of the order of 10 volts.

(e) Standard Attenuator

A key type attenuator (model 32-0) is introduced between amplifier and oscilloscope. It can produce attenuation from 1 to 100 dB in step of 1 dB for electrical pulse upto 1000 MHz. The incident insertion loss is negligible.

(f) Oscilloscope

Systronics (model: 560) Cathode Ray Oscilloscope is a wide band portable oscilloscope (Fig.11a.2). The dual channel DC to 60MHz vertical deflection system provides calibrated deflection factors from 2mV/cm to 10mV/cm. A 140 ns delay line is incorporated in the vertical system, facilitates the full display of triggering edge. The triggering circuit provides stable sweep triggering to beyond the bandwidth of the vertical system. The horizontal deflection system has a dual delay sweep system. The main time base has calibrated sweep from 0.1 μ S/div to 0.5 μ S/div. A 10turn dial provides continuous delay control. A 10 KV PDA provides a bright trace even in the fastest sweep speed. The regulated power supplies ensure that the CRO performance is not affected by variation of line voltage within +/-10% limits.

Measurement of Ultrasonic Absorption

The ultrasonic attenuation coefficient (α) obtained as follows

$$\alpha = \ln(A_1/A_2)/(X_2 - X_1) \text{ Np/cm} \quad (11A.3)$$

where A_1 and A_2 are the amplitude of the peaks positioned at X_1 and X_2

11b.3 Working principle and procedure of single crystal variable path interferometer to evaluate ultrasonic velocity:

The principle of ultrasonic interferometer (M/S Mittal Enterprises, New Delhi) used in velocity measurement is based on the accurate determination of the wavelength (λ) in the

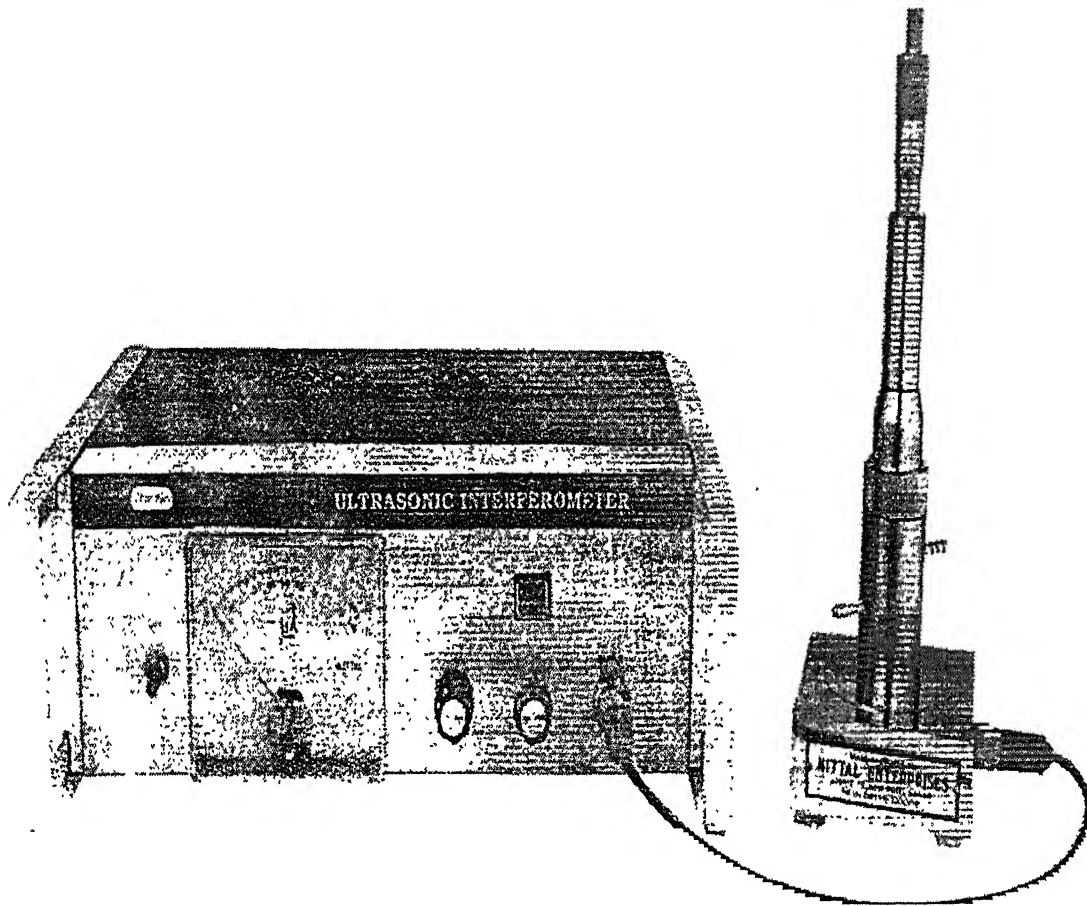


Fig.11a.5 Diagram of ultrasonic interferometer to measure ultrasonic velocity

medium. Ultrasonic waves of known medium. ultrasonic waves of known frequency (f) are produced by a quartz plate fixed at the bottom of the metallic plate kept parallel to the quartz plate. If the separation between these two plates is an exact multiple of sound wavelength, standing waves are formed in the medium. This acoustic resonance gives rise to an electrical impulse on the generator driving the quartz plate and consequently, the anode current of the generator becomes maximum.

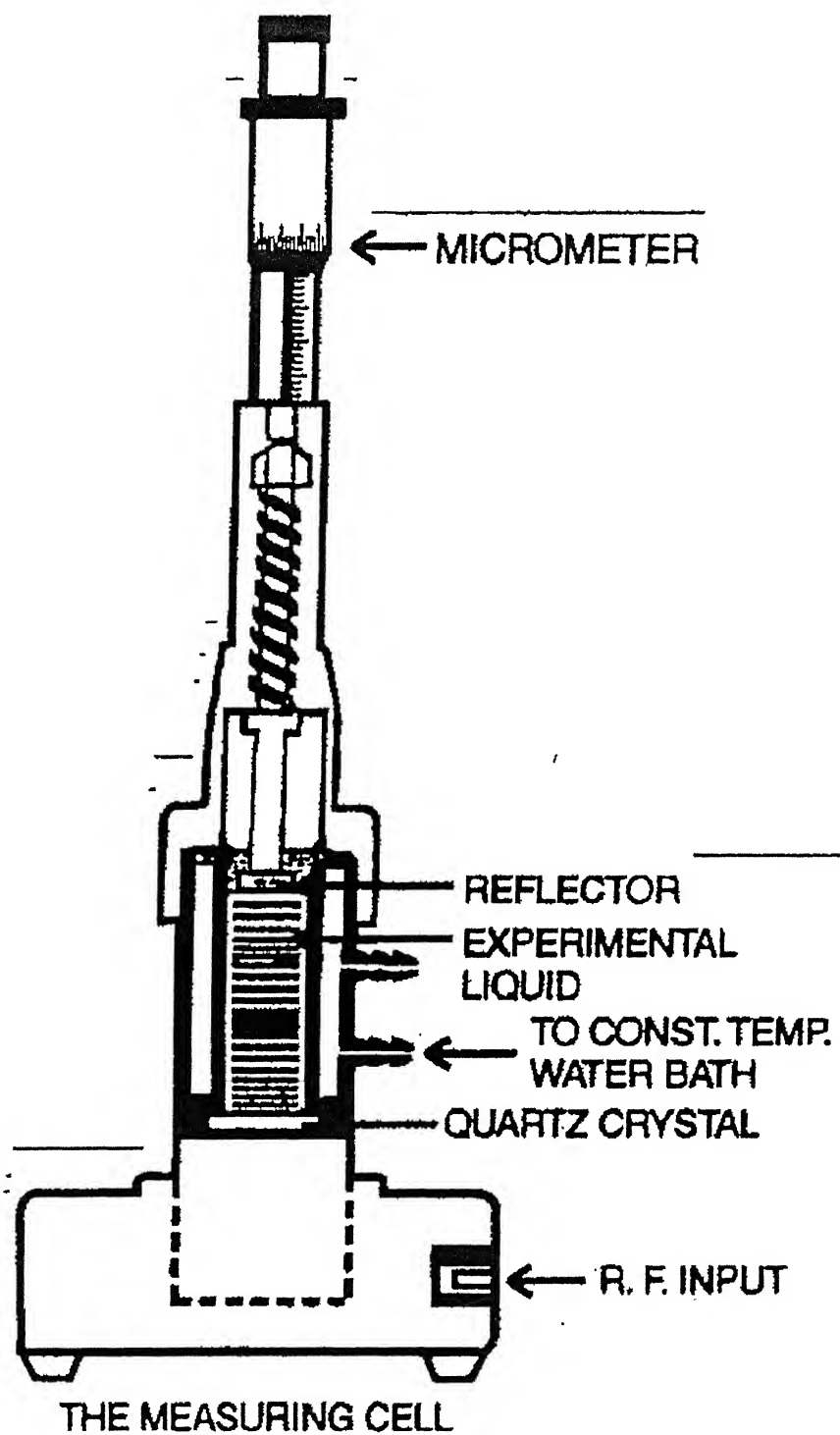


Fig 11a.6 Schematic diagram of Ultrasonic velocity measurement cell

If the distance between the plates is increased or decreased such that the variation is exactly one half wavelength ($\lambda/2$) or multiple of it, anode current again becomes maximum. From the knowledge of wavelength (λ), the velocity can be obtained by the relation

$$V = \lambda \cdot f \quad (11A.4)$$

The ultrasonic interferometer consists of the following parts

- (i) The high frequency ultrasonic wave generator
- (ii) The measuring cell

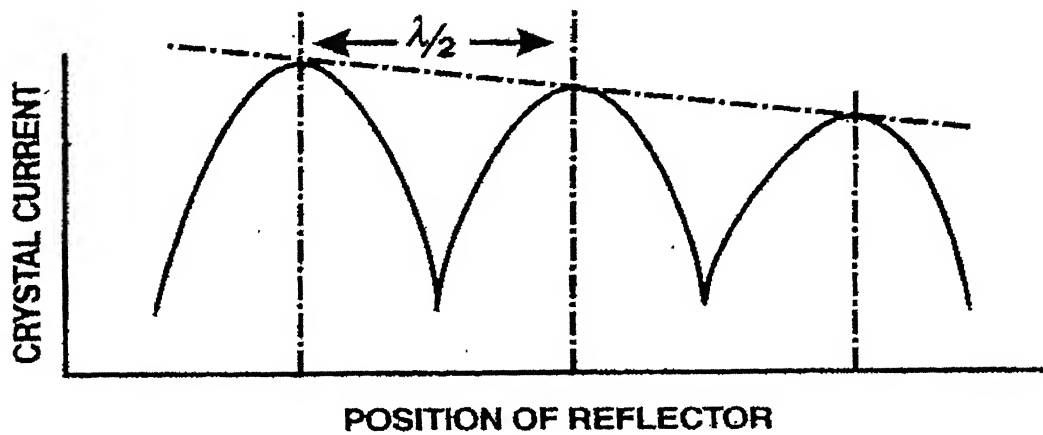


Fig. 11a.7 Variation of position of reflector and crystal current

(i) The high frequency ultrasonic wave generator

It is designed to excite the quartz plate fixed at the bottom of measuring cell at its resonant frequency to generate ultrasonic waves in the experimental liquid filled in the measuring cell. Block diagram of high frequency generator is shown in Fig.11a.5.

(ii) The measuring cell

It is made of a double walled cell so that the temperature of the liquid is kept constant during the observation. A fine micrometer screw has been provided at the top, which can lower or raise the reflector plate in the cell through the known distance. It has a quartz plate fixed at its bottom whose schematic diagram is shown in Figs. 11a.6.

Measurement

The measuring cell is connected to the output terminal of high frequency generator through a shielded cable. The cell is filled with the experimental liquid before switching on the generator. The ultrasonic waves move normal from the crystal till they are reflected back from the movable plate and the standing waves are formed in the liquid in between the reflector plate and the quartz crystal.

The micrometer is slowly moved till the anode currentmeter on high frequency generator shows a maximum. A number of maximum readings of anode current are passed on and their 'n' is counted. The total distance (d) thus moved by the micrometer gives the value of wavelength (λ) with the help of following relation:

$$V=nX\lambda/2 \quad (11A.5)$$

Once the wavelength (λ) is known the velocity (V) in the fluid can be calculated with the help of eqn. (11A.4).

Study with the variation temperature

The variation in the velocity with temperature is to be studied, water at various desired constant temperature is made to circulate through the double walled jacket of the cell with thermostat (Model: NBE 12953). The nipples are provided at the lower cylindrical portion of cell for circulating water around the experimental fluid.

References :

1. C.E.Mulder, Appl.Sc.Res. B1,149(1948) & B1,341(1950).
2. C.J.Moen, J.Acoust.Soc.Am. 23,62(1951).
3. K.Tamm, Der Akademik der Wissens chapten, In Gottingen Mathematische-physikalische klasse No. 10(1952).
4. R.W.Leonard, J.Acoust.Soc.Am. 20,224(1948).
5. O.B.Wilson and R.W.Leonard, J.Acoust.Soc.Am. 26,223(1954).
6. D.A.Beis, J.Chem.Phys. 23,428 (1955).
7. K.Tamm and G.Kurtze, Acustica, 3, 33 (1953).
8. J.Andreac, R.Bass, E.L.Heasell and J.Lamb, Acustica, 8, 131 (1958).
9. E.F.Caldin, "Fast Reactions in Solutions", Black well Scientific Publishers, Oxford, p.90(1964).
10. J.R.Pellam and J.K.Galt, J.Chem.Phys. 14,608 (1948).

11. J.M.M.Pinkerton, Proc. Phys. Soc. (London) B62, 286(1949).
12. G.Atkinson, R.L.Jones and S.K.Kor, J.Scint.Inst. 35,1270(1964).
13. G.S.Darwari, S.Petrucci, J.Chem.Phys. 53,859(1970).

CHAPTER-11B

Ultrasonic Measurements in Lyotropic Liquid Crystal

11b.1 Introduction

Ultrasonics is a versatile tool for studying the properties of solids [1,2], liquids [3,4] and liquid crystals [5,6]. In recent years, in solid (in all type of solids), liquids (pure and electrolytic solutions), the absorption and dispersion are well understood and most of the cases the absorption values are explained. There are several books and review articles, which give in details, the ultrasonic absorption in solid and liquid, however in liquid crystal, the ultrasonic absorption, are not properly explained. Different investigators have tried to explain the ultrasonic absorption in liquid crystals with the different theories and no single theory could explain the ultrasonic absorption as a function of temperature, frequency and concentration.

“Liquid crystals are beautiful and mysterious, I am fond of them for both reason.” –P.G.de Gennes, 1972.

In this first sentence of his seminal book “The Physics of Liquid Crystals,” Pierre Gilles de Gennes [7] has succinctly state that appeal that liquid Crystals for all of us working in this field. The term “liquid Crystals”, in fact, refers to a number of distinct states of matter that have structural order intermediate between that of conventional liquids and solids.

Different workers have investigated the two forms of liquid crystals, thermotropic and lyotropic. Thermotropic liquid crystals [8] the main criteria is the temperature, as the temperature varied the liquid crystalline properties are seen. In the case of lyotropic liquid crystals, concentration of the substance is the main criteria, but the temperature also plays some role in few cases. Lyotropic liquid crystal have been studied mostly in aqueous solutions and recently the studies are extended to non-aqueous solution. Amphiphilic molecules contain two or more functional groups with different chemical affinities. They build interfaces, which limit the contact between these two parts. Interfaces of soap molecule in presence of water separate the paraffinic chain from the water [9] and form aggregates of various shapes. Classically, the aggregates can be infinite with flat or cylindrical interfacial curvatures and packed with long range translational order in the well known lamellar, cubic and hexagonal phases or they can be finite, quasispherical and packed without any long range order in miscellar phase. However,

Rosenblant et al. [10] have shown that long range ordering of finite aggregates is possible. In the translational order, miscellar build a cubic structure while in oriental order, oblate or prolate spheroids are dispersed in the solution with their axis nearly parallel to each other and a nematic phase is formed. The possible factors controlling the shape of aggregates, their interactions and some of their physical properties like ultrasonic velocity and absorption in this chapter. The effect of additive are demonstrated and discussed for selected surfactant systems with respect to phase stability and the induction of neighboring states. In lyotropic liquid crystals the ultrasonic and other studies have been made mostly in aqueous solutions [9,10] and now studies are extended to non-aqueous solutions [11-13].

In the present chapter, Cetyl trimethylammonium bromide (CTAB- $C_{19}H_{42}BrN$) in non-aqueous solution of ethylene glycol ($CH_2(OH)CH_2OH$) has been taken for study. Ultrasonic absorption measurements have been made as a function of concentration and temperature at a fixed frequency of 5 MHz and velocity at 2 MHz. To the knowledge of the author such ultrasonic studies in non-aqueous solution of ethylene glycol have not been reported. The non-aqueous solutions studies are in formamide, glycerol etc.

It seems very important to make the ultrasonic absorption measurements in materials, especially in liquid crystalline phases, because the instruments utilizing the ultrasonics have been used in medical and biological fields. Accumulation of absorption data and the classification of the cause of absorption are so desired in various systems.

11b.2 Molecule studied

Lyotropic amphiphilic nematic phase first found to exist in quaternary system of sodium decyl sulphate, sodium sulphate, decanol and D_2O [16,17]. Quaternary systems have generally been found to be very flexible, frequently stable, when subjected to large variations in composition and temperature. Detergents such as potassium dodecanoate [18], alkyl trimethylammonium bromide [19] and decyl ammonium chloride [20] provides quaternary nematic mesophase. Nematic phase samples can also be obtained by using mixed detergents with oppositely charged head groups [21]. Most quaternary systems can be modified by leaving out the salt [22] or decanol resulting in ternary systems which still maintain a nematic phase under a wide range of temperature and composition variation. The ideal lyotropic amphiphilic nematic phase systems from the theoretical and experimental point of view can be derived from a binary system of detergent and D_2O only. Francois [23] has observed the mesophases in

decaethyleneglycol monolaurylether/water and other soap/water binary systems. A well defined phase diagram of cesium perfluorooctanoate (CePFO)/ D₂O has been demonstrated by Boden et al. [24], where the lamellar phase undergoes a phase transition to isotropic phase by two processes.

- (i) directly via a first order transition
- (ii) indirectly via a second order transition through a nematic phase [25]

In the continuation of above binary system studied, the present chapter deals with the study of ultrasonic velocity and absorption of N-cetyl N, N, N-trimethyl ammonium bromide (CTAB) in non aqueous solution of ethylene glycol as a function of concentration and temperature.

The CTAB used in the present investigation were supplied by Loba Chemmie India Ltd of stated purity 99% and ethylene glycol were supplied by Qualigen Chemical India purity 98%. These substances were used without further purification.

11b.3 Experimental techniques

CTAB and ethylene glycol used are 99% pure and no further purification have been made. The velocity measurements have been made by standard variable path interferometer at 2 MHz. The temperature variation is accurate to $\pm 0.5^{\circ}\text{C}$ and velocity to $\pm 0.1\%$. Standard pulse transmission technique has been used for ultrasonic absorption measurements at 5 MHz. The transmitting-receiving crystals are made parallel to each other by levelling screws and examining the exponential decay of the pulses. The receiving crystal is bigger than the transmitting crystal. The absorption measurements have been made in Frennel's region and therefore no correction is needed. The distance between the crystals are changed and the attenuation (α) is obtained by finding the slope of the curve between the intensity (decibel) and distance moved by the crystal. This (α) divided by the frequency square give (α/f^2). Water from a thermostat is circulated around the sample to keep the temperature constant. The accuracy in the absorption measurement is $\pm 5\%$. Several known values of standard liquids have been checked, including water so as to have satisfaction in absorption and velocity measurements. The observations have been repeated several times.

11b.4 Experimental results

Ultrasonic velocity measurements have been made at frequency of 2 MHz as a function of temperature and concentration. Absorption measurements have been made at 5 MHz as a function of temperature and concentration. Firstly, the velocity measurements have been made as

they are very accurate and ensure the overall behaviour of the liquid crystal. Velocity measurements at 25⁰C as a function of concentration of the substance are presented in Table 11b.1 and Fig 11b.1. It is observed that a distinct velocity minima is observed at 6.5g/100ml of the CTAB in ethylene glycol. Next velocity measurements have been made at 6.5g/100ml as a function of temperature and distinct minima is observed at 15⁰C as shown in Table 11b.2 and Fig. 11b.2. The same type of variation of ultrasonic velocity is observed at 1g/100ml and 8g/100ml. However as the concentration increases the velocity decreases. The velocity minima is most distinct at 6.5g/100ml.

Ultrasonic absorption measurements have been made at 5 MHz as a function of concentration and temperature. Table 11b.3 and Fig. 11b.3 shows the absorption maxima at 6.5g/100ml at 25⁰C for CTAB in ethylene glycol. Ultrasonic absorption measurements have been made at 5MHz as a function of temperature as shown in Table 11b.4 and Fig. 11b.4 and a maxima at 15⁰C is observed.

11b.6 Discussions

Only few ultrasonic measurements have been made in non-aqueous solutions. Mostly the solvents used are formamide and glycerol [14,26], which have similar ultrasonic behaviour as that of water. No relaxation frequency is observed in these solvents in the frequency range studied and thus the complete analysis of the data are possible. However, in the present study we have used ethylene glycol, which has a relaxation frequency [27]. To our knowledge no ultrasonic study in lyotropic liquid crystal has been made using ethylene glycol as solvent. This is obvious by the fact that ethylene glycol itself shows a variation of ultrasonic absorption (α/f^2) with frequency which is characteristic of a relaxation phenomenon.

The aim of the present study is to see that CTAB in ethylene glycol shows micelle formation or not. Using ethylene glycol micellization of cationic surfactant have been studied [28], which shows the micelle formation. Keeping this in mind an attempt has been made to check if micelle formation takes place using CTAB as surfactant in ethylene glycol. In the present study ultrasonic absorption maxima is observed at 6.5g/100ml and velocity minima is also observed at the same concentration. The critical temperature is 15⁰C and the characteristic is very predominant at 6.5g/100ml. Thus, it is conclusively proved in the present work that micelle formation takes place for the surfactant CTAB in ethylene glycol. Such behaviour of absorption maxima and velocity minima is similar to that previously observed in thermotropic liquid

crystals, binary liquids and liquid gas system at the critical point. The behaviour is of the same type as observed by Dyro and Elmonds [11]. No quantitative analysis is possible as the solvent itself shows a relaxation frequency.

The preliminary results obtained in the present work can be used for further investigation using other methods such as polarizing microscope, X-rays, surface tension, NMR and other conventional methods for making a complete analysis.

Table 11b.1 Ultrasonic velocity (m/s) in different concentration of CTAB in nonaqueous solution of ethylene glycol at 25⁰C (2MHz).

Concentration of CTAB /100ml	Velocity (m/s)
1	1653
2	1652
3	1651
4	1650
5	1645
6	1638
7	1640
8	1644
9	1650

Table 11b.2 Ultrasonic velocity (m/s) in 6.5g/100ml of CTAB in nonaqueous solution of ethylene glycol at the temperature range 10-25⁰C (2MHz).

Temperature [C]	Velocity (m/s)
10	1730
12	1650
13	1600
14	1550
15	1490
16	1510
17	1540
18	1560
20	1600
22	1620
24	1630
25	1638

Table 11b.3 Ultrasonic absorption (α/f^2) in different concentration of CTAB in nonaqueous solution of ethylene glycol at 25⁰C (5MHz).

Concentration of CTAB /100ml	$(\alpha/f^2) \times 10^{-17} \text{ Np s}^2/\text{cm}$
1	50
2	72
3	80
4	93
5	100
6	110
6	115
7	110
8	90
9	73

Table 11b.4 Ultrasonic absorption (α/f^2) in 6.5g/100ml of CTAB in nonaqueous solution of ethylene glycol at the temperature range 10-20⁰C (5MHz).

Temperature [C]	$(\alpha/f^2) \times 10^{-17} \text{ Np s}^2/\text{cm}$
11	150
12	155
13	165
14	190
15	242
16	212
17	190
18	170
20	140

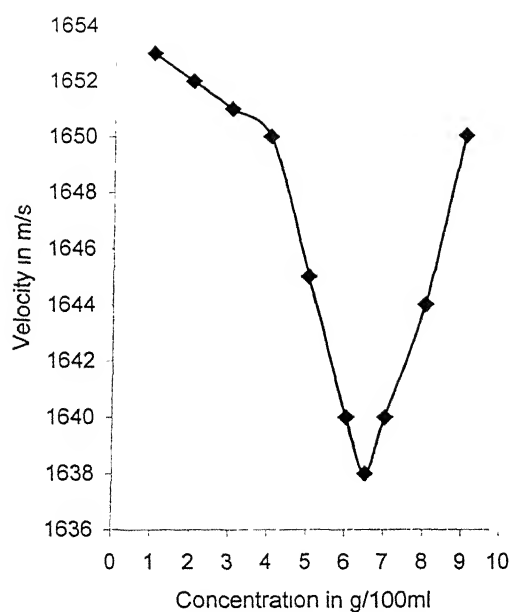


Fig. 11b.1 Concentration vs. ultrasonic velocity at 2 MHz at 25°C

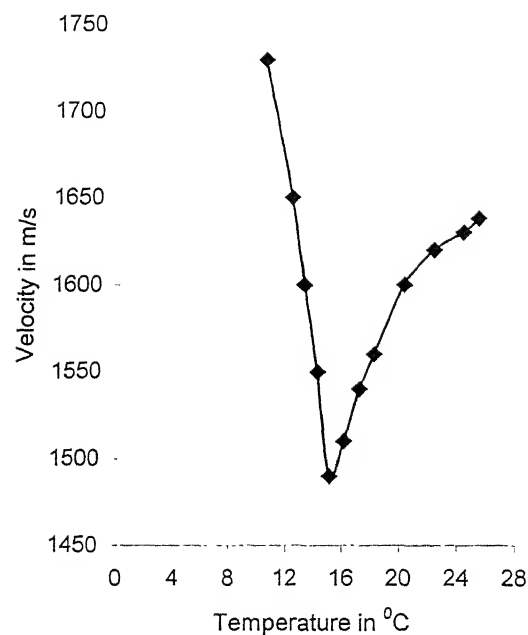


Fig. 11b.2 Temperature vs. velocity at 6.5g/100ml

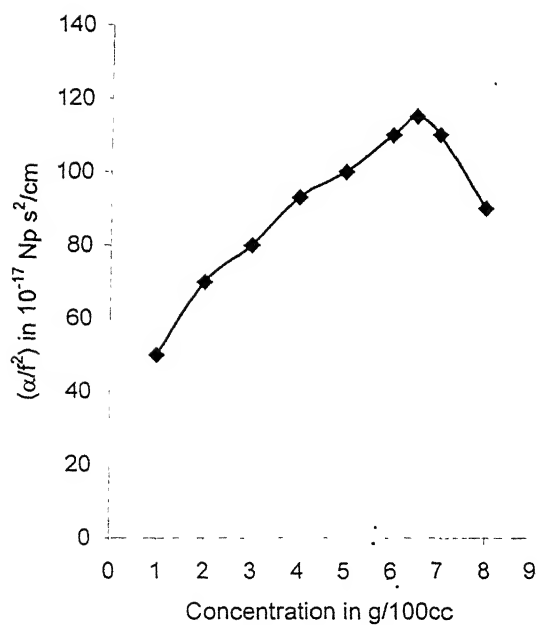


Fig. 11b.3 concentration vs. (α/f^2) at 25°C

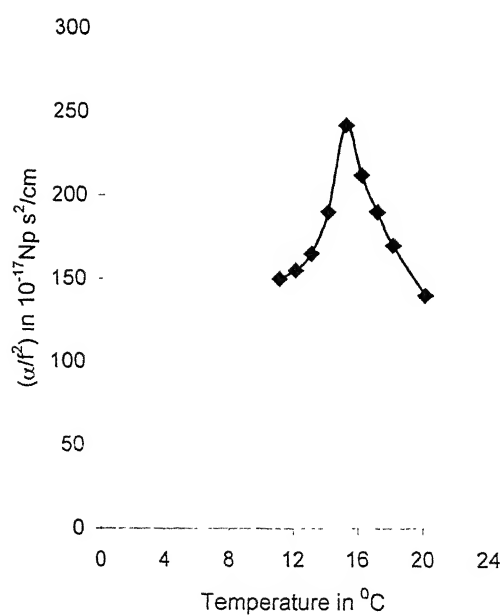


Fig 11b.4 Temperature vs. (α/f^2) at 6.5g/100cc

References:

1. W.P.Mason edited, Physical Acoustics, (Academic Press, New York 1965) Vol.IIIB.
2. F.Bert, G.Bellessa, A.Quivy, Y.Calvayrac, Phys. Rev. B61,32(2000).
3. J.Bae and S.Yun, Jpn.J.Appl.Phys. 37,2801(1998).
4. J.H.So, R.Esquivel-Sirvent, S.S.Yun and F.B.Stumpf, J.Acoust.Soc.Am. 98,659(1995).
5. S.K.Kor and A.K.Srivastava, J.Phys.Soc.Jpn. 54,613(1985).
6. M.A.Thomson, D.M.Bloor and E.Wyn-Jones, Langmuir 8,2107(1992).
7. P.G.de Gennes, The Physics of liquid Crystals, (Oxford University Press, Oxford 1974)
8. S.K.Kor and S.K.Pandey, J.Chem.Phys. 64,1333(1975).
9. C.L.Khetrapal, A.C.Kunwar, A.S.Tracey and P.Diehl, NMR basic principles and progress, Vol.9 (P.Diehl, E.Fluck and R.Kosfeld eds), Springer Verlag, Berlin (1975).
10. C.Rosenblatt, S.Kumar and J.D.Litster, Phys.Rev. A29,1010(1984).
11. J.F.Dyro and P.D. Edmonds, 2nd .Int. Conf.Liquid Crystals, Part II,21(1969).
12. N.K.Sanyal, R.A.Yadav and S.R.Shukla, Phys.Stat.Solid 99,551(1987).
13. David J.Jolue, R.E.Verall, Bodhas Skalski and Emilio Aicard, J.Phys.Chem 96, 6811 (1992).
14. M.A.Thomson, D.M.Bloor and E.Wyn-Jones, Langmuir 8,2107(1992).
15. D.F.Evans, Langmuir 4, 3 (1988).
16. D.Chen, F.Fujiwara and L.W.Reeves, Can.J.Chem. 55,2396(1977).
17. J.Charvolin, Mol.Cryst.Liq.Cryst. 113,1(1984)
18. R.C.Long, J.Mag.Res.12,216(1973).
19. K.Redley and A.S.Tracy, Mol.Cryst.Liq.Cryst. 1,95(1985).
20. L.W.Reeves, A.S.Tracey and M.M.Tracey, J.Am.Chem.Soc. 95,3799(1973).
21. A.S.Tracey and T.L.Boivin, J.Phys.Chem. 88,1017(1984).
22. K.Redley, L.W.Reeves and A.S.Tracy, J.Phys.Chem. 80,174(1976).
23. J.Francois, Kolloid Z. und Z.Polymere 248,606(1971).
24. N.Boden, P.H.Jackson, K.McMullen and H.C.Holmes, Chem.Phys.Lett. 65,476(1979).
25. N.Boden and H.C.Holmes, Chem.Phys.Lett. 109,76(1984).
26. X.Auvray, C.Petipas, R.Anthore, I.Rico and A.Lattes, J.Phys.Chem. 93,7458(1989).
27. N.Chelliah and R.Sabesan, Ind. J.Pure Appl.Phys.,32, 315 (1994).
28. H.Gharibi, R.Polepu, D.M.Bloor, D.G.Hall and E.Wyn-Jones, Langmuir 8, 782 (1992).

Appendix-A

Table A.1 Equations for Grüneisenumbers along <100> for longitudinal waves:

Type of wave	No.of Modes	Equations for $\langle \gamma_1^j \rangle$
Longitudinal	1	$-\frac{3C_{11} + C_{111}}{2C_{11}}$
Shear	2	$-\frac{C_{11} + C_{166}}{2C_{44}}$
Longitudinal	2	$-\frac{C_{11} + C_{112}}{2C_{11}}$
Shear	2	$-\frac{2C_{44} + C_{12} + C_{166}}{2C_{44}}$
Shear	2	$-\frac{C_{12} + C_{144}}{2C_{44}}$
Longitudinal	2	$-\frac{2C_{12} + C_{112} + 2C_{144} + C_{123}}{2(C_{11} + C_{12} + 2C_{44})}$
Shear	2	$-\frac{2C_{12} + C_{112} - C_{123}}{2(C_{11} - C_{12})}$
Shear	2	$-\frac{C_{12} + 2C_{44} + C_{166}}{2C_{44}}$
Longitudinal	4	$-\frac{2(C_{11} + C_{12} + C_{44}) + C_{111}/2 + 3C_{112}/2 + 2C_{166}}{2(C_{11} + C_{12} + 2C_{44})}$
Shear	4	$-\frac{2C_{11} + (C_{111} - C_{112})/2}{2(C_{11} - C_{12})}$
Shear	4	$-\frac{C_{11} + C_{12} + C_{144} + C_{166}}{4C_{44}}$
Longitudinal	4	$-\frac{5C_{11} + 10C_{12} + 8C_{44} + C_{111} + 6C_{112} + 2C_{123} + 4C_{144} + 8C_{166}}{6(C_{11} + 2C_{12} + 4C_{44})}$
Shear	4	$-\frac{4C_{11} + 5C_{12} + C_{44} + (C_{111} + 3C_{112})/2 + (C_{144} + 5C_{166})/2 - 2C_{123}}{6(C_{11} - C_{12} + C_{44})}$
Shear	4	$-\frac{2C_{11} + C_{12} + C_{44} + (C_{111} - C_{112})/2 + (C_{144} + C_{166})/2}{2(C_{11} - C_{12} + C_{44})}$

Table A.2 Equations for Grüneisenumbers along $\langle 100 \rangle$ for shear waves:

Type of wave	No. of Modes	Equations for $\langle \gamma_i^j \rangle$
Longitudinal	2	$\pm \frac{C_{11} + C_{12} + C_{44} + C_{166}}{2(C_{11} + C_{12} + 2C_{44})}$
Shear	2	$\pm \frac{C_{44} + C_{456}}{2C_{44}}$
Shear	2	$\pm \frac{C_{12} - C_{11} + 2C_{44}}{2(C_{11} - C_{12})}$
Longitudinal	4	$\pm \frac{2C_{11} + 4C_{12} + 14C_{44} + 4C_{144} + 8C_{166} + 8C_{456}}{6(C_{11} + 2C_{12} + 4C_{44})}$
Shear	4	$\pm \frac{2C_{11} + 2C_{12} + 4C_{44} - (C_{144} + 2C_{456}) + C_{166}}{6(C_{11} - C_{12} + C_{44})}$
Shear	4	$\pm \frac{2C_{44} - C_{144} + C_{166}}{2(C_{11} - C_{12} + C_{44})}$

Table A.3 Equations for Grüneisenumbers along $\langle 110 \rangle$ for longitudinal waves:

Type of wave	No. of Mode s	Equations for $\langle \gamma_i^j \rangle$
Longitudinal	2	$\frac{3C_{11} + C_{12} + C_{111} + C_{112}}{4C_{11}}$
Shear	1	$\frac{2C_{11} + 2C_{112}}{4C_{11}}$
Longitudinal	2	$\frac{C_{11} + C_{12} + 2C_{44} + 2C_{166}}{4C_{44}}$
Shear	2	$\frac{2C_{12} + 2C_{44} + C_{144} + C_{166}}{4C_{44}}$
Shear	2	$\frac{C_{11} + C_{12} + C_{144} + C_{166}}{2C_{44}}$
Longitudinal	4	$\frac{2C_{11} + 4C_{12} + 2C_{44} + (C_{111} + 5C_{112})/2 + 2C_{144} + 2C_{166}}{4(C_{11} + C_{12} + 2C_{44})}$
Longitudinal	1	$\frac{5C_{11} + 5C_{12} + 7C_{44} + C_{111} + 3C_{112} + 8C_{166}}{4(C_{11} + C_{12} + 2C_{44})}$
Longitudinal	1	$\frac{3C_{11} + 3C_{12} - 3C_{44} + C_{111} + 3C_{112}}{4(C_{11} + C_{12} + 2C_{44})}$
Shear	4	$\frac{2C_{11} + 2C_{12} + (C_{111} + C_{112})/2 - C_{123}}{4(C_{11} - C_{12})}$

Shear	1	$\frac{3C_{11} + C_{12} + 2C_{44} + C_{111} - C_{112}}{4(C_{11} - C_{12})}$
Shear	1	$\frac{3C_{11} - C_{12} - 2C_{44} + C_{111} - C_{112}}{4(C_{11} - C_{12})}$
shear	1	$\frac{3C_{11} + 2C_{12} + 2C_{44} + 2C_{144} + 2C_{166} + 2C_{456}}{8C_{44}}$
Shear	1	$\frac{C_{11} + 3C_{12} + 4C_{44} + C_{144} + 3C_{166}}{8C_{44}}$
Shear	1	$\frac{2C_{11} + 2C_{12} - 2C_{44} + 2C_{144} + 2C_{166} - 2C_{456}}{8C_{44}}$
Shear	2	$\frac{6C_{11} + 12C_{12} + 15C_{44} + C_{111} + 6C_{112} + 2C_{123} + 6C_{144} + 12C_{166} + 4C_{456}}{6(C_{11} + 2C_{12} + 4C_{44})}$
Shear	2	$\frac{4C_{11} + 8C_{12} + C_{44} + C_{111} + 6C_{112} + 2C_{123} + 2C_{144} + 4C_{166} - 4C_{456}}{6(C_{11} + 2C_{12} + 4C_{44})}$
Longitudinal	2	$\frac{9(C_{11} + C_{12} + C_{44}) + C_{111} + 3C_{112} - 3C_{144} + 9C_{166} - 4C_{456}}{12(C_{11} - C_{12} + C_{44})}$
Longitudinal	2	$\frac{7C_{11} + 11C_{12} - 5C_{44} + C_{111} - C_{112} + C_{144} + C_{166} - 4C_{123}}{12(C_{11} - C_{12} + C_{44})}$
Shear	2	$\frac{3(C_{11} + C_{12} + C_{44}) + C_{111} - C_{112} + C_{144} + C_{166} - C_{456}}{4(C_{11} - C_{12} + C_{44})}$
Shear	2	$\frac{5C_{11} + C_{12} + C_{44} + C_{111} - C_{112} + C_{144} + C_{166} + C_{456}}{4(C_{11} - C_{12} + C_{44})}$

Table A.4 Equations for Grüneisen numbers shear waves propagating along <110> direction and polarized along <001> direction:

Type of wave	No.of Modes	Equations for $\langle \gamma_i^j \rangle$
Longitudinal	4	$\pm \frac{C_{11} + C_{12} + 4C_{44} + 4C_{166}}{2\sqrt{2}(C_{11} + C_{12} + 2C_{44})}$
Shear	4	$\pm \frac{C_{11} - C_{12} - 2C_{44}}{2\sqrt{2}(C_{11} - C_{12})}$
Shear	4	$\pm \frac{C_{44} + C_{456}}{2\sqrt{2}C_{44}}$
Longitudinal	2	$\pm \frac{2C_{11} + 4C_{12} + 14C_{44} + 4C_{144} + 8C_{166} + 8C_{456}}{3\sqrt{2}(C_{11} + 2C_{12} + 4C_{44})}$
Shear	2	$\pm \frac{2C_{11} - 2C_{12} - 4C_{44} + C_{144} - C_{166} + 2C_{456}}{3\sqrt{2}(C_{11} - C_{12} + C_{44})}$

Shear	4	$\pm \frac{2C_{44} - C_{144} + C_{166}}{\sqrt{2}(C_{11} - C_{12} + C_{44})}$
-------	---	--

Table A.5 Equations for Grüneisen numbers shear waves propagating along $\langle 110 \rangle$ direction and polarized along $\langle 1\bar{1}0 \rangle$ direction:

Type of wave	No. of Modes	Equations for $\langle \gamma_i^j \rangle$
Longitudinal	2	$\pm \frac{3C_{11} - C_{12} + C_{111} - C_{112}}{2C_{11}}$
Shear	2	$\pm \frac{C_{11} - C_{12} - 2C_{44}}{2C_{44}}$
Shear	2	$\pm \frac{2C_{44} - C_{144} + C_{456}}{2C_{44}}$
Shear	2	$\pm \frac{C_{11} - C_{12} - C_{144} + C_{166}}{2C_{44}}$
Longitudinal	4	$\pm \frac{2C_{11} + 2C_{44} + (C_{111} + C_{112})/2 - C_{123} - 2C_{144} + 2C_{166}}{2(C_{11} + C_{12} + 2C_{44})}$
Shear	2	$\pm \frac{2C_{11} - 2C_{12} + (C_{111} - 3C_{112})/2 + C_{123}}{2(C_{11} - C_{12})}$
Shear	4	$\pm \frac{C_{11} - C_{12} - 4C_{44} + C_{144} - C_{166}}{4C_{44}}$

Table A.6 Equations for Grüneisen numbers along $\langle 111 \rangle$ for longitudinal waves:

Type of wave	No. of Mode s	Equations for $\langle \gamma_i^j \rangle$
Longitudinal	3	$\frac{3C_{11} + 2C_{12} + C_{111} + 2C_{112}}{6C_{11}}$
Shear	6	$\frac{C_{11} + 2C_{12} + 2C_{44} + 2C_{166} + C_{144}}{6C_{44}}$
Longitudinal	3	$\frac{6C_{11} + 8C_{12} + 12C_{44} + C_{111} + 4C_{112} + C_{123} + C_{144} + 12C_{166}}{6(C_{11} + C_{12} + 2C_{44})}$
Longitudinal	3	$\frac{2C_{11} + 4C_{12} - 4C_{44} + C_{111} + 4C_{112} + C_{123} + 2C_{144} - 4C_{166}}{6(C_{11} + C_{12} + 2C_{44})}$
Shear	3	$\frac{2C_{11} + 4C_{12} + 4C_{44} + C_{111} - C_{123}}{6(C_{11} - C_{12})}$
Shear	3	$\frac{6C_{11} - 4C_{44} + C_{111} - C_{123}}{6(C_{11} - C_{12})}$

Shear	3	$\frac{C_{11} + 2C_{12} + 2C_{166} + C_{144} + 2C_{456}}{6C_{44}}$
Shear	3	$\frac{C_{11} + 2C_{12} + 2C_{166} + C_{144} - 2C_{456}}{6C_{44}}$
Longitudinal	1	$\frac{9C_{11} + 18C_{12} + 36C_{44} + C_{111} + 4C_{112} + 2C_{123} + 12C_{144} + 16C_{456}}{6(C_{11} + 2C_{12} + 4C_{44})}$
Longitudinal	3	$\frac{11C_{11} + 22C_{12} - 4C_{44} + 3C_{111} + 12C_{112} + 6C_{123} + 4C_{144} + 8C_{166} - 16C_{456}}{18(C_{11} + 2C_{12} + 4C_{44})}$
Shear	1	$\frac{3C_{11} + 6C_{12} + 12C_{44} + C_{111} - C_{123} - 3C_{144} + 6C_{166} - 2C_{456}}{6(C_{11} - C_{12} + C_{44})}$
shear	2	$\frac{13C_{11} + 4C_{12} - 8C_{44} + 3C_{111} - 3C_{123} + 4C_{144} - 2C_{166} - 2C_{456}}{6(C_{11} - C_{12} + C_{44})}$
Shear	1	$\frac{25C_{11} + 2C_{12} + 4C_{44} + 3C_{111} - 3C_{123} - C_{144} - 10C_{166} + 10C_{456}}{18(C_{11} - C_{12} + C_{44})}$
Shear	1	$\frac{3C_{11} + 6C_{12} + 12C_{44} + C_{111} - C_{123} - 3C_{144} + 6C_{166} - 2C_{456}}{6(C_{11} - C_{12} + C_{44})}$
Shear	2	$\frac{7C_{11} + 2C_{12} + C_{111} - C_{123} - C_{144} + 2C_{166} + 2C_{456}}{6(C_{11} - 2C_{12} + C_{44})}$
Shear	1	$\frac{3C_{11} + 6C_{12} - 4C_{44} + C_{111} - C_{123} + 5C_{144} - 2C_{166} - 2C_{456}}{6(C_{11} - 2C_{12} + C_{44})}$

Table A.7 Equations for Grüneisen numbers shear waves propagating along $\langle 110 \rangle$ direction ϵ polarized along $\langle \bar{1}10 \rangle$ direction:

Type of wave	No.of Modes	Equations for $\langle \gamma_i^j \rangle$
Longitudinal	2	$\pm \frac{3C_{11} - C_{12} + C_{111} - C_{112}}{\sqrt{6}C_{11}}$
Shear	2	$\pm \frac{C_{11} - C_{12} - 2C_{44}}{\sqrt{6}C_{44}}$
Longitudinal	2	$\pm \frac{-5C_{11} - C_{12} - 8C_{44} - C_{111} - 8C_{166} - C_{112} + 2C_{123} + 4C_{144}}{2\sqrt{6}(C_{11} + C_{12} + 2C_{44})}$
Shear	2	$\pm \frac{-3C_{11} + C_{12} - C_{111} - C_{112} + 2C_{123} + 4C_{144}}{2\sqrt{6}(C_{11} + C_{12} + 2C_{44})}$
Shear	2	$\pm \frac{-C_{11} + 3C_{12} - 2C_{44} - C_{111} + 3C_{112} - 2C_{123}}{2\sqrt{6}(C_{11} - C_{12})}$
Shear	2	$\pm \frac{-5C_{11} + 5C_{12} + 2C_{44} - C_{111} + 3C_{112} - 2C_{123}}{2\sqrt{6}(C_{11} - C_{12})}$

Longitudinal	2	$\pm \frac{-C_{11} + C_{12} + 3C_{44} - C_{144} + C_{166} - C_{456}}{2\sqrt{6}C_{44}}$
Shear	2	$\pm \frac{-C_{11} + C_{12} + 5C_{44} - C_{144} + C_{166} - C_{456}}{2\sqrt{6}C_{44}}$
Shear	2	$\pm \frac{2C_{11} + 4C_{12} + 14C_{44} + 4C_{144} + 8C_{166} + 8C_{456}}{3\sqrt{6}(C_{11} + 2C_{12} + 4C_{44})}$
Shear	2	$\pm \frac{-2C_{11} + 2C_{12} + C_{44} - C_{144} - C_{166} - 2C_{456}}{3\sqrt{6}(C_{11} - C_{12} + C_{44})}$
Shear	2	$\pm \frac{2C_{44} - C_{144} + C_{166}}{3\sqrt{6}(C_{11} - C_{12} + C_{44})}$
Longitudinal	2	$\pm \frac{C_{11} - C_{12} - C_{144} + C_{166}}{\sqrt{6}C_{44}}$
Longitudinal	2	$\pm \frac{2C_{44} - C_{144} + C_{166}}{\sqrt{6}C_{44}}$